The reflection and scattering of sound from the seabed

Ainsworth, Stephen E.

Award date:
2001

Awarding institution:
University of Bath

THE REFLECTION AND SCATTERING OF SOUND FROM THE SEABED

submitted by Stephen E Ainsworth

for the degree of PhD

of the University of Bath

February 2001

ProQuest LLC
789 East Eisenhower Parkway
P.O. Box 1346
Ann Arbor, MI 48106-1346

Summary

This thesis shows how the interaction of a pulsed sonar beam with the seabed may be modelled by a modified first order perturbation approach. The seabed is described as a rough surface with a physically realistic impedance determined by its density and wave speeds. A scattering model is developed systematically, by applying the elastic boundary conditions seen in smooth surface reflection theory (chapter 2) to the statistical formalism required to describe a rough surface (chapter 3). Perturbation theory solutions are thus developed for rough surface scattering, for a liquid / liquid interface (chapter 4) and a liquid / solid interface (chapter 5). This is done for plane harmonic waves. In all cases these solutions are shown to reduce analytically to precisely the correct (standard) forms for limiting values of densities and wave speeds. It is then shown, in chapter 6, how these solutions may be used to model the practical application of a pulsed beam interacting with a seabed. The statistics of the scattered solutions derived for many rough surface realisations are also presented.

Acknowledgements

Thanks to Nick Pace and all the staff at Bath University, for their help, encouragement and flexibility.

Thanks to Chris Bevan and Barbara Brookes, for helpful discussions on many aspects of acoustics, and for their friendship and support over many Fridays at Bath University.

Thanks to Geoff Searing, Jim Chalmers, Dave Dunn and Alan Parsons at DERA who helped in getting me started, and to DERA for providing funding for the early years.

Many thanks to Gary Woods and Keith Williams who were, during my time at DERA, good friends, fine scientists, and were most helpful and informative in all sorts of ways in many areas of environmental acoustics.

Thanks are also due to my friends and colleagues at DERA Weymouth, notably Andrew Green, Mark Miller, Jerry Siddle, and Richard Heycock.

Thanks also to Roger Benton and Stephen Long with whom I have had many useful and interesting technical discussions at TMSL, to Malcolm Merritt for the use of his library, and to TMSL for the use of their computing and printing facilities.

As ever, many thanks are due to my parents, Harry and Jen, who have always encouraged me to "just do your best", and have provided me with the love, support and opportunities to do so.

Many thanks are also due to my sister and brother, Cath and Chris, for their love, encouragement and good humour at all times.

Finally, my thanks to my wife, Liz, for her love and support in all things, and to whom this thesis is dedicated.

Contents

Glossary of Symbols and Abbreviations

Unless stated otherwise, the symbols and abbreviations used in this thesis have the following meanings. Unless stated otherwise, all units are standard SI units.

a	dimensionless parameter used to define the Thorsos PSD, chapter 3
a_{nn}	the matrix propagator method terms defined in Appendix 2A
b_i	transverse (shear) wave speed in the i^{th} seabed layer, in m/s
c	sound speed in the sea, 1500m/s
c_0	sound speed in the sea, assumed to be 1500 m/s
c_i	sound speed in the i^{th} seabed layer, in m/s
c_l	sound speed in the i^{th} seabed layer, in m/s
c_t	transverse (shear) wave speed in the i^{th} seabed layer, in m/s
c_{im}	imaginary part of the sound speed (used in defining attenuation)
c_{re}	real part of the sound speed (used in defining attenuation)
corr	correlation length
dB	decibels, used to calculate scattering strength
d_n	layer thickness used for the input impedance method, chapter 2
exp	used to denote "e to the power..." where e is 2.71828182845905
f	frequency, in Hertz
f(z)	displacement-stress vector, chapter 2
g(t)	Gaussian pulse function in the time domain
h	height, in metres, of the array centre from the seabed, chapter 6
i	square root of minus 1
j	used to number the seabed layers used in the matrix propagator method development, chapter 2
k, k_0	sound wavenumber in the sea
k_i	sound wavenumber in the i^{th} seabed layer
k_{im}	imaginary part of the sound wavenumber (used in defining attenuation)
k_{re}	real part of the sound wavenumber (used in defining attenuation)
l	as a subscript, this refers to a longtudinal ("compressional" or "sound") wave
l	distance, in metres, of the array centre from the seabed, chapter 6
m	ratio of seabed layer density to sea density (latter assumed to be 1000 kg/m^3)
m_S	scattering coefficient
n	ratio of sea sound speed to seabed layer sound speed
p	pressure
r	radial vector in x,y plane

r	radial distance in 3 dimensions
rms	root mean square
t	time, in seconds
t	as a subscript, this refers to a transverse (shear) wave
u	particle displacement in a solid, chapter 2
v	particle displacement in a solid, chapter 2
v	also used in chapter 2 as a particle velocity
v_z	vertical particle velocity, used in chapter 2 (input impedance method)
w	particle displacement in a solid, chapter 2
x, y, z	right handed cartesian co-ordinate system
z_i	height of interface of the i^{th} layer with the $i+1^{th}$ layer, chapter 2
A_i	the matrix propagator method layer to layer matrix
A	the matrix propagator method full scenario (i.e. all layers) matrix
$A(\kappa)$	rough surface power spectral amplitude
$A_\alpha(\kappa)$	rough surface spectral scattered reflected amplitude
$A_\beta(\kappa)$	rough surface spectral scattered transmitted amplitude
A_S	scattering area, used in development of scattering strength, chapter 3
$B(\mathbf{r})$	surface autocorrelation function, used in scattering strength development, chapter 3
C(x)	correlation function
C(r)	correlation function
$C_{1\text{-}12}$	parameters set up in chapter 5 to collect terms together
E	constant set up in chapter 4 to collect terms
FT	Fourier Transform operation
G	constant set up in chapter 4 to collect terms
I_i	incident intensity, used in scattering strength development, chapter 3
I_S	scattered intensity, used in scattering strength development, chapter 3
I	incident velocity potential, chapter 5 (assumed to be 1 in calculations)
L	length of scattering surface, used in scattering strength development for 1 dimensional surface, chapter 3
L	length of the array from which the beam is formed, in metres, chapter 6
N	number of points at which a rough surface height is sampled, chapter 3
O	used as origin in figures throughout
P	amplitude of the transmitted shear velocity potential for a liquid / solid interface, chapter 2
$P(\kappa)$	surface wavenumber power spectrum, used in scattering strength development, chapter 3
P	point of observation of scattering strength, chapter 3
PSD	Power Spectral Density
R	distance from scattering area, A_S, to point of observation, P, chapter 3

$S(\kappa, geo)$	function used to represent the affect of the interface geoacoustic parameters on the surface spectral scattered pressure amplitude
V	amplitude of the reflected sound pressure wave for a liquid / liquid interface, chapter 2
V	amplitude of the reflected sound velocity potential for a liquid / solid interface, chapter 2
W	amplitude of the transmitted sound pressure wave for a liquid / liquid interface, chapter 2
W	amplitude of the transmitted sound velocity potential for a liquid / solid interface, chapter 2
X	variable used for correlation function development, chapter 3
Z_i	impedance of the i^{th} layer, chapter 2
Z_{inp}	input impedance of a series of seabed layers, chapter 2
α_i	vertical wavenumber component for sound wave in i^{th} layer, chapter 2
β_i	vertical wavenumber component for shear wave in i^{th} layer, chapter 2
γ	vertical wavenumber component, chapter 4, 5
∂	partial derivative
$\delta(\kappa-\kappa')$	Dirac delta function
ξ	horizontal wavenumber component – the same for all waves in all layers
χ	statistical parameter used in chapter 6
ϕ	azimuthal angle in 3d spherical polar co-ordinates, chapter 3
ϕ	scalar velocity potential, chapters 2, 5
κ	rough surface wavenumber
λ	wavelength
λ	Lamé coefficient, chapters 2, 4, 5
μ	Lamé coefficient, the elasticity modulus, chapters 2, 4, 5
μ	mean value for the Gaussian distribution, used in chapter 6
θ	incident angle
ρ	density, in kg/m^3
σ	stress tensor
σ_{ij}	force per unit area (stress) in the direction j on the face perpendicular to the direction i, chapter 2
σ	standard deviation of Gaussian distribution, used in chapter 6
σ	parameter used to define the Rayleigh distribution, used in chapter 6
ω	angular frequency, radians per second
ψ	vector velocity potential, chapters 2, 5
Δ	used to denote "difference in ..."
∇	gradient operator
$\nabla_\perp$	horizontal (2D) part of the gradient operator

1 Introduction

1.1 Summary

The propagation of sound in the ocean has been used for many years as a means of detecting other vessels both on and below the sea surface. A detailed knowledge of the underlying mechanisms which govern this phenomenon enables continuous improvement to be made in all aspects of sonar research. The basic theory of sound propagation in ideal conditions is well understood and documented (BREKHOVSKIKH & LYSANOV (1990)). In the real world, however, conditions are far from ideal. Geometry, boundary and environmental conditions conspire to produce a physical problem which is far from fully understood.

Of interest here is the role of the seabed boundary in affecting the propagation of sound through the ocean. If sound "echoes" from the seabed then the questions which must be answered are: in what direction and how loud? Ideally these questions should be answered in a mathematically general sense, such that the solutions are widely applicable to a range of sounds and seabed types. It will be shown that this is possible by parameterising the seabed in terms of its geoacoustic properties and in terms of certain statistical properties of its relief.

Neither the standard theories of reflection or scattering alone can accurately model the interaction of sound with the seabed. Reflection theory assumes that the seabed is perfectly smooth: standard scattering theories assume that: either the directional scattering pattern is proportional to that obtained from a perfectly hard surface; or that the seabed is a pressure release interface. Both these assumptions are too simplistic for a general seabed. In the more realistic model presented here the physically correct boundary conditions used in reflection theory are combined with the geometrically correct description of the rough surface used in scattering theory. The assumption is made that the roughness of the surface is small (as defined in chapter 3): the scattered energy is then a small perturbation on the zero order reflected energy, the reflected energy being calculated using standard reflection theory (as defined in chapter 2). In this way the ideas and techniques from reflection and scattering theories are combined in one model, with the assumption that the zero order reflection solution is already known.

It is the goal of this thesis to describe this model for the interaction of low frequency (around 1kHz) sound with the seabed. More specific aims are that this model will:

1 have a firm theoretical basis;

2 make intuitive sense;

3 and be easily applied to naval research scenarios.

Some of the theoretical ideas in this study have been examined in the literature in great mathematical detail, with much rigour (see MOE and JACKSON (1998), IVAKIN (1998) and JACKSON and IVAKIN (1998)); and some of the applications of this study, reverberation modelling, have also been studied in their own right (see LePAGE (1999)). This thesis aims

to present a more tractable, direct route to modelling simple forward- and back- scattering of sound from the seabed for pulsed beams, and a seabed defined by both its surface roughness and its geoacoustic properties.

The features of the model described here are that:

- the lower medium (seabed) is assumed to be elastic (described in chapter 2);
- the lower medium (seabed) is assumed to be rough (as described in chapter 3);
- attenuating media (sediments) are accommodated (described in chapter 2);
- in principle any layered media (seabed) structure can be used (described in chapter 2);
- a Gaussian spectrum is used which is user tuneable, though in principle any other suitable (defined in chapter 3) power spectrum could be used;
- the scattered pressure amplitude has a simple explicit dependence on the geoacoustic parameters at the rough interface (see chapters 4 and 5 for liquid / liquid and for liquid / solid cases respectively);
- the scattering depends on the complex (i.e. including phase) amplitude spectrum for the surface height of the particular rough surface realisation (see chapter 6);
- scattering into the lower medium (seabed,) at grazing angles below the critical grazing angle, is predicted naturally as a consequence of the way in which the scattered wavevectors are calculated (see chapter 4);
- the model generates results for many independent rough surface realisations enabling ensemble scattering statistics to be generated (see chapter 6);
- the incident sound is generated as a pulsed beam of user defined frequency, duration and width (see chapter 6);
- the model is developed in a modular form, such that each can be improved independently of the others.

Although this model has been developed to be consistent with a ray based sound propagation model, it is noted that scattering is relevant to all types of propagation models including normal modes models (see GINGRAS (1998)) and parabolic equation models (see SMITH (1997)). A different approach would be required to fit in with these propagation models than that presented here.

A further qualification is that although phase is included (see chapter 6), which is derived from the relative travel times of different plane waves, the model generates static results. It is not a "time evolution" model such as that developed by BERGEM et al. (1999), POULIQUEN et al. (1999). The model developed here could be used as a component in such a time evolution model, for calculating the interaction at a seabed interface, given the appropriate sonar pulse, geoacoustic and geometric parameters. Similarly the results derived for the rough surface interaction could be used in reverberation models (see BERMAN (1999)) where the time history of the returned field is modelled in terms of many rough surface interactions due to sound propagating within a roughly bounded waveguide.

1.2 Thesis structure

In this first chapter a literature review is presented which gives an overview of the development of the theories of seabed reflection and scattering. This has two important roles: firstly to put the work in this thesis into context and secondly to serve as one source of ideas which may be considered for future work. The latter will be discussed in chapter 8. Further reference to more specific papers from the more recent literature will be made in the following chapters when discussing particular ideas in greater detail than in this first introductory chapter.

In chapter 2 the basic theory of reflection of sound at a smooth interface will be considered. This will be done for both liquid / liquid and liquid / solid interfaces, and the use of each in describing a sea / seabed interface will be explained. The matrix propagator model described by BREKHOVSKIKH and GODIN (1990) is reviewed and corrections are made to their application of this to a simple case. This model is a general seabed reflection model which can, in principle, be used to calculate the reflection coefficient from any system of smooth homogeneous horizontal seabed layers. An example of this is presented for an inhomogeneous sediment layer and the results are compared with those presented by AINSLIE et al. (1998). The main aims of this chapter are to introduce the physical boundary conditions which must be used at any interface (here a smooth interface), and also to explore the effects of the various geoacoustic parameters which are used to describe the seabed.

In chapter 3 the basic considerations for understanding the scattering of sound using first order perturbation theory are described, and it is shown how standard scattering theories must be extended to deal with non-trivial boundary conditions. This includes the development of the co-ordinate transformations required to cope with elastic boundary conditions; and also extends the development of the scattering coefficient and scattering strength. Although using realistic boundary conditions, the theory remains first order, and takes no account of higher order surface scattering terms which would increase the accuracy of the solution (see THORSOS and JACKSON (1989). Neither does it take explicit account of surface waves which may develop on the rough surface and be scattered, leading to complex phenomena such as propagation of sound over curved surfaces into shadow regions (see CHAMBERS and BERTHELOT (1997); and nor does it take into account sediment volume scattering, as described by PACE (1992,1993) and HINES (1990).

Chapters 4 and 5 show the new scattering development for the liquid / liquid and the liquid / solid interface regimes respectively. This approach uses the appropriate elastic boundary conditions described in chapter 2, along with the statistical framework for describing rough surfaces developed in chapter 3. The solutions derived are for plane harmonic waves, for the scattered amplitudes (*pressure* amplitudes in chapter 4: *velocity potential* amplitudes in chapter 5), and are in terms of the surface spectral amplitude (rather than the surface power spectral density).

Chapter 6 shows how the theoretical scattered pressure amplitude results from chapters 4 and 5 can be applied to derive useful results for a realistic rough seabed. This includes: details of the sea / seabed model, in terms of the geoacoustic model and the roughness model; details of how the plane harmonic wave results from chapters 4 and 5 are summed and weighted for different angles and frequencies to give results applicable to a pulsed beam; details of how the results are derived for a single surface and how ensemble statistics are generated for many suface realisations; and describes the statistical measures and techniques used.

In chapter 7 the code used for the models described in the earlier chapters is listed. This includes the matrix propagator method code, and the scattering model code for the liquid / liquid case. The subroutines used for the liquid / liquid model are also listed. These include those used to calculate the scattering statistics, and those used to generate and test the pulse and beam parameters. For the liquid / solid case only one of the subroutines is listed, the one which calculates the scattered pressures for a particular plane harmonic wave given the geoacoustic parameters: all the other subroutines, and the main routine, for the liquid / solid case are very similar to those for the liquid / liquid case.

In chapter 8 ideas for further work in this area are presented. These include ideas for extending the work done in each of the separate areas of reflection theory and scattering theory, as well as ideas for extending the new model developed here so that it could provide an input to other scattering models (those which include other scattering phenomena and are time dependent).

1.3 Literature review

Historically the interaction of sound at the seabed has been categorised into two main phenomena: reflection and scattering. Both are highly intuitive. The former is typical of any energetic impact at a *smooth* boundary, from a ball striking a wall to light reflecting from a mirror. The features of reflection are that it is immediate, at the point of impact, and that all the reflected energy is *coherent*, i.e. with a definite phase and amplitude in the specular direction. Scattering, on the other hand, is the result of energy impacting on a *rough* surface. Energy is now re-radiated in many directions though not necessarily in equal proportion. The energy is now incoherent, i.e. with different amplitudes and phases in the different directions.

The theories of sound reflection and scattering at the seabed have thus developed separately. Reflection theory considers the continuity of force and displacement at a smooth interface between two media. This results in a *reflection coefficient*, a dimensionless number of magnitude less than or equal to 1, which indicates the fraction of the incident energy which is reflected from the interface. Scattering theories most often assume that the reflection coefficient is either -1 or +1, which correspond to a pressure release or rigid surface respectively. In both these cases, therefore, it is assumed that all the incident energy is returned from the interface. The theories concentrate instead upon calculating the angular distribution of this scattered energy.

The open literature may be divided into papers which consider aspects of reflection loss at a smooth interface and those which consider scattering at a rough interface with the assumption of unit modulus reflection coefficient. With the exception of KUO (1964), who considered reflection at a rough liquid / liquid interface, only recently have papers begun to consider general scattering (i.e. not merely backscatter) at elastic boundaries.

Reflection papers have tended to make many simplifying assumptions about the seabed. Typically the seabed is considered to be comprised of a sediment layer on top of a semi-infinite basement layer. Properties of these layers are usually modelled very simply: homogeneity is often assumed or a simple form for the sound speed profile is used. If more than one layer is assumed for the sediment then homogeneity within each layer is the norm.

The purely theoretical reflection problem, however, was solved almost fifty years ago. THOMSON (1950) presented a matrix propagator method for the general case of a layered solid medium. He then went on to evaluate this for some simple cases, though not applicable to the case of interest here.

Later, COOPER (1967) considered the interaction of plane waves at the interface of two viscoelastic media. The work may be used, therefore, to describe reflections from between sediment layers, though these are higher order effects than the main seabed surface reflection. COOPER (1967) also presented a thorough discusson of the complex angles resulting from the fact that attenuation was present, and used this to highlight the conditions under which interface waves would be generated.

VIDMAR and FOREMAN (1979) described a modified propagator model developed to investigate the effect of sediment rigidity on bottom reflection loss. The sediment layers considered had arbitrary sound speed profiles. The boundary values required for the propagator layer matrices were derived by numerically integrating the wave equation for that layer. The propagator method was then used in the usual way for various cases of sediment and substrate.

VIDMAR (1980a) then used the model developed in 1979 to look in more detail at the different waves generated at various frequencies and angles. Again he looked at the effect of sediment rigidity on bottom reflection loss in a typical deep sea sediment. It was found that the effect was most important for thin sediments (< 500m) and that the greatest mechanism for energy loss to S [shear] waves was from compressional wave conversion at the sediment-basement interface. The latter comment seems plausible enough. The former comment will depend upon the attenuation undergone by compressional waves in the sediment layer. For any sediment there will be a thickness above which little (arbitrary) energy is returned by waves travelling down to the basement rock and back due to attenuation. For thin layers this will not be the case and so all waves must be considered.

VIDMAR (1980b) also reviewed a three layer model of a typical deep sea environment. He examined in some detail the sensitivity of the bottom reflection loss estimates to geoacoustic parameter accuracy by varying the parameters from a typical parameter set. Again the emphasis was on thin sediment layers and shear wave exitation. It

was found that the shear and compressional wave velocities in the sediment and substrate were clearly important; the attenuation coefficients in the sediment were important only for certain frequency and thickness ranges; all of these were related to shear wave production. All other parameters were found to be not as important in the sense that their central values could be used quite adequately.

A relatively novel technique was used by SCHMIDT and JENSEN (1985) when considering wave *propagation* in a horizontally stratified viscoelastic medium. The field equations were derived, starting using the usual displacement equations, boundary conditions and elastic coefficients. The equations were then Fourier transformed and solved. This technique is mentioned since it is similar to that used (see later) by BLAKEMORE (1993) when looking at elastic scattering. Reflection and displacement of a beam at a liquid / solid boundary was also discussed, caused partly by the generation of a lateral wave if the incident beam has finite width (a leaky surface wave also contributes at just below the shear critical angle).

WESTWOOD and VIDMAR (1987) presented an eigenray based approach to calculating the time series returned from a layered seabed. The eigenrays contributing to the series received at the receiver were found, broadly speaking, by trial and error. Again the frequency domain is used for combining the effects of multiple layers. This paper showed that the time series received could be severely distorted by even relatively simple layering.

Later, WESTWOOD (1989) presented a thorough exposition of the use of complex ray methods in evaluating acoustic interaction at a fluid / fluid interface. The analysis was of the reflected field from a point sound source being reflected off a seabed. The result was compared to classical ray theory. The main difference was at low frequencies or at angles near the critical angle.

An extension to the simple seabed model consisting of homogeneous layers was made by ROBINS (1991) who considered the transmission of an acoustic plane wave through a horizontally stratified fluid layer whose density and sound speed both varied continuously with depth. The model was, therefore: homogeneous fluid / varying fluid / homogeneous fluid. Although the seabed basement should, more accurately, be modelled as a solid, the use of a middle layer whose properties varied with depth was a significant improvement in modelling a sediment layer. Wave solutions for typical sound speed profiles (constant c, linear k^2, inverse square c) in the middle layer were matched to solutions in the other layers to deduce reflection coefficients. For high and low frequency limits these were shown to be independent of the density and sound speed profiles in the middle layer (sediment).

AINSLIE (1995) presented an explicit form of the solution for the reflection coefficient from a three layered elastic medium: elastic half space / elastic layer / elastic half space. This was done by considering the interface interaction histories contributing to a ray's amplitude, for all the rays contributing to the total outgoing energy. The explicit solution was equivalent to the implicit form obtained (usually) by matrix methods. It should be noted that

any of the layers in this model may be used to model a liquid simply by setting the shear wave speed for that layer equal to zero. Hence the first elastic half space may model the sea, the lower two the sediment and seabed basement.

It is imperative in ray counting methods such as this to ensure that the individual layer reflection and transmission coefficients are accurate. If approximations are used for either of the coefficients then one must ensure that the principle of conservation of energy is not violated. AINSLIE and BURNS (1995) presented a "fix" to this problem for the reflection and transmission coefficients for a solid / solid interface. They calculated the reflection coefficient and then ensured that the transmission coefficient was defined such that the intensities generated by the two coefficients (square then divide by the layer impedance, for each) summed to one. A better solution is simply to use correct layer to layer reflection and transmission coefficients, as calculated in chapter 2.

AINSLIE (1996) presented simple expressions for plane wave reflection and transmission coefficients for a layered fluid sediment layer sandwiched between a semi-infinite fluid and a fluid basement. The layered sediment layer was modelled as a layer with continuously varying geoacoustic properties. Exact solutions were derived for the case where the sediment sound speed and density varied such that the pressure derivative in the sediment was no longer given by a constant multiplied by the pressure (as it would be for the homogeneous layer case), but given by f(z) times the pressure, where z was the depth. The method of input impedances was used. The problem which remained was to find layers with density and / or speed profiles such that the Helmholtz equation could be solved to give a pressure such that the pressure derivative had the required form. This was done for a few simple cases. The method was then extended to deal with a solid basement.

In a paper slightly detached from the general thrust of seabed reflection research BADIEY (1996) *et al.* looked at the effect on bottom reflection loss of the parameters describing porous sediments. To gain a stochastically valid solution the models were run many times with varying parameters in a Monte Carlo type manner. They concluded that the porosity of the seafloor had a "profound" effect on the amplitude and phase of the reflection coefficient. This should be borne in mind when considering sediment volume scattering, one cause of which is porosity within the sediment.

More recently CARBO (1997) looked at modelling the sediment layer as a series of homogeneous layers using a matrix propagator method. Frequency variations in the reflection coefficient were found which were dependent upon the physical property gradients in the uppermost sediment layer. One would certainly expect frequency dependence since attenuation coefficients were included in the model. Generally the effect of attenuation is to limit wave propagation, and so the uppermost sediment layer's greater significance is also what one would expect.

Most theoretical *scattering* papers assume that the reflection coefficient is of unit magnitude. Developments are aimed, instead, at predicting the directional distribution of the scattered energy. Of particular significance is the backscattered energy, since this is

relatively easy to measure experimentally and this is the reverberation against which monostatic sonar systems must be able to discriminate. The complicated nature of scattering is traditionally simplified by considering the scattering surface to satisfy either the small perturbation approximation or the tangent plane approximation (see chapter 3).

MARSH (1961) presented a theoretical development of the "exact" solution for scattering from a rough surface with Dirichlet boundary conditions. The surface wavenumber spectrum was decomposed into plane waves. The boundary conditions were then met for the incident wave interacting with each surface plane wave component, to give many plane scattered waves. These scattered waves were then summed.

Later the same year MARSH et al. (1961) described how sound scattering from the sea surface could be modelled, using the theoretical treatment described in the earlier MARSH paper, if one had a good estimate of the surface wave spectrum. The major problem for the case of seabed scattering is the same - that of finding the correct, or at least useful, surface power spectrum (see chapter 3).

A different approach was taken by KINNEY and CLAY (1988) who considered scattering to be the result of adding many reflections from facets. They proposed a working hypothesis that the reflected amplitude was proportional to the incident signal. The proportionality was modelled as a function of: the facet width; the wavelength corresponding to the peak frequency of the signal; and the distance from the collocated source / receiver to the facet. Again Dirichlet or Neuman boundary conditions were assumed throughout.

A highly theoretical comparison of perturbation theories is given by JACKSON et al. (1988). The different perturbation theories based on the Rayleigh hypothesis and the extinction theorem are compared and found to agree to fifth order terms for a sinusoidal surface. These considerations have been given no further thought here since the perturbation theory used in chapters 4 and 5 is only to first order.

Much experimental work on general scattering (not backscatter) seems to be mostly in the ultrasonic frequencies, including double reflection studies (ROSE and BILGEN (1994)), scattering from Gaussian etched glass (SCHULTZ and TOKSOZ (1996)), as well as the studies of NAGY and ALDER (1987) investigating the effect of surface perturbations (of the order of micrometres) causing attenuation of a coherent high frequency collimated beam.

Modelling of seabed scattering data has most often been limited to backscatter data (since monostatic experiments at sea are much more readily achieved, and are much cheaper!). A model with which data is often compared is "Lambert's law", which states that the scattering coefficient varies as the square of the cosine of the incident angle (e.g. MACKENZIE (1961)). The relative abundance of backscatter data has resulted in an improvement in many scattering models, and an understanding of the requirements for other seabed surface features (rather than simply the power spectrum) in order to make accurate backscatter predictions.

MACKENZIE (1961) presented the results of bottom reverberation measurements made at 530Hz and 1030Hz in deep (4000m) water. The measurements had been made over grazing angles from 90-30° and fits were made to Lambert's law.

BOEHME *et al.* presented (1985) low grazing angle backscattering results and their interpretation in terms of Lambert's law. They looked at grazing angles from 2-10° in 15.5 metres of water. Lambert's law was shown to be followed for all frequencies (30-95kHz) and grazing angles.

A departure from Lambert's law is, however, generally found. MOURAD and JACKSON (1993), for example, using low frequency sound found that the backscatter also depended upon both the water / sediment density and sound speed ratios. They also found that sediment volume scattering could be important - this is discussed later. CARUTHERS and NOVARINI (1993) also concluded that Lambert's law was inaccurate, though decided this due to coherence and forward scattering considerations. It was argued that in real data one saw some energy scattered coherently and a significant forward scattering lobe, neither of which were described by Lambert's law. This concurred with their theoretical examination of how scattering occured from ensemble realisations of facets.

The insufficiency of the surface power spectrum for estimating scattering strength and coherence was discussed by KINNEY and CLAY (1985). Their claim, which was supported by numerical studies, was that the backscattered energy was more sensitive to the actual surface shape than was the forward scattered energy. This lead to the statement that the surface power spectrum alone (which fixes the root mean square (rms) height and the spatial correlation function) was not enough to describe the surface completely as regards backscatter. This seems to be a fairly intuitive result. For forward scatter one is interested in the surface components which have wavevectors equal to or near to zero (see chapter 4). For these, the phases are not important as they only introduce factors less than one, leaving the surface wavevector still near zero, as required. Hence any representation of a surface with some spectral components near zero will be sufficient for forward scatter. For backward scatter one is interested in the surface component wavevectors with magnitude greater than or equal to the incident horizontal wavevector. For surface component wavevectors equal to the incident horizontal wavevector the phase must be exactly π for backscatter. Higher frequency wavevectors will scatter locally if at the correct phase relative to the incident wave, though not generally. Hence the options for backscatter are much more limited and depend on the particular shape of the surface over the area of interest. Of course the relative amplitudes of these spectral components will also come into the argument. The line of reasoning I have given here is for a purely flat surface power spectrum.

THORSOS and JACKSON (1989) studied the accuracy of perturbation theory applied to randomly rough, corrugated surfaces with Gaussian correlation functions. They concluded that in addition to the height restriction there was sometimes a restriction on the correlation length of the surface: the correlation length was required to be less than or equal to the reciprocal of the wavenumber. This restriction did not apply to scattering in the

specular direction but became more severe when scattering was further from the specular direction.

This latter conclusion was similar to that of KINNEY and CLAY (1985), that the surface needed to be more tightly defined for backscatter to be possible. THORSOS and JACKSON explained this in terms of the form of the power spectrum. First order theory predicted that the diffuse field intensity was proportional to the power spectrum evaluated at a wavevector equal to the difference between the incident and scattered x direction wavevectors. The dominant component in second order theory was the corresponding sum of incident and scattered x wavevectors. When the two vectors were in the same quadrant (i.e. backscattering quadrant) then the sum was less than the difference and hence the power spectrum component would be greater for the second order component than for the first (since the power spectrum was Gaussian). The effect was maximised in the backscatter direction where the sum of the vectors was zero and where the power spectrum was at its greatest. It was therefore possible, they argued, for the second order contribution to the scattered field to be comparable with, or greater than, the first order contribution [which leads me to suspect something is formally wrong with this case] even for small heights, with this effect more likely to occur close to the backscattering direction.

The accuracy of Kirchhoff theory was also studied by THORSOS (1988) for 1 dimensional rough surfaces. Again it was assumed that the surface had a Gaussian surface power spectrum. Backscatter solutions using the Kirchhoff approximation were compared to "exact" solutions to integral equations. It was found that the surface correlation length was the most important parameter required for accurate backscatter predictions.

More recent work has brought the perturbation theory (small amplitude roughness) and Kirchhoff theory (smooth, potentially large amplitude roughness) regimes together in multiscale roughness models. Critical in these models is the wavenumber cut-off used to define the limits of the two scales. This was discussed by CARUTHERS and NOVARINI (1994) who considered a multiscale roughness model for a rigid surface where the small scale roughness was described by a facet model. The size of the facets was set by the requirement that the energy bouncing off the facet was totally incoherent.

Most multiscale roughness models use a power law spectrum to describe at least one of the two scales' surface power spectrum. Implicit in the use of a power law is the concept of self-similarity, that the surface looks the same over a range of scales, i.e. is fractal. GOFF (1995) used this approach to investigate the relationships between the scattered energy and the two surface regimes. He concluded that the global scale surface looked simply like a diffuse local scale surface and that the scattering was highly sensitive to the local surface at low grazing angles.

The scattering considered for the model presented in this thesis is only assumed to be due to the roughness of the sea / seabed interface, and not due to any form of sediment volume scattering. Volume scattering (see CHERNOV (1967)) is the scattering produced by density and sound speed anomalies within an otherwise homogeneous volume.

In some cases, this can be the dominant mechanism contributing to backscattered sound and so is discussed briefly here. The fundamental source of density and sound speed anomalies is different for different media. In the sea, volume scattering may be due to resonance scattering of sound due to fish bladders (see FEUILLADE and NERO (1998)) or shoals of fish, or due to resonance scattering off microbubbles at a rough sea surface (see PACE et al (1997)), whilst within a seabed it is most often due to porosity fluctuations giving gas-filled or fluid-filled bubbles, which have large impedance mismatches with the surrounding porous sediment. Studies of seabed volume scattering are motivated by trying to explain the larger than expected scattered returns from relatively smooth seabeds, especially at low grazing angles. As with surface scattering, the problems with validating theories are finding ground truth geoacoustical data and knowing the correct statistics of the volume inhomogeneities (see TRACEY and SCHMIDT (1999)). There is also considerable interest in locating gassy sediments within the oil and gas exploration industry (see GARDNER (2000)).

The earliest significant work applicable to volume scattering studies was done over forty years ago by BIOT (1956) who presented a theoretical method of evaluating the propagation and attenuation of waves in a porous solid. He considered connected isotropic porosity only, by considering the displacements and forces on the edges of a cube which was partly solid and partly fluid on its edges. It was shown that the parameters which affected the propagation were the kinematic viscosity of the fluid and porosity fraction in the solid.

NOLLE (1963) presented a thorough experimental examination of the propagation, reflection and scattering of sound by water filled sands at very high frequencies (400kHz and above). It was found that the reflected signal behaved as expected from the continuity conditions at the surface. The magnitude and autocorrelation properties of the fluctuations in the scattered signal were found to correspond approximately to a model based on a Gaussian distribution of local scattering intensity. A surface model developed in this way, however, failed to account for the marked decrease in scattering below the critical grazing angle. This was because the sediment volume scattering component was much less below the critical grazing angle since acoustic penetration was much less. The argument for including both sediment volume scattering and surface scattering was discussed further. It was reasoned that the fluid and sand in the sediment were both different to the composite created by the two of them, and that they would therefore both act as volume scatterers. It was noted that the surface where the sand met the fluid layer (sea) was a large impedance mismatch and so should also be considered.

Both PACE (1992,1993) and HINES (1990) produced models to describe sediment volume scattering. Both used the particle volume scattering development of CHERNOV (1967), though HINES' development explicitly considered both the refracted and evanescent waves. When the mean scattered intensities were calculated, however, approximations were made: the contribution due to interference of the two types of waves were deemed

negligible. PACE (1993) discussed the roles of the two types of wave and then modelled scattering due to the refracted wave. The resulting model was much simpler (and easier to use) than HINES'. Both models were for backscatter though both then extended their work to include forward scatter in the same vertical plane (PACE (1995), HINES (1996)).

Comparisons of surface and sediment volume scattering have been made over the last ten years or so. JACKSON and BRIGGS (1992) took measurements (15-45kHz) and concluded that at a sandy site rough surface scattering could account for observed backscatter whereas at a silty site sediment volume scattering was dominant.

Similarly, LYONS and ANDERSON (1994) found that in high backscatter areas (with silt-clay layers) continuum sediment volume scattering dominated whereas in low backscatter areas scattering from the interface 10cm below the water sediment boundary was dominant.

YAMAMOTO (1996) recently modelled the seabed such that the scattering fit the data of JACKSON and BRIGGS (1992) and MOURAD and JACKSON (1993). It was found that the sediment volume scattering mechanism was dominant in soft seabeds, with the frequency dependence governed by the power law of the porosity fluctuations.

The volume scattering work may also be used as a potential simplification to the study of a many layered sediment. TANG (1996) investigated the scattering effect of a stack of rough interfaces. The interfaces were assumed to have only small root mean square height deviations and be separated on scales small compared to the wavelength of the incident sound. It was also further assumed that the difference in geoacoustic properties between each layer and the next were so small as to produce no reflected wave. It was found that the stack simply behaved as, and could be treated as, a weakly scattering volume with randomly fluctuating sound speed and density. Given the simplifications made in the model this seems to be an entirely expected conclusion.

There have been relatively few studies which have attempted to model scattering from a rough surface where the reflection coefficient is of magnitude less than one. Most of the studies which have been done have been for small amplitude roughness using perturbation theory. It is significant then that one of the earliest studies, by PARKINS (1967), was aimed at improving the Kirchhoff theory scattering model. He noted that the reflection coefficient would be a function of the surface gradient and that if these gradients were small then the reflection coefficient could be expanded about its value for a mean slope of zero gradient (i.e. for the smooth surface reflection coefficient). The coefficients of the expansion therefore depended on the incident angle. PARKINS substituted this expansion into the usual Kirchhoff-Helmholtz formulation (see BREKHOVSKIKH and LYSANOV (1990)). Terms involving second order height derivatives were neglected and the edge effects ignored. For very rough surfaces an expression was obtained for the far field scattered intensity.

KUPERMAN (1975) also looked at scattering, in the Kirchhoff approximation, from a fluid / fluid interface. The expressions which he derived for the reflection coefficient were,

however, only for the limit of one of the fluid densities approaching zero, and for the pressure release boundary condition.

The elastic scattering problem was partially solved by TOLSTOY (1985) using correct elastic boundary conditions in a perturbation theory approach for a slightly rough liquid / solid interface. The solutions were only for a limited set of ideal surfaces.

A clear exposition of a scattering solution was produced by BLAKEMORE (1993). Firstly the standard analysis for reflection of sound at a smooth fluid-solid interface was reviewed. Zeroth order terms for the (complex in general) amplitudes of the reflected wave and both transmitted waves were derived. The analysis was then repeated for a slightly rough interface. The boundary conditions were now required to be satisfied on the rough surface boundary and so they were derived in terms of a small roughness function which described the statistics of the interface. Hence the expressions for the effective boundary conditions on the mean plane of the interface for the surface stresses and the accelerations were found, utilising the boundary conditions satisfied by the unperturbed fields.

The resulting boundary conditions were in terms of derivatives of the roughness function. To aid solution of the boundary condition equations they were Fourier transformed (c.f. SCHMIDT and JENSEN (1985)) to give the Fourier transforms of the first order solutions to the field quantities (the pressure in the fluid, and the shear and compressional potentials in the solid) in terms of Fourier transformed field quantities for the zeroth order (smooth surface) solutions. The resulting set of simultaneous linear equations were then solved and then inverse Fourier transformed to give the "surface scattering coefficient" for the scattered acoustic pressure in the liquid.

KUPERMAN and SCHMIDT (e.g. 1986, 1989) have produced many papers between them concerning elastic scattering from rough surfaces. In 1989 they introduced a boundary condition operator formalism which allowed the usual Fourier transformed boundary condition approach to be taken a step further. It was shown that using a matrix formalism for the boundary conditions the method could be extended to solve the scattering problem for a seabed with an arbitrary number of layers. The layers had, in general, different roughnesses, though all roughnesses were assumed to be small compared to the layer separations.

Another mechanism which may improve scattering theory is that due to the scattering of interface waves. This, and the relative effects of surface and volume scattering have been assessed by BRADLEY and STEPHEN (1996) in both 2 and 3 dimensions, though details of the scattering models used were not given.

Although the model developed in this thesis is largely theoretical, in order for meaningful results to be achieved it must be used with realistic input data. For modelling the beam and pulse parameters this is relatively straightforward – these concepts are described in many texts (see WAITE (1998)): for the geoacoustic parameters things are not so simple. Firstly, a model must be chosen which accurately describes the structure of the sediment layers and basement which make up the seabed. Secondly, the roughness model for the interface must be determined. These considerations are described more completely in

chapter 6. Finally, the sound speeds, densities and attenuations of each of the sediment and basement layers must be estimated. The classic paper detailing relationships between geological properties and acoustical properties was written by HAMILTON (1980). Since then various improvements to some of the relationships governing shear wave speeds, and both shear and compressional wave attenuations have been made (see BOWLES (1997)). Practical methods of deriving geoacoustic and statistical parameters of the seabed involve inversion techniques (see TURGUT (1997)). These work by running a model with different input parameter values until the one which best matches the measured data is found. Due to the number of combinations of parameter values, rather than conducting an exhaustive search (which would take much too long) a more directed approach is used. This can involve techniques such as genetic algorithms or simulated annealing, to hone in on good sets of parameters until the optimum set is found.

It should be noted that a more empirical approach may be taken towards describing the two processes of reflection and scattering from the seabed. The roughness characteristics of the seabed are described by HEEZEN and HOLISTER (1971) for both deep sea abyssal planes and for continental shelf beds. Seabed roughness features such as sediment ripples and waves with scales from centimetres to kilometres are assessed quantitatively by ALLEN (1968) and others. These features are reported to be dependent on both sediment grain size (LEEDER (1985)) and the current speed (STRIDE (1982)) over the seabed. The link between these parameters and scattering strength is not complete, though it is speculated that these roughness characteristics could be incorporated into a simple surface scattering theory valid for small roughness. Secondly, the geotechnical properties of sediments can be related to the geoacoustic parameters required to predict seabed reflection loss: sediment density, shear and compressional wave speeds, and attenuation coefficients. This may be done using the GEOSEIS database (described by MARKS (1994, 1995)). The reflection coefficient anticipated from these parameters is that for a smooth interface. One may hypothesise, therefore, that given the prevalent local oceanographic conditions and the geotechnical properties of the seabed an estimate of both the bottom reflection loss and roughness characteristics of the surface could be made.

2 Reflection theory

In this chapter the problem of modelling the reflection of sound from the seabed will be reviewed. The general considerations made when modelling the seabed will be discussed before looking at the physical theories used to describe wave interactions at smooth interfaces. The theories considered will be:

1 for a single liquid / liquid interface;

2 for a single liquid / solid interface;

3 the method of input impedance, for multi-layered liquids;

4 the matrix propagator method, for the general multi-layered case.

Using the matrix propagator method a range of interfaces will be examined in order to indicate the effects of the various geoacoustic parameters on the reflection coefficient. This model will also be used to model an inhomogeneous sediment layer on top of a semi-infinite solid seabed, to illustrate the utility of the method as a benchmark.

2.1 Modelling the seabed

The problem of modelling sound reflection from the seabed can be split into three components: that of modelling the sound source; that of modelling the propagation of the sound within the water column, before and after the interaction with the seabed; and that of modelling the seabed interaction itself. It is the latter problem which concerns us here. In order to attempt to solve this problem one must first try to model the seabed itself in such a way that it is both an accurate representation of the real seabed and is able to be analysed acoustically. The conflicting demands of authenticity and simplicity result in most models being a compromise weighted by the requirements for accuracy and applicability. Generally speaking, a more simplified model will be less accurate but more widely applicable than one which uses a highly detailed representation of a particular seabed.

The first simplification which is always made is that the seabed surface is smooth. Without this assumption we would have a scattering problem, as discussed in chapter 3. It is also generally assumed that the seabed is horizontal. These two assumptions are common to all seabed reflection models. Below the seabed surface is where models differ. For many cases the simplest realistic models envisage a three layer regime: the water column; a seabed sediment layer; and a bedrock. The interfaces between all the layers are assumed to be smooth and horizontal.

The uppermost and lowermost layers are always assumed to be homogeneous and semi-infinite, the upper one being a fluid and the lower one a solid. The sediment layer in between is most simply assumed to be homogeneous but is also often modelled as having a simple sound speed or density profile (for example AINSLIE (1996), AINSLIE et al (1998)). For a homogeneous layer the wave equation is solved easily, predicting simple harmonic plane waves. For non-homogeneous layers this is not the case and so often the non-homogeneous case is approximated by a series of homogeneous layers whose layer to layer properties vary appropriately (see section 2.5.6)

Homogeneous sediment layers are most often assumed to support only compressional waves (sound waves): in other words they are assumed to be fluid. For cases where all the sediment layers are fluid the input impedance method, described later, may be used to model the reflections at the layer interfaces. In the cases where sediment layers also support shear waves (i.e. the sediment is solid) these waves are usually assumed to be highly attenuated, this being a mechanism used to account for energy loss within the sediment. More complicated models, such as the matrix propagator model discussed later (section 2.5) can accommodate solid sediment layers with or without attenuation of shear waves.

For now, the implicit assumption is made that the seabed can be thought of as either a solid or a liquid, and that the properties of each are well understood and can be used to accurately represent a real seabed. This is not the case for many sediments, whose inertial properties can be modelled as solid-like, but whose elastic properties are more liquid-like (see VIDMAR (1980)). When the attenuation or "lossy" properties of sediments are investigated the situation is not at all clear. Various loss mechanisms are considered in the literature, due to friction between particles of unconsolidated solids, or due to pore fluid friction in porous solids, for example. Many of these mechanisms fail to explain the fact that attenuation scales roughly with the first power of the sound frequency, for many decades of frequency. BUCKINGHAM (1997) proposes a mechanism which does explain the frequency dependence, which shows that the attenuation can be thought of as due to a temporal convolution between the material response function and the particle velocity.

In order to limit the model developed here (see chapter 7) to depending on a reasonably small number of geoacoustic parameters, the attenuation is modelled as a constant number of decibels per wavelength travelled by the wave. [This is related by a constant factor to a constant attenuation in decibels per metre per kilohertz, which is also often used.] Also, for the model developed here it is assumed that solid behaviour is elastic to the extent defined solely by the shear modulus μ (also known as the "elastic" modulus). It is further assumed that liquids are defined by having a shear modulus equal to zero and that shear waves are not supported in such cases, even though BUCKINGHAM (1998) shows that this is not always true. For porous fluid-filled sediments which exhibit a dissipative characteristic with memory (or hysteresis), he shows that a shear wave solution may be derived even though the shear (or elastic) modulus is zero.

For seabeds comprising homogeneous non-attenuating sediment layers the parameters which must be known for all reflection models are the sound speeds, shear wave speeds (if applicable), densities and thicknesses of all the layers. As stated earlier, homogeneous layers support plane waves. These are of the form

$$p_0 = A_0 \exp[ik(x\sin\theta + z\cos\theta)] \qquad 2\text{-}1$$

where p_0 is the pressure wave at a point (x,z), amplitude A_0, travelling at an incident angle θ to the vertical, with wavenumber k. Note that a constant factor of $\exp(i\omega t)$ for an assumed

harmonic time dependence is omitted here, and throughout this chapter[1]. If the sediment layers do attenuate a wave type then this is easily incorporated into models by making the wavenumber k complex. The imaginary part of k introduces an exponential decay term which models the decrease in amplitude of the wave as it travels through the medium.

For an attenuation coefficient, α_c, given in dB per wavelength travelled we have

$$k_{im} = \frac{\alpha_c}{8.686}\frac{f}{c} \qquad 2\text{-}2$$

or, equivalently, using ($k=\omega/c$ and) the approximation that the real part of k is much bigger than the imaginary part of k, and using the value of the imaginary part of k given above, we find that the imaginary part of the wave speed is given by

$$c_{im} \approx \frac{-c_{re}\alpha_c}{54.575} \qquad 2\text{-}3$$

where c_{im} and c_{re} are the imaginary and real parts of the (now complex) sound speed.

2.2 Reflection at a liquid / liquid interface

It is assumed that the incident sound wave is an infinite plane harmonic wave of unit amplitude at an angle θ to the vertical. This incident wave will give rise to both a transmitted plane wave, of amplitude W, and a reflected plane wave, of amplitude V. For real sound pulses two Fourier decompositions must be performed before applying any plane harmonic wave reflection coefficients. A spatial decomposition of the beam into plane waves must be performed, as must a temporal decomposition of the pulse into harmonic wave components. Wave reflection theory may then be applied to each harmonic plane wave and the resulting reflected and transmitted waves summed repectively. This is described in more detail in chapter 6 where a pulsed beam is constructed for the scattering model.

For a liquid / liquid interface the boundary conditions which must be satisfied during the reflection of the pressure wave are that the pressures and the normal particle accelerations (or, equivalently, velocities or displacements, since they are all related by constant factors of $i\omega$ for harmonic waves) must be equal on either side of the interface, hence:

$$p = p_l \qquad 2\text{-}4$$

and

$$\frac{1}{\rho}\frac{\partial p}{\partial z} = \frac{1}{\rho_l}\frac{\partial p_l}{\partial z} \qquad 2\text{-}5$$

[1] A Gaussian *pulse* is used later, in chapter 6. This is made up from a sum of weighted harmonic waves of *different* frequencies. In this case the $\exp(i\omega_n t)$, where ω_n is different for each contributing harmonic wave, is essential, and is included in the calculation.

where ρ and ρ_1 are the densities in the upper (where the incident wave is from) and lower liquids respectively.

From the first of these conditions we immediately obtain the refraction law, *Snell's law*, which requires that the components of the wavevectors parallel to the interface on either side of the interface, for incident, reflected and transmitted waves, be equal:

$$k \sin\theta = k_1 \sin\theta_1 \qquad \text{2-6.}$$

From the second equation and Snell's law, by considering the pressures on either side of the interface to be due to incident, reflected and transmitted waves the relative amplitudes of each are easily deduced. It is found that

$$V = \frac{Z_1 - Z_0}{Z_1 + Z_0} \qquad \text{and} \qquad W = \frac{2Z_1}{Z_1 + Z_0} \qquad \text{2-7}$$

where Z_i is the *characteristic impedance* of the i^{th} layer given by

$$Z_i = \frac{\rho_i c_i}{\cos\theta_i} \qquad \text{2-8}$$

and where θ_1 is deduced for the reflecting (lower) layer from Snell's law.

Although relatively simple, the expressions shown here do highlight the main features of reflection at most seabeds. Firstly, the magnitude of the reflection coefficient can be anywhere between zero, when the layer impedances are equal, and one, when Z_1 is very large or when Z_1 is imaginary. The latter occurs for incident angles equal to or greater than the *critical angle*. In this case $\sin\theta_1$, deduced from Snell's law, becomes greater than one and so $\cos\theta_1$ becomes imaginary. This type of reflection is known as *total internal reflection*. Note that if attenuation is present in the reflecting medium then the sound speed, and $\sin\theta_1$ and $\cos\theta_1$, will all be complex and so total internal reflection cannot occur, though reflection coefficients near one, and evanescent waves within the lower medium, will be observed if the attenuation is low. Evanescent waves produced in this way may be important if there is only a thin sediment, since some energy will "tunnel" through to the basement and be reflected or scattered.

Strictly, critical angle effects are only expected for plane waves. For a smooth flat surface, for an incident *beam*, as used in chapter 6, one can expect these effects to be smoothed out since the beam is made from a number of plane waves at different angles. For a beam made from an infinite number of plane waves then there will never be a true critical angle, though, depending on the width of the beam (i.e. the amount contributed by a few plane waves at angles near to the main beam angle) there may be effects seen at the "beam" critical angle.

Figure 1 shows the reflection power coefficient (the square of the modulus of the reflection coefficient) for 4 different combinations of basement sound speeds, densities, and in one case shear wave speed. It is seen that higher densities and sound speeds both give

higher reflection coefficients. The sound speed also controls the critical angle, above which the reflection coefficient is one, i.e. total internal reflection occurs. The green, red and blue plots are all for liquid / liquid interfaces. By introducing a shear wave speed the reflection coefficient from a liquid / solid interface is shown in the magenta plot. It is seen that for a range of incident angles, above the critical angle (critical with respect to the sound wave speed), this solid reflects less energy than the liquid. For all the cases shown in Figure 1 the liquid above the interface has a density of 1000kg/m^3 and a sound speed of 1500m/s and the frequency of the incident sound was 800Hz.

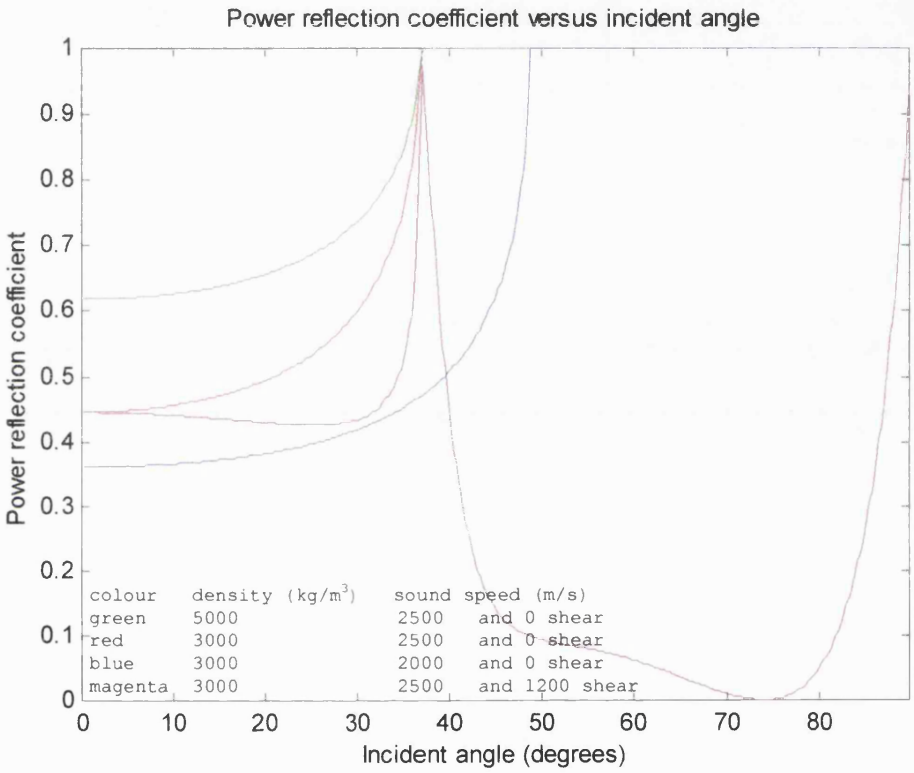

Figure 1: Power reflection coefficients versus incident angle, for three liquid / liquid interfaces (green, red, blue) and one liquid / solid interface (magenta). For each case the liquid above the interface has a density of 1000kg/m^3 and a sound speed of 1500m/s and the frequency of the incident sound was 800Hz. It is seen that higher densities and sound speeds in the lower medium both give higher reflection coefficients. The sound speed also controls the critical angle, above which the reflection coefficient is one, i.e. total internal reflection occurs. It is also seen that for the liquid / solid case, for a range of incident angles, this solid reflects much less energy than the liquid.

2.3 Reflection at a liquid / solid interface

The analysis for reflection at a liquid / solid interface is similar to that from a liquid / liquid interface except that account must be taken of the shear waves generated at the

boundary which then propagate within the solid. Also, it is appropriate now to formulate the development in terms of velocity potentials rather than pressures (see BREKHOVSKIKH and LYSANOV (1990)). This will be seen in the matrix propagator method development later in section 2.5. The three boundary conditions are that the normal components of the particle velocity and the stress tensor are continuous across the interface; and that the tangential component of the stress tensor is continuous at the interface. The first two of these boundary conditions are entirely equivalent to the liquid / liquid boundary conditions. For the case of a liquid / solid or solid / liquid interface the third boundary condition amounts to the tangential component of the stress tensor being zero at the interface, since liquids cannot support shear stresses. The stress tensor will be discussed in more detail in 2.5 when looking at the matrix propagator method.

From equality of the normal components of the stress tensor we obtain Snell's law again, now including a term for the shear wave:

$$k \sin\theta = k_1 \sin\theta_1 = \kappa_1 \sin\gamma_1 \qquad 2\text{-}9$$

where κ_1 is the shear wavenumber ($=\omega/b_1$ where b_1 is the shear wave speed) and γ_1 is the shear wave propagation angle, relative to the inward normal direction to the interface.
Using this and the other boundary conditions and considering two transmitted waves now (compressional *and* shear waves), the relative amplitude of the reflected wave is deduced:

$$V = \frac{Z_{input} - Z_0}{Z_{input} + Z_0} \qquad 2\text{-}10$$

where Z_{input} is the *input impedance* of the solid layer given by:

$$Z_{input} = Z_l \cos^2 2\gamma_1 + Z_t \sin^2 2\gamma_1 \qquad 2\text{-}11$$

where Z_l and Z_t are the compressional and shear wave impedances given by 2-8.

Here we find two critical angles: when $\sin\gamma_1$ equals one and when $\sin\theta_1$ equals one. Since the shear wave speed in the lower layer is always less than the compressional wave speed in this layer, total internal reflection only occurs when $\sin\theta$ is greater than c/b_1, i.e. at angles greater than the larger of the two critical angles. Between the two critical angles the reflection coefficient dips below one.

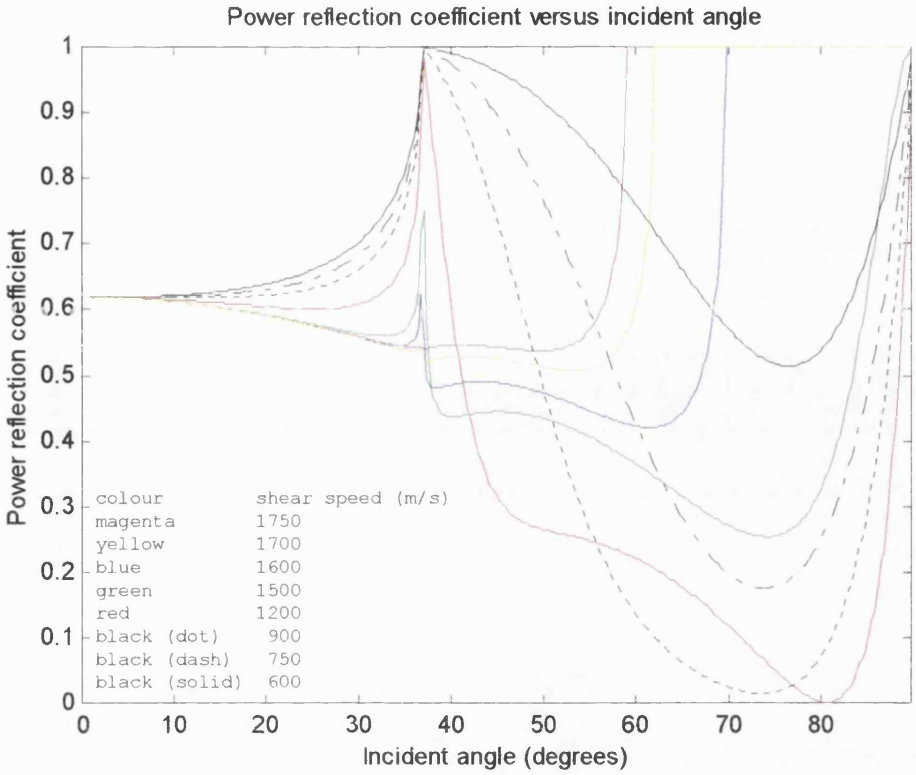

Figure 2: Power reflection coefficients versus incident angle, for eight different liquid / solid interfaces. For each case the liquid has a density of 1000kg/m^3 and the sound wave speed is 1500m/s. The solids all have densities of 5000kg/m^3 and sound speeds of 2500m/s. The frequency of the incident sound is 800Hz. It can be seen that for each of the solids there is a critical angle due to the sound wave speed, at 36.9° (= arcsin(1500/2500)) at which the reflection coefficient goes to one (the resolution of the figure is to 0.25° and so some of the peaks to R=1 are not seen exactly). For the solids with shear wave speeds above 1500m/s there is then a second critical angle corresponding to arcsin (1500 / shear wave speed). Between these two critical angles the reflected power coefficient is less than one, and so less than what it would be for a liquid which would be in a total internal reflection regime for these angles. The solids with shear wave speeds less than or equal to the sound speed in the liquid do not have critical angles. Their reflected power coefficients approach one only as the incident angle approaches 90°. For the solids with shear wave speeds above 1200m/s the effect of decreasing the shear wave speed is to decrease the reflected power coefficient for angles greater than the critical incident angle. For the solids with shear wave speeds below 1200m/s it can be seen that the effect of decreasing the shear wave speed is to increase the reflected power coefficient for these angles.

As the shear speed goes to zero the terms on the right hand side of 2-11 reduce to Z_1 and then 2-10 is the same as 2-7 for the liquid / liquid case. Many sediments are modelled as being solid but with a low shear speed and often with a high shear wave attenuation

coefficient. This enables reflection coefficients to be calculated that accomodate the fact that the sediment is not truly rigid and only weakly supports shear waves.

Figure 2 shows the power reflection coefficient for 8 different liquid / solid interfaces. It can be seen that the effect of the shear wave speed is a complex one. Typically, very hard solids have high shear speeds, of the order 2500m/s or more, whereas liquids are the opposite limit not supporting shear waves, nominally having shear wave speeds of zero. For the calculations shown in Figure 2 the liquid has a density of 1000kg/m^3 and the sound wave speed is 1500m/s. The solids all have densities of 5000kg/m^3 and sound speeds of 2500m/s. It can be seen that for each of the solids there is a critical angle due to the sound wave speed, at 36.9° (= arcsin(1500/2500)) at which the reflection coefficient goes to one (the resolution of Figure 2 is to 0.25° and so some of the peaks to R=1 are not seen exactly). For the solids with shear wave speeds above 1500m/s there is then a second critical angle corresponding to arcsin (1500 / shear wave speed). Between these two critical angles the reflected power coefficient is less than one, and so less than what it would be for a liquid which would be in a total internal reflection regime for these angles. The solids with shear wave speeds less than or equal to the sound speed in the liquid do not have critical angles. Their reflected power coefficients approach one only as the incident angle approaches 90°. For the solids with shear wave speeds above 1200m/s the effect of decreasing the shear wave speed is to decrease the reflected power coefficient for angles greater than the critical incident angle. For the solids with shear wave speeds below 1200m/s it can be seen that the effect of decreasing the shear wave speed is to increase the reflected power coefficient for these angles.

The conclusions to be drawn from this are:

1 the presence of a shear wave will always reduce the reflected energy at the angles between the critical angle for the sound wave and the critical angle for the shear wave;

2 if the shear wave speed is less than the liquid sound speed then there will be no shear wave critical angle;

3 for a range of shear wave speeds down to a critical speed the reflected power will decrease with decreasing shear wave speed. This critical speed is different for each incident angle. Thereafter, a decreasing shear wave speed will result in increasing reflected power – the limit for decreasing shear wave speed is when the shear wave speed is zero and the liquid limit is reached.

2.4 Input impedance method

The cases examined in the previous two sections are for simple interfaces between two semi-infinite media. This is appropriate for a seabed which consists of one very thick sediment, or just a basement rock with no overlying sediment. For a seabed consisting of a layered sediment on top of a basement rock, a method is needed which combines the effects of all the reflections at all the layer interfaces.

The input impedance method is used to calculate the input impedance of a whole system of *liquid layers*[2] and then this system input impedance used in a reflection coefficient amplitude equation such as 2-10. In order to relate the impedance at the top of one layer to that at the top of the layer above the continuous impedance function is defined as

$$Z_{input} = \frac{p}{v_z} \qquad 2\text{-}12$$

where v_z is the vertical component of the particle velocity, given by:

$$v_z = \frac{1}{i\omega\rho}\frac{\partial p}{\partial z} \qquad 2\text{-}13.$$

Note that within a layer this definition is exactly equal, within a phase factor, to the impedance given by 2-8. By considering each layer to have waves traversing it in both up and downward directions the function $Z_{input}(z)$ is derived[3]. The values it must have at the interfaces ($Z_{input}(n\text{-}1)$ and $Z_{input}(n)$) are used to find the relative amplitudes of the traversing waves and hence the layer to layer relation:

$$Z_{input_n} = \frac{Z_{input_{n-1}} - iZ_n \tan\alpha_n d_n}{Z_n - iZ_{input_{n-1}} \tan\alpha_n d_n} Z_n \qquad 2\text{-}14$$

where the layers are numbered from bottom to top, the topmost layer being that from which the sound approaches.

This method has been extended by AINSLIE (1996) to cover the case when the layers are non-homogeneous. In this case the restrictions are only such that dp/dz is any function f(z), multiplied by p, rather than simply $ik_z p$ as it is for the homogeneous case when harmonic plane waves propagate. The solutions are somewhat more involved but are evaluated by AINSLIE (1996) for a simple 3 layer case.

2.5 Matrix propagator method

2.5.1 Introduction

The classical method for solving the reflection problem for the case of many liquid or solid sediment layers is the matrix propagator method. The main features and assumptions of this method are discussed here, though the details and equations are given in Appendix 2A and Appendix 2B. The equation numbering continues in the appendices, and those

[2] The fact that only liquid / liquid interfaces are considered results in only two boundary condition equations requiring solution at each interface. Two compressional waves exist in each layer (one going up, the other going down) and the interface equations are easily solved to give equation 2-14. For the case of solid / solid interfaces two more boundary conditions are imposed and two more waves are considered (the shear waves, upward and downward). The system of four equations is solved to give a matrix equation (rather than a relatively simple equation such as 2-14). This method is the matrix propagator method discussed in 2.5.

[3] Each layer is considered to contain upward and downward travelling waves since the theory considers a steady state for plane harmonic waves. Such waves are infinite in temporal and spatial extent, so at any point in a layer there will be waves travelling in both directions having had any number of reflections at the bounding interfaces. It should also be noted that the reflection coefficient will have zero time lag or horizontal displacement, since the reflection will be occurring at each point along the interface and at all times.

equations also presented in this section have their Appendix numbers.

In summary, the matrix propagator method expresses the relationship between the *velocity potentials* and the *displacement-stress vector* as a matrix equation equivalent to the boundary conditions used when solving the case of reflection at a single solid-solid interface. The displacement-stress vector is used since it is continuous across all interfaces, and hence throughout the system as a whole. Using the fact that the velocity potential amplitudes are constant within a layer it is relatively easy to find the matrix equations linking displacement-stress vectors on neighbouring boundaries. These equations reduce directly into one equation, the matrix in this equation being the product of the layer to layer matrices. Solution of this equation yields the reflection coefficient.

It was pointed out earlier that an inhomogeneous sediment layer can usefully be modelled as many thin (compared to a wavelength) layers, each layer being homogeneous. The propagator method is therefore a *complete solution* to the general seabed reflection problem, though it is mathematically very detailed and the main features of a reflection coefficient (versus grazing angle) solution are not always easy to pick out from such a formal analysis. Given the fact that it provides a complete solution the method has been coded up to provide a useful benchmark bottom reflection loss model, and compared to the solutions presented by AINSLIE et al in section 2.5.6.

The matrix propagator method may therefore be used as a benchmark solution to the general plane wave reflection problem. In some cases, for certain sound speed profiles, the reflection solution may be derived analytically, rather than using a many layered approach, as presented by ROBINS (1998) and by AINSLIE et al (1998). The latter present a study of reflection from sediments with geoacoustic properties defined by the BLUG model (this is the "Bottom Loss Up-Grade" model, see references given by AINSLIE et al (1998)), and also a sediment where k^2 is linear with depth. The advantage of using an analytical solution rather than a many layered approach is not just in the savings to be made in computer processor power and memory. With any layered system there will be resonances set up at various specific angles, leading to local maxima in the reflection coefficient which are not representative of the true reflection coefficient of the sediment. Indeed, ROBINS (1998) comments that many layers are needed to arrive at an accurate result for a seabed with realistic sediment and basement properties. An application of the matrix propagator method to a seabed comprising an inhomogeneous sediment overlying a solid basement is presented in section (2.5.6). This shows that although significant, the problem concerning the number of layers required to model inhomogeneous sediments is not insuperable.

A further advantage in using analytical solutions is that behavioural features of the surface can be deduced from them. The simplest case of this is through the analysis of Snell's law (BREKHOVSKIKH and LYSANOV) to deduce the critical angles for an interface. Similarly the expressions for the reflection coefficient for a simple liquid / liquid or a simple liquid / solid interface may be analysed to help understand surface waves, which occur when the effective reflection coefficient is infinite (found by setting the denominator of expressions

such as 2-10 to zero). At certain frequencies, for liquid / solid interfaces, there may be more than one surface wave (ALENITSYN), and these surface waves may interfere with one another. Also, TOLLEFSON shows that energy may be lost through coupling to guided elastic waves in thin sediments.

2.5.2 Wave propagation within a solid

The following notes describe and explain the theoretical route used to derive the matrix propagator method used to calculate the bottom reflection loss from a layered seabed. The layers are each assumed to be homogeneous and horizontal with smooth interfaces. Shear and compressional waves are supported in each layer. The derivation follows that of BREKHOVSKIKH and GODIN (1990) though it should be noted that their final expression for the reflection coefficient from a liquid / solid interface (the solid being layered) is incorrect. I have derived a correct expression here[4].

Firstly it is instructive to look at the basic theory for wave propagation in solids since this will reveal the equations required when considering the boundary conditions which must be satisfied when a wave is reflected from an interface[5]. When a wave propagates through a solid it does so by inducing elastic deformations in the solid. The relation between stresses and deformations in the linear theory of elasticity and in the most simple case of locally isotropic solids, is given by *Hooke's law*:

$$\sigma_{ij} = \lambda \frac{\partial u_k}{\partial x_k} \delta_{ij} + \mu \left(\frac{\partial u_i}{\partial x_j} + \frac{\partial u_j}{\partial x_i} \right) \qquad 2\text{-}14$$

where λ and μ are the *Lamé coefficients*, σ_{ij} is the force per unit area in the direction j on the face perpendicular to the direction i, and u is the particle displacement in the solid, as shown in Figure 3 below.

[4] Godin has been contacted (e-mail) and was aware of the problem. It will be corrected in future revisions.
[5] These boundary condition equations are relevant not only here but also for the liquid / solid scattering solution derived in chapter 5.

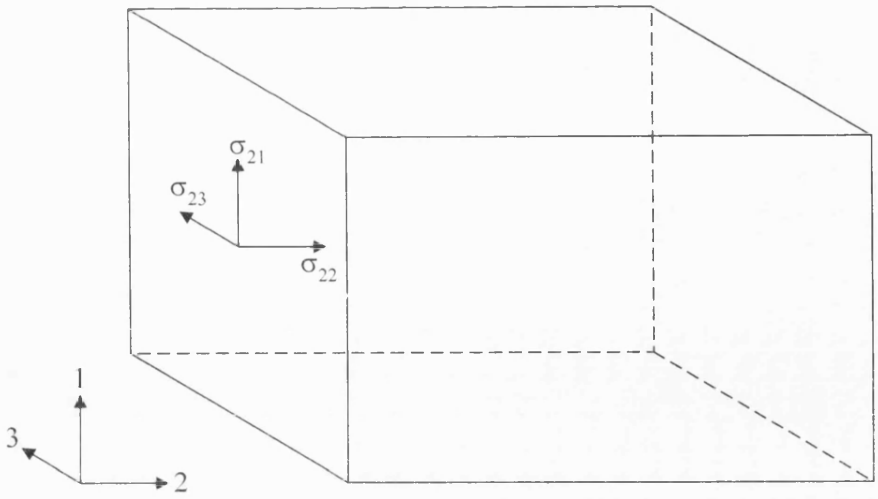

Figure 3: An elemental cube of an elastic solid is shown. σ_{ij} is the force per unit area in the direction j on the face perpendicular to the direction i. The forces on the cube face perpendicular to the "2" direction are shown. Sets of σ_{ij} can be written for each of the faces of the cube (not shown here).

Hooke's law is very general and a statement of the obvious: a pressure or tension force will cause stresses on all faces whereas a purely shearing force will cause no stress in the direction perpendicular to the shear[6]. Newton's second law (where ρ is the density) relates the stresses required to produce particle displacements in the solid:

$$\rho \frac{\partial^2}{\partial t^2} u_j = \frac{\partial}{\partial x_i} \sigma_{ij} \qquad 2\text{-}15$$

From this equation the three equations governing particle displacement within a solid are derived, equations 2-23a, b, and c. In doing so, it is shown (see Appendix 2A) that the displacement can be written as the sum of two components, related to a scalar potential and a vector potential. These are shown to represent particle motions which are compressional and shear in nature, respectively. These particle displacements are shown to be governed by a harmonic dependence on time and position (see equation 2-19, Appendix 2A). Also, the compressional and shear displacements (also known as "longitudinal" and "transverse" displacements) are shown to propagate independently of each other, at different speeds, c_l and c_t, which are functions of the Lamé coefficients and the solid density. It is important that these compressional and shear waves propagate independently of each other. This means that the conversion of one wave type to the other need only be considered at the layer interfaces. The wave speeds themselves are given by:

[6] Equation 2-14 is also a statement of the fact that for small forces, elasticity is a *linear* effect. This is crucial, since for linear equations the principle of superposition holds, which allows a solution for a complicated input to be

$$c_l = \sqrt{(\lambda + 2\mu)/\rho} \qquad 2\text{-}20$$

$$c_t = \sqrt{\mu/\rho} \qquad 2\text{-}21.$$

It is seen that the compressional wave speed will always be greater than the shear wave speed. In fact, the shear speed can at most be 1/sqrt(2) times the compressional wave speed. It can also be seen that as μ approaches zero then the shear wave speed approaches zero whereas the compressional wave speed does not.

The three equations governing particle displacement within a solid, 2-23a, b, and c, have been derived assuming that the x axis is directed such that it is in the same direction as the horizontal component of the incident sound wavevector. In other words, the wave propagation direction is in the xz plane. The critical property of these equations is that the one for particle displacements in the y direction is independent of the other two. Hence waves with particle displacement along the y axis propagate independently of the waves polarized in the xz plane. The case when $u_1 = u_3 = 0$ is usually referred to as an *SH wave*, the polarisation being in the horizontal plane (along the y axis) and so the wave is a shear wave. For the second case, when the displacement is in the xz plane, the wave may be either a compressional wave, referred to as a *P wave*, or a shear wave, referred to as an *SV wave*, or a combination of both. Since the P (and SV) waves do not interact with the SH waves then a pure compressional wave incident upon the seabed will produce only P and SV waves in the first sediment layer. These will, in turn, produce only P and SV waves in the next layer. This will be the case at all the sediment layer interfaces. Hence SH waves are not considered since they will never be produced by a sound wave interacting with the seabed, and hence u_2 is set to zero.

The argument above, for neglecting SH waves, is dependent on the incident wave's x and z co-ordinate system being set up parallel and perpendicular (respectively) to the smooth interface. For a 1 dimensional rough interface, the incident wave will still be in the xz plane, and the roughness will be in the xz plane, and so no SH waves will be produced. If a 2 dimensional case is considered, then there will be plane waves (part of the beam decomposition into plane waves – see chapter 6) whose polarisations have components in the y direction. The surface roughness will be in two dimensions, and so even incident waves polarised in the xz plane may produce scattered waves into the sediment which are polarised in the y direction. In terms of the zero order reflection solution required for the scattering solutions developed in chapters 4 and 5, these are secondary concerns and are not considered further.

2.5.3 Boundary conditions

For the case of vertically polarised elastic waves for non-slip contact between two

---

constructed from the sum of solutions to simpler inputs. This will be used (implicitly) in chapter 6 when considering the scattered solution from a pulsed beam.

solids there are four boundary conditions. These are given here in terms of the particle displacement, u, and the stress tensor, σ:

$$[\sigma_{13}]_s = 0 , [\sigma_{33}]_s = 0 , [u_1]_s = 0 \text{ and } [u_3]_s = 0 \qquad 2\text{-}24$$

where $[]_s$ indicates that the difference between the values of the variable on both sides of the boundary is to be taken. These boundary conditions are simply that there is net particle displacement and no net shear or stress at the interface: the corollary of them not being true would be a net force at the boundary (hence relative bulk layer movement) or net particle loss from one of the layers at the interface, neither of which must happen. The u_3 and σ_{33} boundary conditions are the equivalent of those used for the liquid / liquid interface earlier (2.2); the σ_{13} is the equivalent of the additional boundary condition used for the liquid / solid interface (2.3); and the u_1 condition is one more necessary for the solid / solid interface.

It should noted that these boundary conditions are for non-slip contact at the interfaces. This assumption may be incorrect for the case where the seabed consists of a saturated unconsolidated sediment layer. In such cases, the equations derived from these boundary conditions will not be able to completely describe the wave interactions within or on the boundaries of these media (as found by BUCKINGHAM (1998)).

2.5.4 Matrix propagation

The matrix propagator method is most easily formulated in terms of the velocity potentials defined in Appendix 2A by equations 2-17. Since the particle displacement varies harmonically with position the scalar and vector potentials ϕ and ψ must be picked such that this is the case. Also, since $u_2 = 0$, the vector potential $\underline{\Psi}$ must be chosen such that only the component ψ_2 is non-zero and so the y component of $\underline{\nabla}\times\underline{\Psi}$ is zero. The potentials ϕ and ψ within a layer are therefore each given by a set of upward and downward travelling waves (see equation 2-26 in Appendix 2A). Within a layer the amplitudes of ϕ_1 and ϕ_2 (the amplitudes of the upward and downward components of the potential ϕ) and ψ_1 and ψ_2 are constant, as are the propagation directions of these waves. It should be noted that there is an implicit assumption being made here, that the fields within each layer are in a steady state. This is the same assumption as was made when looking at the input impedance method (2.4), see footnote 3.

In terms of the ϕ and ψ potentials the particle displacement is given by

$$\underline{u} = (i\xi\phi - \frac{\partial\psi}{\partial z}, 0, \frac{\partial\phi}{\partial z} + i\xi\psi) \qquad 2\text{-}28.$$

This equation enables two of the boundary conditions to be evaluated in terms of the velocity potentials ϕ and ψ. Substituting equation 2-28 into equation 2-14 for the stress tensor the σ_{13} and σ_{33} components are also found in terms of the velocity potentials (see equation 2-29, and 2-30 in Appendix 2A).

All the variables required for the matrix propagator method have now been established. The incident wave and boundary values may now be propagated between layers. This is shown in detail in Appendix 2A. The variables required for the boundary conditions are expressed as a column vector, f, which is constant across an interface (see equation 2-32). For between interfaces, i.e. within a layer, the propagation is described by a column vector $\underline{\phi}$, the amplitudes of the upward and downward components of ϕ and ψ (see equation 2-33). The relationship between f and $\underline{\phi}$ is given by equations 2-34, 2-35 and 2-36. This relationship may be evaluated at the two interfaces which bound a layer, and for which $\underline{\phi}$ is constant. Since $\underline{\phi}$ is constant these two relationships may be equated and solved to give the relationship between the values of f on each of the interfaces (see equation 2-37). This relationship is in terms of a matrix $A^{(j)}$ which is specific to the particular layer between the two interfaces. It is layer-specific in that it contains terms such as the density and wave speeds and wave directions for that layer. Precisely equivalent relationships can be written for each layer. Using (2-37) the values of f on the boundaries of layers 1 and 2 can be connected to those on the boundary between between layers n and n+1 by:

$$f(z_n) = [A] f(z_1) \qquad 2\text{-}40$$

where

$$[A] = [A^{(n)}][A^{(n-1)}].....[A^{(3)}][A^{(2)}] \qquad 2\text{-}41.$$

Once the matrix [A] has been calculated it is possible to calculate the reflection coefficient. This is now done for the case of interest where the top layer is a fluid. The total field of the incident and reflected waves in the fluid half-space is written as:

$$\phi^{(n+1)} = \exp[-i\alpha(z - z_n)] + V \exp[i\alpha(z - z_n)] \qquad 2\text{-}42$$

where V is the reflection coefficient. In the lower elastic half-space are only waves departing from the boundary, the potentials of which are written as:

$$\phi^{(1)} = W_1 \exp(-i\alpha_1 z) \text{ and } \psi^{(1)} = W_1 \exp(-i\beta_1 z) \qquad 2\text{-}43$$

The reflection coefficient may now be solved for. This is shown in Appendix 2A. The matrix coefficients for the matrix [A] are found by multiplying the individual layer matrices, in the order specified by equation 2-41, where the individual layer matrix coefficients are found at Appendix 2B. These coefficients for each layer are given in terms of the density, shear and compressional wave speeds within the layer as well as the propagation angles of these waves within that layer. The propagation angles are found for each wave using Snell's law.

Attenuation of any of the waves in any layer is incorporated by making the appropriate wave speed complex, the imaginary part of the wave speed being given by equation 2-3. It should be noted that this will render the angle of propagation complex (through Snell's law) and so the matrix coefficients will generally be complex also.

2.5.5 Sediment layer attenuation

The theory described above and in the appendices has been applied to the case of a seabed consisting a 5m thick sediment overlying a semi-infinite basement. The reflected power coefficients have been calculated for 4 different combinations of attenuation coefficients for the sound and shear waves in the sediment. For the (liquid) sea the density is assumed to be 1000kg/m^3 and the sound speed 1500m/s. The sediment is modelled as having a density of 2000kg/m^3 and a sound speed of 2000m/s and a shear wave speed of 1200m/s. The basement has a density of 5000kg/m^3, a sound speed of 3000m/s and a shear wave speed of 2000m/s. The basement is assumed to have zero attenuation (for simplicity rather than reality) and the sediment is assumed to have attenuation in dB per wavelength given by $\alpha(1)$ and $\alpha(2)$ for sound and shear waves respectively. The frequency is 800Hz. The reflected power coefficients are shown in Figure 4.

At low incident angles energy is lost to the seabed due to both attenuation within the sediment layer and due to sound being transmitted into the basement layer (never to return). For incident angles above 30° (= arcsin(1500/3000)) all compressional wave energy is reflected from the basement. Whatever energy is lost above this incident angle is due to attenuation within the sediment and energy converted to shear waves which is either attenuated or transmitted into the basement. Above 48.6° (=arcsin(1500/2000)) both wave types are reflected completely from the basement. Also, this is the critical angle for the sound wave within the sediment, and so energy loss is now due entirely to shear wave attenuation within the sediment. It is seen that much energy may be lost to the seabed due to shear wave attenuation when the sediment shear wave speed is less than the sea water sound speed.

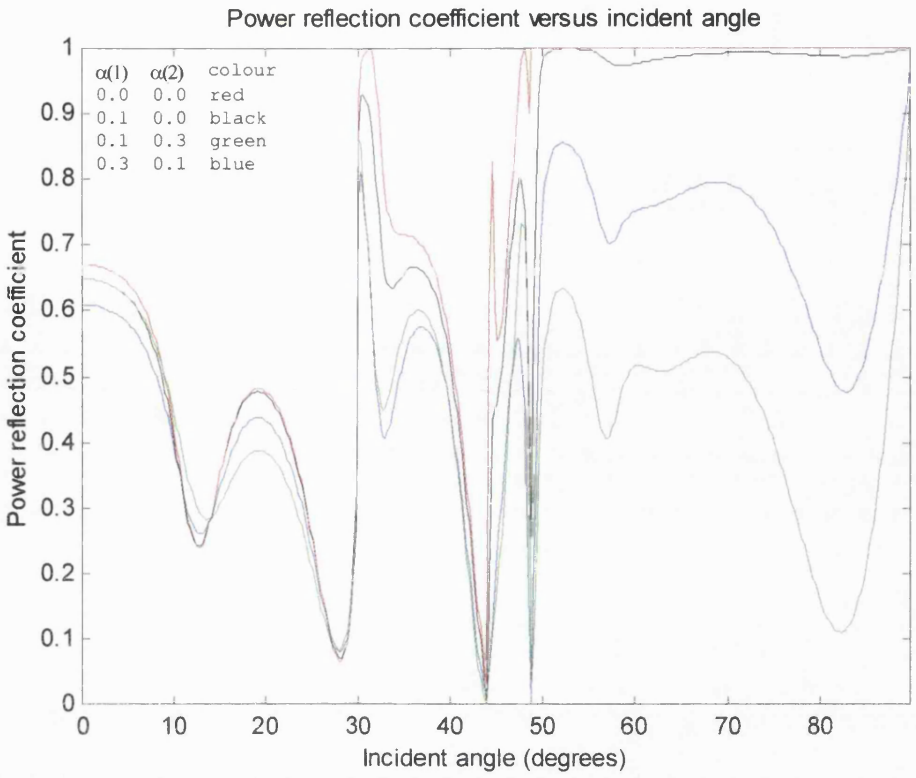

Figure 4: Power reflection coefficient versus incident angle for a seabed consisting of a 5m thick sediment layer overlying a semi-infinite basement, for different sediment attenuation coefficients. The reflected power coefficients have been calculated for 4 different combinations of attenuation coefficients for the sound and shear waves in the sediment. For the (liquid) sea the density is assumed to be 1000kg/m^3 and the sound speed 1500m/s. The sediment is modelled as having a density of 2000kg/m^3 and a sound speed of 2000m/s and a shear wave speed of 1200m/s. The basement has a density of 5000kg/m^3, a sound speed of 3000m/s and a shear wave speed of 2000m/s. The basement is assumed to have zero attenuation (for simplicity rather than reality) and the sediment is assumed to have attenuation in dB per wavelength given by α(1) and α(2) for sound and shear waves respectively. The frequency of the incident sound is 800Hz. At low incident angles energy is lost to the seabed due to both attenuation within the sediment layer and due to sound being transmitted into the basement layer. For incident angles above 30° all compressional wave energy is reflected from the basement. Above 48.6° both wave types are reflected completely from the basement. It is seen that much energy may be lost to the seabed due to shear wave attenuation.

2.5.6 Use of the matrix propagator method as a benchmark

For reflection from a simple liquid / solid or liquid / liquid interface the methods shown in sections 2.2 and 2.3 are more straightforward to use than the more generalised

matrix propagator method. For seabeds modelled with sediment layers and / or layers with non-homogeneous properties the matrix propagator method is the default benchmark which should be used.

AINSLIE et al (1998) have presented "benchmark" solutions to reflection from a non-homogeneous sediment overlying a semi-infinite solid substrate. In Figures 5 and 6 the equivalent matrix propagator solutions are presented by way of comparison. In each case the sediment is modelled as having an analytic sound speed profile and analytic sound speed attenuation coefficient profile, thus allowing an analytic solution to be derived. Here, the 20m thick sediment has been split into 200 x 0.1 metre thick homogeneous layers and the matrix propagator method allowed to calculate the solution. These solutions both compare well with those presented by AINSLIE et al and indicate the usefulness of the matrix propagator method. For sediments with sound speed profiles *which do not lend themselves to analytic solution* the sediment may be split into thin layers, each of which is then assumed to be homogeneous, and then the matrix propagator method used to compute the solution. It should be stressed that the matrix propagator method can be used to calculate the solution for a sediment with *any* geoacoustic profile; it is this fact that enables it to be used as a benchmark for calculating bottom reflection loss from seabeds.

One caveat with the matrix propagator method is that large attenuation coefficients can lead to problems. This is due to the fact that some of the terms involved in propagating the waves between the layers involve cosines and sines of "kz" type terms, where k is the wavenumber and z is the layer thickness. For real k, this is not a problem. When attenuation is included, however, the k becomes complex, and the cosine and sine terms also become complex, with potentially very large imaginary parts. These can easily become too large for the software package and lead to null results. When using MATLAB such problems are made obvious since an "Inf" or a "NaN" error message is produced. Other lower level languages are not as user-friendly and will just produce spurious results. For Figures 5 and 6 the sediment was modelled as having no attenuation (thus explaining the slight differences compared to the results of AINSLIE et al). Solutions to this problem are discussed in chapter 8.

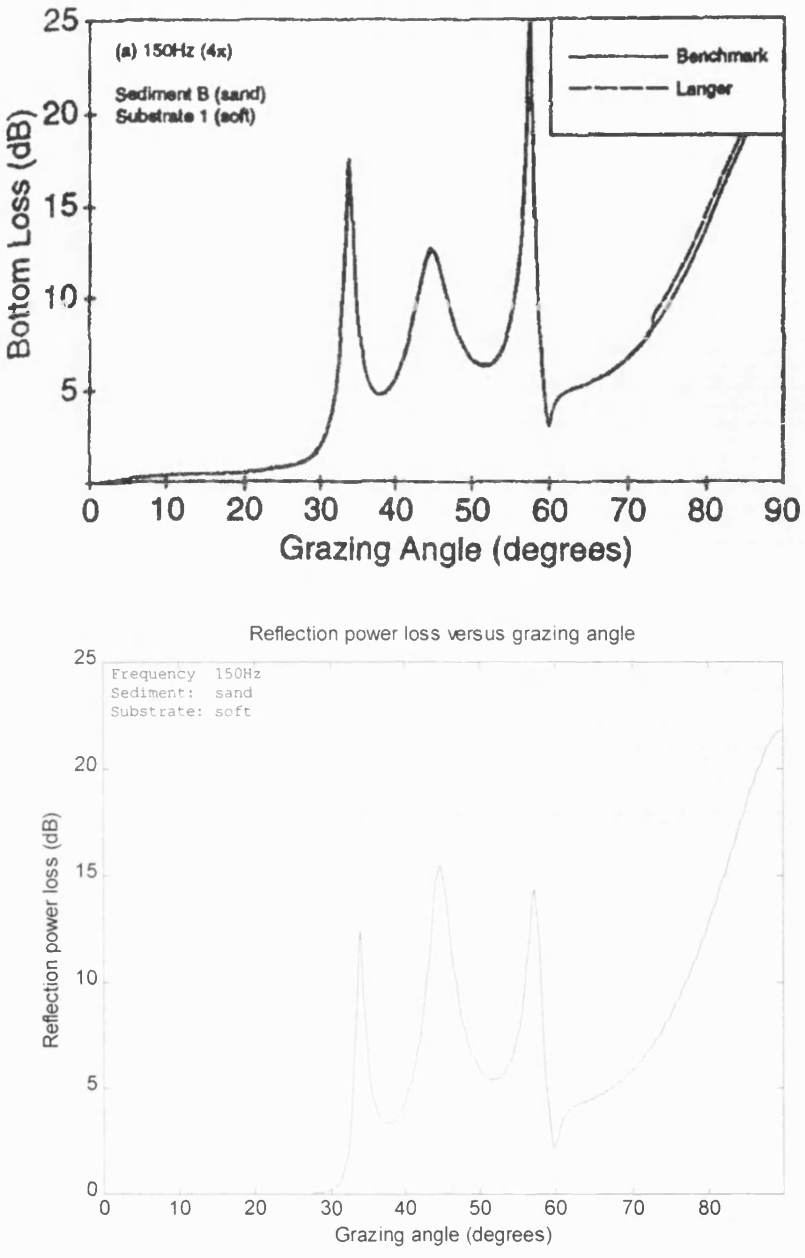

Figure 5: Reflected power loss versus grazing angle for an inhomogeneous sand sediment overlying a soft basement. The sound speed and attenuation profiles within the sediment, and the geoacoustic parameters within the basement, are those given in Tables I and II by AINSLIE et al (1998). The incident sound frequency is 150Hz. The top plot shows the analytical solution presented by by AINSLIE et al (1998). The lower plot has been computed using the matrix propagator method, with 200 x 0.1 metre thick homogeneous sediment layers, with no attenuation. The solutions are very similar. The main differences are due to the fact that attenuation has not been included in the matrix propagator method solution: the zero loss below 30° and the size of the loss peaks. It is clear, however, that the matrix propagator method can be used to provide

a benchmark solution by using a large number of thin homogeneous layers to represent a geoacoustic profile.

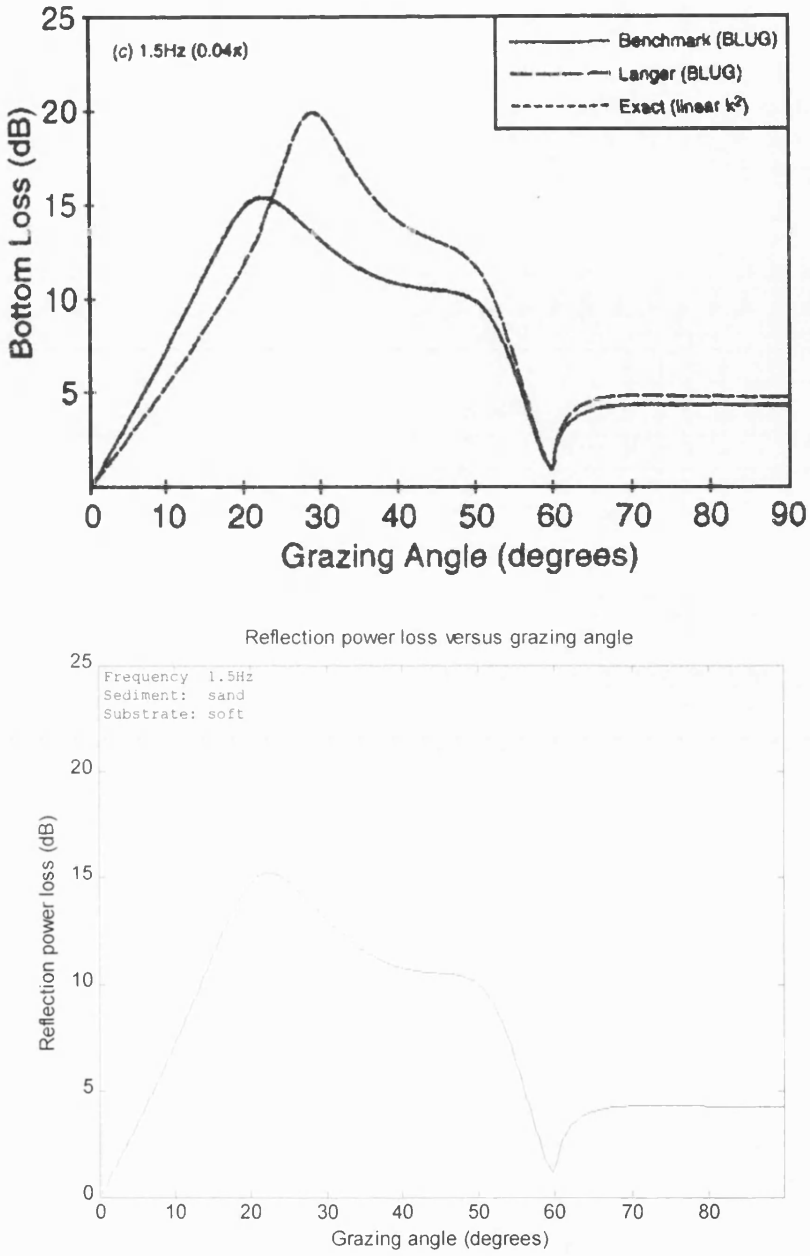

Figure 6: Reflected power loss versus grazing angle for an inhomogeneous sand sediment overlying a soft basement. The sound speed and attenuation profiles within the sediment, and the geoacoustic parameters within the basement, are those given in Tables I and II by AINSLIE et al (1998). The Incident sound frequency is 1.5Hz. The top plot shows the analytical solution presented by by AINSLIE et al (1998). The lower plot has been computed using the matrix propagator method, with 200 x 0.1 metre thick homogeneous sediment layers, with no attenuation. The solutions are virtually identical, and again show the utility of the matrix propagator method in providing a benchmark bottom reflection loss solution.

Appendix 2A

The development of the matrix propagator method presented here follows that given by BREKHOVSKIKH and GODIN (1990). The final part of the development, to calculate the reflection coefficient for a liquid / solid interface, is new work, and is the basis of the code used to produce the reflection results presented in sections 2.5.5 and 2.5.6.

Fundamental equations

The relation between stresses and deformations in the linear theory of elasticity and in the most simple case of locally isotropic solids, is given by *Hooke's law*:

$$\sigma_{ij} = \lambda \frac{\partial u_k}{\partial x_k} \delta_{ij} + \mu \left(\frac{\partial u_i}{\partial x_j} + \frac{\partial u_j}{\partial x_i} \right) \qquad 2\text{-}14$$

where λ and μ are the *Lamé coefficients*, σ_{ij} is the force per unit area in the direction j on the face perpendicular to the direction i, and u is the particle displacement in the solid, as shown in Figure 1 below.

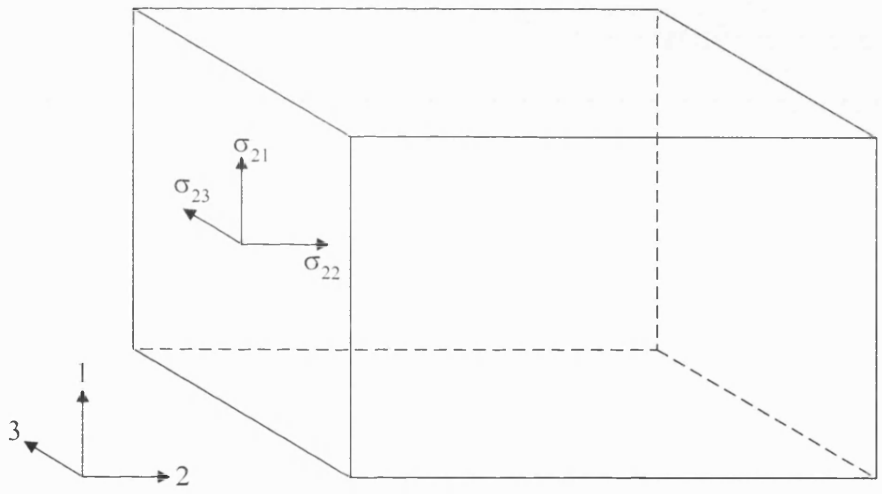

Figure 1: An elemental cube of an elastic solid is shown. σ_{ij} is the force per unit area in the direction j on the face perpendicular to the direction i. The forces on the cube face perpendicular to the "2" direction are shown. Sets of σ_{ij} can be written for each of the faces of the cube (not shown here).

Newton's second law (where ρ is the density) relates the stresses required to produce particle displacements in the solid to the stress tensor σ:

$$\rho \frac{\partial^2}{\partial t^2} u_j = \frac{\partial}{\partial x_i} \sigma_{ij} \qquad 2\text{-}15$$

Wave equations within a solid

Substituting for σ_{ij} from (2-14) into (2-15) gives the equation describing the propagation of elastic waves in a locally isotropic solid:

$$\rho\frac{\partial^2 \underline{u}}{\partial t^2} = (\lambda+\mu)\underline{\nabla}(\underline{\nabla}.\underline{u}) + \_\mu\nabla^2\underline{u} + \underline{\nabla}\lambda\underline{\nabla}.\underline{u} + (\underline{\nabla}\mu)\times(\underline{\nabla}\times\underline{u}) + 2(\underline{\nabla}\mu.\underline{\nabla})\underline{u} \qquad \text{2-16a}$$

which can be simplified for a homogeneous solid, for which case the Lamé coefficient derivatives are zero, to:

$$\frac{\partial^2 \underline{u}}{\partial t^2} = \frac{\lambda+2\mu}{\rho}\underline{\nabla}(\underline{\nabla}.\underline{u}) - \frac{\mu}{\rho}\underline{\nabla}\times(\underline{\nabla}\times\underline{u}) \qquad \text{2-16b}$$

In general the displacement vector $\underline{u}$ can be related to scalar, ϕ and vector, ψ velocity potentials by:

$$\underline{u} = \underline{u_l} + \underline{u_t} \qquad \text{2-17a}$$

$$\underline{u_l} = \underline{\nabla}\phi \qquad \text{2-17b}$$

$$\underline{u_t} = \underline{\nabla}\times\underline{\psi} \qquad \text{2-17c}$$

Introducing (2-17) into (2-16) gives:

$$\frac{\partial^2 \underline{u_l}}{\partial t^2} - \frac{\lambda+2\mu}{\rho}\nabla^2\underline{u_l} + \frac{\partial^2 \underline{u_t}}{\partial t^2} - \frac{\mu}{\rho}\nabla^2\underline{u_t} = 0 \qquad \text{2-18.}$$

After successive applications of the div and curl operators to (2-18) it is found that the $\underline{u}_l$ parts and the $\underline{u}_t$ parts are each only dependent on t. Defining $\underline{u}_l$ and $\underline{u}_t$ to within an accuracy of additive vectors depending only on t, results in wave equations for $\underline{u}_l$ and $\underline{u}_t$. That for $\underline{u}_l$ is given:

$$\frac{\partial^2 \underline{u_l}}{\partial t^2} - c_l{}^2\nabla^2\underline{u_l} = 0 \qquad \text{2-19}$$

with

$$c_l = \sqrt{(\lambda+2\mu)/\rho} \qquad \text{2-20}$$

An equivalent equation exists for u_t with c_t defined as:

$$c_t = \sqrt{\mu/\rho} \qquad \text{2-21.}$$

The relations (2-17) and (2-19) - (2-21) imply that two types of displacements occur in solids, each associated with a wave propagation whose speed is determined by the Lamé coefficients and the solid density. These two types of displacement and wave are independent. By considering the change in volume which occurs when the solid is deformed,

$\underline{\nabla}.\underline{u}$, using (2-17) it is seen that the displacement $\underline{u}_l$ is concerned with volume changes, and so is a compressional displacement, whereas $\underline{u}_t$, which is not, is a shear displacement.
From equation (2-19) it may be assumed that the waves propagating within the solid produce displacements which have a harmonic dependence on time and on the horizontal co-ordinates, and so can be written as:

$$\underline{u}(\underline{r},\omega) = \underline{u}(z,\underline{\xi},\omega)\exp(i\underline{\xi}.\underline{r} - i\omega t) \qquad 2\text{-}22.$$

Here the x axis is directed such that it is in the same direction as the horizontal component of $\underline{\xi}$. Substituting (2-22) into (2-16a), and remembering that only the z derivatives of the Lamé coefficients are non-zero at an interface, the equations governing particle displacements are found:

$$-\omega^2 \rho u_1 = i\xi[(\lambda+\mu)\frac{\partial u_3}{\partial z} + \frac{\partial \mu}{\partial z}u_3] + \frac{\partial}{\partial z}(\mu\frac{\partial u_1}{\partial z}) - \xi^2(\lambda+2\mu)u_1 \qquad 2\text{-}23a$$

$$-\omega^2 \rho u_2 = \frac{\partial}{\partial z}(\mu\frac{\partial u_2}{\partial z}) - \xi^2 \mu u_2 \qquad 2\text{-}23b$$

$$-\omega^2 \rho u_3 = i\xi[\frac{\partial}{\partial z}(\lambda u_1) + \mu\frac{\partial u_1}{\partial z}] + \frac{\partial}{\partial z}[(\lambda+2\mu)\frac{\partial u_3}{\partial z}] - \xi^2 \mu u_3 \qquad 2\text{-}23c$$

where subscripts 1,2,3 refer to x,y,z components respectively. The equations cease to be coupled when ξ=0, i.e when the propagation is normal to the layers. For arbitrary incidence the u_2 equation is not coupled with the other two equations. Hence waves with displacement along the y axis propagate independently of the waves polarized in the xz plane. Thus, shear waves polarised in the xz plane are independent of shear waves polarised along the y axis. Hence SH waves are not considered any further since they will never be produced by a sound wave interacting with the seabed, and hence u_2 is set to zero.

Boundary conditions

For the case of vertically polarised elastic waves for welded (i.e. non-slip) contact between two solids there are four boundary conditions:

$$[\sigma_{13}]_s = 0, [\sigma_{33}]_s = 0, [u_1]_s = 0 \text{ and } [u_3]_s = 0 \qquad 2\text{-}24$$

where $[]_s$ indicates that the difference between the values of the variable on both sides of the boundary is to be taken.
Now that it is known that the displacement varies harmonically with position (see equation 2-19) the scalar and vector potentials must be defined such that this is the case. It follows from (2-17) that the potentials must therefore both be harmonic functions of position. Since u_2 = 0 the vector potential $\underline{\Psi}$ must be chosen such that only the component ψ_2 is non-zero and so the y component of $\underline{\nabla}\times\underline{\Psi}$ is zero. The shear displacement components, are now given by:

$$u_x = \frac{-\partial \psi}{\partial z} \text{ and } u_z = \frac{\partial \psi}{\partial x} \qquad 2\text{-}25$$

where ψ_2 is now written simply as ψ. A general elastic wave (hence components travelling both upwards and downwards) in a layered solid is described by the two scalar functions ϕ and ψ given by:

$$\phi = \phi_1 \exp(i\alpha z) + \phi_2 \exp(-i\alpha z)$$

$$\psi = \psi_1 \exp(i\beta z) + \psi_2 \exp(-i\beta z) \qquad 2\text{-}26$$

where

$$\alpha = (k_1^2 - \xi^2)^{\frac{1}{2}} \text{ and } \beta = (k_t^2 - \xi^2)^{\frac{1}{2}} \qquad 2\text{-}27$$

and where $k_i = \omega/c_i$. Substituting into (2-17) gives the general particle displacement:

$$\underline{u} = (i\xi\phi - \frac{\partial \psi}{\partial z}, 0, \frac{\partial \phi}{\partial z} + i\xi\psi) \qquad 2\text{-}28.$$

Substituting (2-28) into (2-14) and using (2-20) and (2-21) the values of σ_{13} and σ_{33} are also found in terms of the velocity potentials:

$$\sigma_{13} = -2\mu\xi(\gamma\psi - i\frac{\partial \phi}{\partial z}) \qquad \text{and} \qquad \sigma_{33} = 2\xi\mu(\gamma\phi + i\frac{\partial \psi}{\partial z}) \qquad 2\text{-}29$$

where γ is given by:

$$\gamma = \xi - \frac{k_1^2}{2\xi} \qquad 2\text{-}30.$$

In (2-28) and (2-29) are the four boundary condition variables required for calculating wave transmission and reflection coefficients at an interface. Having derived the general form of the scalar and vector potentials, and their relationships with the particle displacement and stresses, the matrix propagator method is now considered.

Calculating the A matrix

For the j^{th} layer equation (2-26) is replaced by:

$$\phi^{(j)} = \phi_1^{(j)} \exp(i\alpha(z - z_{j-1})) + \phi_2^{(j)} \exp(-i\alpha(z - z_{j-1}))$$

$$\psi^{(j)} = \psi_1^{(j)} \exp(i\beta(z - z_{j-1})) + \psi_2^{(j)} \exp(-i\beta(z - z_{j-1})) \qquad 2\text{-}31$$

for $z_j \geq z \geq z_{j-1}$.

The co-ordinate and layer numbering system is as shown in Figure 2 below.

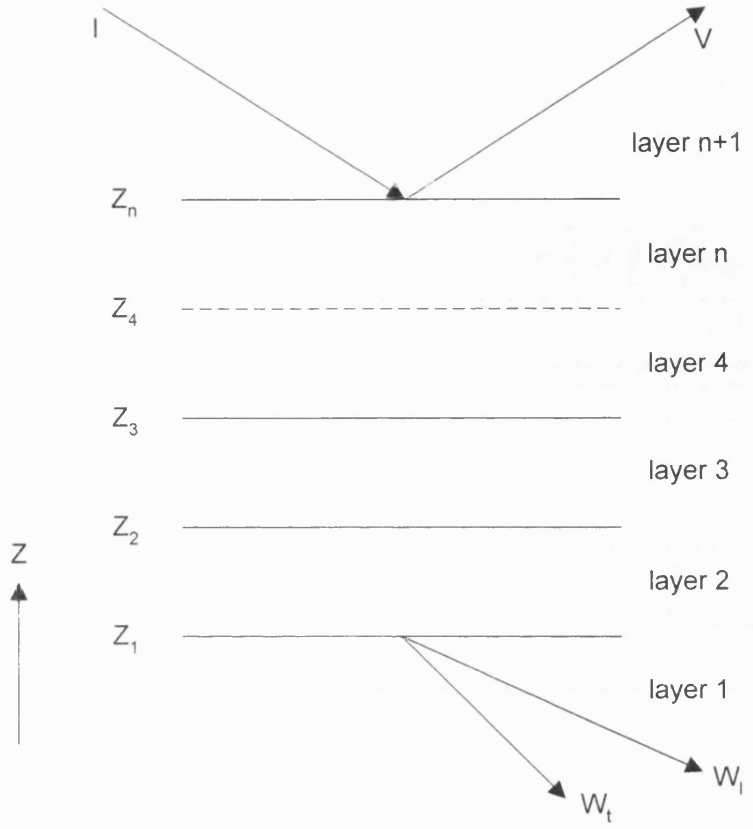

Figure 2: Co-ordinate and layer numbering system used for the matrix propagator method for the sea / seabed interface. The incident and reflected waves, amplitude I (assumed equal to 1) and V respectively, are in the n+1th layer, assumed to be liquid (representing the sea). The seabed basement, assumed solid, is layer 1, and it is into this layer that the transmitted longitudinal wave (W_l) and transverse (or shear) wave (W_t) propagate. In all the intermediate layers there are longitudinal and transverse waves propagating (diagonally) both upwards and downwards. The co-ordinate system has z increasing upwards, and z_n is at the top of the nth layer.

The α, β, $\phi_{1,2}$ and $\psi_{1,2}$ are constant within the layer. It is assumed that the layers are numbered from the lower half-space (layer 1) to the fluid half-space (layer n+1) with z_j being at the top of layer j.

Assuming that the field in the jth layer is known, the aim is to calculate it in the j+1th layer. For this purpose it is useful to characterise the field by a *displacement-stress vector* $\underline{f}$:

$$\underline{f}(z) = (u_1, u_3, \sigma_{33}, \sigma_{3l})^T \qquad 2\text{-}32.$$

The vector $\underline{f}$ is useful since it is continuous across each interface (in fact it is continuous everywhere), as stated by the boundary conditions in equations (2-24). The vector $\underline{\phi}$ on the other hand is constant within a layer but transforms in a complicated manner across interfaces: ϕ is given by:

$$\underline{\phi} = (\phi_1, \phi_2, \psi_1, \psi_2)^T \qquad \text{2-33.}$$

The relationship between $\underline{f}$ and $\underline{\phi}$ is given by:

$$\underline{f}(z) = [B(z, z_{j-1})]\phi \qquad \text{2-34a}$$

i.e.

$$\underline{f}(z_j) = [B(z_j, z_{j-1})]\phi \qquad \text{2-34b}$$

$$\underline{f}(z_{j-1}) = [B(z_{j-1}, z_{j-1})]\phi \qquad \text{2-34c}$$

where ϕ is that within layer j and where

$$[B(z_j, z_{j-1})] = [L][a, a^{-1}, b, b^{-1}] \qquad \text{2-35}$$

and

$$[L] = \begin{bmatrix} i\xi & i\xi & -i\beta & i\beta \\ i\alpha & -i\alpha & i\xi & i\xi \\ 2\mu\xi\gamma & 2\mu\xi\gamma & -2\mu\xi\beta & 2\mu\xi\beta \\ -2\mu\xi\alpha & 2\mu\xi\alpha & -2\mu\xi\gamma & -2\mu\xi\gamma \end{bmatrix} \qquad \text{2-36a}$$

$$a = \exp(i\alpha(z_j - z_{j-1})) \text{ and } b = \exp(i\beta(z_j - z_{j-1})) \qquad \text{2-36b}$$

and where $[a_1, a_2, a_3, a_4]$ is defined as having elements $c_{ij} = a_i \delta_{ij}$. Direct substitution of 2-36, 2-35, 2-32 and 2-33 into 2-34 prove that the latter relation is valid. Using the fact that ϕ is constant within a layer the relation between the f vectors on neighbouring boundaries is found by comparing equations 2-34b and 2-34c:

$$f(z_j) = [A^{(j)}]f(z_{j-1}) \qquad \text{2-37}$$

where

$$[A^{(j)}] = [B(z_j, z_{j-1})][B(z_{j-1}, z_{j-1})]^{-1} \qquad \text{2-38}$$

hence

$$[A^{(j)}] = [L][a, a^{-1}, b, b^{-1}][L]^{-1} \qquad \text{2-39}$$

The elements of $[A^{(j)}]$ can now be calculated. The results of evaluating this matrix are shown at Appendix 2B.

The matrix propagator method

Using (2-37) the values of f on the boundaries of media 1 and 2 and n and n+1 are related by the matrix [A]:

$$f(z_n) = [A]f(z_1) \qquad 2\text{-}40$$

where

$$[A] = [A^{(n)}][A^{(n-1)}].....[A^{(3)}][A^{(2)}] \qquad 2\text{-}41.$$

Once the matrix [A] has been calculated it is possible to calculate the reflection coefficient. Using equation 2-34 at both top and bottom interfaces the potentials at these interfaces can be related through equation 2-40. This is now done for the case of interest where the top layer is a fluid. The origin of the co-ordinate system is set to be on the boundary of media 1 and 2. The total field of the incident and reflected waves in the fluid half-space is written as:

$$\phi^{(n+1)} = \exp[-i\alpha(z - z_n)] + V\exp[i\alpha(z - z_n)] \qquad 2\text{-}42$$

where V is the reflection coefficient. In the lower elastic half-space there are only waves departing from the boundary, the potentials of which are written as:

$$\phi^{(1)} = W_1\exp(-i\alpha_1 z) \text{ and } \psi^{(1)} = W_1\exp(-i\beta_1 z) \qquad 2\text{-}43$$

for the compressional (sound) and shear waves respectively. Modifying equation (2-34) for ϕ in layer n+1 and then setting $z=z_n$ the displacement stress vector at the boundary where the incident wave hits the layered system is found:

$$f(z_n) = [B(z_n, z_n)](V,1,0,0)^T \qquad 2\text{-}44.$$

The displacement stress vectors at the two outer interfaces are related by $f(z_n) = [A]f(z_1)$. For $f(z_1)$ equation (2-34) is applied again with an arbitrary layer boundary in the (homogeneous) lower half-space an arbitrarily small distance from z_1, the latter being at z=0. This gives:

$$f(z_n) = [A][B(0,0)](0,W_1,0,W_1)^T \qquad 2\text{-}45.$$

Comparing equations (2-44) and (2-45) and eliminating the displacement stress vector, $f(z_n)$, gives:

$$[B(z_n, z_n)](V,1,0,0)^T = [A][B(0,0)](0,W_1,0,W_1)^T \qquad 2\text{-}46.$$

Using equation (2-35) for [B] and equation (2-36) for [L], and using the equality $\mu\gamma = -\omega^2\rho/2\xi$ which is valid for the fluid, the matrix equation linking the reflected and transmitted wave amplitudes is found:

$$\begin{bmatrix} i\xi(1+V) \\ -i\alpha(1-V) \\ -\omega^2\rho(1+V) \\ 0 \end{bmatrix} = [A].\begin{bmatrix} i\xi W_l + i\beta_l W_t \\ -i\alpha_l W_l + i\xi W_t \\ 2\mu_l\xi(\gamma_l W_l + \beta_l W_t) \\ 2\mu_l\xi(\alpha_l W_l - \gamma_l W_t) \end{bmatrix} \qquad 2\text{-}47.$$

By equating the values of the fourth elements in the vectors on the left hand side and right hand side of (2-47) the ratio $q = W_t / W_l$ can be found. This is written at Appendix 2B. Using the second and third components of (2-47) eliminating V gives W_l and hence W_t.

Calculating the reflection coefficient, V

It is in calculating the reflection coefficient that the development presented here deviates from that presented BREKHOVSKIKH and GODIN (1990). Substituting for W_t with qW_l equation (2-47) can be written as:

$$\begin{bmatrix} i\xi(1+V) \\ -i\alpha(1-V) \\ -\omega^2\rho(1+V) \\ 0 \end{bmatrix} = [A].W_l\begin{bmatrix} (1) \\ (2) \\ (3) \\ (4) \end{bmatrix} \qquad 2\text{-}48$$

where

$$\begin{bmatrix} (1) \\ (2) \\ (3) \\ (4) \end{bmatrix} = \begin{bmatrix} i\xi + i\beta_l q \\ -i\alpha_l + i\xi q \\ 2\mu_l\xi(\gamma_l + \beta_l q) \\ 2\mu_l\xi(\alpha_l - \gamma_l q) \end{bmatrix} \qquad 2\text{-}49.$$

Equating the second elements in the vectors on the left hand side and right hand side of equation (2-48) gives:

$$1 - V = \frac{i}{\alpha} W_l [A_{21}(1) + A_{22}(2) + A_{23}(3) + A_{24}(4)] \qquad 2\text{-}50.$$

Similarly the third elements of equation (2-48) give:

$$1 + V = \frac{-1}{\omega^2\rho} W_l [A_{31}(1) + A_{32}(2) + \_ A_{33}(3) + A_{34}(4)] \qquad 2\text{-}51.$$

Defining E_j by

$$E_j = [A_{j1}(1) + A_{j2}(2) + A_{j3}(3) + A_{j4}(4)] \qquad 2\text{-}52$$

and dividing equation (2-50) by equation (2-51) gives:

$$\frac{1-V}{1+V} = \frac{-i\omega^2\rho}{\alpha}\frac{E_2}{E_3} \qquad 2\text{-}53.$$

Now (1-V)/(1+V) = N/D can be re-arranged to give V=(D-N)/(D+N) and hence:

$$V = \frac{E_3 - \frac{-i\omega^2\rho}{\alpha}E_2}{E_3 + \frac{-i\omega^2\rho}{\alpha}E_2} \qquad 2\text{-}54.$$

Equation (2-54) is re-arranged to give:

$$V = \frac{\frac{-E_3}{i\omega E_2} - \frac{\omega\rho}{\alpha}}{\frac{-E_3}{i\omega E_2} + \frac{\omega\rho}{\alpha}} \qquad 2\text{-}55.$$

Defining Z_{inp} by:

$$Z_{inp} = \frac{-E_3}{i\omega E_2} \qquad 2\text{-}56$$

and evaluating α as $(\omega/c)\cos\theta$ the reflection coefficient, V, may be given by:

$$V = \frac{Z_{inp} - Z}{Z_{inp} + Z} \qquad 2\text{-}57$$

where:

$$Z = \frac{\rho c}{\cos\theta} \qquad 2\text{-}58.$$

Note that equations (2-55), (2-56), (2-57) agree with the expressions given by BREKHOVSKIKH and GODIN (1990, p102). The only difference in the results derived here comes in the definition of E_j, as shown below (equations (2-67) and (2-68)).

Notes

Before evaluating the brackets (1), (2), (3) and (4) from equation (2-49) it is instructive to note a few relationships between the commoner variables:

$$\alpha_l = k_l \cos\theta_l$$

$$\beta_l = k_t \cos\theta_t$$

$$\xi = k_{index} \sin\theta_{index} \qquad 2\text{-}59$$

and equation (2-30) may also be re-arranged to show:

$$\xi\gamma_l = \frac{-1}{2} k_l^{\,2} \cos 2\theta_l \qquad 2\text{-}60.$$

Equation (2-21) and the definition of k also gives:

$$\mu_l k_l^{\,2} = \omega^2 \rho_l \qquad 2\text{-}61$$

and hence:

$$\mu_l \xi\gamma_l = \frac{-1}{2} \omega^2 \rho_l \cos 2\theta_l \qquad 2\text{-}62.$$

Using $\kappa = k_t \sin\theta_t$ and equations (2-59) and (2-61) it is found that $\mu_1\xi\beta_1$ is given by:

$$2\mu_l \xi\beta_l = \omega^2 \rho_l \sin 2\theta_l \qquad 2\text{-}63.$$

To evaluate $\mu_1\xi\alpha_1$ it is multiplied by $k_t \sin\theta_t / k_l \sin\theta_l$ (which equals 1 of course – Snell's Law) giving:

$$2\mu_l \xi\alpha_l = 2\omega^2 \rho_l \sin^2\theta_l \cot\theta_l \qquad 2\text{-}64.$$

Substituting brackets (1), (2), (3) and (4) from equation (2-49) into equation (2-52) and using equations (2-62), (2-63) and (2-64) gives:

$$\begin{aligned} i E_j = &- A_{j1}\xi + A_{j2}\alpha_l - i\omega^2\rho_l (A_{j3}\cos 2\theta_l - A_{j4} 2\sin^2\theta_l \cot\theta_l) \\ &- q[A_{j1}\beta_l + A_{j2}\xi - i\omega^2\rho_l (A_{j3}\sin 2\theta_l + \_ A_{j4}\cos 2\theta_l)] \end{aligned} \qquad 2\text{-}65.$$

The factor i can be discarded since it will cancel out when E_3 is divided by E_2 (see equation (2-56)). Hence we have:

$$\begin{aligned} E_j = &- A_{j1}\xi + A_{j2}\alpha_l - i\omega^2\rho_l (A_{j3}\cos 2\theta_l - A_{j4} 2\sin^2\theta_l \cot\theta_l) \\ &- q[A_{j1}\beta_l + A_{j2}\xi - i\omega^2\rho_l (A_{j3}\sin 2\theta_l + \_ A_{j4}\cos 2\theta_l)] \end{aligned} \qquad 2\text{-}66.$$

The reflection problem is now solved. The reflection coefficient, V, is given by equation (2-57) where Z and Z_{input} are given by equations (2-58) and (2-56) respectively and where E_j is given by (2-66). The matrix coefficients for [A] are found by multiplying the individual layer matrices, in the order specified by equation (2-41), where the individual layer matrix coefficients are found at Appendix 2B. These coefficients are given for each layer in terms of the density, shear and compressional wave speeds within that layer as well as the propagation angles of these waves within that layer. The propagation angles are found for each wave in each layer using Snell's Law.

Instead of equation (2-66) BREKHOVSKIKH and GODIN (1990, p102) find:

$$E_j = M_{j2}\alpha_1 - i\omega^2\rho_1(M_{j3}\cos 2\theta_1 + M_{j4}2\sin^2\theta_1\cot\theta_1) - q[M_{j2}\xi + i\omega^2\rho_1(M_{j3}\sin 2\theta_1 - M_{j4}\cos 2\theta_1)] \quad 2\text{-}67$$

where

$$M_{jk} = A_{jk} - \frac{A_{j1}}{A_{41}} \quad 2\text{-}68.$$

Expanding equation (2-67) by substituting for M from equation (2-68) gives:

$$\begin{aligned} E_j = {} & A_{j2}\alpha_1 - i\omega^2\rho_1(A_{j3}\cos 2\theta_1 + A_{j4}2\sin^2\theta_1\cot\theta_1) \\ & - q[A_{j2}\xi + i\omega^2\rho_1(A_{j3}\sin 2\theta_1 - A_{j4}\cos 2\theta_1)] \\ & + \frac{-A_{j1}}{A_{41}}[\alpha_1 - i\omega^2\rho_1(\cos 2\theta_1 + 2\sin^2\theta_1\cot\theta_1)] \\ & - q\frac{-A_{j1}}{A_{41}}[\xi + i\omega^2\rho_1(\sin 2\theta_1 - \cos 2\theta_1)] \end{aligned} \quad 2\text{-}69.$$

It is clear that this is not in general equivalent to equation (2-66) or any scalar multiple thereof. A comparison of the two reflection coefficient solutions is shown in Figure 3 and Figure 4 for a simple liquid / liquid and liquid / solid interface respectively. Both of these comparisons show the solution calculated here to be correct, and the one developed by BREKHOVSKIKH and GODIN (1990) to be incorrect, for a very simple case. The BREKHOVSKIKH and GODIN (1990) solution becomes even more excessive (peaks much greater than 10 for the reflection coefficient) for layered media (not shown here). There are very few papers in the literature which present results using implementations of the matrix propagator solution – none are known to the author – perhaps this is why.

It is also clear that the solution derived here is a correct implementation of the matrix propagator method. This defines the reflection coefficient in terms of the equations presented above (2-57, 2-58, 2-56, 2-66, 2-41) and the individual layer matrix coefficients derived at Appendix 2B. Its validity is shown firstly in the fact that for single liquid / liquid and liquid / solid interfaces it predicts the same solutions as those derived earlier in chapter two using simpler standard developments in sections 2.2 and 2.3 to give equations (2-7), (2-8), (2-10) and (2-11). Its validity is shown secondly in the comparison against the analytical results presented by AINSLIE et al (1998) for scenarios with a sediment on top of a seabed basement, shown earlier in chapter 2 (at 2.5.6). The sediment was assumed to have an analytic sound speed profile and analytic sound speed attenuation profile: the matrix propagator code was run using 200 homogeneous layers, each with slightly different sound speed and attenuation. The excellent agreement shows the utility of the matrix propagator method as a benchmark code for any sediment with known geoacoustic profile.

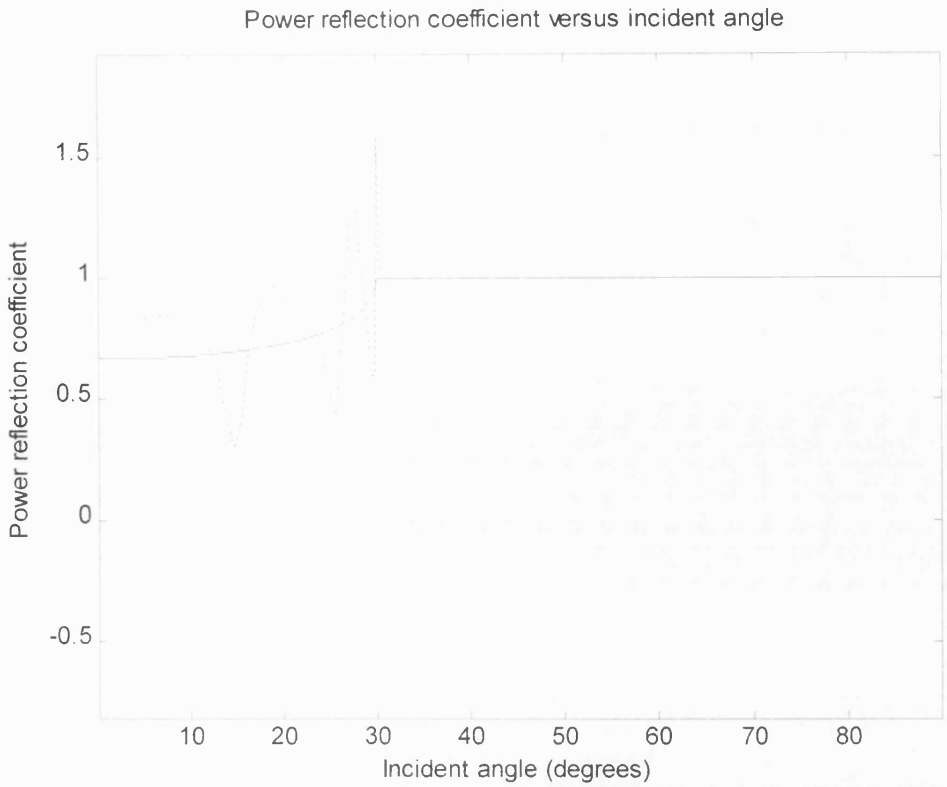

Figure 3: Power reflection coefficient versus incident angle for a simple liquid / liquid interface. The results shown are for incident sound at 800Hz from an upper liquid of density 1000kg/m^3 and sound speed 1500m/s. The lower liquid has a density of 5000kg/m^3 and a sound speed of 3000m/s. The two solutions presented are the matrix propagator method solution developed here (solid line) and the one given by BREKHOVSKIKH and GODIN (dotted). For this simple case the solutions may be compared with those developed earlier in chapter two using the simpler liquid / liquid interface results, equations (2-7) and (2-8). Clearly the matrix propagator method solution developed here (solid line) is perfectly correct: and the solution given by BREKHOVSKIKH and GODIN (dotted) is clearly wrong. Significantly, the BREKHOVSKIKH and GODIN (dotted) solution predicts a reflection coefficient which for some angles is greater than one: this is physically impossible, since it violates conservation of energy.

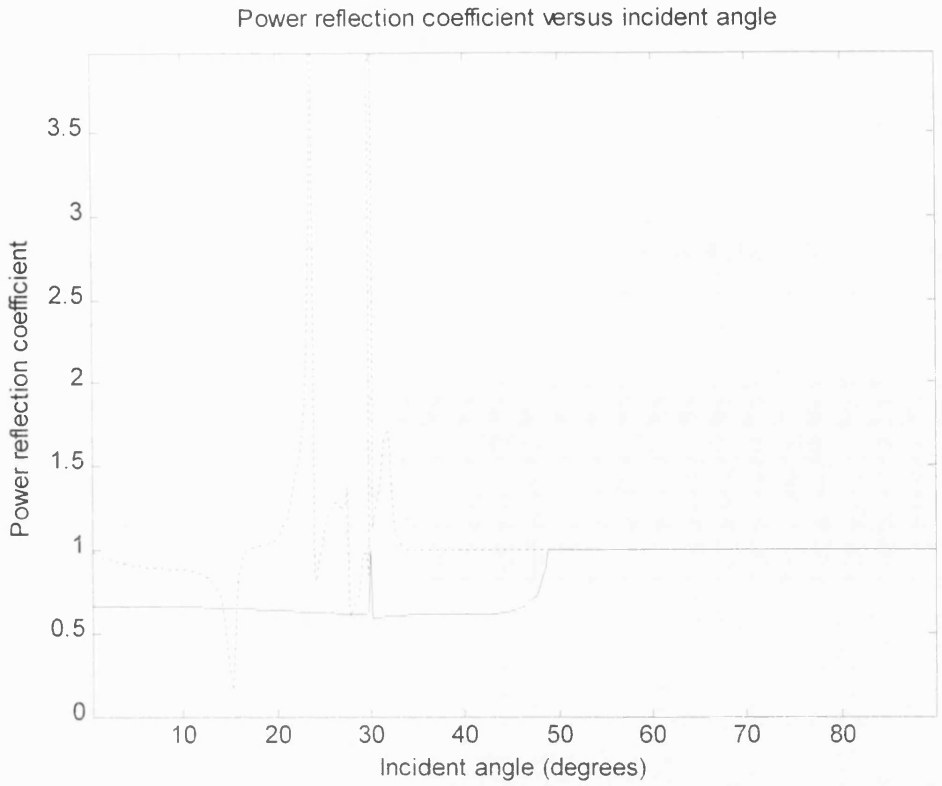

Figure 4: Power reflection coefficient versus incident angle for a simple liquid / solid interface. The results shown are for incident sound at 800Hz from an upper liquid of density 1000kg/m^3 and sound speed 1500m/s. The lower solid has a density of 5000kg/m^3, a sound speed of 3000m/s, and a shear wave speed of 2000m/s. The two solutions presented are the matrix propagator method solution developed here (solid line) and the one given by BREKHOVSKIKH and GODIN (dotted). For this simple case the solutions may be compared with those developed earlier in chapter two using the simpler liquid / solid interface results, equations (2-10) and (2-11). Clearly the matrix propagator method solution developed here (solid line) is perfectly correct: and the solution given by BREKHOVSKIKH and GODIN (dotted) is clearly wrong. Significantly, the BREKHOVSKIKH and GODIN (dotted) solution predicts a reflection coefficient which for some angles has peaks which are greater than one: this is physically impossible, since it violates conservation of energy. Adding layers to the seabed increases the number and magnitude of these peaks (not shown here). The attenuation was assumed to be zero here. Adding attenuation does not change the form of the solutions presented above, and the incorrect peaks remain well above one.

Appendix 2B

Continuing from equation (2-39) to calculate the matrix A. Firstly the inverse of [L] must be calculated. This requires finding the determinant of [L]. Much simple but laborious algebra yields:

$$|L| = -4\alpha\beta\rho^2\omega^4 \qquad 2\text{-}70$$

The co-factors of [L] are then found and the inverse matrix constructed (remember + and - signs on the co-factors and also remember to swap rows and columns). This is found to be given by:

$$[L]^{-1} = \frac{-1}{2\alpha\beta\omega^2\rho}\begin{bmatrix} 2i\mu\xi\alpha\beta & -2i\mu\xi\beta\gamma & \alpha\beta & \xi\beta \\ 2i\mu\xi\alpha\beta & 2i\mu\xi\beta\gamma & \alpha\beta & -\xi\beta \\ 2i\mu\xi\alpha\gamma & 2i\mu\xi\alpha\beta & \xi\alpha & -\alpha\beta \\ -2i\mu\xi\alpha\gamma & 2i\mu\xi\alpha\beta & -\xi\alpha & -\alpha\beta \end{bmatrix} \qquad 2\text{-}71$$

and can be verified by checking $[L][L]^{-1} = [I]$.

The elements of $[A^{(j)}]$ can now be found relatively quickly. From equation (2-39) the elements of $[A^{(j)}]$ are given by:

$$A^{(j)} = \begin{bmatrix} i\xi & i\xi & -i\beta & i\beta \\ i\alpha & -i\alpha & i\xi & i\xi \\ 2\mu\xi\gamma & 2\mu\xi\gamma & -2\mu\xi\beta & 2\mu\xi\beta \\ -2\mu\xi\alpha & 2\mu\xi\alpha & -2\mu\xi\gamma & -2\mu\xi\gamma \end{bmatrix}\begin{bmatrix} 2i\mu\xi\alpha\beta a & -2i\mu\xi\beta\gamma a & \alpha\beta a & \xi\beta a \\ 2i\mu\xi\alpha\beta a^{-1} & 2i\mu\xi\beta\gamma a^{-1} & \alpha\beta a^{-1} & -\xi\beta a^{-1} \\ 2i\mu\xi\alpha\gamma b & 2i\mu\xi\alpha\beta b & \xi\alpha b & -\alpha\beta b \\ -2i\mu\xi\alpha\gamma b^{-1} & 2i\mu\xi\alpha\beta b^{-1} & -\xi\alpha b^{-1} & -\alpha\beta b^{-1} \end{bmatrix}\frac{-1}{2\alpha\beta\omega^2\rho} \qquad 2\text{-}72$$

Again, much laborious but simple algebra yields the coefficients of the propagator matrix A:

$a_{11} = 2\sin^2\theta_t\cos P + \cos 2\theta_t\cos Q$

$a_{12} = i(\tan\theta_L\cos 2\theta_t\sin P - \sin 2\theta_t\sin Q)$

$a_{13} = i\sin\theta_t(\cos Q - \cos P)/\omega\rho c_t$

$a_{14} = (\tan\theta_L\sin\theta_t\sin P + \cos\theta_t\sin Q)/\omega\rho c_t$

$a_{21} = i(2\cot\theta_L\sin\theta_t\sin P - \tan\theta_t\cos 2\theta_t\sin Q)$

$a_{22} = \cos 2\theta_t\cos P + 2\sin^2\theta_t\cos Q$

$a_{23} = (\cot\theta_L \sin\theta_t \sin P + \sin\theta_t \tan\theta_t \sin Q)/\omega\rho c_t$

$a_{24} = a_{13}$

$a_{31} = -2i\omega\rho c_t \sin\theta_t \cos 2\theta_t (\cos Q - \cos P)$

$a_{32} = -\omega\rho c_t (\tan\theta_L \cos^2 2\theta_t \sin P + \sin^2 2\theta_t \tan\theta_t \sin Q)/\sin\theta_t$

$a_{33} = a_{32}$

$a_{34} = a_{12}$

$a_{41} = -\omega\rho c_t (4\cot\theta_L \sin^3\theta_t \sin P + (\cos^2 2\theta_t/\cos\theta_t)\sin Q)$

$a_{42} = a_{31}$

$a_{43} = a_{21}$

$a_{44} = a_{11}$ 2-73

where:

$P=\alpha(z_j - z_{j-1})$ and $Q=\beta(z_j - z_{j-1})$; $\alpha=(\omega/c_L)\cos\theta_L$ $\beta=(\omega/c_t)\cos\theta_t$ 2-74.

The ratio of the transmitted shear to compressional wave amplitudes (W_t/W_L) is given by q = Numerator/Denominator where:

$\text{Numerator} = a_{41} - a_{42}\cot\theta_L + ia_{43}\mu k_t \cos 2\theta_t \sin^{-1}\theta_t - 2a_{44} i\mu k_t \sin\theta_t \cot\theta_L$ 2-75

$\text{Denominator} = -a_{41}\cot\theta_t - a_{42} + 2ia_{43}\mu k_t \cos\theta_t + ia_{44}\mu k_t \cos 2\theta_t \sin^{-1}\theta_t$ 2-76.

The transmitted compressional wave amplitude is given by:

$$W_L = -2\omega^2\rho\cot\theta_L\{(\omega^2\rho a_{21} + i\alpha a_{31})(1 + q\cot\theta_t) + (\omega^2\rho a_{22} + i\alpha a_{32})(q - \cot\theta_L) + \mu k_t \cos 2\theta_t \sin^{-1}\theta_t [(i\omega^2\rho a_{23} - \alpha a_{33})(1 - q\tan 2\theta_t) - (i\omega^2\rho a_{24} - \alpha a_{34})(q + 2\sin^2\theta_t \cot\theta_L / \cos 2\theta_t)]\}^{-1}$$ 2-77.

3 Scattering from a rough surface

In this chapter the theories concerning the scattering of waves from a rough surface will be examined. In the first three sections, the ways in which surface roughness may be described are discussed, and the large and small scale roughness limits are examined. In the last three sections, the mathematics required to cope with the rough surface boundary conditions and rough surface power spectra, used in chapters 4 and 5, are developed. This is based on standard scattering theory (see BREKHOVSKIKH and LYSANOV 1990)) but extended here to be applicable to the new development shown in chapters 4 and 5.

3.1 Describing a rough surface

There are many ways of describing a rough surface, each with advantages and disadvantages depending on the type of data being collected or theory being developed. OGILVY (1992) discusses many of these, the most useful for the purposes of this thesis being the surface power spectrum (or "power spectral density") discussed later.

3.1.1 The Rayleigh parameter

It is very important, when considering the rather subjective idea of "roughness" to be aware of the physical scales of the waves and the surface which are interacting. In this regard, the Rayleigh parameter is, perhaps, the single most useful value which is used to provide a yardstick for the roughness of a surface (BREKHOVSKIKH and LYSANOV (1990)). In Figure 1 consider the difference between a specular reflection from a rough surface (ray 1) and a specular reflection from a smooth surface (ray 2).

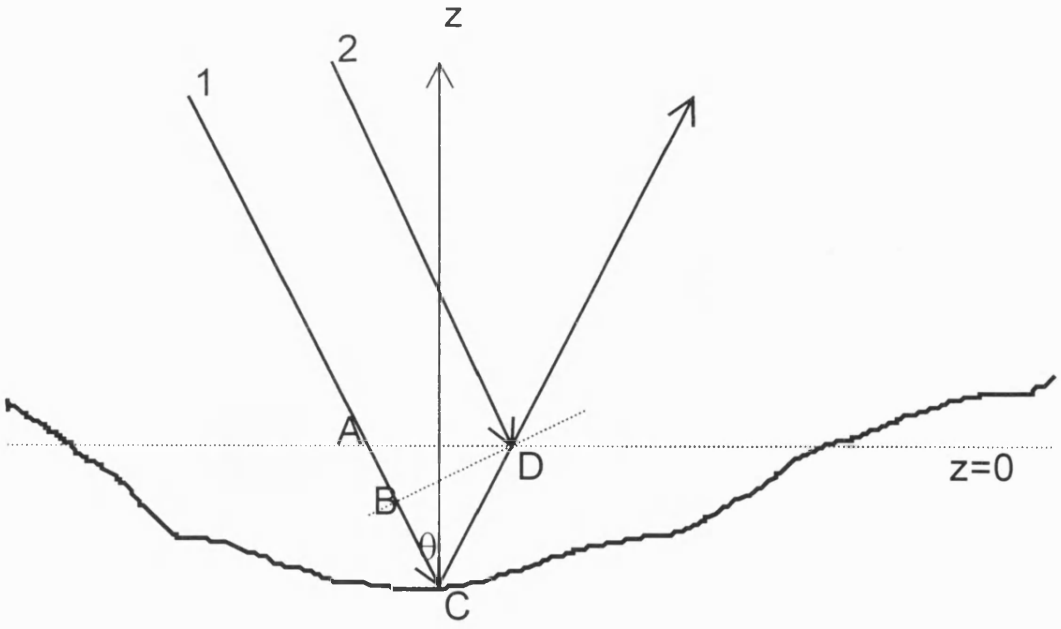

Figure 1: To show the phase difference between a ray reflected from a rough surface and one reflected from a smooth surface.

By comparing the paths of rays 1 and 2 the phase difference, $\Delta\phi$, is seen to be given by

$$\Delta\phi = 2kh\cos\theta \qquad 3\text{-}1$$

where h is the depth at the point C relative to the mean surface at z=0; k is the wavenumber of the incoming sound and θ is the incident angle of the incoming sound. The root mean square value of $\Delta\phi$ over the rough surface is given by P, the Rayleigh parameter, where

$$P=2k\sigma\cos\theta \qquad 3\text{-}2$$

and σ is the root mean square surface height deviation. The Rayleigh parameter is, therefore, a measure of the average phase difference a rough surface will make to a ray reflecting from its surface as compared to a flat surface[1]. For P much less than 1 (the criterion $P << \pi/4$ is also often used) the roughness of the surface is said to be small. The surface produces only slight scattering and most of the sound energy propagates coherently in the specular direction. For P much less than 1, then the limit on the surface root mean square height deviation is:

$$\sigma << \lambda/4\pi\cos\theta \qquad 3\text{-}3$$

In the code used for the Gaussian power spectrum (see chapter 7) the value of σ is taken to be given by:

$$\sigma = 0.01\ \lambda/4\pi \qquad 3\text{-}4$$

thus fulfilling the requirement for small roughness. A value of P much greater than 1 generally indicates large scale roughness. For this case considerable incoherent scattering occurs over a relatively wide angular interval.

3.1.2 Rough surface statistics

It is assumed in most rough surface scattering studies that whatever analytic function is used to describe the seabed is valid for the whole of the seabed, i.e. that the surface shows stationarity and ergodicity (see VORONOVICH). This amounts to saying that the same surface roughness function represents the statistical properties of any part of the surface, and further, that spatial averaging and ensemble averaging give the same measured statistics. Thus the height distribution of the surface is represented in a general sense, without describing any particular *features* of any particular surface. This methodology

[1] THORSOS (1988) also uses $P=2kR\cos^3\theta$, where R is the local radius of curvature of the rough surface. This gives a greater range on the validity of perturbation theory.

is not suitable, therefore, for studying scattering caused by discrete objects on the seabed, (see FAWCETT et al., HWANG, MAST et al). Nor is it suitable for studying areas of surfaces which are comparable in size to the largest feature within that area. OGILVY suggests that the length of any surface from which scattering measurements are to be made should be at least ten times the surface roughness correlation length. Rippled seabeds are well within the capability of the approach used here (the power spectral density would have one dominant component), though this special case is best studied as such (see SCHMIDT and LEE).

The implications of the above requirements on the types of surfaces which can be studied are quite subtle. Surfaces which are modelled as power laws have the same rough "appearance" at all scales, they are fractal. As such, they have infinite power and infinite correlation length, and so do not fit with the ideas of stationarity discussed above. In practice, any specific feature can be represented by a power law, and there will always be features on the scale of the surface measured, and so there will not be any ergodicity. Also, in practice, no surface will be truly fractal. And, again also in practice, no surface will ever be measured as completely fractal since it is only measured to a certain scale. The apparent problem with the infinite power is no longer, since the integral over surface wavenumber is only over a finite range. A fractal surface, implied by a power law, seems reasonable enough if it is realised that the power law, or "fractal-ness" only covers a specific range of spatial scales. Less intuitive is the approach taken by QIAN, who constructs a "generalised fractal" surface and derives its scattering strength.

3.1.3 Rough surface realisations and phase

It is true, however, that the approach to describing a surface by means of a power spectrum with analytic correlation length and mean square surface height deviation yields a convenient, but incomplete, picture of the surface. This is true regardless of the type of power spectrum used. A more complete description of a surface must include what LUPIEN refers to as "scale structure". That is, information about the sizes of actual features of the rough surface, if there are any. These features are the spurious odd parts of the surface which prevent the surface from looking isotropically rough, and prevent the apparent statistics of the surface from being stationary. In fact, the statistics of the surface as a whole may be stationary. The parameters which always change with position over a rough surface are the relative phases of the *amplitude* spectral components of the surface. It is these phases which coherently add to produce the rough surface. It is also these phases which are omitted in the power spectrum description of the surface, since each power spectral component is the square of the magnitude of each amplitude spectral component. The scale structure, then, reveals how the phases of the amplitude spectral components have combined locally (i.e. where the surface is being sampled, or observed) to create visible features.

Clearly the phase of each amplitude spectral component will affect the scattering in a significant way, since the phase will affect how that amplitude spectral component interacts

with an incident plane wave. During resonance scattering (see later) the outgoing horizontal wavevector, k_{out}, is simply the sum of the incident horizontal wavevector, k_{in}, and the surface wavevector, κ. A phase difference of 180° in the surface amplitude spectral component is the difference between the outgoing wavevector being given by

$$k_{out} = k_{in} + (+\kappa) \qquad 3\text{-}5$$

and

$$k_{out} = k_{in} + (-\kappa) \qquad 3\text{-}6$$

For large enough κ this can be the difference between forward and backward scattering. This is very intuitive – think of a tennis ball thrown down to bounce off a corrugated surface, where the corrugated grooves are perpendicular to the radial direction the ball has come from. It only takes a shift of the corrugated surface to change what would have been a bounce forward off the surface to be a bounce back. Also, if the corrugations were very gradual (i.e. κ small), then the ball would always bounce forward.

LUPIEN concludes that the power spectrum is dominant in affecting the mean scattering strength in the back quadrant and that the scale structure affects the amount of forward scatter and feature-like behaviour. It will be shown in chapters 4 and 5 that the scattered pressure can be derived in terms of the surface spectral amplitude: they are calculated without regard for phase initially, then in chapter 6 it is shown how the phases are included.

3.2 Large scale roughness

For surfaces which, relative to the incident sound's wavelength, have power spectra dominated by low frequency components, a large scale roughness approximation is used. In this case the surface is locally smooth and only undulating "slowly". This is the same as saying that the surface correlation length is large compared to the incident sound wavelength. For these surfaces it is reasonable to assume that the surface is locally flat, and that the smooth surface reflection coefficient can be used to calculate the field scattered from the local surface. The scattered solution is written as an integral over the local reflected solutions, each local reflected solution taking into account the incident angle of the sound and the local gradient of the rough surface (see BREKHOVSKIKH and LYSANOV).

In writing the solution as an integral equation over all the surface, it is assumed that all points on the surface interact directly with the incident wave. This may not be true at low grazing angles. Even at higher grazing angles, the integral equation solution assumes that the incident wave scatters only once from any point on the surface. In other words, no sound scatters from the surface back towards another point on the surface, to be re-scattered. Such assumptions lead to careful consideration of the regimes of validity of this approach

(see DeSANTO and MARTIN), particularly for when the observation point is not above the highest point on the surface (see PURCELL). For most practical naval applications, where the receiving array is far from the rough surface, the applicability of this large scale roughness (or Kirchhoff) approach is governed mainly by the relative scale of the roughness to the incident sound wavelength (see THORSOS (1988)).

3.3 Small scale roughness

For surfaces which, relative to the incident sound's wavelength, have only small deviations from the mean plane, a small scale approximation is used, called the method of small perturbations. For such surfaces, as well as the surface height being small, it is also assumed that the surface correlation length is small compared to the incident wavelength. In the standard theory, presented here for comparison with the new methods developed in chapters 4 and 5, it is generally assumed that the medium from which the sound is scattering has density and sound speed which approach one of two limits. The first is the limit of zero sound speed and density. This is the Dirichlet boundary condition. The second is the Neumann boundary condition, when the limits of infinite sound speed and density are assumed.

In the method of small perturbations the particular boundary conditions imposed (Dirichlet or Neumann) on the rough surface are transferred to a smooth mean plane (z=0) by expanding them as a power series in a small surface roughness parameter $\zeta(\underline{r})$. Similarly the theoretical smooth plane sound field in the half space $z>\zeta$ is expanded in powers of ζ and the (transferred rough surface) conditions which must be satisfied by successive approximations at the mean surface are found. These equations are solved to give the sound field to various levels of approximation. Usually the theoretical smooth plane sound field is assumed to be due to a surface with a reflection coefficient of magnitude unity (known reflection coefficient solutions, constant with incident angle, for the Dirichlet or Neuman boundary conditions).

The solution for the Dirichlet, or "pressure release" boundary condition is reviewed here for comparison with the new methods developed in chapters 4 and 5. For a flat pressure release surface the boundary condition is that the total pressure is zero:

$$p = 0 \qquad 3\text{-}7$$

Expanding the boundary condition for a rough surface, in terms of the local height deviation from the mean, ζ, gives:

$$p + \zeta \frac{\partial p}{\partial z} = 0 \qquad 3\text{-}8$$

The pressure field is defined as the sum of a zero order term and a first order scattered term

$$p = p_0 + p_s \qquad 3\text{-}9$$

and hence on the mean plane (z=0) :

$$p_0 = 0 \qquad 3\text{-}10$$

and

$$p_s = -\zeta \frac{\partial p_0}{\partial z} \qquad 3\text{-}11$$

The solution for p_0 is then taken to be given by the sum of the incident wave and the reflected wave, which for a pressure release surface has an amplitude of –1 relative to the incident wave

$$p_0 = e^{i\underline{\xi}_0 \cdot \underline{r}}\left(e^{-i\gamma_0 z} - e^{i\gamma_0 z}\right) \qquad 3\text{-}12$$

where: ξ_0 is the horizontal component of the incident wavevector, and, from Snell's law, the horizontal component of the specularly reflected wavevector; $-\gamma_0$ is the vertical component of the incident wavevector; and $+\gamma_0$ is the vertical component of the specularly reflected wavevector.

For the new method shown in chapters 4 and 5, the –1 will be replaced by a V, the reflection coefficient. Also, the V will be a function of the incident angle: for the pressure release surface the reflection coefficient of –1 is true for all incident angles. Hence the solution for p_s at z=0 is found and a factor of $\exp(i\gamma z)$ then gives the solution for all z. This is:

$$p_s(\underline{r}, z) = 2i\gamma_0 \zeta(\underline{r}) \exp\left(i\underline{\xi}_0 . \underline{r} + i\gamma z\right) \qquad 3\text{-}13$$

where γ is the vertical component of the scattered reflected wavevector. [Further details on the horizontal and vertical components of the scattered wavevectors are given in chapter 4, see section 4.4.1.]

At this stage the surface parameter $\zeta(\underline{r})$ is written in terms of the Fourier transform of the surface wavenumber amplitude spectrum, giving

$$p_s(\underline{r}, z) = \frac{1}{2\pi} 2i\gamma_0 \int_{-\infty}^{\infty} A(\underline{\kappa}) \exp\left[i\left(\underline{\xi}_0 + \underline{\kappa}\right)\underline{r} + i\gamma z\right] d\underline{\kappa} \qquad 3\text{-}14$$

where $A(\kappa)$ is the rough surface spectral amplitude. The surface height $\zeta(\underline{r})$ and the rough surface spectral amplitude $A(\kappa)$ are a Fourier transform pair defined by

$$\zeta(r) = \frac{1}{2\pi} \int_{-\infty}^{\infty} A(\kappa) \exp(i\kappa r) d\kappa$$

$$A(\kappa) = \int_{-\infty}^{\infty} \zeta(r) \exp(-i\kappa r) dr$$

[This is discussed in detail in section 3.5.1 and is used in chapter 4, section 4.4.1.]

The $2i\gamma_0$ in equation (3-14) is a constant term with respect to the integral over κ, since it depends only on the geoacoustic properties of the interface, and so can be taken inside the integral. Hence we now have

$$p_s(\underline{r}, z) = \frac{1}{2\pi} \int_{-\infty}^{\infty} (2i\gamma_0) A(\underline{\kappa}) \exp\left[i\left(\underline{\xi_0} + \underline{\kappa}\right)\underline{r} + i\gamma z\right] d\underline{\kappa} \qquad 3\text{-}15$$

The scattered pressure is therefore an integral over a function which is a product of the surface amplitude spectrum, a geoacoustics term ($2i\gamma_0$), and an exponential function which determines the scattering directions. For each scattering direction the horizontal wavevector may now be given by ξ, which is the sum of the incident horizontal wavevector, ξ_0, and a particular value of the surface wavenumber κ This is called *resonance scattering*:

$$\xi = \xi_0 + \kappa \qquad 3\text{-}16$$

Note that equation 3- 15 is for a z axis pointing upwards. For a z axis pointing downwards, consistent in direction with the one used later (chapters 4, 5) this expression becomes:

$$p_s(\underline{r}, z) = \frac{1}{2\pi} \int_{-\infty}^{\infty} (-2i\gamma_0) A(\underline{\kappa}) \exp\left[i\left(\underline{\xi_0} + \underline{\kappa}\right)\underline{r} - i\gamma z\right] d\underline{\kappa} \qquad 3\text{-}17$$

In the new method presented in the next two chapters a departure from this standard method is taken in the solution for p_0. When solving the general case of reflection at a smooth boundary one has *two* boundary conditions: continuity of pressure (i.e. Newton's third law) and continuity of particle displacement (i.e. no net transfer of particles from one medium to the other). From these two boundary conditions two unknowns are calculated: the reflection and transmission coefficients; and these are functions of the incident angle. For special cases where the density of the second medium is infinite or zero the results for the reflected and transmitted waves are simple: the reflected wave has amplitude ± 1

respectively and the transmitted wave has zero amplitude, for all incident angles. These two cases are often described as having Neuman or Dirichlet "boundary conditions" (respectively) however it must be remembered that these are not the *boundary conditions* used to solve the general case.

3.4 Co-ordinate transformations

3.4.1 Co-ordinate transformations in 1 dimension

To solve the scattering problem for a rough surface with elastic boundary conditions the elastic boundary condition equations must be written in terms of the rough surface co-ordinates, rather than the cartesian co-ordinates of x and z. Generalising the approach used by BREKHOVSKIKH (1990), consider the rough surface shown below (Figure 2) in which the local surface unit normal vector, $\underline{n}$ and unit tangent vector, $\underline{s}$ are shown, as well as the vertical and horizontal components of the unit normal vector, $\underline{n}_z$ and $\underline{n}_\perp$ respectively.

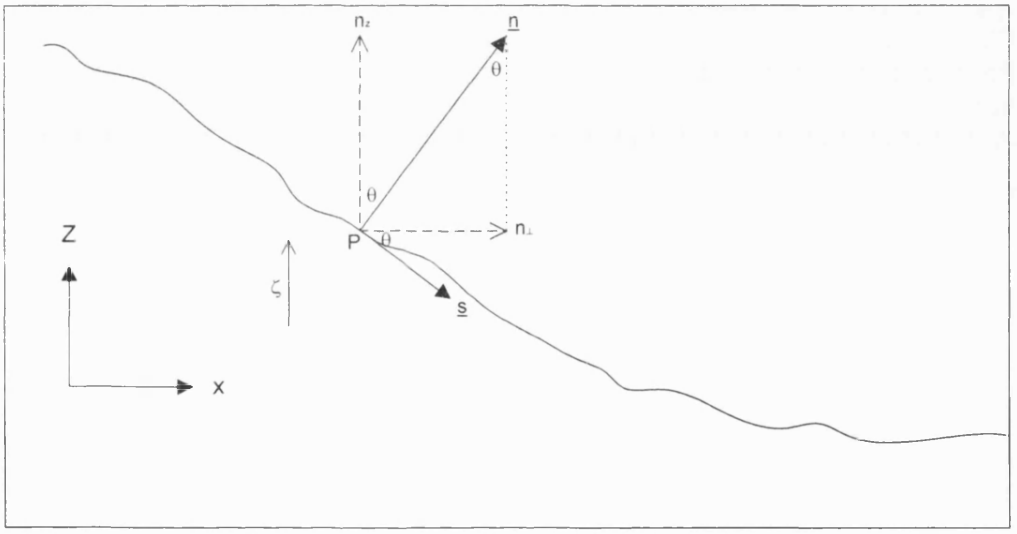

Figure 2: Geometry for the co-ordinate transformations required for a rough interface.

The axes normal and parallel to the surface, n and s[2], respectively, are given by

$$n = z\cos\theta + x\sin\theta$$
$$s = -z\sin\theta + x\cos\theta \qquad \text{3- 18}$$

or equivalently

[2] The s axis is assumed here to be in the xz plane, though in principal could be anywhere in the plane perpendicular to n.

$$z = n\cos\theta - s\sin\theta$$
$$x = n\sin\theta + s\cos\theta \qquad \text{3- 19}$$

Now for ϕ, which is a function of both n and s, its normal derivative is given by

$$\frac{\partial\phi}{\partial n} = \frac{\partial\phi}{\partial x}.\frac{\partial x}{\partial n} + \frac{\partial\phi}{\partial z}.\frac{\partial z}{\partial n} \qquad \text{3- 20}$$

hence

$$\frac{\partial\phi}{\partial n} = \frac{\partial\phi}{\partial x}.\sin\theta + \frac{\partial\phi}{\partial z}.\cos\theta \qquad \text{3- 21}$$

and so

$$\frac{\partial}{\partial n} = \sin\theta\frac{\partial}{\partial x} + \cos\theta\frac{\partial}{\partial z} \qquad \text{3- 22}$$

since θ is an independent variable.

Similarly

$$\frac{\partial\phi}{\partial s} = \frac{\partial\phi}{\partial x}.\frac{\partial x}{\partial s} + \frac{\partial\phi}{\partial z}.\frac{\partial z}{\partial s} \qquad \text{3- 23}$$

hence

$$\frac{\partial\phi}{\partial s} = \frac{\partial\phi}{\partial x}.\cos\theta + \frac{\partial\phi}{\partial z}.(-\sin\theta) \qquad \text{3- 24}$$

and so

$$\frac{\partial}{\partial s} = \cos\theta\frac{\partial}{\partial x} - \sin\theta\frac{\partial}{\partial z} \qquad \text{3- 25}$$

From equations (3- 22) and (3- 25) the second derivatives are found:

$$\frac{\partial^2}{\partial n^2} = \sin^2\theta\frac{\partial^2}{\partial x^2} + \cos^2\theta\frac{\partial^2}{\partial z^2} + 2\sin\theta\cos\theta\frac{\partial^2}{\partial x\partial z} \qquad \text{3- 26}$$

$$\frac{\partial^2}{\partial s^2} = \cos^2\theta \frac{\partial^2}{\partial x^2} + \sin^2\theta \frac{\partial^2}{\partial z^2} - 2\sin\theta\cos\theta \frac{\partial^2}{\partial x \partial z} \qquad 3\text{-}27$$

$$\frac{\partial^2}{\partial n \partial s} = \sin\theta\cos\theta\left(\frac{\partial^2}{\partial x^2} - \frac{\partial^2}{\partial z^2}\right) + \left(\cos^2\theta - \sin^2\theta\right)\frac{\partial^2}{\partial x \partial z} \qquad 3\text{-}28$$

The equations for the partial derivatives with respect to n and s are now in terms of x, z, and θ and are simply a co-ordinate conversion, for which at any point, θ is constant. Over the rough surface, however, θ varies, and so it is useful to express it in terms of the local surface gradient. If the height above the mean surface (z=0) is given by ζ then the local surface gradient is given by:

$$\frac{\partial \zeta}{\partial x} = \frac{-\sin\theta}{\cos\theta} \qquad 3\text{-}29$$

The equations for the partial derivatives may now be written as

$$\frac{\partial}{\partial n} = \cos\theta\left(\frac{\partial}{\partial z} - \frac{\partial \zeta}{\partial x}\frac{\partial}{\partial x}\right) \qquad 3\text{-}30$$

$$\frac{\partial}{\partial s} = \cos\theta\left(\frac{\partial}{\partial x} + \frac{\partial \zeta}{\partial x}\frac{\partial}{\partial z}\right) \qquad 3\text{-}31$$

$$\frac{\partial^2}{\partial n^2} = \cos^2\theta\left(\frac{\partial^2}{\partial z^2} - 2\frac{\partial \zeta}{\partial x}\frac{\partial^2}{\partial x \partial z}\right) \qquad 3\text{-}32$$

$$\frac{\partial^2}{\partial s^2} = \cos^2\theta\left(\frac{\partial^2}{\partial x^2} + 2\frac{\partial \zeta}{\partial x}\frac{\partial^2}{\partial x \partial z}\right) \qquad 3\text{-}33$$

$$\frac{\partial^2}{\partial n \partial s} = \cos^2\theta\left(\frac{\partial^2}{\partial z \partial x} - \frac{\partial \zeta}{\partial x}\left(\frac{\partial^2}{\partial x^2} - \frac{\partial^2}{\partial z^2}\right)\right) \qquad 3\text{-}34$$

where the higher order terms containing $\left(\frac{\partial \zeta}{\partial x}\right)^2$ terms have been neglected since it is assumed that ζ is small.

These equations for the first and second partial derivatives, with respect to the surface normal and with respect to the surface tangent, are the co-ordinate transformation equations which will be used in chapters 4 and 5. They will be used to re-state the boundary

condition equations for the rough surface back into a form dependent upon Cartesian co-ordinates and the rough surface amplitude ζ. It will be seen that these boundary condition equations will be such that the cosine and cosine squared terms will occur on both sides, and so cancel out.

3.4.2 Co-ordinate transformations in 2 dimensions

For a 2 dimensional treatment of the scattering problem the situation is as shown in Figure 2. The vertical component of the surface normal stays the same, the difference now is that the horizontal component has both x and y components, since it is no longer constrained to the (x,z) plane. Similarly, the vector, $\underline{s}$, parallel to the surface now has both x and y components. The unit vectors normal and parallel to the surface, $\underline{n}$ and $\underline{s}$ respectively, shown in Figure 2 are now given by

$$\begin{aligned} \underline{n} &= \left(\underline{n}_\perp, n_z\right) \\ \underline{s} &= \left(n_z, -\left|\underline{n}_\perp\right|\right) \end{aligned} \qquad 3\text{-}35$$

where $\underline{n}.\underline{s} = 0$. Note that the unit vector parallel to the surface may be in any direction on the plane perpendicular to the surface normal, $\underline{n}$. With the vector $\underline{s}$ written above, its x and y components are not specified uniquely, but together have magnitude equal to n_z. For simplicity, without loss of generality, it may be assumed that the y component of $\underline{s}$ is zero. These equations are the 2 dimensional equivalent of equations (3- 18) derived for the 1 dimensional earlier. A horizontal derivative shorthand is now defined by

$$\nabla_\perp \zeta = \frac{-n_\perp}{n_z} = \left(\frac{\partial}{\partial x}, \frac{\partial}{\partial y}\right)\zeta \qquad 3\text{-}36$$

Finally, the derivative of any function, f, with respect to a vector, can be defined as the dot product of the gradient of the function and the vector, hence

$$\frac{\partial f}{\partial n} = \left(\underline{\nabla f} \bullet \underline{n}\right) = \left(\underline{\nabla_\perp f}, \frac{\partial f}{\partial z}\right) \bullet \left(\underline{n}_\perp, n_z\right)$$

$$\frac{\partial f}{\partial s} = \left(\underline{\nabla f} \bullet \underline{s}\right) = \left(\underline{\nabla_\perp f}, \frac{\partial f}{\partial z}\right) \bullet \left(n_z, -\left|\underline{n}_\perp\right|\right) \qquad 3\text{-}37$$

This pair of equations for the 2 dimensional case is the equivalent of equations (3- 20) and (3- 23) for the 1 dimensional case. Using equation (3- 36) to substitute for $n_\perp$ the normal and surface derivatives are found to be given by

$$\frac{\partial}{\partial n} = n_z\left(-\underline{\nabla_\perp \zeta}.\underline{\nabla_\perp} + \frac{\partial}{\partial z}\right)$$

$$\frac{\partial}{\partial s} = n_z\left(\underline{\hat{x}}.\underline{\nabla_\perp} - \left|\underline{\nabla_\perp \zeta}\right|\frac{\partial}{\partial z}\right) \qquad 3\text{- }38$$

where

$\underline{\hat{x}}$ = unit vector in the x direction 3- 39

These equations for the 2 dimensional normal and surface derivatives are the equivalent of equations (3- 22) and (3- 25) for the 1 dimensional case. Apart from notation, the only real difference is that there is now also a derivative with respect to the y direction, brought in through equation (3- 36). The second derivatives are found by straightforward manipulations of the equations (3- 38). The application of the 2 dimensional co-ordinate transformations to the boundary condition equations is, again, straightforward, though involves much more algebra. For this reason the new developments shown in chapters 4 and 5 are for the 1 dimensional case, using the 1 dimensional co-ordinate transformation equations (3- 30) to (3- 34). It should be noted that for the 2 dimensional case exactly the same physical principles apply as for the 1 dimensional case, the only difference is that the equations become more complicated. For the 2 dimensional case, to be consistent, the power spectrum must also be two dimensional (see 3.5.4), as must the scattering coefficient (see 3.6) and the incident sound beam (see chapter 6).

3.5 The rough surface power spectral density

In this section the roughness of a surface is discussed in terms of its power spectral density, PSD, (often referred to as simply the "power spectrum"), for both the 1 dimensional and 2 dimensional regimes. The power spectral densities used to derive the scattering results shown in chapter 6 will be derived and compared here. For both the Gaussian spectrum, and the one used by THORSOS (1999), the importance of the ratio of the wavelength of the sound to the roughness statistics of the surface will be highlighted.

3.5.1 Roughness in 1 dimension

The amplitude, or height, of a rough surface relative to its mean (assumed to be at height ζ=0) may be given by $\zeta(x)$, where x is the distance from an arbitrary origin. Alternatively the surface height distribution may be thought of in terms of its Fourier components $A(\kappa)$:

$$\zeta(x) = \frac{1}{2\pi} \int_{-\infty}^{\infty} A(\kappa) \exp(i\kappa x) d\kappa \,. \qquad 3\text{-}40$$

Each of the components, $A(\kappa)$, is a sinusoidal wave of a particular spatial frequency and amplitude. In this case the surface is represented by an amplitude spectrum $A(\kappa)$, which defines the amplitude of the sinusoidal component with wavelength $2\pi/\kappa$.

In order to find the total power associated with the rough surface the square of the surface height function is integrated over all x. From Parseval's theorem (see RILEY) it is known that this gives the same result as integrating $\frac{1}{2\pi} |(A(\kappa)|^2$ over all κ:

$$\int_{-\infty}^{\infty} \zeta^2(x) dx = \frac{1}{2\pi} \int_{-\infty}^{\infty} A^2(\kappa) d\kappa = TotalPower = \sigma^2 N \qquad 3\text{-}41$$

where σ is the surface height standard deviation (or the root mean square surface height if the mean height is set to zero) and where N is the number of height samples taken. More useful than the total power is a "power" which is normalised with respect to the sample size. Such a "power" function may be derived from the surface correlation function. Firstly, it is noted from the Wiener Khinchine theorem [see PRESS et al.] that the Fourier transform of surface autocovariance function is equal to the square of the amplitude spectrum:

$$\int_{-\infty}^{\infty} \exp(-i\kappa x) \left[\int_{-\infty}^{\infty} \zeta(X + x) \zeta(X) dX \right] dx = A^2(\kappa) \qquad 3\text{-}42$$

where the autocovariance function is in the square brackets. If there are N samples of the surface height, $\zeta(x)$, then the value of the autocovariance function at x=0 is simply $\sigma^2 N$, since the autocovariance function reduces to the total power equation above. If a surface correlation function, C(x), is defined by

$$C(x) = \frac{1}{\sigma^2 N} \left[\int_{-\infty}^{\infty} \zeta(X + x) \zeta(X) dX \right] \qquad 3\text{-}43$$

then this is normalised such that it has a maximum value of 1 at x=0. Re-arranging this gives:

$$C(x)\sigma^2 = \frac{1}{N} \left[\int_{-\infty}^{\infty} \zeta(X + x) \zeta(X) dX \right] \qquad 3\text{-}44$$

Taking the Fourier transform of both sides of this equation leads to the result that the Fourier transform of σ^2 times the correlation function is equal to the power spectral density:

$$FT\left[C(x)\sigma^2\right] = \int_{-\infty}^{\infty} \exp(-i\kappa x)\frac{1}{N}\left[\int_{-\infty}^{\infty}\zeta(X+x)\zeta(X)dX\right]dx = \frac{1}{N}A^2(\kappa) \qquad 3\text{-}45$$

where $A^2(\kappa)/N$ is the power spectral density. From the total power equation above (equation (3- 41)) it is clear that the integral of the power spectral density over all κ is equal to $2\pi\sigma^2$.

It is now clear how to define a power spectral density: a surface correlation function, C(x) is defined, or measured, which is normalised such that it has a maximum value of 1 at x=0; the power spectral density is then simply the Fourier transform of $\sigma^2 C(x)$. In practice, this allows a functional form for the autocorrelation function to be assumed, the autocorrelation function to be measured and its parameters evaluated, and then a surface power spectrum to be derived from it. More specifically, if it is assumed that the autocorrelation function for the surface is a Gaussian decay with range r, then one can experimentally determine the surface correlation length λ_x. From this an explicit form for the surface power spectrum can be derived.

3.5.2 Gaussian Power Spectral Density

If the autocorrelation function, $C(x)$, is given by a Gaussian envelope

$$C(x) = \exp\left(-\frac{x^2}{\lambda_x^2}\right) \qquad 3\text{-}46$$

where λ_x is the surface correlation length, then the power spectral density is given by the Fourier transform

$$P(\kappa) = \sigma^2 \int_{-\infty}^{\infty} \exp\left(-i\kappa x - \frac{x^2}{\lambda_x^2}\right)dx \qquad 3\text{-}47$$

which is easily evaluated to give

$$P(\kappa) = \sigma^2 \pi^{0.5} \lambda_x \exp\left(-\frac{\kappa^2 \lambda_x^2}{4}\right) \qquad 3\text{-}48$$

This is the form of the Gaussian power spectral density used to generate the results shown in chapter 6. It can be seen that this power spectral density function depends upon both the

mean square surface height deviation and upon the surface correlation length.

3.5.3 Thorsos Power Spectral Density

The scattering code algorithms (described in chapters 4 and 5) are verified mathematically against standard expressions and limiting cases. They are also validated against the results described by THORSOS (1999), though for this comparison the power spectral density used is not a Gaussian one. The Thorsos power spectral density is defined in 1 dimension, without explicitly using a correlation length, by:

$$P(\kappa) = a/(\kappa^2 + b^2) \qquad 3\text{-}49$$

where a and b are constants which enable the power spectral density to be parameterised in terms of the incident sound and the mean square surface height, σ^2. For consistency with the convention used here the integral of $P(\kappa)$ over κ must equal $2\pi\sigma^2$. Evaluating this integral in terms of a and b leads to a relation between them:

$$a\pi/b = 2\pi\sigma^2 \qquad 3\text{-}50$$

With the power spectral density defined in terms of the constants a and b, as above, then a and b can be determined uniquely if two products are defined in terms of the wavenumber k ($k=2\pi/\lambda$ where λ is the wavelength, not the correlation length):

$$ka = \alpha \text{ and } k\sigma = \beta. \qquad 3\text{-}51$$

It is easily shown that

$$a = \alpha / k \text{ and } b = k\alpha/2\beta^2. \qquad 3\text{-}52$$

Therefore the Thorsos power spectral density can be defined for any pair of values of ka and $k\sigma$, and for each pair of values the integral of $P(\kappa)$ over κ will give $2\pi\sigma^2$. Note that since only one condition has been used to derive a ratio between a and b, defined by the equations above, there is still a degree of freedom in the Thorsos power spectral density.

3.5.4 Roughness in 2 dimensions

The results for the one dimensional case are easily extended to model a 2 dimensional surface. In this case the surface correlation function is, in general, a function of both x and y, and the surface will generally have different correlation lengths along these axes. This would be the case for a seabed which was strongly influenced by tidal forces or geostrophic currents (see LEEDER (1985), STRIDE (1982)).

A Gaussian correlation function would now have the form

$$C(x,y) = \exp\left(-\left(\frac{x^2}{\lambda_x^2} + \frac{y^2}{\lambda_y^2}\right)\right) \qquad 3\text{-}53$$

and the surface power spectral density is now calculated from σ^2 multiplied by the 2 dimensional Fourier transform:

$$P(\kappa_x, \kappa_y) = \sigma^2 \int_{-\infty}^{\infty} \exp\left(-i\kappa_x x - i\kappa_y y - \frac{x^2}{\lambda_x^2} - \frac{y^2}{\lambda_y^2}\right) dxdy \qquad 3\text{-}54$$

This integral separates into two integrals which depend on x and y uniquely, to give the solution

$$P(\kappa_x, \kappa_y) = \sigma^2 \pi^{0.5} \lambda_x \exp\left(-\frac{\kappa_x^2 \lambda_x^2}{4}\right) \pi^{0.5} \lambda_y \exp\left(-\frac{\kappa_y^2 \lambda_y^2}{4}\right) \qquad 3\text{-}55$$

For an isotropic 2 dimensional surface the surface correlation length is the same in all directions, and so λ_x and λ_y may be replaced by λ_0. The surface power spectral density then becomes:

$$P(|\kappa|) = \pi\sigma^2 \lambda_0^2 \exp\left(-\frac{\kappa^2 \lambda_0^2}{4}\right) \qquad 3\text{-}56$$

The scattering coefficient derivations later all assume a surface which is rough in only one dimension, and so the power spectrum used corresponds to that derived earlier (equation (3- 48)). Note that the correlation length used must fit with the requirements for small scale roughness discussed earlier: it must be small compared to the wavelength of the incident sound. This means that the rough surface power spectrum must contain high frequency components (c.f. the case for large scale scattering where the surface consists of only low frequency components).

For completeness it is worth noting that the form of the Thorsos power spectral density used in the 1 dimensional case can only be used for a finite range of surface wavenumbers in the 2 dimensional case. This is because the integral over all κ in 2 dimensions is unbounded:

for $P(\kappa)$ in 2 dimensions

$$P(\kappa) = P(\kappa_x, \kappa_y) = a/(\kappa_x^2 + \kappa_y^2 + b^2); \qquad 3\text{-}57$$

integrating over κ_y gives

$$a\pi/(\kappa_x^2 + b^2)^{1/2} \qquad 3\text{-}58$$

and then integrating over κ_x gives

$$[a\pi * \ln(p \pm (p^2+1)^{1/2})] \qquad 3\text{-}59$$

evaluated for p between $\pm$ infinity. This is an infinite result.

3.5.5 Scattering spectral amplitudes

For the rough surface scattering amplitudes used in the code (see chapter 7) the square roots of the values obtained from either equation (3- 48) or equation (3- 49) are taken. For each power, since this is done for each of the respective values of κ. The amplitude thus obtained is given a random phase (see chapter 6), since each surface roughness wavenumber component will have a particular phase at the point of impact of the sound beam.

3.5.6 Comparison of Gaussian and Thorsos Power Spectral Densities

When Gaussian and Thorsos power spectral densities (PSDs) are compared for arbitrary values of α (for α as discussed earlier) the resulting power spectra may be very different. Although both PSDs do integrate over all κ to give the same σ^2 the PSDs' shapes may be very different. At very small and very large κ the two PSDs can be orders of magnitude different. For ka = 0.0175 and kσ = 0.2 the values of the PSDs at κ=0 are of the order 10^3 apart. The Gaussian one falls off rapidly for large κ, whereas the Thorsos power spectral density falls off as κ^{-2} for large κ.

At κ=0 the value of the Gaussian power spectral density is given by

$$\pi^{1/2}\lambda_0 * \sigma^2 \qquad 3\text{-}60$$

whereas that from Thorsos is given by

$$4\sigma^2/a * \sigma^2 \qquad 3\text{-}61$$

There are two degrees of freedom with each of the PSD. The Gaussian PSD is determined by σ and λ_0: the Thorsos PSD is determined by a and b. If the two are to be equal for a defined value of κ, and they have both been normalised so that they integrate over κ to give $2\pi\sigma^2$, then the solution is to either:

1 fix λ_0 and then calculate a;

2 fix a and then calculate λ_0.

To force the two PSD to be equal for relatively small κ, which is the region of interest here, these expressions for the PSDs at κ=0 are equated. Solving for a or λ_0 gives:

$a = 4\sigma^2 / (\lambda_0 \pi^{1/2})$ solution 1 3- 62

or equivalently

$\lambda_0 = 4\sigma^2 / (a\pi^{1/2})$ solution 2 3- 63

3.6 The scattering coefficient

When the scattered pressure is calculated it is, strictly, only valid for the particular angle at which the sound pressure scatters. To calculate the intensity of sound scattered onto a finite area some distance from the scattering medium one must consider the pressure contributions scattered in the directions over which the finite area spreads. The scattering coefficient enables this to be done in a consistent manner. It is more intuitive to think of the scattering coefficient in terms of scattering onto a 2 dimensional surface, and so the 2 dimensional case will be presented first. The 1 dimensional case, which is used in the code (see chapter 7), is presented thereafter.

3.6.1 Scattering coefficient in 2 dimensions

The derivation of the scattering coefficient here in 2 dimensions follows the development by BREKHOVSKIKH and LYSANOV (1990), though is extended here for a more generalised case, so that it can be applied to the new scattering solutions developed in chapters 4 and 5. BREKHOVSKIKH and LYSANOV's development is for a scattered pressure derived for a pressure release surface – the standard Dirichlet boundary condition. More significantly, for this standard case, the reflection coefficient has been assumed to be constant over all angles, and the scattered pressure is a function of only the surface amplitude spectrum and the incident geometry. In the more generalised development here the scattered pressure is taken to be a function of both the surface scattering amplitude and the geoacoustic properties of the sea / seabed interface (anticipating the results of chapters 4 and 5), as well as geometry of course.

Both pressure release, and rigid surface scattered pressures, and, indeed, any general scattered pressure (scattered under the assumptions of the small perturbation theory) may be written in the following form (cf. equation 3-17):

$$p(\mathbf{r}, z) = \frac{1}{(2\pi)^2} \int_{-\infty}^{\infty} \int_{-\infty}^{\infty} A(\kappa)[S(\kappa, \text{geo})] \exp[i(\xi_0 + \kappa).\mathbf{r} + i\gamma z] d\kappa \qquad 3\text{- }64$$

[For example in equation (3-17) the $S(\kappa, geo)$ is replaced by the $-2i\gamma_0$.] Equation 3-64 is a double integral since the 2 dimensional case is being considered, and so κ and $\mathbf{r}$ are 2 dimensional. In this representation the scattered pressure is still an integral over all wavenumber components. This integral is weighted in this case by two factors, assumed here to be independent of each other (it will be shown in chapters 4 and 5 that this is a valid assumption). These factors are: the surface spectral scattering amplitudes, $A(\kappa)$; and a function $S(\kappa,geo)$, which represents the effect of the geoacoustics of the interface. For the pressure release interface the value of $S(\kappa,geo)$ would be given by the relatively simple term $2i\gamma_0$ (see equation 3-17) though for the elastic scattered pressures calculated in chapters 4 and 5 the value of $S(\kappa,geo)$ is somewhat more complicated.

The relative scattered intensity in the incident medium, I_S, is given by

$$I_S = \left\langle |\, p\,|^2 \right\rangle \qquad 3\text{-}65$$

where the angled brackets indicate taking the mean value over the surface. Writing the modulus of the square of the scattered pressure as the product of the pressure with its complex conjugate, the scattered intensity is given by

$$I_S = \frac{1}{(2\pi)^4} \int_{\Gamma_1}\int_{\Gamma_1} \left\langle A(\kappa)S(\kappa, geo)A(\kappa')^* S(\kappa', geo)^* \right\rangle \exp\left[i(\xi_0 + \kappa).\mathbf{r} + i\gamma z - i(\xi_0 + \kappa').\mathbf{r} - i\gamma' z\right] d\kappa\, d\kappa' \qquad 3\text{-}66$$

The average over the surface does not include the exponential terms since these only relate to the phase of the wave once it has been scattered, and not to determining the amplitude of the scattered wave itself. If the scattering function $S(\kappa,geo)$ depends on only the geoacoustics of the interface, then this too will be independent of position on the scattering surface, and so may be taken outside the angled brackets. Equation (3- 66) can thus be simplified to

$$I_S = \frac{1}{(2\pi)^4} \int_{\Gamma_1}\int_{\Gamma_1} \left\langle A(\kappa)A(\kappa')^* \right\rangle S(\kappa, geo)S(\kappa', geo)^* \exp\left[i(\kappa - \kappa').\mathbf{r} + i(\gamma - \gamma')z\right] d\kappa\, d\kappa' \qquad 3\text{-}67$$

To proceed further the statistics of the surface amplitude must be considered. In the spatial domain the surface amplitude is given by $\zeta(\mathbf{r}_1)$ where the Fourier transform of $\zeta(\mathbf{r}_1)$ is the surface spectral scattering amplitude $A(\kappa)$

$$A(\kappa) = \int_{-\infty}^{\infty}\int_{-\infty}^{\infty} \zeta(\mathbf{r}_1)\exp(-i\kappa.\mathbf{r}_1)\, d\mathbf{r} \qquad 3\text{-}68$$

If it is assumed that the statistics of the surface are stationary, i.e. that all statistical properties such as mean surface height, and surface power, are the same no-matter which area of surface is used to measure them, then the surface autocorrelation function may be written as $B(\mathbf{r})$ where

$$B(\mathbf{r}) = \langle \zeta(\mathbf{r}_1)\zeta(\mathbf{r}_2) \rangle \qquad 3\text{-}69$$

where

$$\mathbf{r} = \mathbf{r}_2 - \mathbf{r}_1 \qquad 3\text{-}70$$

It is now easily shown, using the result

$$\frac{1}{(2\pi)^2} \int_{-\infty}^{\infty}\int_{-\infty}^{\infty} \exp(i\mathbf{r}_1(\kappa - \kappa'))d\mathbf{r}_1 = \delta(\kappa - \kappa') \qquad 3\text{-}71$$

that the average over the surface for the terms in equation (3- 67) is given by

$$\frac{1}{(2\pi)^2} \langle A(\kappa)A(\kappa')^* \rangle = P(\kappa)\delta(\kappa - \kappa') \qquad 3\text{-}72$$

where

$$P(\kappa) = \int_{-\infty}^{\infty} B(\mathbf{r})\exp(-i\kappa.\mathbf{r})d\mathbf{r} \qquad 3\text{-}73$$

is the surface wavenumber power spectrum. Substituting equation (3- 72) into equation (3- 67) for the intensity gives

$$I_S = \frac{1}{(2\pi)^2} \int_{\Gamma_1}\int_{\Gamma_1} P(\kappa)\delta(\kappa - \kappa')S(\kappa, geo)S(\kappa', geo)^* \exp[i(\kappa - \kappa').\mathbf{r} + i(\gamma - \gamma')z]d\kappa\, d\kappa' \qquad 3\text{-}74$$

Integrating over κ' gives

$$I_S = \frac{1}{(2\pi)^2} \int_{\Gamma_1} P(\kappa)S(\kappa, geo)S(\kappa, geo)^* d\kappa \qquad 3\text{-}75a$$

where the integral over κ is a double integral over both κ_x and κ_y. Note: for the 1 dimensional case an equivalent derivation yields:

$$I_S = \frac{1}{2\pi} \int_{\Gamma_1} P(\kappa) S(\kappa, geo) S(\kappa, geo)^* d\kappa \qquad 3\text{-}75b$$

where the integral over κ is now a single integral.

This equation for the scattered intensity is in terms of an integral over κ, the surface wavenumber, and has no explicit dependence on the scattered direction. To derive an expression for the scattering coefficient, a second equation is now derived for the scattered intensity, in terms of the scattering coefficient, and the two equations are compared.

The scattering coefficient, m_S, is defined as the ratio of the scattered to incident intensity, normalised by the solid angle over which the scattered intensity, I_S, is measured:

$$m_S = \frac{I_S}{I_i} \cdot \frac{R^2}{A_S} \qquad 3\text{-}76$$

where I_i is the intensity of sound incident on the rough surface and A_S is the area from which the sound is scattered, to be measured at a point P which is at a distance R from the scattering area. Re-arranging for I_S gives

$$I_S = I_i \frac{A_S}{R^2} m_S(\theta, \phi) \qquad 3\text{-}77$$

To evaluate the intensity scattered in a particular direction consider the intensity observed at the point P, in Figure 3 overleaf. To calculate the total scattered intensity the scattering surface must be split into small sections for which the scattering coefficient is constant. These sections, of area dA_S, must be large in comparison with the wavelength of the sound and the correlation radius of the rough surface, and must be far from the point P at which the scattered sound is measured.

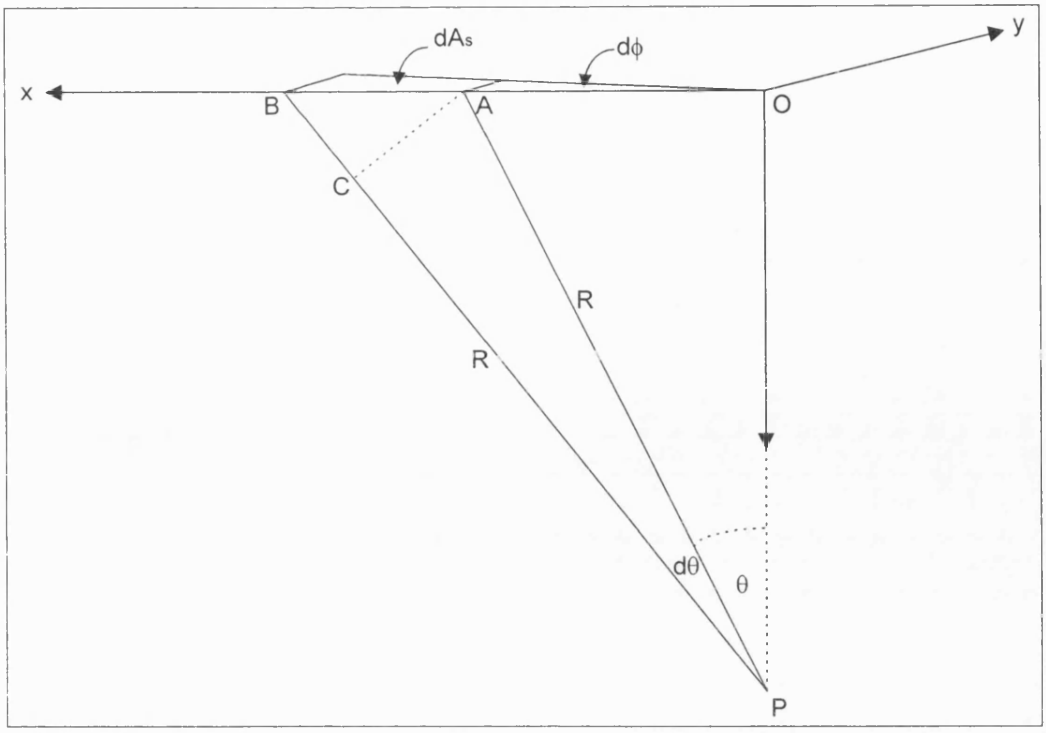

Figure 3: Geometry for the scattering coefficient calculation. The total scattered intensity is a sum over that scattered from all elemental rough surface areas dA_S.

For a unit incident intensity the scattered intensity now becomes an integral over these areas:

$$I_S = \iint R^{-2} m_S(\theta,\phi) dA_S \qquad 3\text{- }78$$

Evaluating the sides of the rectangular area dA_S it is seen that length OA is equal to $R\sin\theta$ and AB is equal to $AC/\cos\theta$, hence AB is equal to $Rd\theta/\cos\theta$. Hence dA_S is given by

$$dA_S = R^2 \tan\theta d\theta d\phi \qquad 3\text{- }79$$

and so the intensity is now given by

$$I_S = \int_0^{2\pi} \int_0^{\pi/2} m_S \tan\theta d\theta d\phi \qquad 3\text{- }80$$

This equation for the scattered intensity may be compared with equation (3- 75a) derived earlier, in terms of an integral over κ. The term $d\kappa$ is clearly equal to $d\xi$ (see equation (3- 16) for resonance scattering) and the vector $d\xi$ may be written as

$$d\xi = \xi d\xi d\phi = k^2 \sin\theta\cos\theta d\theta d\phi \qquad 3\text{- }81$$

and so equation (3- 75a) for the scattered intensity becomes

$$I_S = \frac{1}{(2\pi)^2}\int_0^{2\pi}\int_0^{\pi/2} P(\theta,\phi)S(\theta,\phi,geo)S(\theta,\phi,geo)^* k^2 \sin\theta\cos\theta d\theta d\phi \qquad 3\text{- }82$$

Comparing equations (3- 80) and (3- 82) for the scattered intensity, it can be seen that the scattering coefficient is given by

$$m_S(\theta,\phi) = \frac{1}{(2\pi)^2} P(\kappa)|S|^2 k^2 \cos^2\theta \qquad 3\text{- }83$$

3.6.2 Scattering coefficient in 1 dimension

For the scattering coefficient in 1 dimension the equations (3- 76) and (3- 78) are replaced by the two below:
the 1 dimensional scattering coefficient is defined by

$$m_S = \frac{I_S}{I_i}.\frac{R^1}{L_S} \qquad 3\text{- }84$$

where L_S is the length of surface from which the sound is scattered; and the total scattered sound is therefore given by

$$I_S = \int R^{-1} m_S(\theta) dL_S \,. \qquad 3\text{- }85$$

It is seen from Figure 3 that this may be written as

$$I_S = \int (m_S(\theta)/\cos\theta) d\theta \qquad 3\text{- }86$$

This equation for the scattered intensity is compared to the 1 dimensional intensity equation (3- 75b),

$$I_S = \frac{1}{2\pi}\int_L P(\kappa)S(\kappa,geo)S(\kappa,geo)^* d\kappa \qquad 3\text{- }87$$

where $P(\kappa)$ is now the square of the 1 dimensional scattering amplitude spectral density,

$A(\kappa)$. Similarly to the two dimensional case the one dimensional $d\kappa$ can be re-written as $d\xi = k\cos\theta\, d\theta$, and so the scattering strength may be written as

$$I_S = \frac{1}{2\pi}\int_L P(\kappa)S(\kappa, geo)S(\kappa, geo)^* k\cos\theta d\theta \qquad 3\text{- }88$$

Comparing equations (3- 86) and (3- 88) for the 1 dimensional scattered intensity it is seen that the 1 dimensional scattering coefficient is given by

$$m_S(\theta) = \frac{1}{2\pi}P(\kappa)|S|^2\, k\cos^2\theta \qquad 3\text{- }89$$

3.6.3 Dimensions and Scattering Strength

It should be noted that in the 2 dimensional case the 2 dimensional power spectral density, $P(\kappa)$ has dimensions of σ^2L^2 since it must be integrated over $d\kappa = d\kappa_x\, d\kappa_y$ to get $(2\pi)^2\sigma^2$, whereas in the 1 dimensional case the power spectral density, $P(\kappa)$, has dimensions of σ^2L^1 since it is integrated only over $d\kappa$ to get $2\pi\sigma^2$.

The term $S(\kappa,geo)$ has dimensions of $1/\sigma$ in both 1 and 2 dimensional cases. This is easily seen for the standard cases – and is also true for the results derived in the later chapters. The 1 and 2 dimensional scattering coefficients are therefore both seen to be dimensionless, as required.

$$m_S(\theta) = \frac{1}{2\pi}P(\kappa)|S|^2\, k\cos^2\theta \qquad \text{1 dimensional} \qquad 3\text{- }90$$

$$m_S(\theta,\phi) = \frac{1}{(2\pi)^2}P(\kappa)|S|^2\, k^2\cos^2\theta \qquad \text{2 dimensional.} \qquad 3\text{- }91$$

The scattering strength, SS, is simply calculated as

$$SS = 10log_{10}(m_s) \qquad 3\text{- }92$$

in both cases. In the code (see chapter 7) which was used to display the results from the equations derived in chapters 4 and 5 the 1 dimensional scattering coefficient was used.

4 Scattering from a liquid / liquid interface

This chapter shows how a perturbation theory method can be developed which uses the fact that we already know the true zeroth order scattering solution for any reflecting surface, since this is the smooth surface reflection and transmission coefficients. This, along with a derivation which uses elastic boundary conditions, will be used to find the first order scattered field. Using this development it will be seen that the solution for the spectral amplitudes of the scattered pressure fields are a product of the rough surface spectral amplitude and a function of the geoacoustic parameters. In other words, the solution is separable into a roughness factor and a geoacoustics factor. The solution is, therefore, equally valid for any rough surface spectrum which satisfies the amplitude and correlation length conditions discussed in chapter 3.

4.1 Introduction

In the standard method of small perturbations (see BREKHOVSKIKH and LYSANOV (1990)) the particular "boundary condition" imposed (Dirichlet or Neumann) on the rough surface is transferred to a smooth mean plane (z=0) by expanding it as a power series in a small surface roughness parameter $\zeta(r)$. Similarly the theoretical smooth plane sound field in the half space $z>\zeta$ is expanded in powers of ζ and the (transferred rough surface) boundary conditions which must be satisfied by successive approximations at the mean surface are found. The terms of various orders are equated and solved to give the sound field to various levels of approximation. Using this method the first order pressure was derived in chapter 3.

In the new method presented here a departure from the usual method is taken on two distinct fronts: for the assumed zero order solution p_0; and for the boundary conditions used to solve for the higher order terms. Here the boundary conditions which are used in the smooth surface reflection theory of chapter 2 are combined with the rough surface statistical methodology of chapter 3. This is done in a self-consistent manner here for a liquid / liquid interface, and in chapter 5 for a liquid / solid interface.

When solving the general case of reflection at a smooth boundary one has two boundary conditions: continuity of pressure (i.e. Newton's third law) and continuity of particle displacement (i.e. no net transfer of particles from one medium to the other). From these two boundary conditions two unknowns are calculated: the smooth surface reflection and transmission coefficients. In general, for finite densities and sound speeds, these coefficients are functions of the incident angle. For special cases where the density of the second medium is infinite or zero the results for the reflected and transmitted waves are simple: the reflected wave has amplitude ± 1 respectively and the transmitted wave has zero amplitude, for all incident angles. The fact that these special case coefficients are independent of angle makes them ideal "standard" cases to study for scattering. These two cases are often described as having Neuman or Dirichlet "boundary conditions" (respectively) however it

must be remembered that these are not the *boundary conditions* used to solve the general case.

In the method described here it is recognised that both media will have finite densities and sound speeds, and so must be treated with the elastic boundary conditions derived earlier, since these elastic boundary conditions are valid at any point on any interface. For consistency, the zero order solutions for the scattered pressures must be the zero order – i.e. smooth surface – solutions to the elastic boundary condition equations. The zero order solutions are therefore the V and W coefficients derived in chapter 2.

4.2 New liquid / liquid perturbation theory

As in chapter 2, the starting point is the liquid / liquid interface boundary conditions in terms of pressure:

$$p_{in} + p_{out_V} = p_{out_W} \qquad 4\text{-}1$$

$$\frac{1}{\rho_0}\frac{\partial\left(p_{in} + p_{out_V}\right)}{\partial n} = \frac{1}{\rho_1}\frac{\partial\left(p_{out_W}\right)}{\partial n} \qquad 4\text{-}2$$

where p_{in} is the incident pressure, p_{out_V} is the total scattered reflected pressure and p_{out_W} is the total scattered transmitted pressure. To evaluate these equations for a rough surface, however, it must be understood how they change when they are transformed to the usual cartesian co-ordinates. Consider the rough surface normal $\underline{n}$ with components $(n_\perp, n_z)$ shown below:

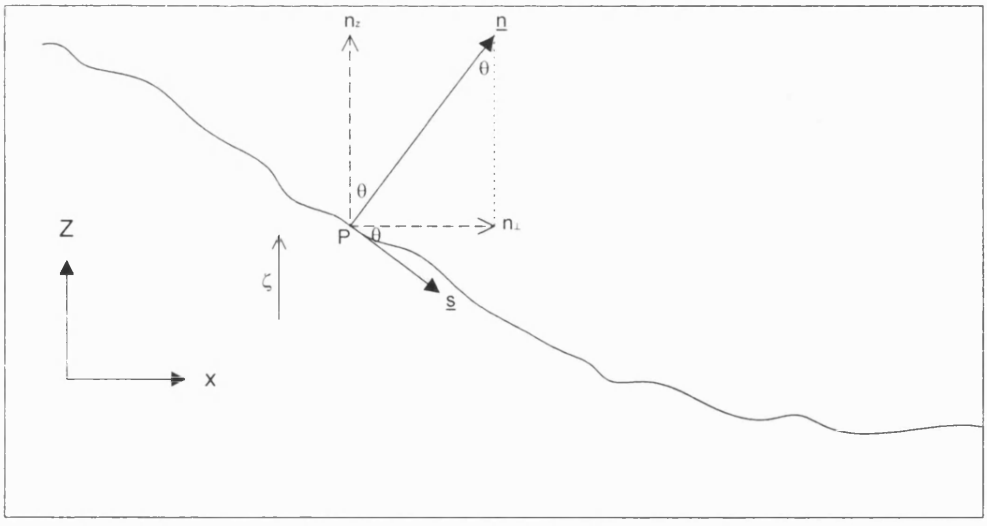

Figure 1: Geometry for the co-ordinate transformations required for a rough interface.

This is the same figure as presented in chapter 3. There, the transformations from local rough surface co-ordinates to cartesian co-ordinates were derived. It was shown (see equation (3-30)) that if the analysis is restricted to surfaces which have roughness in only the x-z plane, then $\partial p/\partial n$ reduces to

$$\frac{\partial p}{\partial n} = \left(-\frac{\partial \zeta}{\partial x}\frac{\partial p}{\partial x} + \frac{\partial p}{\partial z} \right) \cos\theta \qquad \text{4- 3}$$

where ζ is the height deviation of the rough surface away from the mean plane at z=0. The boundary condition equations are now therefore:

$$p_{in} + p_{out_l} = p_{out_W} \qquad \text{4- 4}$$

$$\frac{1}{\rho_0}\left(\left(-\frac{\partial \zeta}{\partial x}\frac{\partial}{\partial x} + \frac{\partial}{\partial z} \right)\left(p_{in} + p_{out_l} \right) \right) = \frac{1}{\rho_1}\left(\left(-\frac{\partial \zeta}{\partial x}\frac{\partial}{\partial x} + \frac{\partial}{\partial z} \right) p_{out_W} \right) \qquad \text{4- 5}$$

where the $\cos\theta$ terms have been cancelled on both sides of equation (4-5). These boundary condition equations hold on the rough surface. In general, a point P on the rough surface will be at a height ζ above the mean surface height (the z co-ordinate is set such that the mean surface height is z=0), where ζ varies with position (x co-ordinate) on the rough surface. This is shown in Figure 2 below.

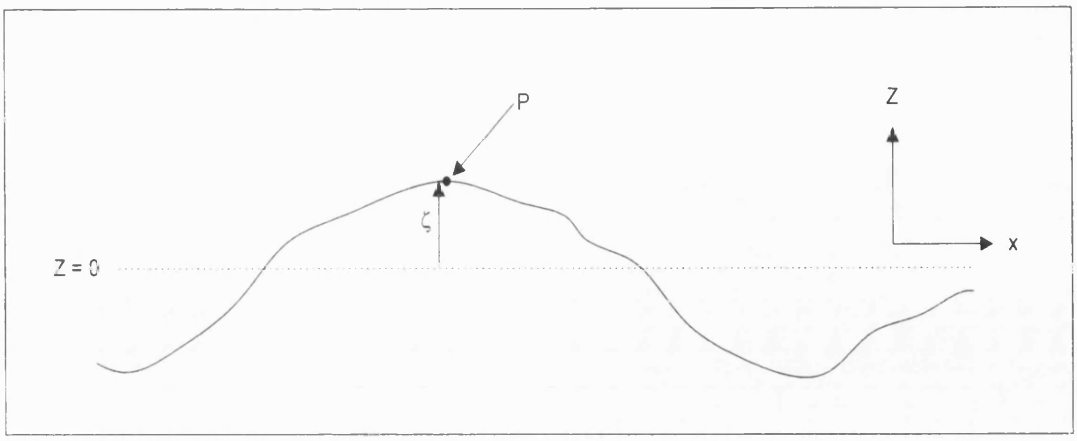

Figure 2: A point P on a rough surface is at a height ζ above the mean surface height at z=0, where ζ varies with position (x co-ordinate) on the rough surface. The boundary condition equations (4-4) and (4-5) hold on the rough surface. In order to simplify the evaluation of the subsequent equations the boundary condition equations (4-4) and (4-5) are re-written in terms of equivalent boundary condition equations which hold at z=0. This is done by assuming that ζ is small, and therefore assuming that the boundary condition equations at the rough surface may be written as a Taylor series expansion (in ζ) of the boundary condition equations written to apply at z=0.

In order to simplify the evaluation of the subsequent equations the boundary condition equations (4-4) and (4-5) are re-written in terms of equivalent boundary condition equations which hold at z=0. This is done by assuming that ζ is small, and therefore assuming that the boundary condition equations at the rough surface may be written as a Taylor series expansion (in ζ) of the boundary condition equations written to apply at z=0. This is done by re-writing the boundary condition equations (4-4) and (4-5) and applying the operator

$$\left(1+\zeta\frac{\partial}{\partial z}\right)$$

to both sides of each equation. In applying this operator only zero and first order terms are kept. It is assumed that ζ and its gradient are small and hence first order quantities, and so terms involving both of these are therefore second order and are neglected. Thus equations (4-4) and (4-5) which hold on the rough surface may be replaced by equations (4-6) and (4-7) which hold on the mean surface z=0:

$$\left(1+\zeta\frac{\partial}{\partial z}\right)\left(p_{in}+p_{out_I}\right)=\left(1+\zeta\frac{\partial}{\partial z}\right)\left(p_{out_{II}}\right) \qquad 4\text{-}6$$

$$m\left(\left(\frac{\partial}{\partial z}+\zeta\frac{\partial^2}{\partial z^2}-\frac{\partial\zeta}{\partial x}\frac{\partial}{\partial x}\right)\left(p_{in}+p_{out_I}\right)\right)=\left(\left(\frac{\partial}{\partial z}+\zeta\frac{\partial^2}{\partial z^2}-\frac{\partial\zeta}{\partial x}\frac{\partial}{\partial x}\right)p_{out_{II}}\right) \qquad 4\text{-}7$$

where m is given by: $m=\frac{\rho_1}{\rho_0}$ 4- 8

The elastic scattering boundary conditions have now been written in terms of cartesian co-ordinates, to apply at the mean plane, and in terms of the total ingoing and outgoing pressures. To evaluate the scattered components, the outgoing pressures must be expressed as the sum of zero and first order components. The zero order components are the smooth interface reflection and transmission pressure coefficients, and the first order components are the scattered pressures – the unknowns – p_α and p_β:

$$p_{out_I} = p_0 + p_\alpha$$
$$p_{out_{II}} = p_1 + p_\beta \qquad 4\text{-}9$$

where for an incoming wave defined by

$$p_{in} = I\exp\left(ik\left(x\sin\theta + z\cos\theta\right)\right) \qquad 4\text{-}10$$

(where I = 1 in the subsequent equations) the zero order reflected solutions are known to be given by:

$$p_0 = V\exp\left(ik\left(x\sin\theta - z\cos\theta\right)\right)$$
$$p_1 = W\exp\left(ik_1\left(x\sin\theta_1 + z\cos\theta_1\right)\right) \qquad 4\text{-}11$$

where

$$k\sin\theta = k_1\sin\theta_1 = \xi$$
$$k_i\cos\theta_i = \gamma_i$$
$$k_i = \omega/c_i \qquad 4\text{-}12$$

Substituting the zero order solutions into the rough surface boundary condition equations (4-6) and (4- 7) gives:

$$\left(1+\zeta\frac{\partial}{\partial z}\right)\left(p_{in}+p_0+p_\alpha\right)=\left(1+\zeta\frac{\partial}{\partial z}\right)\left(p_1+p_\beta\right) \qquad 4\text{-}13$$

$$m\left(\left(\frac{\partial}{\partial z}+\zeta\frac{\partial^2}{\partial z^2}-\frac{\partial\zeta}{\partial x}\frac{\partial}{\partial x}\right)\left(p_{in}+p_0+p_\alpha\right)\right)=\left(\left(\frac{\partial}{\partial z}+\zeta\frac{\partial^2}{\partial z^2}-\frac{\partial\zeta}{\partial x}\frac{\partial}{\partial x}\right)\left(p_1+p_\beta\right)\right) \qquad 4\text{- }14$$

Equations (4- 13) and (4- 14) are now the two rough surface boundary condition equations in two unknowns, p_α and p_β. To proceed further the zero order terms (p_{in}, p_0 and p_1) must be substituted for, and the surface function ζ must be defined. The derivatives must then be evaluated and the simultaneous equations solved.

4.3 Solving the scattered pressure equations

The equations for the incoming and outgoing zeroth order plane waves (equations (4- 10) and (4- 11)) must be substituted for into the rough surface boundary condition equations (4- 13) and (4- 14) and then the derivatives evaluated where appropriate. The expressions are then evaluated at z=0, the mean scattering surface. Starting with equation (4- 13), this gives:

$$(1+V)\exp(i\xi x)+i\gamma_0\zeta(1-V)\exp(i\xi x)+p_\alpha+\zeta\frac{\partial p_\alpha}{\partial z}=(1+i\gamma_1\zeta)W\exp(i\xi x)+p_\beta+\zeta\frac{\partial p_\beta}{\partial z} \qquad 4\text{- }15$$

This is an equation involving zero, first and second order terms. The zero order terms should correspond to those found when solving the smooth interface case. Separating out the zero order terms it is found that this is indeed so:

$$1+V=W \qquad 4\text{- }16$$

The second order terms are $\zeta\frac{\partial p_\alpha}{\partial z}$ and $\zeta\frac{\partial p_\beta}{\partial z}$ since each is a product of two first order terms. These may be neglected since they will be small compared to the first order (and zero order) ones. The first order terms give the equation concerning the scattered pressure:

$$i\zeta(\gamma_0(1-V)-\gamma_1 W)\exp(i\xi x)=p_\beta-p_\alpha \qquad 4\text{- }17$$

A similar process of substituting, differentiating and evaluating using the second boundary condition equation (4- 14) gives:

$$\exp(i\xi x)\left(mi\gamma_0(1-V)-m\left(\zeta\gamma_0^2+i\xi\frac{\partial\zeta}{\partial x}\right)(1+V)-\left(i\gamma_1-\zeta\gamma_1^2-i\xi\frac{\partial\zeta}{\partial x}\right)W\right)=\left(\frac{\partial}{\partial z}+\zeta\frac{\partial^2}{\partial z^2}-\frac{\partial\zeta}{\partial x}\frac{\partial}{\partial x}\right)\left(p_\beta-mp_\alpha\right) \qquad 4\text{- }18$$

Again, this is an equation involving zero, first and second order terms, and the zero order terms should correspond to those found when solving the smooth interface case. Separating out the zero order terms it is found again that this is so:

$$mi\gamma_0(1-V)=i\gamma_1 W \qquad 4\text{- }19$$

The second order terms are $\left(\zeta\frac{\partial^2}{\partial z^2}-\frac{\partial\zeta}{\partial x}\frac{\partial}{\partial x}\right)(p_\beta - mp_\alpha)$. Again, these are small and can be neglected. The first order terms collect to give

$$\exp(i\xi x)\left(-m\left(\zeta\gamma_0^2+i\xi\frac{\partial\zeta}{\partial x}\right)(1+V)+\left(\zeta\gamma_1^2+i\xi\frac{\partial\zeta}{\partial x}\right)W\right)=\left(\frac{\partial}{\partial z}\right)(p_\beta - mp_\alpha) \qquad 4\text{- }20$$

Hence from the two boundary condition equations, (4- 13) and (4- 14), the two first order scattered pressure equations, (4- 17) and (4- 20), have been derived. For each of these the left hand sides contain terms which, for any defined media (in terms of densities and sound speeds) with defined rough interface between them, are known; the right hand sides contain an operator term (unit operator for (4- 17)) which acts on the scattered pressures terms. It appears that the scattered pressures have been separated out, though this is only a consequence of the way in which the equations have been written. For the two equations the scattered pressures are acted on by different operators and since the scattered pressures themselves are unknown the derivative terms are, effectively, further unknowns. In order to proceed any further some consideration must be given to the assumed form of the solutions.

4.4 Defining a solution

To solve equations (4- 17) and (4- 20) the type of solutions which are sought for the scattered pressures must be more clearly defined. A form for these solutions must be given to allow the unknowns in them to be solved for. A schematic of the problem is shown below.

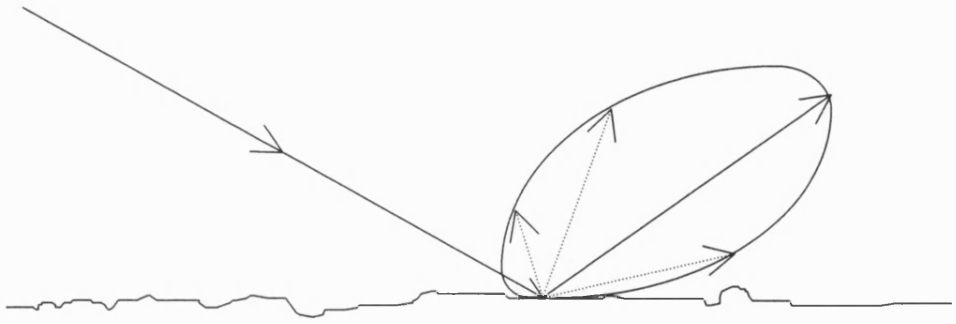

Figure 3: Schematic showing how an incoming wave is scattered in different directions with different amplitudes. The lengths of the arrows represent the amplitudes scattered in the directions of the arrows.

The incoming wave is shown from the left. The outgoing scattered waves (just shown for the reflected scattered waves here) are in all outgoing directions with different magnitudes. The magnitudes of the outgoing waves are represented by the lengths of the arrows. For the different directions these trace out a tilted oval type shape. It is this shape, in terms of scattering strength versus angle, which must be calculated and plotted.

4.4.1 Scattered angles

One would expect the distribution of the scattering angles for the reflected scattered energy to be the same as those already calculated for the "ideal" scattering case (where V = ±1), since the reflected *directions* only depend upon the direction of the local surface normal relative to the direction of the incoming wave. The statistical distribution of this local surface normal across the whole surface determines the distribution of the scattering directions. The local surface normal is a function of the geometry of the surface, i.e. is a function of the surface amplitude $\zeta(x)$ and is not explicitly related to the geoacoustic properties of either of the media at the interface.

In the smooth surface case the surface normal is always vertical and so no boundary forces act in any horizontal direction to alter the incoming wave. Hence the horizontal wavevector of the reflected wave is the same as that of the incoming wave. For the "ideal" scattering cases there are many scattered waves, each corresponding to the interaction of the incoming wave with a harmonic surface wave, each harmonic wave corresponding to one component of the Fourier decomposition of the surface. Each outgoing wave has a horizontal wavevector equal to its incoming horizontal wavevector plus that of the particular harmonic wave with which it interacted. This is the "*resonant scattering*" shown in chapter 3.

One would expect this to be the case also for the true scattered reflected wave, since exactly the same *geometrical conditions* are involved. Hence for a scattered reflected wave from an incoming horizontal wavevector ξ (=ksinθ) the outgoing horizontal wavevector, ξ_α, is given by:

$$\xi_\alpha = \xi + \kappa \qquad \text{4- 21}$$

where the Fourier decomposition of the surface amplitude $\zeta(x)$ is given by

$$\zeta(x) = \frac{1}{2\pi} \int_{-\infty}^{\infty} A(\kappa) \exp(i\kappa x) d\kappa \qquad \text{4- 22}$$

The values of κ range from minus to plus infinity and so backscatter is included in the range of possible ξ_α values, backscatter occuring when

$$\xi_\alpha = -\xi \qquad \Leftrightarrow \qquad \kappa = -2\xi$$

Clearly forward scatter occurs when

$$\xi_\alpha = \xi \qquad \Leftrightarrow \qquad \kappa = 0$$

In other words the smooth surface ("d.c.") component of the surface spectrum determines the specularly scattered component. It should be noted however that the range of κ values integrated over in equation (4-22) need not be infinite. Once each ξ_α has been calculated the corresponding vertical wavevector, γ_α, may be deduced from the identity

$$\gamma_\alpha^2 = k^2 - \xi_\alpha^2 \qquad \text{4- 23}$$

For values of ξ_α greater in magnitude than k the corresponding vertical wavenumber is imaginary and from the form of the scattered pressure (seen later) a rapid attenuation of the wave amplitude then occurs with increasing distance from the interface. Hence the limits of the integration over κ may be restricted, depending on the distance (number of wavelengths) the observer is from the interface.

The horizontal wavevectors of the scattered *transmitted* waves must be governed by a similar relation to equation (4- 21) above since the surface looks the same, statistically, from either side: it has a surface decomposition which is symmetrical about the plane z=0. It is easier to see that this is relevant for the transmitted scattered wave by considering the time-reversed case for which ξ may be "deduced" from

$$-\xi = -\xi_\beta + \kappa \qquad \text{4- 24}$$

Re-arranging this gives the time-forward equation (which must be derived from this equality since the boundary conditions are time-independent)

$$\xi_\beta = \xi + \kappa \qquad \text{4- 25}$$

For each scattered wave the scattered angle from the normal is calculated using:

$$\xi_\alpha = k \sin \varphi(\kappa)$$
$$\xi_\beta = k_1 \sin \varphi_1(\kappa) \qquad \text{4- 26}$$

As for the scattered reflected wave the vertical wavenumbers for the scattered transmitted waves, γ_β, are calculated from

$$\gamma_\beta^2 = k_1^2 - \xi_\beta^2 \qquad 4\text{-}27$$

Again it is prudent to consider only κ values which result in real values of γ_β.

4.4.2 Assumed form for the solutions

Having now defined the directions for the scattered waves the full form of the scattered pressure solutions must be defined. Again, the solution for the ideal case shown in chapter 3 shows the type of function which can be expected. The solutions here are assumed to be of precisely the same form, except with the surface amplitude spectrum and the geoacoustic terms rolled into one term, A_α or A_β. Hence

$$p_\alpha = \frac{1}{2\pi}\int_{-\infty}^{\infty} A_\alpha(\kappa)\exp(i(\kappa+\xi)x)\exp(-i\gamma_\alpha z)d\kappa \qquad 4\text{-}28$$

$$p_\beta = \frac{1}{2\pi}\int_{-\infty}^{\infty} A_\beta(\kappa)\exp(i(\kappa+\xi)x)\exp(i\gamma_\beta z)d\kappa \qquad 4\text{-}29$$

The spectral amplitude functions $A_\alpha(\kappa)$ and $A_\beta(\kappa)$ are yet to be determined. These are the functions which define the individual amplitudes for each of the scattered waves. In terms of Figure 3 these are the lengths of the scattered wave arrows inside the oval. Using the expressions for the surface amplitude ζ (equation (4- 22)) and for p_α and p_β above the spectral amplitude functions $A_\alpha(\kappa)$ and $A_\beta(\kappa)$ can now be derived from the first order scattered pressure equations (4- 17) and (4- 20).

4.5 Evaluating A_α and A_β

Firstly it is useful to further simplify equations (4- 17) and (4- 20). From equation (4- 17) the constant, E, is defined by

$$E = \gamma_0(1-V) - \gamma_1 W \qquad 4\text{-}30$$

and equation (4- 17) becomes

$$iE\zeta\exp(i\xi x) = p_\beta - p_\alpha \qquad 4\text{-}31$$

Similarly equation (4- 20) may be simplified by defining a constant, G, by:

$$G = -m(1+V) \qquad 4\text{-}32$$

and so equation (4- 20) becomes

$$\exp(i\xi x)\left(\left(\zeta\gamma_0^2 + i\xi\frac{\partial\zeta}{\partial x}\right)G + \left(\zeta\gamma_1^2 + i\xi\frac{\partial\zeta}{\partial x}\right)W\right) = \left(\frac{\partial}{\partial z}\right)\left(p_\beta - mp_\alpha\right) \qquad 4\text{- }33$$

Substituting the assumed forms for the surface amplitude ζ, and for p_α and p_β into the first of the first order scattered pressure equations (4- 31) gives

$$\frac{1}{2\pi}\int_{-\infty}^{\infty} A_\beta(\kappa)\exp(i(\kappa+\xi)x)\exp(i\gamma_\beta z)d\kappa \quad = \quad iE\exp(i\xi x)\frac{1}{2\pi}\int_{-\infty}^{\infty} A(\kappa)\exp(i\kappa x)d\kappa$$
$$-\frac{1}{2\pi}\int_{-\infty}^{\infty} A_\alpha(\kappa)\exp(i(\kappa+\xi)x)\exp(-i\gamma_\alpha z)d\kappa \qquad 4\text{- }34$$

Both sides of this equation can be simplified greatly. On the left hand side both terms can be taken inside one integral. On the right hand side the term (iEexp(iξx)) is constant with respect to κ and so can be taken inside the integral. Hence

$$\int_{-\infty}^{\infty}\left(A_\beta(\kappa)\exp(i\gamma_\beta z) - A_\alpha(\kappa)\exp(-i\gamma_\alpha z)\right)\exp(i(\kappa+\xi)x)d\kappa = \int_{-\infty}^{\infty} iE\exp(i\xi x)A(\kappa)\exp(i\kappa x)d\kappa \qquad 4\text{- }35$$

More simplifications are now apparent. Both sides of the equation are Fourier transforms using the same variable, κ. The quantities being transformed must therefore equate[1]. Looking at these quantities themselves, it can be seen that they both have factors of exp(iξx) which therefore cancel. Evaluating the expression at z=0 gives

$$A_\beta - A_\alpha = iEA \qquad 4\text{- }36$$

where the dependence upon κ has been omitted for brevity here.

The second of the first order scattered pressure equations (4- 33) contains $\partial/\partial x$ and $\partial/\partial z$ terms. These can both be evaluated inside the integral expressions for ζ and p_α and p_β as appropriate. Specifically

$$\frac{\partial p_\alpha}{\partial z} = \frac{1}{2\pi}\int_{-\infty}^{\infty} -i\gamma_\alpha A_\alpha(\kappa)\exp(i(\kappa+\xi)x)\exp(-i\gamma_\alpha z)d\kappa$$

[1] Note: it is not enough to say that the integrals equate and so the integrands must equate, since one of the integrands may contain a function which integrates over the limits to zero. One of the properties of a Fourier transform is that if the Fourier transforms of two functions are equal, then the two functions are themselves equal. It is this property that is invoked here.

$$\frac{\partial p_\beta}{\partial z} = \frac{1}{2\pi}\int_{-\infty}^{\infty} i\gamma_\beta A_\beta(\kappa)\exp(i(\kappa+\xi)x)\exp(i\gamma_\beta z)d\kappa$$

$$\frac{\partial \zeta}{\partial x} = \frac{1}{2\pi}\int_{-\infty}^{\infty} i\kappa A(\kappa)\exp(i\kappa x)d\kappa \qquad 4\text{- }37$$

Equation (4- 33) now gives

$$\begin{aligned}\frac{1}{2\pi}\int_{-\infty}^{\infty} i\gamma_\beta A_\beta(\kappa)\exp(i(\kappa+\xi)x)\exp(i\gamma_\beta z)d\kappa \quad &= \quad \frac{1}{2\pi}\exp(i\xi x)\gamma_0^2 G\int_{-\infty}^{\infty} A(\kappa)\exp(i\kappa x)d\kappa \\ -\frac{1}{2\pi}\int_{-\infty}^{\infty} -i\gamma_\alpha A_\alpha(\kappa)\exp(i(\kappa+\xi)x)\exp(-i\gamma_\alpha z)d\kappa \quad &+ \frac{1}{2\pi}\exp(i\xi x)i\xi G\int_{-\infty}^{\infty} i\kappa A(\kappa)\exp(i\kappa x)d\kappa \\ &+ \frac{1}{2\pi}\exp(i\xi x)\gamma_1^2 W\int_{-\infty}^{\infty} A(\kappa)\exp(i\kappa x)d\kappa \\ &+ \frac{1}{2\pi}\exp(i\xi x)i\xi W\int_{-\infty}^{\infty} i\kappa A(\kappa)\exp(i\kappa x)d\kappa \qquad 4\text{- }38\end{aligned}$$

Just as for the first scattered pressure equation, all the constant factors on the right hand side can be taken inside the integrals. Again, both sides of the equation are Fourier transforms using the same variable, κ. The quantities being transformed must therefore equate. Looking at these quantities themselves, it can be seen that they again both have factors of exp(iξx) which therefore cancel. Evaluating the expression at z=0 gives:

$$i\gamma_\beta A_\beta + mi\gamma_\alpha A_\alpha = A\left(\left(\gamma_0^2 - \kappa\xi\right)G + \left(\gamma_1^2 - \kappa\xi\right)W\right) \qquad 4\text{- }39$$

The two liquid / liquid boundary conditions have led to two equations, (4- 36) and (4- 39), which are linear equations in only two unknowns, A_α and A_β, and so can be solved simultaneously. Substituting for A_β from (4- 36) into (4- 39), gives

$$i\gamma_\beta\left(A_\alpha + iEA\right) + mi\gamma_\alpha A_\alpha = A\left(\left(\gamma_0^2 - \kappa\xi\right)G + \left(\gamma_1^2 - \kappa\xi\right)W\right) \qquad 4\text{- }40$$

which may be re-arranged to give

$$A_\alpha = A\frac{\left(\gamma_0^2 - \kappa\xi\right)G + \left(\gamma_1^2 - \kappa\xi\right)W + \gamma_\beta E}{mi\gamma_\alpha + i\gamma_\beta} \qquad 4\text{- }41$$

and similarly A_β can be found to be given by

$$A_\beta = A\frac{\left(\gamma_0^2 - \kappa\xi\right)G + \left(\gamma_1^2 - \kappa\xi\right)W - m\gamma_\alpha E}{mi\gamma_\alpha + i\gamma_\beta} \qquad 4\text{-}42$$

Substituting these expressions for A_α and A_β into the defined forms for p_α and p_β (equations (4- 28) and (4- 29)) results in the scattered pressures being given by

$$p_\alpha = \frac{1}{2\pi}\int_{-\infty}^{\infty} A(\kappa)\frac{\left(\gamma_0^2 - \kappa\xi\right)G + \left(\gamma_1^2 - \kappa\xi\right)W + \gamma_\beta E}{mi\gamma_\alpha + i\gamma_\beta}\exp\left(i(\xi+\kappa)x\right)\exp\left(-i\gamma_\alpha z\right)d\kappa \qquad 4\text{-}43$$

$$p_\beta = \frac{1}{2\pi}\int_{-\infty}^{\infty} A(\kappa)\frac{\left(\gamma_0^2 - \kappa\xi\right)G + \left(\gamma_1^2 - \kappa\xi\right)W - m\gamma_\alpha E}{mi\gamma_\alpha + i\gamma_\beta}\exp\left(i(\xi+\kappa)x\right)\exp\left(i\gamma_\beta z\right)d\kappa \qquad 4\text{-}44$$

where

$$G = -m(1+V)$$
$$E = \gamma_0(1-V) - \gamma_1 W \qquad 4\text{-}45$$

4.6 Consistency checks for scattered solution

A consistency check for the scattered solutions is now to verify that the expression for p_α reduces to the standard expressions for the scattered pressures for both a pressure release boundary and a rigid boundary. The pressure release case, where ρ_1 and c_1 go to zero, has:

V = -1 from smooth surface reflection theory
W = 0 from smooth surface reflection theory
m=0

and so

G=0
$E = 2\gamma_0$

and hence

$$p_\alpha = \frac{1}{2\pi}\int_{-\infty}^{\infty} A(\kappa)\frac{0+0+2\gamma_0\gamma_\beta}{i\gamma_\beta}\exp\left(i(\xi+\kappa)x\right)\exp\left(-i\gamma_\alpha z\right)d\kappa \qquad 4\text{-}46$$

giving

$$p_\alpha = \frac{1}{2\pi}\int_{-\infty}^{\infty} -2i\gamma_0 A(\kappa)\exp(i(\xi+\kappa)x)\exp(-i\gamma_\alpha z)d\kappa \qquad 4\text{-}47$$

This equation is exactly as required for a pressure release surface, as derived earlier in chapter 3. Secondly, the rigid boundary condition case, where ρ_1 and c_1 tend to infinity, has:

V = 1 from smooth surface reflection theory

W = 2 from smooth surface reflection theory

$m \to \infty$

and so

G=-2m

E = 0

and hence

$$p_\alpha = \frac{1}{2\pi}\int_{-\infty}^{\infty} A(\kappa)\frac{-2m(\gamma_0^2 - \kappa\xi) + 2(\gamma_1^2 - \kappa\xi) - 2\gamma_1\gamma_\beta}{mi\gamma_\alpha + i\gamma_\beta}\exp(i(\xi+\kappa)x)\exp(-i\gamma_\alpha z)d\kappa$$

The terms containing factors of m are dominant and so this reduces to

$$p_\alpha = \frac{1}{2\pi}\int_{-\infty}^{\infty} 2i(\gamma_0^2 - \kappa\xi)A(\kappa)\gamma_\alpha^{-1}\exp(i(\xi+\kappa)x)\exp(-i\gamma_\alpha z)d\kappa \qquad 4\text{-}48$$

Again this equation is exactly as required when compared to the standard expression (BREKHOVSKIKH and LYSANOV (1990)).

The fact that the elastic scattering solutions (equations (4-43) and (4-44)) tend to the correct standard solutions for both high and low limiting densities and sound speeds provides great confidence that these elastic scattering solutions are correct. In terms of the physics of the scattering solution equations (4-43) and (4-44) provide two insights. Firstly, that the scattering directions are independent of the elastic properties of the scattering interface. Secondly, that the amplitude of the scattered pressure is derived from the product of the rough surface amplitude spectrum ($A(\kappa)$) and a term which depends on the elastic properties of the scattering interface.

The results predict that there is scattered reflected energy in all directions. As such, this model can be used for calculating backwards and forwards scattering. This is true for both the reflected and transmitted scattered energy, with the horizontal wavevectors being

given by equations (4- 21) and (4- 25) respectively. Scattering in this way leads naturally to there even being sound energy within the sediment as a result of an incident wave below the (smooth surface) grazing angle. This will occur when the amplitude and phase of a surface wavenumber component is such that it subtracts from the incident horizontal wavenumber to give a horizontal wavenumber which is less than the maximum allowed wavenumber (ω/c_1 or ω/b_1) in the seabed. For seabeds which weakly support shear waves, where b_1 is small, then one might expect this effect to be more pronounced. This is one of the sub-critical penetration mechanisms reviewed by MAGUER et al (2000) the other mechanism being evanescent waves due to the attenuation of the sediment (see chapter 2 where this is described for a smooth surface), examined by THORSOS et al (2000).

4.7 Scattering strength

The scattering strength is defined in chapter 3 (see equations (3-90), (3-91) and (3-92)). Using the results derived above the scattering strength has been calculated for six rough liquid / liquid interfaces, shown in Figure 5 below. For each of these rough interfaces the liquid from which the sound is incident has a density of 1000kg/m^3 and a soundspeed of 1500m/s. The incident sound frequency is 800Hz, and is at an angle of 45°. The details of the scattering media are given in Table 1 below. In all cases the attenuation coefficients in both incident and scattering media have been set to zero. Each rough surface has a Gaussian power spectral density defined by equation (3-48). This definition is such that the integral of the power spectral density over all κ is equal to $2\pi\sigma^2$, for all root mean square surface heights and all surface correlation lengths.

medium	density (kg/m^3)	sound speed (m/s)	rms surface height/λ	correlation length/λ
data 1	0	0	0.053	0.45
data 2	2000	2000	0.053	0.45
data 3	3000	3000	0.053	0.45
data 4	3000	3000	0.100	0.45
data 5	2000	2000	0.053	0.20
data 6	10000	10000	0.053	0.45

Table 1: Geoacoustic parameters and surface roughness characteristics for the scattering media in Figure 5.

Standard first order pertubation theory results from THORSOS (1988) are shown in Figure 4 for a rough "pressure release" interface. The scattering strength curve shown in Figure 5 for "data 1" is produced using the equations developed here, using the appropriate geoacoustic (zero density and soundspeed) and interface parameters, and compares well with the benchmark case. The equations developed here are also used with other geoacoustic and rough surface parameters to produce the other curves in Figure 5, to show

how the scattering strength is dependent on the elastic properties of the rough interface, as well as the statistical properties of the roughness itself.

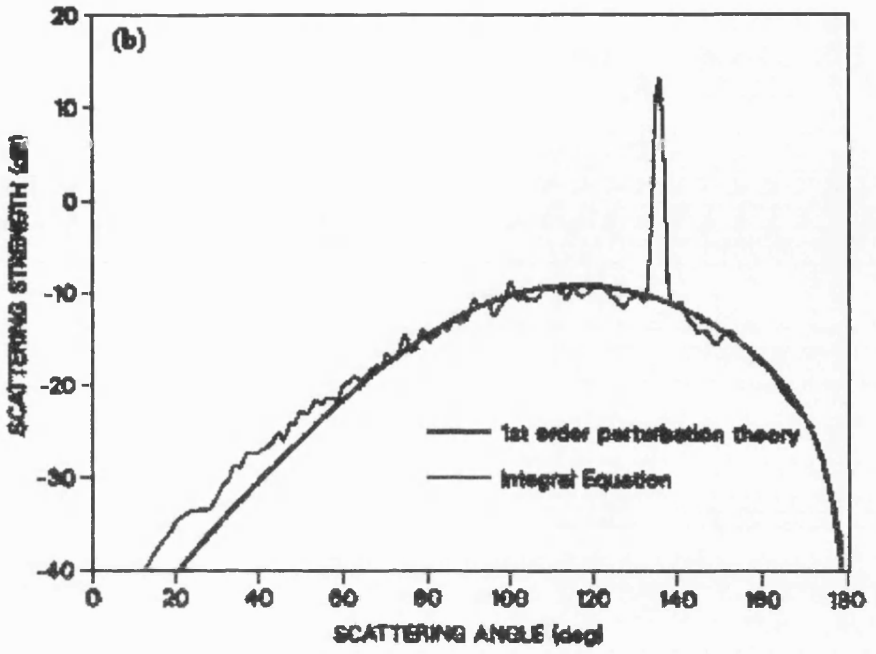

Figure 4: Standard first order perturbation theory results (excluding coherent component) for the scattering of sound from a rough surface, compared with integral equation results (including coherent component) from THORSOS 1988. The plot shows scattering strength versus scattering angle, for an incident wave at 45°. The scattering angle is numbered such that 135° is forwardscatter and 45° is backscatter. The rough surface has a Gaussian roughness spectrum with root mean square height of 0.053λ and surface correlation length 0.45λ where λ is the wavelength of the incident sound. The scattering medium has "pressure release boundary conditions", i.e. it has zero density and sound speed.

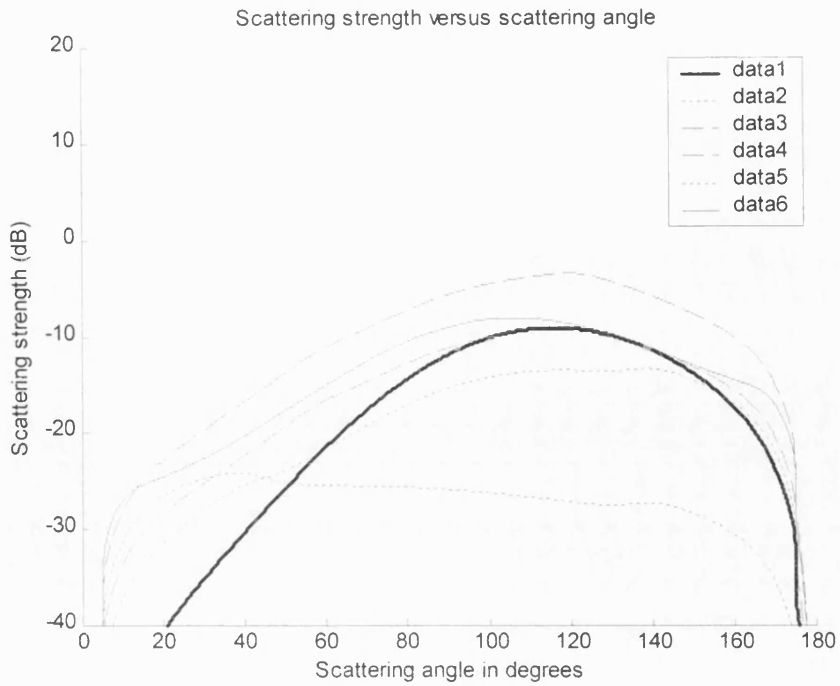

Figure 5: First order perturbation theory results calculated using the development of chapters 3 and 4. The figure shows plots of scattering strength versus scattering angle, each for an incident wave at 45°, for liquid / liquid interfaces with different Gaussian roughness spectra and impedances. The incident medium is modelled as having a sound speed of 1500m/s and a density of 1000kg/m^3. The scattering media geoacoustic and interface properties are:

medium	*density (kg/m^3)*	*sound speed (m/s)*	*rms surface height/λ*	*correlation length/λ*
data 1	*0*	*0*	*0.053*	*0.45*
data 2	*2000*	*2000*	*0.053*	*0.45*
data 3	*3000*	*3000*	*0.053*	*0.45*
data 4	*3000*	*3000*	*0.100*	*0.45*
data 5	*2000*	*2000*	*0.053*	*0.20*
data 6	*10000*	*10000*	*0.053*	*0.45*

It can be seen that the plot for the scattering medium with "pressure release boundary conditions", "data 1", matches the first order perturbation theory solution presented by THORSOS (1988) – see Figure 4 earlier. When the scattering medium has realistic densities and sound speeds, but the same roughness spectrum, the scattering strength varies significantly from that for the interface with "pressure release boundary conditions": the plots for "data 2" (upper dotted line) and for "data 3" (lower dashed line) show this to be the case, particularly at low scattering angles. The plot for "data 4" shows that an increase in rms surface height increases the level, but not the shape, of the scattering strength curve. The plot for "data 5" shows that a reduction in correlation length, for a surface with Gaussian power spectral density, has the effect of increasing the proportion of the scattering in the backscattering quadrant (0 – 90°), and decreasing the mean level of the scattering strength curve.

5 Scattering from a liquid / solid interface

In this chapter it is shown how a perturbation theory method can be developed to calculate the scattering from a rough liquid / solid interface. In terms of the physics of the interface, the only difference between a solid and a liquid is that a solid has a non-zero elasticity modulus, μ: in other words a solid is able to support shear waves as well as compressional waves. Instead of solving for two waves, the reflected scattered and transmitted scattered compressional waves, it is now required therefore to solve for three waves: reflected scattered and transmitted scattered compressional waves, and the transmitted scattered shear wave. In the limit of the elasticity modulus going to zero, the liquid / solid solutions tend to the liquid / liquid solution.

The development here follows almost exactly the same methodology as that used for calculating the scattered pressures for the liquid / liquid interface in chapter 4. The first difference is that for the case of scattering from a liquid / solid interface it is simpler to express the boundary condition equations in the form of the *velocity potentials*, just as when calculating the smooth surface reflection coefficient shown earlier in chapter 2. The second difference is that for the liquid / solid case there are 3 boundary conditions (rather than 2 used for the liquid / liquid case), again just as shown in chapter 2, and the application of each of these to a rough surface will be considered in turn.

As for the liquid / liquid case, again it will be seen that the solutions for the spectral amplitudes of the scattered pressure fields are a product of the rough surface spectral amplitudes and functions of the geoacoustic parameters. In other words, the solutions are separable into a roughness factor and a geoacoustics factor. The solutions are, therefore, equally valid for any rough surface spectrum which satisfies the amplitude and correlation length conditions discussed in chapter 3.

It is assumed now that the velocity potential above the interface is given by

$$\phi_0 = I\exp\left[i\xi x + i\alpha z\right] + V\exp\left[i\xi x - i\alpha z\right] + \phi_V \qquad 5\text{-}1$$

and that the velocity potential within the solid is given by

$$\phi_1 = W\exp\left[i\xi x + i\alpha_1 z\right] + \phi_W \qquad 5\text{-}2$$

$$\psi_1 = P\exp\left[i\xi x + i\beta_1 z\right] + \phi_P \qquad 5\text{-}3$$

where the I, V, W and P are the zero order terms calculated using smooth surface reflection theory (see chapter 2) and the ϕ_V, ϕ_W, and ϕ_P terms are the first order scattered terms. The α and β terms are the vertical wavevectors for the compressional waves and transverse wave respectively, while the ξ is the horizontal wavevector which is the same in both media.

5.1 Continuity of particle velocity

The boundary condition equation for a smooth surface (BREKHOVSKIKH & LYSANOV (1990)) is written as

$$\frac{\partial \phi_0}{\partial z} = \frac{\partial \phi_1}{\partial z} + \frac{\partial \psi_1}{\partial x} \qquad 5.1\text{-}1$$

which for a rough surface may be re-written as

$$\frac{\partial \varphi_0}{\partial n} = \frac{\partial \varphi_1}{\partial n} + \frac{\partial \psi_1}{\partial s} \qquad 5.1\text{-}2$$

Substituting for $\partial/\partial n$ and $\partial/\partial s$ using the expressions derived in chapter 3, equations (3-30) and (3-31), and cancelling the cosine factors on both sides gives

$$\frac{\partial \phi_0}{\partial z} - \frac{\partial \zeta}{\partial x}\frac{\partial \phi_0}{\partial x} = \frac{\partial \phi_1}{\partial z} - \frac{\partial \zeta}{\partial x}\frac{\partial \phi_1}{\partial x} + \frac{\partial \psi_1}{\partial x} + \frac{\partial \zeta}{\partial x}\frac{\partial \psi_1}{\partial z} \qquad 5.1\text{-}3$$

This boundary condition equation holds on the rough surface. In general, a point P on the rough surface will be at a height ζ above the mean surface height (the z co-ordinate is set such that the mean surface height is z=0), where ζ varies with position (x co-ordinate) on the rough surface. This is shown in Figure 1 below.

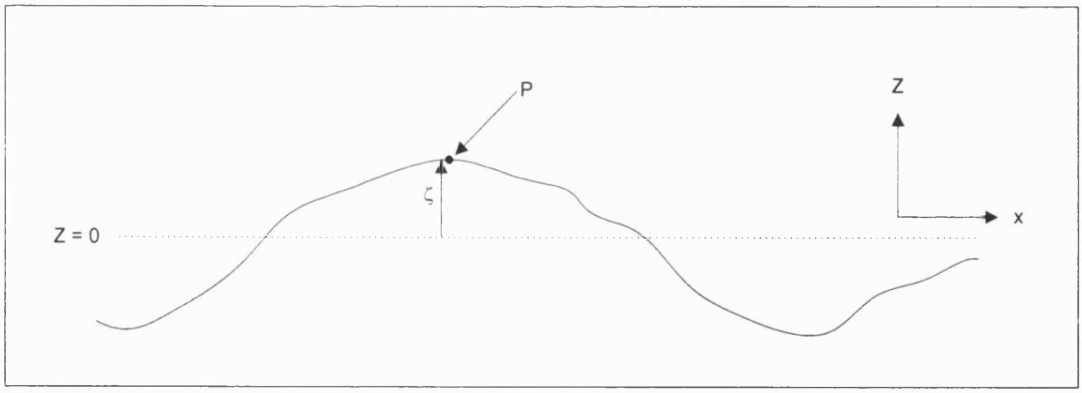

Figure 1: A point P on a rough surface is at a height ζ above the mean surface height at z=0, where ζ varies with position (x co-ordinate) on the rough surface. The boundary condition equation (5.1- 3) holds on the rough surface. In order to simplify the evaluation of the subsequent equations the boundary condition equation (5.1- 3) is re-written in terms of equivalent boundary condition equation which holds at z=0. This is done by assuming that ζ is small, and therefore assuming that the boundary condition equation at the rough surface may be written as a Taylor series expansion (in ζ) of the boundary condition equation written to apply at z=0.

In order to simplify the evaluation of the subsequent equations the boundary condition equation (5.1- 3) is re-written in terms of equivalent boundary condition equation which holds at z=0. This is done by assuming that ζ is small, and therefore assuming that the boundary condition equation at the rough surface may be written as a Taylor series expansion (in ζ) of the boundary condition equation written to apply at z=0. This is done by re-writing the boundary condition equation (5.1- 3) and applying the operator

$$\left(1+\zeta\frac{\partial}{\partial z}\right)$$

to both sides of each equation. In applying this operator only zero and first order terms are kept. It is assumed that ζ and its gradient are small and hence first order quantities, and so terms involving both of these are therefore second order and are neglected. Thus equation (5.1- 3) which holds on the rough surface may be replaced by equation (5.1- 4) which holds on the mean surface z=0:

$$\frac{\partial\phi_0}{\partial z}+\zeta\frac{\partial^2\phi_0}{\partial z^2}-\frac{\partial\zeta}{\partial x}\frac{\partial\phi_0}{\partial x}=\frac{\partial\phi_1}{\partial z}+\zeta\frac{\partial^2\phi_1}{\partial z^2}-\frac{\partial\zeta}{\partial x}\frac{\partial\phi_1}{\partial x}+\frac{\partial\psi_1}{\partial x}+\zeta\frac{\partial^2\psi_1}{\partial z\partial x}+\frac{\partial\zeta}{\partial x}\frac{\partial\psi_1}{\partial z} \qquad 5.1\text{- }4$$

In this equation the first, fourth and seventh terms are zero order, the rest are first order. Substituting for ϕ_0, ϕ_1 and ψ_1 from equations (5-1, 5-2 and 5-3) and keeping only the first order terms gives

$$\frac{\partial\phi_V}{\partial z}+\left(\zeta\frac{\partial^2}{\partial z^2}-\frac{\partial\zeta}{\partial x}\frac{\partial}{\partial x}\right)\left(I\exp(i\xi x+i\alpha z)+V(i\xi x-i\alpha z)\right)=\frac{\partial\phi_W}{\partial z}+\left(\zeta\frac{\partial^2}{\partial z^2}-\frac{\partial\zeta}{\partial x}\frac{\partial}{\partial x}\right)W\exp(i\xi x+i\alpha_1 z)$$
$$+\frac{\partial\phi_P}{\partial x}+\left(\zeta\frac{\partial^2}{\partial z\partial x}+\frac{\partial\zeta}{\partial x}\frac{\partial}{\partial z}\right)P\exp(i\xi x+i\beta_1 z) \qquad 5.1\text{- }5$$

Performing the differentiations with respect to z, and evaluating this at z=0 gives

$$\frac{\partial\phi_V}{\partial z}-\left(\zeta\alpha^2+\frac{\partial\zeta}{\partial x}\frac{\partial}{\partial x}\right)(I+V)\exp(i\xi x)=\frac{\partial\phi_W}{\partial z}-\left(\zeta\alpha_1^2+\frac{\partial\zeta}{\partial x}\frac{\partial}{\partial x}\right)W\exp(i\xi x)$$
$$+\frac{\partial\phi_P}{\partial x}+\left(\zeta i\beta_1\frac{\partial}{\partial x}+i\beta_1\frac{\partial\zeta}{\partial x}\right)P\exp(i\xi x) \qquad 5.1\text{- }6$$

To proceed further the expressions for the scattered velocity potentials, ϕ, and the surface, ζ, must be substituted for. These are assumed to be of exactly the same form as used in

chapter 4 for the liquid / liquid case, except that now the scattered solutions are in terms of velocity potentials, *viz*.

$$\zeta(x) = \frac{1}{2\pi}\int_{-\infty}^{\infty} A(\kappa)\exp(i\kappa x)d\kappa \qquad 5.1\text{-}7$$

and

$$\phi_V = \frac{1}{2\pi}\int_{-\infty}^{\infty} A_V(\kappa)\exp(i(\kappa+\xi)x)\exp(-i\gamma_V z)d\kappa \qquad 5.1\text{-}8$$

with similar expressions for ϕ_W and ϕ_P but with the exponential terms indicating waves travelling into the solid since these are the transmitted waves. These are substituted into equation (5.1- 6). All the constant multiplicative terms are taken inside the integrals. The derivative terms simplify as follows:

$$\frac{\partial\zeta}{\partial x} \quad \Rightarrow \quad i\underline{\kappa}\zeta$$

$$\frac{\partial\phi}{\partial x} \quad \Rightarrow \quad i(\underline{\kappa} + \underline{\xi})\phi$$

All the terms in the equation are Fourier transforms using the same variable, κ. The quantities being transformed must therefore equate[1]. The equation is then evaluated at x=0. The factors of $1/2\pi$ cancel. Hence equation (5.1- 6) becomes

$$-i\gamma_V A_V + A\left(\kappa\xi - \alpha^2\right)(I+V) = i\gamma_W A_W + A\left(\kappa\xi - \alpha_1^2\right)W + i(\kappa+\xi)A_P - A\beta_1(\kappa+\xi)P \qquad 5.1\text{-}9$$

where all the A and $A_{V,W,P}$ terms are functions of κ. Multiplying both sides by minus 1 gives

$$i\gamma_V A_V - A\left(\kappa\xi - \alpha^2\right)(I+V) = -i\gamma_W A_W - A\left(\kappa\xi - \alpha_1^2\right)W - i(\kappa+\xi)A_P + A\beta_1(\kappa+\xi)P \qquad 5.1\text{-}10$$

Equation (5.1- 10) is a linear equation in terms of the three unknowns, A_V, A_W and A_P, representing the first boundary condition, continuity of particle velocity. This equation will be solved simultaneously with the other two equations which will be derived in the following two sections.

[1] Note: it is not enough to say that the integrals equate and so the integrands must equate, since one of the integrands may contain a function which integrates over the limits to zero. One of the properties of a Fourier transform is that if the Fourier transforms of two functions are equal, then the two functions are themselves equal. It is this property that is invoked here.

5.2 Continuity of force (normal)

The boundary condition equation for σ_{33} continuity (BREKHOVSKIKH & LYSANOV (1990)) is

$$\lambda_0\left(\frac{\partial^2\phi_0}{\partial x^2}+\frac{\partial^2\phi_0}{\partial z^2}\right)=\lambda_1\left(\frac{\partial^2\phi_1}{\partial x^2}+\frac{\partial^2\phi_1}{\partial z^2}\right)+2\mu_1\left(\frac{\partial^2\phi_1}{\partial z^2}+\frac{\partial^2\psi_1}{\partial x\partial z}\right) \qquad 5.2\text{- }1$$

which for a rough surface may be re-written as

$$\lambda_0\left(\frac{\partial^2\phi_0}{\partial s^2}+\frac{\partial^2\phi_0}{\partial n^2}\right)=\lambda_1\left(\frac{\partial^2\phi_1}{\partial s^2}+\frac{\partial^2\phi_1}{\partial n^2}\right)+2\mu_1\left(\frac{\partial^2\phi_1}{\partial n^2}+\frac{\partial^2\psi_1}{\partial s\partial n}\right) \qquad 5.2\text{- }2$$

Substituting for $\partial^2/\partial n^2$, $\partial^2/\partial s^2$ and $\partial^2/\partial s\partial n$ using the equations derived in chapter 3, equations (3-32), (3-33) and (3-34), gives

$$\lambda_0\left(\frac{\partial^2}{\partial z^2}+\frac{\partial^2}{\partial x^2}\right)\phi_0=\lambda_1\left(\frac{\partial^2}{\partial z^2}+\frac{\partial^2}{\partial x^2}\right)\phi_1+2\mu_1\left(\frac{\partial^2}{\partial x^2}-2\frac{\partial\zeta}{\partial x}\frac{\partial^2}{\partial x\partial z}\right)\phi_1+2\mu_1\left(\frac{\partial^2}{\partial x\partial z}+\frac{\partial\zeta}{\partial x}\left(\frac{\partial^2}{\partial z^2}-\frac{\partial^2}{\partial x^2}\right)\right)\psi_1 \qquad 5.2\text{- }3$$

where ζ is the rough surface amplitude, as described earlier. This boundary condition equation holds on the rough surface. As for the first boundary condition (section 5-1), in order to simplify the evaluation of the subsequent equations the boundary condition equation (5.2- 3) is re-written in terms of equivalent boundary condition equation which holds at z=0. This is done by assuming that ζ is small, and therefore assuming that the boundary condition equation at the rough surface may be written as a Taylor series expansion (in ζ) of the boundary condition equation written to apply at z=0. This is done by re-writing the boundary condition equation (5.2- 3) and applying the operator

$$\left(1+\zeta\frac{\partial}{\partial z}\right)$$

to both sides of each equation. In applying this operator only zero and first order terms are kept. It is assumed that ζ and its gradient are small and hence first order quantities, and so terms involving both of these are therefore second order and are neglected. Thus equation (5.2- 3) which holds on the rough surface may be replaced by equation (5.2- 4) which holds on the mean surface z=0:

$$\lambda_0\left(\frac{\partial^2}{\partial z^2}+\frac{\partial^2}{\partial x^2}\right)\phi_0 \quad = \quad \lambda_1\left(\frac{\partial^2}{\partial z^2}+\frac{\partial^2}{\partial x^2}\right)\phi_1+2\mu_1\left(\frac{\partial^2}{\partial x^2}-2\frac{\partial\zeta}{\partial x}\frac{\partial^2}{\partial x\partial z}\right)\phi_1$$
$$+\lambda_0\zeta\left(\frac{\partial^3}{\partial z^3}+\frac{\partial^3}{\partial z\partial x^2}\right)\phi_0 \qquad +2\mu_1\left(\frac{\partial^2}{\partial x\partial z}+\frac{\partial\zeta}{\partial x}\left(\frac{\partial^2}{\partial z^2}-\frac{\partial^2}{\partial x^2}\right)\right)\psi_1$$
$$+\lambda_1\zeta\left(\frac{\partial^3}{\partial z^3}+\frac{\partial^3}{\partial z\partial x^2}\right)\phi_1+2\mu_1\zeta\left(\frac{\partial^3}{\partial z\partial x^2}\right)\phi_1+2\mu_1\zeta\left(\frac{\partial^3}{\partial z^2\partial x}\right)\psi_1 \qquad 5.2\text{- }4$$

In this equation the terms containing ζ and its derivative with respect to x are all first order: the rest of the terms are zero order terms. Looking only at the left hand side (*lhs*) of this equation and substituting for ϕ_0 from equation (5-1) and keeping only first order terms gives:

$$lhs=\lambda_0\left(\frac{\partial^2}{\partial z^2}+\frac{\partial^2}{\partial x^2}\right)\phi_V+\lambda_0\zeta\left(\frac{\partial^3}{\partial z^3}+\frac{\partial^3}{\partial z\partial x^2}\right)\left(I\exp(i\xi x+i\alpha z)+V\exp(i\xi x-i\alpha z)\right) \qquad 5.2\text{- }5$$

Performing the differentiations and evaluating this equation at z=0 gives

$$lhs=\lambda_0\left(\frac{\partial^2}{\partial z^2}+\frac{\partial^2}{\partial x^2}\right)\phi_V-i\lambda_0\zeta\alpha\left(\alpha^2+\xi^2\right)(I-V)\exp(i\xi x) \qquad 5.2\text{- }6$$

For the ϕ_1 terms from equation (5.2- 4), equation (5-2) is substituted and only first order terms are kept to give:

$$\phi_1 terms \Rightarrow \lambda_1\left(\frac{\partial^2}{\partial z^2}+\frac{\partial^2}{\partial x^2}\right)\phi_W+2\mu_1\left(\frac{\partial^2}{\partial x^2}\right)\phi_W$$
$$-4\mu_1\left(\frac{\partial\zeta}{\partial x}\frac{\partial^2}{\partial x\partial z}\right)W\exp(i\xi x+i\alpha_1 z)$$
$$+\left(\lambda_1\zeta\left(\frac{\partial^3}{\partial z^3}+\frac{\partial^3}{\partial z\partial x^2}\right)+2\mu_1\zeta\left(\frac{\partial^3}{\partial z\partial x^2}\right)\right)W\exp(i\xi x+i\beta_1 z) \qquad 5.2\text{- }7$$

Performing the differentiations and evaluating at z=0 gives

$$\phi_1 terms \Rightarrow \lambda_1\left(\frac{\partial^2}{\partial z^2}+\frac{\partial^2}{\partial x^2}\right)\phi_W+2\mu_1\left(\frac{\partial^2}{\partial x^2}\right)\phi_W$$
$$+4\mu_1\alpha_1\xi\left(\frac{\partial\zeta}{\partial x}\right)W\exp(i\xi x)$$
$$-i\alpha_1\left(\lambda_1\zeta\left(\alpha_1^2+\xi^2\right)+2\mu_1\zeta\xi^2\right)W\exp(i\xi x) \qquad 5.2\text{- }8$$

For the ψ_1 terms from equation (5.2- 4), equation (5-3) is substituted and only first order terms are kept to give:

$$\psi_1 terms \Rightarrow 2\mu_1\left(\frac{\partial^2}{\partial x \partial z}\right)\phi_P + 2\mu_1\left(\frac{\partial \zeta}{\partial x}\left(\frac{\partial^2}{\partial z^2} - \frac{\partial^2}{\partial x^2}\right) + \zeta\left(\frac{\partial^3}{\partial z^2 \partial x}\right)\right)P\exp(i\xi x + i\beta_1 z) \qquad 5.2\text{- } 9$$

Performing the differentiations and evaluating at z=0 gives

$$\psi_1 terms \Rightarrow 2\mu_1\left(\frac{\partial^2}{\partial x \partial z}\right)\phi_P - 2\mu_1\left(\frac{\partial \zeta}{\partial x}\left(\beta_1^2 - \xi^2\right) + i\zeta\beta_1^2\xi\right)P\exp(i\xi x) \qquad 5.2\text{- } 10$$

Partial equations (5.2-6, 5.2-8, and 5.2-10) are now re-combined to give:

$$\begin{aligned}
\lambda_0\left(\frac{\partial^2}{\partial z^2} + \frac{\partial^2}{\partial x^2}\right)\phi_V \quad &= \quad \lambda_1\left(\frac{\partial^2}{\partial z^2} + \frac{\partial^2}{\partial x^2}\right)\phi_W + 2\mu_1\left(\frac{\partial^2}{\partial x^2}\right)\phi_W \\
-i\lambda_0\zeta\alpha\left(\alpha^2 + \xi^2\right)(I - V)\exp(i\xi x) \quad &\qquad + 4\mu_1\alpha_1\xi\left(\frac{\partial \zeta}{\partial x}\right)W\exp(i\xi x) \\
&\qquad - i\alpha_1\left(\lambda_1\zeta\left(\alpha_1^2 + \xi^2\right) + 2\mu_1\zeta\xi^2\right)W\exp(i\xi x) \\
&\qquad 2\mu_1\left(\frac{\partial^2}{\partial x \partial z}\right)\phi_P - 2\mu_1\left(\frac{\partial \zeta}{\partial x}\left(\beta_1^2 - \xi^2\right) + i\zeta\beta_1^2\xi\right)P\exp(i\xi x)
\end{aligned} \qquad 5.2\text{- } 11$$

To proceed further the expressions for the scattered velocity potentials, ϕ, and the surface, ζ, are substituted for using the same equations as in section 5.1. All the constant multiplicative terms, (I-V), W etc., are taken inside the integrals. The derivative terms simplify as described earlier (see section 5.1). As for the first boundary condition equation, all the terms which remain are Fourier transforms using the same variable, κ. The quantities being transformed must therefore equate. After simple but involved algebra equation (5.2- 11) reduces to:

$$\begin{aligned}
-\lambda_0 k_0^2 A_V \quad &= \quad -\lambda_1 k_1^2 A_W - 2\mu_1(\kappa + \xi)^2 A_W \\
-i\lambda_0 A\alpha k_0^2 (I - V) \quad &\qquad +4i\mu_1\alpha_1\xi\kappa A W \\
&\qquad - i\alpha_1\left(\lambda_1 A k_1^2 + 2\mu_1 A\xi^2\right)W \\
&\qquad - 2\mu_1\gamma_P(\kappa + \xi)A_P - 2i\mu_1 A\left(\kappa\left(\beta_1^2 - \xi^2\right) + \beta_1^2\xi\right)P
\end{aligned} \qquad 5.2\text{- } 12$$

Multiplying both sides by minus 1 gives

$$\lambda_0 k_0^2 A_V = {}_1k_1^2 A_W \quad 2\ {}_1(\quad \xi)^2 A_W$$

5.3 Continuity of force (shear)

On the liquid side of the interface there can be no net shear forces and so the boundary condition equation for σ_{31} continuity (BREKHOVSKIKH & LYSANOV (1990)) is relatively simple:

$$2\frac{\partial^2\phi_1}{\partial x\partial z}+\frac{\partial^2\psi_1}{\partial x^2}-\frac{\partial^2\psi_1}{\partial z^2}=0 \qquad 5.3\text{- }1$$

which for a rough surface may be re-written as

$$2\frac{\partial^2\phi_1}{\partial s\partial n}+\frac{\partial^2\psi_1}{\partial s^2}-\frac{\partial^2\psi_1}{\partial n^2}=0 \qquad 5.3\text{- }2$$

Substituting for $\partial^2/\partial s\partial n$, $\partial^2/\partial s^2$ and $\partial^2/\partial n^2$ (see equations derived in chapter 3) gives:

$$2\left(\frac{\partial^2}{\partial x\partial z}+\frac{\partial\zeta}{\partial x}\left(\frac{\partial^2}{\partial z^2}-\frac{\partial^2}{\partial x^2}\right)\right)\phi_1+\left(\frac{\partial^2}{\partial x^2}-\frac{\partial^2}{\partial z^2}+4\frac{\partial\zeta}{\partial x}\frac{\partial^2}{\partial x\partial z}\right)\psi_1=0 \qquad 5.3\text{- }3$$

This boundary condition equation holds on the rough surface. As for the first two boundary conditions (sections 5-1 and 5-2), in order to simplify the evaluation of the subsequent equations the boundary condition equation (5.3- 3) is re-written in terms of equivalent boundary condition equation which holds at z=0. This is done by assuming that ζ is small, and therefore assuming that the boundary condition equation at the rough surface may be written as a Taylor series expansion (in ζ) of the boundary condition equation written to apply at z=0. This is done by re-writing the boundary condition equation (5.3- 3) and applying the operator

$$\left(1+\zeta\frac{\partial}{\partial z}\right)$$

to both sides of each equation. In applying this operator only zero and first order terms are kept. It is assumed that ζ and its gradient are small and hence first order quantities, and so terms involving both of these are therefore second order and are neglected. Thus equation (5.3- 3) which holds on the rough surface may be replaced by equation (5.3- 4) which holds on the mean surface z=0:

$$2\left(\frac{\partial^2}{\partial x\partial z}+\zeta\frac{\partial^3}{\partial x\partial z^2}+\frac{\partial\zeta}{\partial x}\left(\frac{\partial^2}{\partial z^2}-\frac{\partial^2}{\partial x^2}\right)\right)\phi_1+\left(\left(\frac{\partial^2}{\partial x^2}-\frac{\partial^2}{\partial z^2}\right)+\zeta\left(\frac{\partial^3}{\partial z\partial x^2}-\frac{\partial^3}{\partial z^3}\right)+4\frac{\partial\zeta}{\partial x}\frac{\partial^2}{\partial x\partial z}\right)\psi_1=0$$

5.3- 4

In this equation the terms containing ζ and its derivative with respect to x are all first order: the rest of the terms are zero order terms. Substituting for ϕ_0, ϕ_1 and ψ_1 from equations (5-1, 5-2, 5-3) and keeping only first order terms gives:

$$2\left(\frac{\partial^2\phi_W}{\partial x\partial z}+\zeta\frac{\partial^3}{\partial x\partial z^2}W\exp(i\xi x+i\alpha_1 z)+\frac{\partial\zeta}{\partial x}\left(\frac{\partial^2}{\partial z^2}-\frac{\partial^2}{\partial x^2}\right)W\exp(i\xi x+i\alpha_1 z)\right)$$

$$+\left(\frac{\partial^2}{\partial x^2}-\frac{\partial^2}{\partial z^2}\right)\phi_P+\zeta\left(\frac{\partial^3}{\partial z\partial x^2}-\frac{\partial^3}{\partial z^3}\right)P\exp(i\xi x+i\beta_1 z)+4\frac{\partial\zeta}{\partial x}\frac{\partial^2}{\partial x\partial z}P\exp(i\xi x+i\beta_1 z) \quad = \quad 0 \qquad 5.3\text{-}5$$

Performing the differentiations and evaluating this equation at z=0 gives

$$2\left(\frac{\partial^2\phi_W}{\partial x\partial z}-i\zeta\xi\alpha_1^2W\exp(i\xi x)-\frac{\partial\zeta}{\partial x}\left(\alpha_1^2-\xi^2\right)W\exp(i\xi x)\right)$$

$$+\left(\frac{\partial^2}{\partial x^2}-\frac{\partial^2}{\partial z^2}\right)\phi_P-i\beta_1\zeta\left(\xi^2-\beta_1^2\right)P\exp(i\xi x)-4\frac{\partial\zeta}{\partial x}\beta_1\xi P\exp(i\xi x) \quad = \quad 0 \qquad 5.3\text{-}6$$

To proceed further the expressions for the scattered velocity potentials, ϕ, and the surface, ζ, are substituted for using the same equations as in section 5.1. All the constant multiplicative terms, W, P etc., are taken inside the integrals. The derivative terms simplify as follows:

$$\frac{\partial\zeta}{\partial x} \quad \Rightarrow \quad i\kappa\zeta$$

$$\frac{\partial\phi}{\partial x} \quad \Rightarrow \quad i(\kappa+\xi)\phi$$

As for the other boundary condition equations, all the terms which remain are Fourier transforms using the same variable, κ. The quantities being transformed must therefore equate. The equation is then evaluated at x=0. Hence equation (5.3- 6) becomes

$$-2\left(\gamma_W(\kappa+\xi)A_W+iA\xi\alpha_1^2W+i\kappa A\left(\alpha_1^2-\xi^2\right)W\right)$$

$$-\left((\kappa+\xi)^2-\gamma_P^2\right)A_P-i\beta_1A\left(\xi^2-\beta_1^2\right)P-4i\kappa A\beta_1\xi P \quad = \quad 0 \qquad 5.3\text{-}7$$

This can be tidied up, and both sides can be multiplied by minus 1, to give

$$2\left(\gamma_W(\kappa+\xi)A_W+\left(i\xi\alpha_1^2-i\kappa\left(\xi^2-\alpha_1^2\right)\right)AW\right)+\left((\kappa+\xi)^2-\gamma_P^2\right)A_P+i\beta_1\left(\xi^2-\beta_1^2+4\kappa\xi\right)AP=0 \quad \text{5.3- 8}$$

This is a linear equation in terms of two of the three unknowns, A_W and A_P, representing the third boundary condition, continuity of shear stress across the interface. This equation will be solved simultaneously with the equations derived from the other two boundary conditions in sections 5.1 and 5.2.

5.4 Solution of the boundary condition equations

The three first order scattered pressure equations derived in sections 5.1, 5.2 and 5.3 are linear equations with three unknowns: A_V, A_W, and A_P. These are the spectral amplitude coefficients of the scattered velocity potentials. The parameter A is the spectral amplitude coefficient of the rough surface, ζ. In this section these first order scattered pressure equations will be solved simultaneously. It is, of course, possible to use a matrix approach and solve these equations numerically using a standard matrix inversion routine such as the MATLAB singular value decomposition (SVD) function. The analytical approach is preferred here initially since the properties of the solutions which are derived may then be more easily elucidated.

From sections 5.1, 5.2 and 5.3 earlier, the first order scattered pressure equations derived from the three elastic boundary conditions equations may be re-called:

$$i\gamma_V A_V - A\left(\kappa\xi - \alpha^2\right)(I+V) = -i\gamma_W A_W - A\left(\kappa\xi - \alpha_1^2\right)W - i(\kappa+\xi)A_P + A\beta_1(\kappa+\xi)P \qquad 5.4\text{- }1$$

$$\begin{aligned}\lambda_0 k_0^2 A_V \quad &= \quad \lambda_1 k_1^2 A_W + 2\mu_1(\kappa+\xi)^2 A_W \\ + i\lambda_0 A\alpha k_0^2 (I-V) \quad &\quad -4i\mu_1\alpha_1\xi\kappa AW \\ &\quad + i\alpha_1\left(\lambda_1 A k_1^2 + 2\mu_1 A\xi^2\right)W \\ &\quad + 2\mu_1\gamma_P(\kappa+\xi)A_P + 2i\mu_1 A\left(\kappa\left(\beta_1^2 - \xi^2\right) + \beta_1^2\xi\right)P\end{aligned} \qquad 5.4\text{- }2$$

$$2\left(\gamma_W(\kappa+\xi)A_W + \left(i\xi\alpha_1^2 - i\kappa\left(\xi^2 - \alpha_1^2\right)\right)AW\right) + \left((\kappa+\xi)^2 - \gamma_P^2\right)A_P + i\beta_1\left(\xi^2 - \beta_1^2 + 4\kappa\xi\right)AP = 0 \qquad 5.4\text{- }3$$

Factors of A can be taken out of everything as long as the factors of A are put back into the solutions for A_V, A_W, and A_P when they are derived. The constants in equation (5.4- 1) can be taken to the right hand side to give:

$$\begin{aligned}&i\gamma_V A_V + i\gamma_W A_W + i(\kappa+\xi)A_P = C_1 \\ &C_1 = \left(\kappa\xi - \alpha^2\right)(I+V) - \left(\kappa\xi - \alpha_1^2\right)W + \beta_1(\kappa+\xi)P\end{aligned} \qquad 5.4\text{- }4$$

Similarly equation (5.4- 2) can be re-arranged to give:

$$\begin{aligned}&\lambda_0 k_0^2 A_V - \left(\lambda_1 k_1^2 + 2\mu_1(\kappa+\xi)^2\right)A_W - 2\mu_1\gamma_P(\kappa+\xi)A_P = C_2 \\ &C_2 = -i\lambda_0\alpha k_0^2(I-V) + \left(i\alpha_1\left(\lambda_1 k_1^2 + 2\mu_1\xi^2\right) - 4i\mu_1\alpha_1\xi\kappa\right)W + 2i\mu_1\left(\kappa\left(\beta_1^2 - \xi^2\right) + \beta_1^2\xi\right)P\end{aligned} \qquad 5.4\text{- }5$$

and equation (5.4- 3) can be re-arranged to give:

$$2\gamma_W(\kappa+\xi)A_W + \left((\kappa+\xi)^2 - \gamma_P^2\right)A_P = C_3$$

$$C_3 = -2W\left(i\xi\alpha_1^2 - i\kappa\left(\xi^2 - \alpha_1^2\right)\right) - i\beta_1\left(\xi^2 - \beta_1^2 + 4\kappa\xi\right)P \qquad \text{5.4- 6}$$

Now that the constants have been separated out it is relatively simple to solve the three simultaneous equations. Starting with equation (5.4- 6): A_P can be separated out:

$$A_P = \frac{C_3 - C_4 A_W}{C_5} \qquad \text{5.4- 7}$$

where

$$C_4 = 2\gamma_W(\kappa + \xi)$$
$$C_5 = (\kappa + \xi)^2 - \gamma_P^2 \qquad \text{5.4- 8}$$

The unknown A_P must be substituted into the other two boundary condition equations to leave two equations in two unknowns. Firstly, substitution of equation (5.4- 7) into equation (5.4- 5) gives:

$$\lambda_0 k_0^2 A_V - C_6 A_W - C_7\left(\frac{C_3 - C_4 A_W}{C_5}\right) = C_2 \qquad \text{5.4- 9}$$

where

$$C_6 = \lambda_1 k_1^2 + 2\mu_1(\kappa + \xi)^2$$
$$C_7 = 2\mu_1\gamma_P(\kappa + \xi) \qquad \text{5.4- 10}$$

Secondly, substitution of equation (5.4- 7) into equation (5.4- 4) gives:

$$i\gamma_V A_V + i\gamma_W A_W + i(\kappa + \xi)\left(\frac{C_3 - C_4 A_W}{C_5}\right) = C_1$$

This is easily re-arranged to give:

$$i\gamma_V A_V + C_8 A_W = C_9 \qquad \text{5.4- 11}$$

where

$$C_8 = i\gamma_W - i\frac{C_4}{C_5}(\kappa + \xi)$$

$$C_9 = C_1 - i\frac{C_3}{C_5}(\kappa + \xi) \qquad \text{5.4- 12}$$

There are now two equations, (5.4- 9) and (5.4- 11), in two unknowns, A_V and A_W. Equation (5.4- 9) can be tidied up to give:

$$A_W = C_{10}A_V - C_{11} \qquad \text{5.4- 13}$$

where

$$C_{10} = \lambda_0 k_0^2 \Big/ \left(C_6 - \frac{C_7 C_4}{C_5}\right)$$

$$C_{11} = \left(C_2 + \frac{C_7 C_3}{C_5}\right) \Big/ \left(C_6 - \frac{C_7 C_4}{C_5}\right) \qquad \text{5.4- 14}$$

The unknown A_W from equation (5.4- 13) can be substituted into equation (5.4- 11) to give:

$$i\gamma_V A_V + C_8(C_{10}A_V - C_{11}) = C_9$$

Hence

$$A_V = \frac{C_9 + C_8 C_{11}}{i\gamma_V + C_8 C_{10}} \qquad \text{5.4- 15}$$

Putting the factors of A back in now gives:

$$A_V = A\left(\frac{C_9 + C_8 C_{11}}{i\gamma_V + C_8 C_{10}}\right)$$

$$A_W = A(C_{10}(A_V/A) - C_{11})$$

$$A_P = A\left(\frac{C_3 - C_4(A_W/A)}{C_5}\right) \qquad \text{5.4- 16}$$

These equations are the solutions for the spectral amplitudes of the scattered velocity potentials A_V, A_W and A_P respectively.

5.5 Consistency check as μ_1 goes to zero

The solutions derived in the last section for the spectral amplitudes of the scattered velocity potentials for a liquid / solid interface may be checked for consistency with those derived for a liquid / liquid interface. It must be remembered that for the liquid / liquid interface the scattered *pressures* rather than the scattered *velocity potentials* were used, so the solutions for the compressional and transverse waves scattered into the solid will differ by a factor of m ($=\rho_1/\rho_0$).

The solution for the liquid / solid interface may be reduced to that for a liquid / liquid interface by looking at the limit when the shear coefficient, μ_1, goes to zero. A few of the immediate consequences of this are seen if a couple of equations from chapter 2 are recalled:

$$c_t = \sqrt{\mu/\rho} \qquad 5.5\text{-}1$$

$$k_t = \omega/c_t \qquad 5.5\text{-}2$$

Firstly, the shear wave speed in the solid reduces to zero, and hence k_t is infinite. The corollary of this is that the shear waves do not exist, since any arbitrarily small attenuation coefficient will ensure that the waves are attenuated to zero. More formally, the smooth surface shear wave transmission coefficient, P, goes to zero, as shown in chapter 2, and the vertical wavevectors for the scattered shear waves, γ_P, go to zero. For this case, from chapter 2, we also find that the Lamé coefficient λ_1 is given by

$$\lambda_1 = \rho_1 c_1^2 \qquad 5.5\text{-}3$$

and $\lambda_1 k_1^2$ is given by

$$\lambda_1 k_1^2 = \rho_1 \omega^2 \qquad 5.5\text{-}4$$

Similarly in the upper (liquid) medium we have

$$\lambda_0 = \rho_0 c_0^2 \qquad 5.5\text{-}5$$

$$\lambda_0 k_0^2 = \rho_0 \omega^2 \qquad 5.5\text{-}6$$

Under these conditions the constants C_1 to C_7 used in section 5.4 tend to the following limits:

$$C_1 \Rightarrow \left(\kappa\xi - \alpha^2\right)\left(I + V\right) - \left(\kappa\xi - \alpha_1^2\right)W$$

$$C_2 \Rightarrow -i\alpha\rho_0\omega^2(I-V)+i\alpha_1\rho_1\omega^2 W$$

$$C_3 \Rightarrow -2W\left(i\xi\alpha_1^2 - i\kappa\left(\xi^2-\alpha_1^2\right)\right)$$

$$C_4 \Rightarrow 2\gamma_W(\kappa+\xi)$$

$$C_5 \Rightarrow -\infty$$

$$C_6 \Rightarrow \rho_1\omega^2$$

$$C_7 \Rightarrow 0\,. \qquad \text{5.5- 7}$$

The rest of the constants, C_8 to C_{11}, which are functions of the constants C_1 to C_7 can now be seen to have the following limits:

$$C_8 \Rightarrow i\gamma_W$$

$$C_9 \Rightarrow C_1 \Rightarrow \left(\kappa\xi-\alpha^2\right)(I+V)-\left(\kappa\xi-\alpha_1^2\right)W$$

$$C_{10} \Rightarrow \frac{\rho_0}{\rho_1}$$

$$C_{11} \Rightarrow -i\alpha\left(\frac{\rho_0}{\rho_1}\right)(I-V)+i\alpha_1 W \qquad \text{5.5- 8}$$

Substituting these limits into equation (5.4-16) for A_V gives:

$$A_V \Rightarrow A\left(\frac{\left(\kappa\xi-\alpha^2\right)(I+V)-\left(\kappa\xi-\alpha_1^2\right)W+i\gamma_W\left(-i\alpha\left(\frac{\rho_0}{\rho_1}\right)(I-V)+i\alpha_1 W\right)}{i\gamma_V+i\gamma_W\left(\frac{\rho_0}{\rho_1}\right)}\right) \qquad \text{5.5- 9}$$

Multiplying the numerator and denominator by m ($=\rho_1/\rho_0$) and multiplying out some of the bracketed terms then gives:

$$A_V \Rightarrow A\left(\frac{m\left(\kappa\xi-\alpha^2\right)(I+V)-\left(\kappa\xi-\alpha_1^2\right)mW+\gamma_W\left(\alpha(I-V)-\alpha_1 mW\right)}{mi\gamma_V+i\gamma_W}\right) \qquad \text{5.5- 10}$$

This equation for A_V is *exactly* the same as that derived for the liquid / liquid case in chapter 4, where W in that case is replaced by mW here since equation (5.5- 10) is in terms of velocity potential rather than pressure. For the scattered transmitted wave the limits for the constants C_{10} and C_{11} can be substituted into equation (5.4-16) for A_W to give

$$A_W = A\left(\frac{\rho_0}{\rho_1}(A_V/A)-\left(-i\alpha\left(\frac{\rho_0}{\rho_1}\right)(I-V)+i\alpha_1 W\right)\right) \qquad \text{5.5- 11}$$

and the derived value of A_V can also be substituted from equation (5.5- 10) to give:

$$A_W = A\left(\frac{\rho_0}{\rho_1}\left(\frac{m\left(\kappa\xi-\alpha^2\right)(I+V)-\left(\kappa\xi-\alpha_1^2\right)mW+\gamma_W\left(\alpha(I-V)-\alpha_1 mW\right)}{mi\gamma_V+i\gamma_W}\right)-\left(-i\alpha\left(\frac{\rho_0}{\rho_1}\right)(I-V)+i\alpha_1 W\right)\right) \qquad 5.5\text{- }12$$

This is easily re-arranged to give

$$mA_W = A\left(\frac{m\left(\kappa\xi-\alpha^2\right)(I+V)-\left(\kappa\xi-\alpha_1^2\right)mW-m\gamma_V\left(\alpha(I-V)-\alpha_1 mW\right)}{mi\gamma_V+i\gamma_W}\right) \qquad 5.5\text{- }13$$

Again this is *exactly* the same as the solution for the transmitted scattered wave for the liquid / liquid case, where, again, mA_W and mW here replace the A_W and W for the liquid / liquid case since equation (5.5- 13) is in terms of velocity potential rather than pressure. Lastly, looking at equation (5.4-16) for A_P and noting that the denominator C_5 goes to infinity, it is seen that A_P goes to zero, *exactly* as required for a liquid / liquid interface.

The fact that the scattered velocity potentials derived for a liquid / solid interface reduce (when converted into pressures by the factors of m) exactly to the scattered pressures derived for the liquid / liquid case shows that the latter is a subset of the general case of scattering at a liquid / solid interface. Just as for the smooth surface reflection coefficients, the liquid / liquid interface scattering coefficients can be derived from the liquid / solid scattering coefficients by setting the elastic coefficient μ_1 to zero. Rather than having separate algorithms for scattering from a liquid or a solid, it is sufficient therefore to consider scattering from just the liquid / solid interface.

As well as being consistent with the coefficients derived for the liquid / liquid case the scattered velocity potentials must approach the correct values for the limits of totally rigid and pressure release boundary conditions. The totally rigid limit can be examined by making the density ρ_1 infinitely large and setting just c_1, or both b_1 and c_1 to infinity. [Note that b_1 cannot arbitrarily go to infinity since b_1 is always less than c_1.] For the first of these with just ρ_1 and c_1 going large the situation is the same as for the liquid / liquid case, which was shown to tend to the correct limits earlier (chapter 4). The more general case for both c_1 and b_1 (and ρ_1) going large and small is considered in section 5.6.

The scattering strength is defined in chapter 3 (see equations (3-90), (3-91) and (3-92)). In Figure 1 the scattering strength is shown for a liquid / liquid interface calculated using the liquid / solid equations derived earlier in this chapter and calculated using the liquid / liquid equations derived in chapter 4. This is done for two different lower liquid layers: the first one has density 2000kg/m^3 and sound speed 2000m/s; the second has density

3000kg/m^3 and sound speed 3000m/s. In each case the scattering strength curves coincide perfectly[1], in agreement with the theoretical development above.

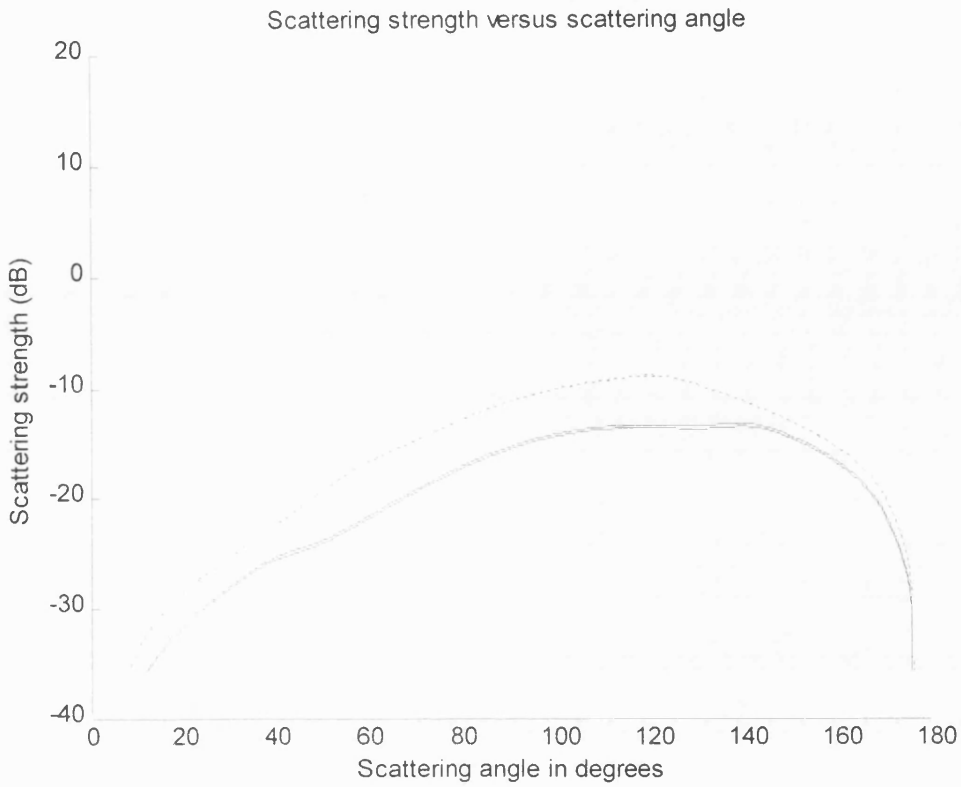

Figure 1: The plot shows scattering strength versus scattering angle, for an incident wave at 45°, for a liquid / liquid interface, calculated using the liquid / solid equations derived earlier in this chapter (see blue lines) and calculated using the liquid / liquid equations derived in chapter 4 (see red lines). This is done for two different lower liquid layers: the first one (solid lines) has density 2000kg/m^3 and sound speed 2000m/s; the second (dotted lines) has density 3000kg/m^3 and sound speed 3000m/s. In each case the incident medium has a density of 1000kg/m^3 and a soundspeed of 1500m/s. The scattering angle is numbered such that 135° is forwardscatter and 45° is backscatter. The rough surface has a Gaussian roughness spectrum with root mean square height of 0.053λ and surface correlation length 0.45λ where λ is the wavelength of the incident sound.

Figure 1 shows, therefore, that the liquid / solid scattering development in this chapter is consistent with the liquid / liquid scattering development from chapter 4.

[1] The lines ***do*** coincide perfectly, so, to enable them to be seen, densities of 1990 kg/m^3 and 2010 kg/m^3 and sound speeds of 1990 m/s and 2010 m/s were used for one comparison, and densities of 2990 kg/m^3 and 3010 kg/m^3 and sound speeds of 2990 m/s and 3010 m/s were used for the other.

5.6 Consistency checks for pressure release and rigid boundary conditions

The case for a totally rigid solid is considered first, in which the density and wave speeds in the solid tend to infinity. For this case the smooth surface velocity potential reflection and transmission coefficients, V, W and P, tend to +1, 0 and 0 respectively. Also, the wavenumbers k_1 and k_b tend to zero. The vertical components of the wavenumbers of the smooth surface coefficients, α_1 and β_1, do not tend to zero however. Since the horizontal component of all the smooth surface wavenumbers is fixed (ξ) then the vertical components must be $i\xi$. Similarly the vertical components of the wavenumbers for the scattered waves are $i(\kappa+\xi)$. It should also be noted that although k_1 and k_b tend to zero, the factors $\lambda_1 k_1^2$ and $\mu_1 k_b^2$ both tend to infinity (see the definitions of the Lamé coefficients in chapter 2). With these limits in mind the constants C_1 to C_7 tend to the following limits:

$$
\begin{aligned}
C_1 &\Rightarrow 2\left(\kappa\xi - \alpha^2\right) \\
C_2 &\Rightarrow 0 \\
C_3 &\Rightarrow 0 \\
C_4 &\Rightarrow 2i(\kappa+\xi)^2 \\
C_5 &\Rightarrow 2(\kappa+\xi)^2 \\
C_6 &\Rightarrow \infty \\
C_7 &= 2i\mu_1(\kappa+\xi)^2
\end{aligned}
\qquad \text{5.6- 1}
$$

The rest of the constants, C_8 to C_{11}, which depend on constants C_1 to C_7 can now be seen to have the following limits:

$$
\begin{aligned}
C_8 &\Rightarrow 0 \\
C_9 &\Rightarrow 2\left(\kappa\xi - \alpha^2\right) \\
C_{10} &\Rightarrow 0 \\
C_{11} &\Rightarrow 0
\end{aligned}
\qquad \text{5.6- 2}
$$

Substituting these limits into equation (5.4-16) for A_V gives:

$$
A_V = A\left(\frac{2\left(\kappa\xi - \alpha^2\right)}{i\gamma_V}\right) \qquad \text{5.6- 3}
$$

This is exactly the same as the scattered velocity potential for the rigid boundary case calculated in the standard texts (see BREKHOVSKIKH and LYSANOV (1990)). For the

scattered transmitted wave the limits for the constants C_3, C_{10} and C_{11} ensure that both A_W and A_P tend to zero (see equation (5.4-16). Again this is what one would expect for the velocity potentials at a rigid interface.

Secondly, the case for a pressure-release boundary is checked. In this case the density and wave speeds in the solid go to zero. As a result the smooth surface velocity potential reflection and transmission coefficients, V, W and P tend to –1, 0 and 0 respectively. Since the wave speeds are zero the wavenumbers k_1 and k_b tend to infinity, and the vertical components of the wavenumbers, α_1, β_1, γ_1 and γ_b also tend to infinity. In this case the factors $\lambda_1 k_1^2$ and $\mu_1 k_b^2$ both tend to zero. With these limits in mind the constants C_1 to C_7 tend to the following limits.

$$C_1 \Rightarrow 0$$

$$C_2 \Rightarrow -2i\alpha\rho_0\omega^2$$

$$C_3 \Rightarrow 0$$

$$C_4 \Rightarrow \infty$$

$$C_5 \Rightarrow -\infty$$

$$C_6 \Rightarrow 0$$

$$C_7 \Rightarrow 0 \qquad \text{5.6- 4}$$

The rest of the constants, C_8 to C_{11}, which depend on constants C_1 to C_7, must be evaluated carefully

$C_8 \Rightarrow i\gamma_W$ since C_4 / C_5 goes to zero (note that γ_W tends to infinity)

$C_9 \Rightarrow 0$

$C_{10} = \rho_0\omega^2 \Big/ \left(C_6 - \dfrac{C_7 C_4}{C_5} \right)$ which has a denominator of zero and so tends to infinity

$C_{11} = -2i\alpha\rho_0\omega^2 \Big/ \left(C_6 - \dfrac{C_7 C_4}{C_5} \right)$ which has a denominator of zero and so tends to infinity

5.6- 5

Substituting these limits into equation (5.4-16) for A_V it is seen that in the numerator the C_8C_{11} term dominates, and in the denominator the C_8C_{10} term dominates. Hence for A_V the factor C_{11} / C_{10} must be evaluated (since the C_8 now cancels). Looking at both C_{10} and C_{11} it is seen that their denominators cancel. Hence it is found that:

$$A_V = -2i\alpha A \qquad \text{5.6- 6}$$

This is exactly the same as the scattered velocity potential for the pressure release boundary case calculated in the standard texts (see BREKHOVSKIKH and LYSANOV (1990)). It is trivial to substitute this into equations (5.4-16) for A_W and A_P and obtain zero for them both.

It has been shown therefore that the elastic scattering solutions derived at section 5.4 reduce to exactly the correct limits for the standard cases of totally rigid and pressure release interfaces, for rough surfaces which hold to the approximations required by the first order small perturbation theory approach. This again is an indication that these solutions are indeed the general first order perturbation theory solutions to the case of scattering at a rough interface with elastic boundary conditions.

5.7 Scattering strength

The scattering strength is defined in chapter 3 (see equations (3-90), (3-91) and (3-92)). Using the results derived above the scattering strength has been calculated for six rough liquid / solid interfaces, shown in Figure 3 below. For each of these rough interfaces the liquid from which the sound is incident has a density of 1000kg/m^3 and a soundspeed of 1500m/s. The incident sound frequency is 800Hz, and is at an angle of 45°. The details of the scattering media are given in Table 1 below. In all cases the attenuation coefficients in both incident and scattering media have been set to zero. Each rough surface has a Gaussian power spectral density defined by equation (3-48), with rms surface height set to 0.053 λ and rough surface correlation length set to 0.45 λ, where λ is the wavelength of the incident sound.

medium	density (kg/m^3)	sound speed (m/s)	shear wave speed (m/s)
green line	0	0	0
data 1	2000	2000	600
data 2	2000	2000	900
data 3	3000	3000	1100
data 4	3000	3000	1200
data 5	2000	2000	1300

Table 1: Geoacoustic parameters for the scattering media in Figure 3.

Standard first order pertubation theory results from THORSOS (1988) are shown in Figure 2 for a rough "pressure release" interface. The scattering strength curve shown in Figure 3 for the "green line" is produced using the equations developed here, using the appropriate geoacoustic (zero density, soundspeed and shear wave speed) and interface parameters, and compares well with the benchmark case. The equations developed here are also used with other geoacoustic parameters to produce the other curves in Figure 3, to show how the scattering strength is dependent on the elastic properties of the rough interface, as well as the statistical properties of the roughness itself.

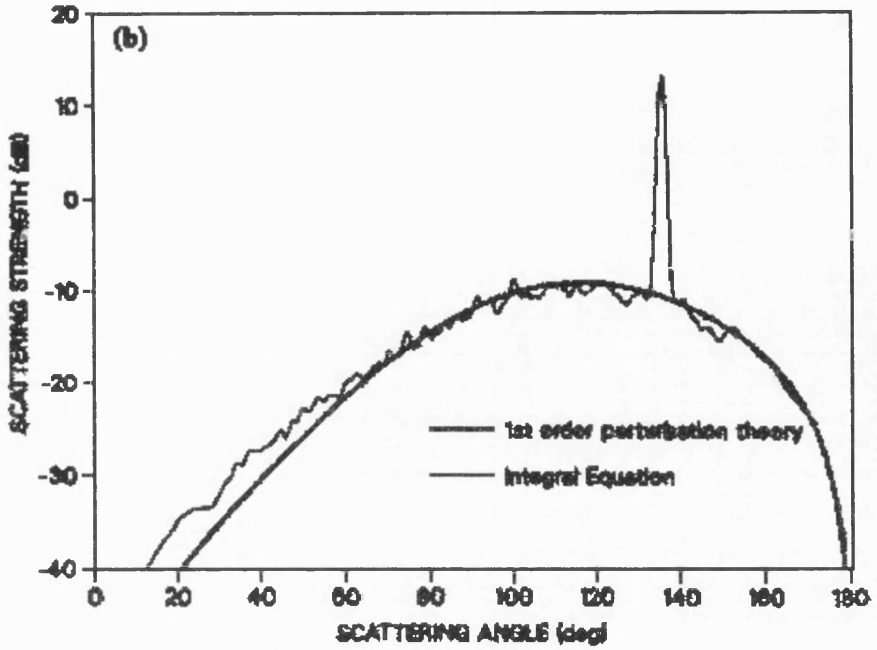

Figure 2: Standard first order perturbation theory results (excluding coherent component) for the scattering of sound from a rough surface, compared with integral equation results (including coherent component) from THORSOS 1988. The plot shows scattering strength versus scattering angle, for an incident wave at 45°. The scattering angle is numbered such that 135° is forwardscatter and 45° is backscatter. The rough surface has a Gaussian roughness spectrum with root mean square height of 0.053λ and surface correlation length 0.45λ where λ is the wavelength of the incident sound. The scattering medium has "pressure release boundary conditions", i.e. it has zero density, zero sound speed, and zero shear wave speed.

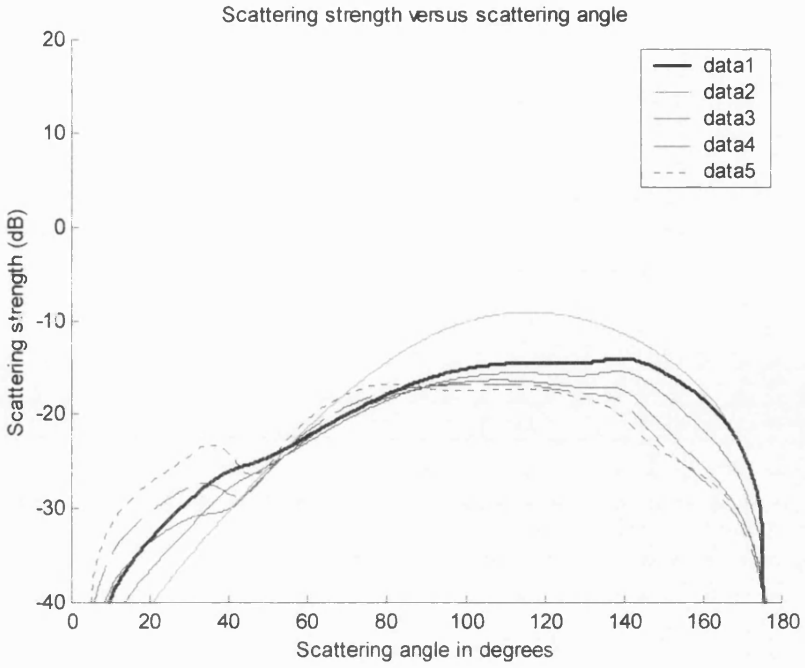

Figure 3: First order perturbation theory results calculated using the development of chapters 3 and 5. The figure shows plots of scattering strength versus scattering angle, each for an incident wave at 45°, for rough liquid / solid interfaces with different impedances. Each rough interface has a Gaussian power spectral density defined by equation (3-48), with rms surface height set to 0.053 λ and rough surface correlation length set to 0.45 λ, where λ is the wavelength of the incident sound. The incident medium is modelled as having a sound speed of 1500m/s and a density of 1000kg/m^3. The scattering media geoacoustic properties are:

medium	*density (kg/m^3)*	*sound speed (m/s)*	*shear wave speed (m/s)*
green line	*0*	*0*	*0*
data 1	*2000*	*2000*	*600*
data 2	*2000*	*2000*	*900*
data 3	*3000*	*3000*	*1100*
data 4	*3000*	*3000*	*1200*
data 5	*2000*	*2000*	*1300*

It can be seen that the plot for the scattering medium with "pressure release boundary conditions", "green line", matches the first order perturbation theory solution presented by THORSOS (1988) – see Figure 2 earlier. When the scattering medium has realistic densities and wave speeds, but the same roughness spectrum, the scattering strength varies significantly from that for the interface with "pressure release boundary conditions" (as did the liquid / liquid plots in chapter 4). The plots for "data 1" to "data 5" also show that the scattering strength varies markedly with shear wave speed, in a non-trivial manner – much as was the case for the reflection coefficient shown in chapter 2. The scattering strength in the backscattering quadrant (0 – 90°) is

particularly sensitive to shear wave speed, and is possibly indicative of some instability in the solution (discussed briefly in chapter 6).

6 Scattering from the seabed

In the previous chapters theoretical algorithms have been derived for the scattering of harmonic plane waves from a rough interface. These algorithms have all been derived to be as generally applicable as possible, within the constraints of first order perturbation theory discussed in chapter 3. In this chapter these algorithms will be applied specifically to the problem of calculating the sound scattered from a seabed.

For the algorithm inputs, consideration will be given to the seabed model, scattering model, and to having a more realistic representation of the sound source. It will be shown how the algorithm outputs can be calculated for many different rough surface realisations, and the statistics of the scattering solutions will be calculated.

6.1 Seabed model

In terms of the scattering model there are two functions of the seabed interface model. Firstly it directly affects the zero order smooth surface reflection and transmission coefficients, V, W and (for a solid) P. Secondly it affects which first order development and subsequent equations are used for the scattered pressures. The earlier chapters described the scattering of sound from elastic interfaces which were between an upper liquid medium and a lower liquid (chapter 4) or solid (chapter 5) medium. Of interest now is which one of these developments to use here to describe scattering from the interface between the sea and the seabed.

The liquid / liquid model is the simplest of the two models. In chapter 2 the reflection coefficient was shown to be a relatively simple function of the relative densities and sound speeds at the interface. The effect of shear waves on the reflection coefficient varies considerably depending on the speed of the shear wave – it was shown in chapter 2 that there is not a straightforward relationship between shear wave speed and reflection coefficient.

The geoacoustical model chosen as input to the scattering model used to calculate the results shown later is one comprising a single fluid / fluid interface at the seabed. Although this is the simplest case which can be considered, it is nevertheless representative of a large number of seabeds. Many sediments are formed from deposits of unconsolidated solid grains of silt, sand, carbonates (broken shells from dead marine life) and mud. These sediments are often saturated and exhibit little structure or elasticity. In terms of the reflection coefficient VIDMAR (1980) showed that the main effect of a fluidy sediment was to attenuate sound entering the sediment layer (see chapter 1), due to the large shear wave attenuation coefficients found for many mud and silt sediments.

Any elasticity (i.e. "solidness") will, however, increase[1] the total amount of sound energy entering the seabed (see chapter 2). More energy entering the seabed will increase the possibility of scattering from sediment volume inhomogeneities, notwithstanding the fact that any scattered energy may also be attenuated. This simple argument could, depending

on the shear wave speeds, attenuation coefficients, and depth of scattering volume, help explain the result found by IVAKIN and JACKSON (1998) that the shear elasticity increases the relative importance of sediment volume scattering.

By contrast, the liquid / solid model represents the general case of seabed interface scattering and so should be applicable to any seabed. In practice, this model has proved less stable than the liquid / liquid model. This is due to the fact that there are 3 simultaneous equations to be solved, which contain terms of differing orders of magnitudes. For some angles this has led to numerical instabilities when solving these equations. It is speculated that this problem could be solved by solving the simultaneous equations numerically. One way would be to solve the 3 simultaneous equations using a matrix inversion technique such as singular value decomposition (SVD, see PRESS et al.).

It is often the case that the seabed is more accurately described by a multilayered model. In the simplest of these the upper liquid layer (the sea) is separated from the solid seabed basement by a thin sediment layer, the properties of which vary from model to model. Of course in reality the geoacoustic properties of the seabed change continuously. In theory, this can be modelled by a series of thin layers, the geoacoustic properties varying slightly from layer to layer. If these layers are all liquid layers then their effects can be combined using the method of input impedances (see chapter 2). Similarly, if they are solid layers, then their effects can be combined using the matrix propagator method (again see chapter 2).

For the simple liquid / liquid interface used here, the appropriate single interface reflection coefficient code has been used to calculate the reflection coefficient for each incident angle. To use this scattering model to interpret trials data, it would be more appropriate to model the seabed layer structure realistically, calculate the reflection coefficient versus incident angle off-line, using the matrix propagator method code (see chapter 7), and store the results for reflected and transmitted waves in a look-up file. The scattering code could then read from the look-up file instead of calling the simple reflection code.

6.2 Roughness model

The scattering model has been developed such that there are no functional constraints on the form of the roughness amplitude. In the model a Gaussian surface power spectral density is used (see chapter 3). In principle, the user could develop any set of parameters for $A(\kappa)$, as long as they satisfied the conditions for small amplitude and slope required for the perturbation theory approach to be valid (see chapter 3).

As stated in the introduction in chapter 1, the model developed here is for the static solution to the scattering problem. It is not a time evolution model such as that developed by POULIQUEN (1999), BERGEM et al (1999). The POULIQUEN model includes the effects of seafloor and seabed volume scattering, and takes into account the geometric positions of the

[1] This is true for all incident angles except the sound speed critical angle at which the reflection coefficient is 1.

scatterers, the spatial characteristics of the incident beam, and the phases of the returns from each scatterer. It does this by considering each infinitesimal element of scattering surface or scattering volume separately, and coherently summing their effects to derive the full solution. Here, a similar but different approach is taken. The elements of the surface are its wavenumber components: the uniqueness of a surface is determined by the phases of these components.

6.3 Scattering from an incident pulse

The development thus far has made two assumptions throughout: that the incident (and hence reflected and transmitted) wave is a plane wave which is infinite in extent in both space and time. Being infinite in space means that the wavefront is perfectly straight, having no curvature at any point, and so the incident angle at all points on the interface is the same. In other words there are no "edge effects". This is a significant simplification, and enables the use of a ray to represent the whole of the wavefront. Being infinite in time allows the solution developed to be independent of any transient effects one might see at the start and end of a pulse's interaction with the seabed. More practically, it allows the solutions to be developed considering only one frequency, another significant simplification. In this and the next sub-section it is shown how these two assumptions are overcome to enable the scattering to be determined for a generalised pulsed beam: a Gaussian pulse[2] of arbitrary frequency with arbitrary pulse length, focussed into a beam.

Firstly, the time dependence of the wave is considered. Clearly an infinite harmonic wave is not sufficient. In truth, any physical sound source such as a hydrophone, will produce a sound which has a finite duration: a "pulse". From Fourier analysis it can be shown that a pulse can be made by combining a set of harmonic waves of different frequencies, each harmonic wave having a different amplitude. Consider the general pulse shown below. This is a wave of frequency f_0 but with a Gaussian envelope.

[2] In principle any pulse shape and beam pattern can be used.

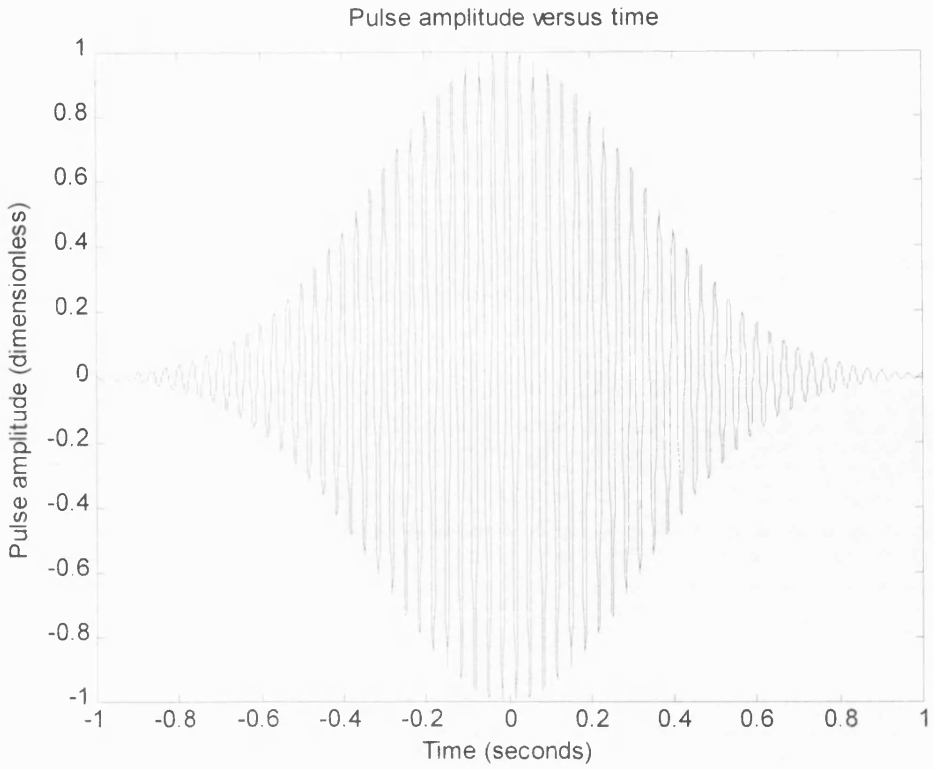

Figure 1: Sound pulse of duration 2 seconds. A centre frequency of 30Hz is used for illustration here: a frequency of 800Hz is used to produce the results presented later.

This wave, in the time domain, can be thought of as the product of a Gaussian envelope with a pure harmonic wave. Alternatively, the convolution theory (see RILEY (1987)) shows that in the frequency domain this product is the same as the convolution of the Fourier transforms of the Gaussian envelope and the harmonic wave. The Fourier transform of the harmonic wave is simply a delta function at the appropriate frequency. The Gaussian envelope transforms into the frequency domain still as a Gaussian envelope: for a mean frequency μ_f and frequency standard deviation of σ_f the Gaussian envelope, $G(f)$, is defined by

$$G(f) = \frac{1}{\left(2\pi\sigma_f{}^2\right)^{0.5}} \exp\left(-\frac{(f-\mu_f)^2}{2\sigma_f{}^2}\right) \qquad 6\text{-}1$$

In the time domain the equivalent Gaussian function $g(t)$ is given by the Fourier transform of $G(f)$

$$g(t) = \int_{-\infty}^{\infty} G(f)\exp(i2\pi ft)df = \frac{1}{\left(2\pi\sigma_f{}^2\right)^{0.5}} \int_{-\infty}^{\infty} \exp\left(-\frac{(f-\mu_f)^2}{2\sigma_f{}^2} + i2\pi ft\right)df \qquad 6\text{-}2$$

The exponential term is integrated by firstly "completing the square", in other words defining constants a, b and c such that

$$-(af+b)^2 + c \equiv -\frac{(f-\mu_f)^2}{2\sigma_f{}^2} + i2\pi ft \qquad 6\text{-}3$$

Solving for a, b and c in turn it is easily shown that

$$a = \frac{1}{\left(2\sigma_f{}^2\right)^{0.5}} \qquad 6\text{-}4$$

$$b = -\left(\frac{\mu_f}{\left(2\sigma_f{}^2\right)^{0.5}} + \frac{i2\pi t\left(2\sigma_f{}^2\right)^{0.5}}{2}\right) \qquad 6\text{-}5$$

$$c = -\frac{4\pi^2\sigma_f{}^2 t^2}{2} + i2\pi\mu_f t \qquad 6\text{-}6$$

Since the constant c is independent of the frequency it can be written outside the integral and the expression for $g(t)$ can now be written

$$g(t) = \frac{\exp(c)}{\left(2\pi\sigma_f{}^2\right)^{0.5}} \int_{-\infty}^{\infty} \exp\left(-(af+b)^2\right) df \qquad 6\text{-}7$$

A further change of variables within the integrand allows the integral to be reduced to a standard form: let

$$q = af + b \qquad 6\text{-}8$$

hence

$$g(t) = \frac{\exp(c)}{\left(2\pi\sigma_f{}^2\right)^{0.5}} \frac{1}{a} \int_{-\infty}^{\infty} \exp\left(-(q)^2\right) dq = \frac{\exp(c)}{\left(2\pi\sigma_f{}^2\right)^{0.5}} \frac{\pi^{0.5}}{a} \qquad 6\text{-}9$$

Re-writing the expression for $g(t)$ with the constants a and c explicitly and seeing that many of the terms cancel leads to

$$g(t) = \exp\left(-2\pi^2 \sigma_f{}^2 t^2\right)\exp\left(i2\pi\mu_f t\right) \qquad 6\text{-}10$$

which is clearly the form of a sinusoid at frequency μ_f within a Gaussian envelope centred at time zero with a standard deviation σ_t given by

$$\sigma_t = \frac{1}{2\pi\sigma_f} \qquad 6\text{-}11$$

allowing $g(t)$ to be written in the standard form

$$g(t) = \exp\left(-\frac{t^2}{2\sigma_t^2}\right)\exp\left(i2\pi\mu_f t\right) \qquad 6\text{-}12$$

This result shows that the signal which has a frequency spectrum given by $G(f)$ is a Gaussian weighted (enveloped) sinusoid at a frequency μ_f. Equivalently, to represent a Gaussian envelope pulse with frequency μ_f it is only necessary to consider the sum of sinusoids with frequencies which have amplitude weightings given by $G(f)$.

In calculating the scattering coefficient for a pulse the scattered pressure solutions for the harmonic waves developed in chapters 4 and 5 are used, and a weighted coherent sum of these solutions is formed. The sum of these pressures is then normalised by the number of frequencies used, and then squared to give the intensity, and the scattering coefficient and scattering strength are calculated from this.

The frequencies of the harmonic waves are such that they represent a pulse of the required centre frequency and duration. It should be noted that the length of the pulse in the time domain is, theoretically, infinite, since the Gaussian function continually decreases but never reaches zero. For a Gaussian function over 95% of the area under the curve lies within ±3 standard deviations of the mean. Hence for a pulse of "duration" t_0 seconds (which is user defined at run time) the time domain Gaussian envelope used to describe it will be taken to have a standard deviation, σ_t, of $t_0/6$. This value of σ_t will be used to determine the required standard deviation of the frequencies, σ_f, to be summed over, using equation (6-11). To improve the accuracy of the pulse the spread of frequencies used will run between plus and minus four σ_f.

6.4 Scattering from an incident beam

For the spatial dependence of the incident sound, a focussed beam is formed from an arbitrary number of hydrophones which are separated at half the Nyquist spacing (see PRESS et al). Using a normal modes approach, GINGRAS (1998) shows that by a judicious use of multiple sources with appropriate weightings and phases one can minimise the backscatter generated from a seabed: these ideas are not used here, and are discussed in

chapter 8. The benefits and disadvantages of focussing the incident sound is discussed by STEPHEN (2000) for the case of Gaussian beams, and optimum beams are derived theoretically. The code used here (see chapter 7) employs Chebychev weightings (MATLAB) to allow virtually any width of beam to be constructed, by enabling the user to define sidelobe level and number of hydrophones. A separate piece of code (see chapter 7) allows different beam configurations to be viewed off-line, so that the user may use the best parameters when running the scattering model. For the delays calculated for the different hydrophones the exact (32 bit) facilities offered by MATLAB have been used, since there were no constraints on processing power or memory. If these phase delays were being calculated repeatedly it would be wise to use a least squares approximation for the delays, as advocated by TRUCCO (1998).

The application for which this theory is intended is that of an active sonar pulse[3] of some sort, produced by an array, and so having a finite width: a "beam". In a precisely analogous manner to the pulse being a weighted sum of a series of plane waves, a beam can also be modelled as a weighted sum of plane waves. In this case one plane wave is associated with each of the hydrophones producing the sound. Each plane wave is at a different incident angle, and each has a different phase relative to the centre hydrophone.

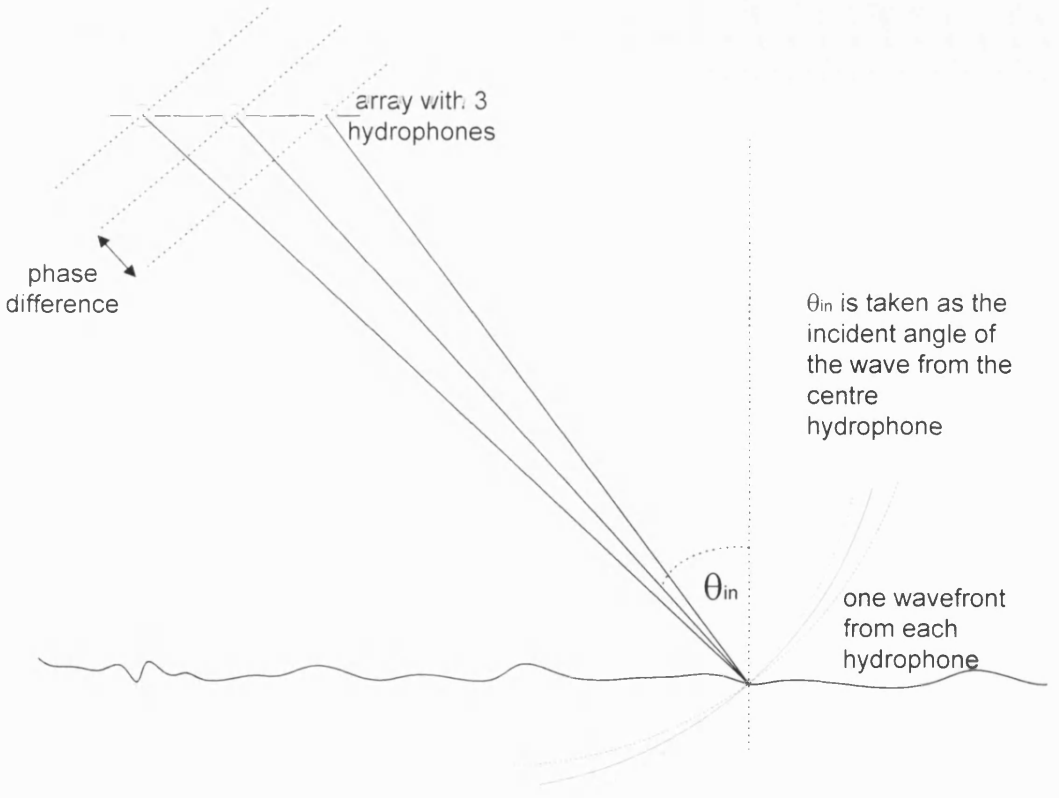

Figure 2: The geometry of the waves from an array with 3 hydrophones incident upon a rough seabed.

[3] Though the underlying physics for passive sonar consists of the same plane harmonic wave solutions.

In Figure 2 above it is assumed that each of the hydrophones produces a spherical continuous wave of constant frequency. As long as the seabed is many wavelengths from the array of hydrophones then each wave can be assumed to be planar by the time it reaches the seabed. In order for the waves to be in phase with each other at the seabed they must be given phase shifts relating to the difference in their path lengths to the seabed. If the centre hydrophone is taken to be the one which is at the incident angle of the beam, and which has the reference phase, then for a horizontal array with hydrophones at s metres apart the phase shift of the nth hydrophone is given by the difference in distances from the surface to each hydrophone, expressed as a fraction of the wavenumber. For a centre hydrophone at a height h and a horizontal distance l from the point of interaction with the seabed, the difference in distance, *diff*, to the nth hydrophone is given by

$$diff = \left(l^2 + h^2\right)^{0.5} - \left((l + ns)^2 + h^2\right)^{0.5} \qquad 6\text{- }13$$

which, when sn is small compared to l may be given by

$$diff = \frac{-lsn}{\left(l^2 + h^2\right)^{0.5}} \qquad 6\text{- }14$$

The phase difference for the nth hydrophone, $\Delta\phi_n$, is then given by

$$\Delta\phi_n = \frac{-lsn}{\left(l^2 + h^2\right)^{0.5}} \frac{2\pi f}{c} \qquad 6\text{- }15$$

For this geometry the incident angle, θ_{in}, is given by

$$\theta_{in} = \tan^{-1}\left(\frac{l}{h}\right) \qquad 6\text{- }16$$

and for the nth hydrophone the incident angle, θ_n, is given by

$$\theta_n = \tan^{-1}\left(\frac{l + ns}{h}\right) \qquad 6\text{- }17$$

For the weightings of the plane waves, instead of using a Gaussian function as with the pulse, a set of Chebyshev weights (PRESS et al., MATLAB) are used. These weights can be used to control the level of the sidelobes of the beam which is produced from the sum of the plane waves from the hydrophones. In theory any level of sidelobes can be achieved, though a trade-off must be sought between sidelobe level and width of the main beam. In general, a

lower sidelobe level will result in a wider main beam. A typical beam produced using a weighted sum of plane waves is shown below in Figure 3. Although the geometry for only 3 hydrophones was shown in Figure 2 earlier, the number of hydrophones used for the beam can be any number: the more that are used the narrower the main beam will be. The separation of the hydrophones must also be carefully considered. To prevent undersampling the spacing must be at least $\lambda/2$, where λ is the sound wavelength, this being the Nyquist limit. In the code used here (see chapter 7) the spacing is set at half the Nyquist limit.

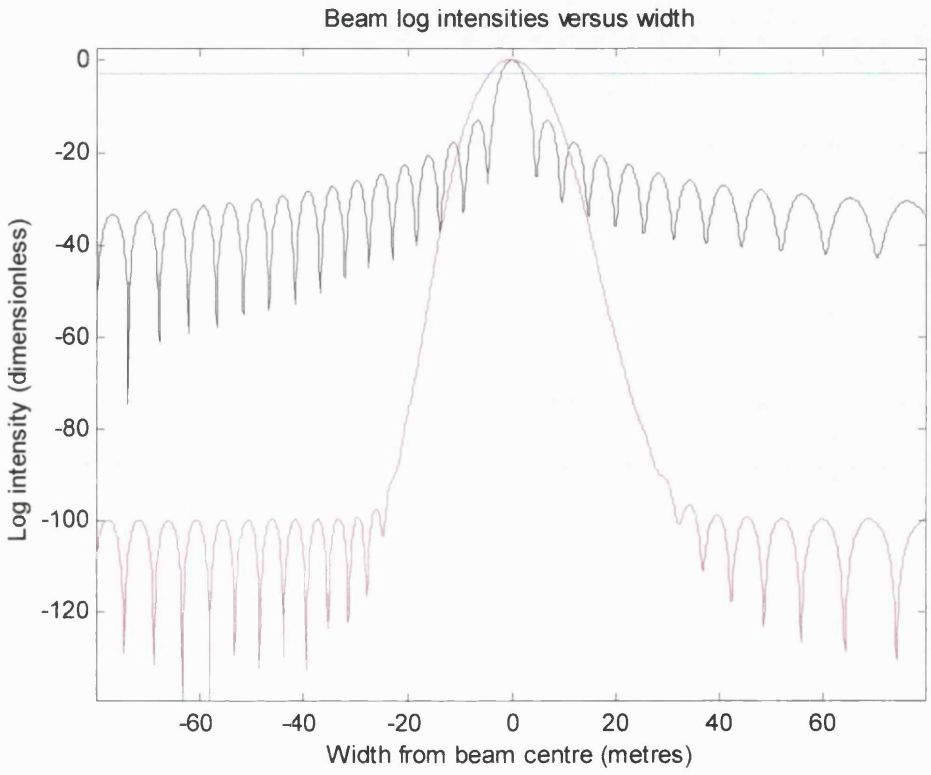

Figure 3: Beampattern produced by an array with 107 hydrophones at $\lambda/4$ apart; the array is 100m above the seabed at 50m horizontal displacement from the point of interaction with the rough surface; the frequency of the sound is 1000Hz and the soundspeed is 1500m/s. The black line shows the beampattern with no weighting on the plane waves: the magenta line shows the Chebyshev weighted solution for a sidelobe level of –100dB. The cyan line is drawn at the –3dB intensity, equal to half the maximum intensity. The Chebyshev weighted beam has a –3dB width of about 8.5m: the unweighted beam is about 4m wide, but with poor sidelobe rejection. In principle, an even greater level of sidelobe rejection could be achieved with the Chebyshev weights, with an appropriate increase in the width of the main beam. Note: the asymmetry in the sidelobes is caused by the fact that the waves are not perfectly planar at the seabed.

For simplicity, in the code described in chapter 7, an odd number of hydrophones are used. Each plane wave is given its phase delay and its weight, W_n, by simply multiplying its amplitude by $W_n\exp(i^*\Delta\phi_n)$. Since this whole term is simply a constant factor it can be taken outside the calculation for the scattered pressure. Hence the scattered pressures are calculated as if they were for the original incident waves (one for each hydrophone) at their respective incident angles, θ_n, and the weighting and phase factors are applied to the scattered pressures afterwards. These phased, weighted, scattered pressure solutions are then added coherently, then normalised by the number and weightings of hydrophones used. The resulting pressure is then squared to give the intensity used to calculate the scattering coefficient.

6.5 Scattering from a pulsed beam

6.5.1 From a 1 dimensional array

To consider a pulsed beam it is necessary to sum, in a nested loop, over both the harmonic frequencies with their Gaussian weights, as described earlier (6.3), and over the plane waves in different directions with different phases and with their Chebyshev weightings. Since the phase terms for the plane waves are dependent upon the frequency (see equation (6- 15)) the nesting must be such that the sum over the plane waves is done within the sum over the harmonic waves. This is how the code presented in chapter 7 is structured.

6.5.2 From a 2 dimensional array

If a 2 dimensional array had been used then there would have to be sums over two lots of plane waves. These plane wave sums could be done either way around as long as they were both within the sum over harmonic waves. In the 2 dimensional case the sum over plane waves is weighted differently to in the 1 dimensional case. In the 1 dimensional case the radially spreading wave was treated as if planar by the time it reached the seabed. For the 2 dimensional case the "free space" solution of the wave equation with a point source must be used for each hydrophone. This is the Green's function for a point source (RILEY (1987)):

$$G_0(\underline{R}) = -\frac{i}{8\pi^2}\int \exp\left[i\underline{k}.\underline{r} + iq(k)|z|\right]q^{-1}(k)d\underline{k} \qquad 6\text{- }18$$

and for this 2 dimensional case is known as the *Weyl formula* (VORONOVICH (1994)), where:

$$q(k) = q_k = \left(K^2 - k^2\right)^{1/2} \qquad 6\text{- }19$$

These equations give the Green's function representation of the field in the form of a superposition of plane waves propagating upwards above the source and downwards below the source. The basis for the plane waves may be set with amplitude $q^{-1/2}$ so that the energy flux in the z direction is constant and independent of $\underline{k}$. It should be noted that the magnitudes of the plane waves satisfying the Helmholtz equation can be set as any function independent of $\underline{R}$ (hence a function of $\underline{k}$ will be fine).

The field incident upon the rough surface may be expressed in terms of an integral over all space of the product of the free space Green's function for a source at arbitrary point $\underline{R}_0$ and the source function Q:

$$\Psi_{in}(\underline{R}) = \int G_0(\underline{R} - \underline{R}')Q(\underline{R}')d\underline{R}' \qquad 6\text{-}20$$

Substituting for the Greens function from equation (6- 18) gives a field which is a weighted ($a(\underline{k})$) integral over plane waves travelling away from the point source:

$$\Psi_{in} = \int a(\underline{k})q^{-1/2}(k)\exp[i\underline{k}.\underline{r} + iq(k)z]d\underline{k} \qquad 6\text{-}21$$

where:

$$a(\underline{k}) = \frac{-i}{8\pi^2}\int q^{-1/2}(k)\exp[-i\underline{k}.\underline{r} - iq(k)z']Q(\underline{r}', z')d\underline{r}'dz' \qquad 6\text{-}22$$

Hence the general solution for a space with many sources can be expressed in terms of 2 dimensional plane waves.

6.6 Interpreting the scattered pressure solutions

The chapter thus far has described how the scattering problem was formulated and how the MATLAB code (see chapter 7) was set up to derive solutions for scattered pressure. A number of code modules have also been written to interpret the scattered pressure solutions: this interpretation has removed spurious effects, caused by the limitations of the way in which the solutions were calculated, and presents the scattered pressure solutions to an accuracy consistent with the definition of the incident pressure field (the pulsed beam discussed earlier).

6.6.1 Angle sorting

The scattered pressure solution for each plane harmonic wave is calculated in the "p_calc_liq_09.m" subroutine using the angles, wavenumbers and frequencies appropriate to that harmonic plane wave (see chapter 7). It was seen in chapters 4 and 5 that the scattered

solution for a plane harmonic wave is conveniently expressed as a "weighted" integral over the surface wavenumber, κ. In chapters 4 and 5 the "weights" required for this integral were derived; these weighting factors are in terms of κ, the geometry of the incident sound, and the geoacoustic parameters of the seabed. The solution for each plane harmonic wave is therefore with respect to these terms as well.

To sum the plane harmonic wave solutions in a consistent manner their scattering solutions must be summed coherently with respect to common *outgoing* angle. This angle, θ_{out}, is calculated from

$$\theta_{out} = \arctan (\gamma_{out} / k_{out}) \qquad 6\text{-}23$$

where k_{out} and γ_{out} are the outgoing horizontal and vertical wavevectors respectively, given by

$$k_{out} = \xi + \kappa \qquad 6\text{-}24$$

$$\gamma_{out} = \text{sqrt} (k^2 - (\xi + \kappa)^2) \qquad 6\text{-}25$$

where k is the incident wavevector and ξ is the horizontal component of the incident wavevector.

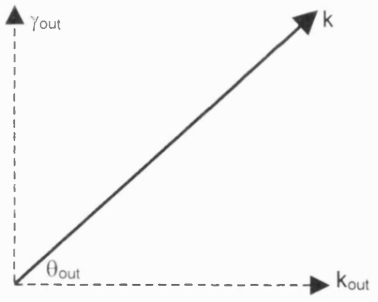

It can be seen that for each incident plane wave, with the same k but with slightly different ξ, the outgoing angles for the solutions for a particular κ will be different. To take account of this effect a routine called "angle_sort_05.m" has been written. This routine converts each solution from a solution in an array corresponding to certain values of κ to a solution in an array corresponding to values of θ_{out}. This is done for each plane harmonic wave solution directly before it is added to the running total of the other plane harmonic wave solutions.

The summed pressure solutions are then used to calculate the scattering coefficient, as described in chapter 3.

6.6.2 Interpolation to remove drop outs

In deriving a solution for the scattering coefficient in terms of the outgoing angle, occasionally an outgoing angle bin would have no value assigned to it, since none of the κ values had mapped to this value of θ. This does not mean that no energy is scattered at that particular angle. The problem is that there is not always a one-to-one mapping between the κ used to calculate the scattered pressures, and the θ used to sort the scattered solutions so that they can be added consistently.

This problem is particularly apparent when the number of θ bins is far greater than the number of κ bins. Indeed, the delta_kappa and the angle_factor parameters should always be set such that the number of θ bins exceeds the number of κ bins, otherwise there will be cases where more than one κ solution is binned into a particular θ bin, resulting in a solution which is badly normalised.

To overcome this situation the scattering coefficient solutions have an interpolation applied to them using a routine called "smooth_03.m". This looks for scattering coefficient array elements which are still set to zero, and sets these equal to a value calculated from a linear interpolation of the values in the nearest non-zero array elements either side. At the ends of the array any zero elements are set to just the nearest non-zero array element value. The use of a linear interpolation, as opposed to any other form of interpolation, is preferred primarily because it is simple, and makes the least assumptions about the form of the scattered solution with respect to scattering angle[4].

6.6.3 Solution accuracy

The scattering coefficient solution is calculated to an apparent degree of angular accuracy determined by the parameter "angle_factor", the angular resolution (in degrees) of the solution being given by:

$$\text{angular resolution} = (1 / \text{angle\_factor}) \qquad 6\text{-}26$$

In reality however, the energy received at the hydrophones of a sonar system is "beamformed" (see WAITE (1998)), the entirely opposite process to that I have described in section 6.4 earlier. The "beams" formed by the sonar system only resolve the incoming energy to a finite angular resolution, or beamwidth, which is dependent upon the frequency of the sound, the number of hydrophones, the geometry of the array upon which the hydrophones are mounted, and any weightings applied to the hydrophone outputs. It is therefore not meaningful to present the scattering results to a greater resolution than that which can be detected.

In order to reduce the angular resolution of the scattering coefficient solution a routine called "box_03" is used. This simply smooths the data by calculating a moving "box-

car" mean. The size of the box used for this routine is set to a nominal beamwidth which is defined by assuming that the array which detects the sound is the same as that which produced the incident beam in the first place. (The user could, alternatively, model a different receive array using the code listed in chapter 7 used to check the beamforming, and take the calculated beamwidth from this.) The beamwidth which is calculated is for the beam in the direction perpendicular to the length of the array, and is the full width at half maximum intensity for the beam response, given by

$$\text{beamwidth}^\circ = 72.5/\,Lf \qquad 6\text{-}27$$

where L is the length of the array in metres and f is the frequency of the sound in kilohertz.

The code is configured so that the user can choose the number of hydrophones used to generate the incident beam. The user also chooses the incident pulsed beam's centre frequency. The spacing of the hydrophones is set to one quarter of the incident sound's wavelength (i.e. twice as accurate as the Nyquist limit) and the length of the array is therefore calculated once the frequency and number of hydrophones are decided by the user. For the case that a small number of hyrophones is used, a maximum beamwidth is set to 10°, since the assumption that the receive array has the same resolution as the transmit array is probably not now valid.

6.7 Scattering from a single surface realisation

The role of the phases of the surface amplitude spectral components is discussed in chapter 3, in the light of the comments from LUPIEN (1999) concerning scale structure. In this section it is shown how the phases of the surface amplitude components are included in the solutions calculated using the models developed in chapter 4 and 5.

For both the liquid / liquid and the liquid / solid models, the scattered pressure amplitude is calculated[5] using the surface scattering amplitude spectrum, as shown in chapters 4 and 5, and in the code presented in chapter 7. The surface scattering amplitude spectrum for a particular rough surface contains information on both the magnitude and phase of each of the rough surface wavenumber components. The magnitudes of the surface wavenumber components are simply the square root of the surface power spectral density. For a particular surface realisation it is the relative phases of these wavenumber components that gives the surface its uniqueness. For the scattering model results presented at section 6.8, the scattering amplitude spectrum has been derived for a number of unique rough surface realisations, each with the same rough surface power spectral density. This has been done by calculating a number of surface scattering amplitude spectra,

[4] This linear interpolation (and the smoothing done in the box car mean process discussed later) is done for the magnitude and the phase of the (in general) complex pressures, since this preserves the trend of the energy versus angle (smoothing the real and imaginary parts instead does not do this).

[5] For the liquid / solid case the derivation in chapter 5 shows that the velocity potential is calculated. In the code (presented in chapter 7) it is shown that this is converted to a pressure by simply multiplying by an appropriate density ratio.

each from square rooting the power spectral density; and then, for each surface scattering amplitude spectrum generating a random phase for each wavenumber component[6].

The random phases were then applied by multiplying each surface amplitude spectrum wavenumber component by a complex exponential with these phases. Thus a whole ensemble of unique sets of complex surface amplitude spectral components are produced. These represent a set of unique individual surface realisations, all with the same *power* spectral density. For each surface realisation the calculations proceed as per the equations in chapters 4 and 5, where each $A(\kappa)$ is now a complex value, which is different per κ for each surface realisation. In the code shown in chapter 7 it can be seen that the calculations are done for all the surface realisations at once, using a matrix approach (which MATLAB is particularly suited to), where each row of the matrix represents the surface amplitude spectrum for a particular rough surface realisation.

From the scattering results from the ensemble of surfaces the statistics of the scattering can be observed, to show that the different phased surfaces do have different scattered profiles. This is done (below) for backscatter and for forward scatter. The analysis of the scattering statistics is relatively simple here, since the aim is to show the utility of the method, rather than conduct a detailed statistical analysis. For a high frequency statistical analysis of backscatter see LYONS and ABRAHAM (1999).

6.8 Ensemble scattering statistics

Using the code described in chapter 7 scattering solutions may be produced for an arbitrary number of surface realisations. It is then possible to look at the distribution of the scattering strength in any scattering direction and examine both the mean and the spread of the distribution.

For the case considered here the sea density and sound speed are 1000kg/m^3 and 1500m/s respectively, the seabed density and wavespeeds are 2000kg/m^3, 2000m/s and 0.01m/s (i.e. the seabed is taken to be a liquid). Also, the pulse centre frequency is 800Hz and the incident angle is 45°. The geoacoustic parameters used here are in fact arbitrary[7]. The *geoacoustic parameters are important in that they affect the mean scattering strength* (at any particular angle): rather than the *distribution of scattering strengths* around the mean. The scattering strength distribution is affected only by parameters which have an impact on the phase of the scattered wave: the pulse centre frequency and the incident angle; the pulse length, since this affects the number of different harmonic frequency components; the number of hydrophones and array gain; the surface power spectral density; and the number of surface realisations – this affects only the accuracy to which the distribution may be measured.

[6] The phase for each negative wavenumber component is minus that for its respective positive wavenumber component: so the real part of the amplitude is the same and the imaginary part is minus that of the positive wavenumber component.

[7] See HAMILTON (1980) for details of real seabed geoacoustic parameters.

The incident pulsed beam was produced using 11 hydrophones at 100m above the seabed, with -20dB Chebyshev weighting. The pulse was 5s long resulting in 4 harmonic frequencies being used. The rough surface power spectral density was Gaussian, with correlation length = 0.45 λ and root mean square surface height, σ, given by $\sigma = 0.053\lambda$, as described in chapter 3, where λ is the wavelength of the incident sound pulse (at centre frequency). For this scenario 1000 independent rough surface realisations were used.

To look at the statistics of the forward and backward scattering distributions their histograms are plotted. See Figures 4 and 5 below. [This is done using the MATLAB "hist" command.] The histograms are compared to best-fit Gaussian and Rayleigh distributions and for each a probability is calculated, the probability that the scattered data are from a dataset with Gaussian or Rayleigh statistics. This is shown in Table 1 below. For each set of data, the histogram is centred on the mean scatter strength, and scatter strength bins are taken out to ± 4 standard deviations either side of the mean.

Data	Test Distribution	χ^2	Degrees of freedom	Prob of being from the test distribution
Backscatter	Gaussian	99	33	1E-15
Forward scatter	Gaussian	124	33	0
Backscatter	Rayleigh	40	32	0.13
Forward scatter	Rayleigh	39	32	0.14

Table 1: Forward and backward scattering statistics for a 5s pulsed beam from 11 hydrophones onto a surface with Gaussian roughness, for 1000 surface realisations. The tests suggest that the samples of backscatter and forward scatter data come from data sets with distributions which are likely to be neither Gaussian nor Rayleigh in nature. The shape of the histograms suggest that the data is more "Rayleigh-like".

6.8.1 Gaussian statistics

A Gaussian distribution, f(z) with a mean μ and a standard deviation σ is given by

$$f(z) = \frac{1}{\left(2\pi\sigma^2\right)^{0.5}} \exp\left(-\frac{(z-\mu)^2}{2\sigma^2} \right) \qquad 6\text{-}28$$

The Gaussian best-fit curve is calculated using the mean and standard deviation of the particular scatter coefficient data set being investigated. It is then normalised by multiplying by the number of surface realisations and by the histogram scatter coefficient bin width.

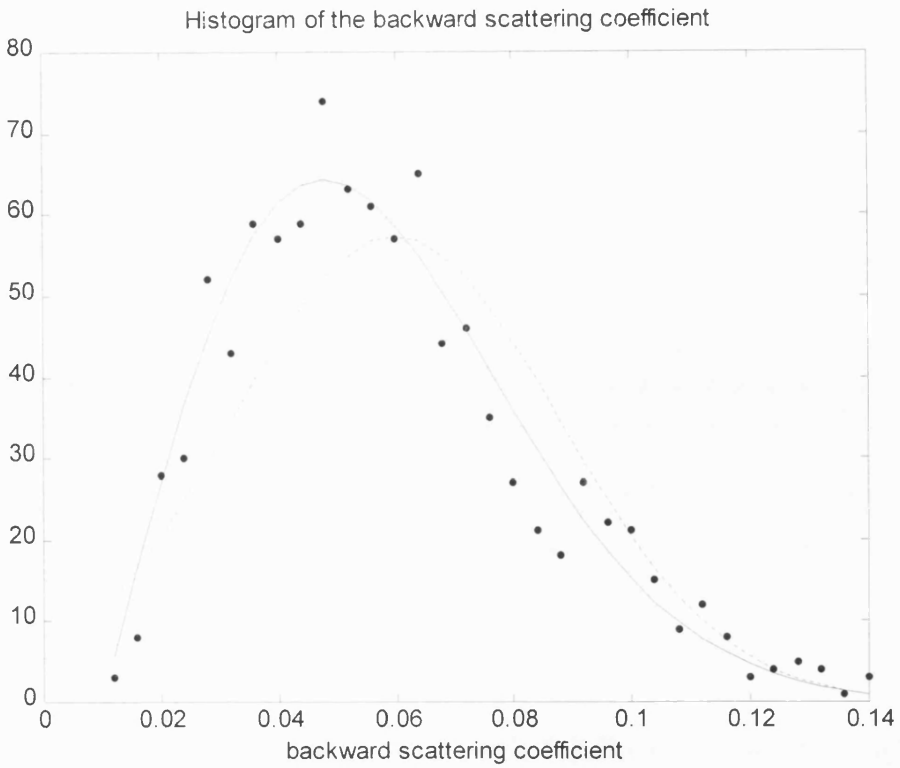

Figure 4: Histogram of the backward scattering coefficient for an incident pulsed beam at 45°. The incident pulsed beam was produced using 11 hydrophones at 100m above the seabed, with -20dB Chebyshev weighting. The pulse was 5s long resulting in 4 harmonic frequencies being used. The rough surface power spectral density was Gaussian, with correlation length = 0.45 λ and root mean square surface height, σ, given by $\sigma = 0.053\lambda$, where λ is the incident wavelength (at centre frequency). For this scenario 1000 independent rough surface realisations were used. For each, the sea density and sound speed are 1000kg/m^3 and 1500m/s respectively, the seabed density and wavespeeds are 2000kg/m^3, 2000m/s and 0.01m/s (i.e. the seabed is taken to be a liquid). Also, the pulse centre frequency is 800Hz. "Best –fit" Gaussian (dotted) and Rayleigh (solid) curves have also been derived and are plotted for comparison.

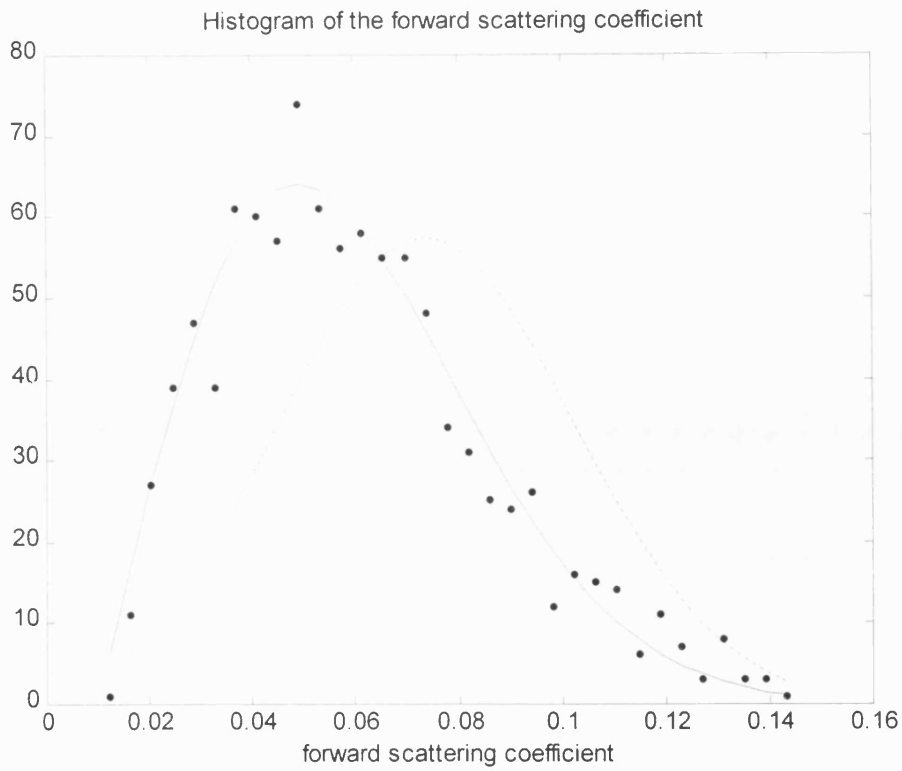

Figure 5: Histogram of the forward scattering coefficient for an incident pulsed beam at 45°. The incident pulsed beam was produced using 11 hydrophones at 100m above the seabed, with -20dB Chebyshev weighting. The pulse was 5s long resulting in 4 harmonic frequencies being used. The rough surface power spectral density was Gaussian, with correlation length = 0.45 λ and root mean square surface height, σ, given by $\sigma = 0.053\lambda$, where λ is the incident wavelength (at centre frequency). For this scenario 1000 independent rough surface realisations were used. For each, the sea density and sound speed are 1000kg/m^3 and 1500m/s respectively, the seabed density and wavespeeds are 2000kg/m^3, 2000m/s and 0.01m/s (i.e. the seabed is taken to be a liquid). Also, the pulse centre frequency is 800Hz. "Best –fit" Gaussian (dotted) and Rayleigh (solid) curves have also been derived and are plotted for comparison.

6.8.2 Rayleigh statistics

A Rayleigh distribution, f(z), is described in terms of a parameter, σ, which is not the standard deviation, by

$$f(z) = \frac{z}{\sigma^2} \exp\left(-\frac{z^2}{2\sigma^2} \right) \qquad 6\text{-}29$$

Although the Rayleigh distribution appears simpler than the Gaussian distribution one must, in fact, be more careful when fitting it to measured data. This is because the Rayleigh distribution is written in terms of one parameter, σ. Three different properties of the Rayleigh distribution may also be written in terms of σ:

Rayleigh mean value, μ_R is given by	$\mu_R = \sigma\ (\pi/2)^{0.5}$	6- 30
Rayleigh standard deviation, σ_R is given by	$\sigma_R^2 = \sigma^2\ (2 - \pi/2)$	6- 31
Rayleigh maximum value, f_{Rmax}, is given by	$f_{Rmax} = 1/\sigma\ \exp(-0.5)$	6- 32
which occurs at	$z = \sigma$.	6- 33

Any one of these 4 parameters, the mean, standard deviation, maximum value, and position of the maximum value, can be found for the measured data and used to define a value of σ from which a theoretical Rayleigh distribution may be derived. The method used here was based on looking at the peak of the histogram of the measured data set, and then performing some heuristic scaling to get a better fit. The "measured" data set here is that calculated using the many different surface ensembles, each generated randomly. For true measured data, an estimate of the mean would be safest to use initially, since it would be more accurate than an estimate of the maximum value, or the standard deviation, since these are both more greatly affected by spurious data points than the mean. In the case of trials data, however, the best solution would simply be to have an algorithm crunch through all candidate Rayleigh curves and select the best fit.

6.8.3 Probability calculation

To compare a measured distribution to a theoretical distribution the chi squared value, χ^2, is calculated and the incomplete gamma function is then used to calculate the probability that the measured data are from the same distribution as the theoretical distribution. This is the chi-squared test. Details of the chi square value and the incomplete gamma function are given by PRESS et al (1992), and MATHEWS and WALKER (1970). The chi squared value is calculated by comparing the scattering coefficient data with the

theoretical distribution. A sum is done over each of the M bins in the histogram, comparing the number in each for both distributions:

$$\chi^2 = \sum_{i=1}^{M} \frac{(N_i - n_i)^2}{n_i} \qquad 6\text{- }34$$

where N_i is the number in the particular scattering coefficient bin from the scattering coefficient data and n_i is the number in the scattering coefficient bin from the theoretical distribution (Gaussian or Rayleigh, whichever is being tested).

The probability that the scattering coefficient data come from data with the same distribution to that being compared with (Gaussian or Rayleigh) is then given by:

$$prob = 1 - gammainc\left(\chi^2, M\right) \qquad 6\text{- }35$$

where "*gammainc*" is the incomplete gamma function. The inputs to the incomplete gamma function are the chi squared value, and also the degrees of freedom. The latter is, for the Gaussian case, the number of histogram bins for which the distributions were compared. For the Rayleigh case, since the zero point is fixed, then M-1 is used.

For the data assessed above (Table 1), the probability of the data being from one of the theoretical distributions is low, even though for the Rayleigh curves the fits look, by eye, to be fairly good. To understand this one must appreciate the subtlety of the chi-squared test. The chi-squared test gives ***the probability that the distribution to which the whole of the measured data belongs is the same as the test distribution***. It is ***not*** a proportional measure of how well the two histograms match. The difference between these two measures of data matching may be illustrated by considering a coin tossing experiment. After 4 coin tosses one would not be surprised if 3 were heads. Clearly 2 heads would be most likely but 3 heads does not indicate an unfair coin. If, after 4 million tosses of the coin, 3 million were heads, then one would be sure that the coin was biased, even though the proportion of coin tosses which were heads was the same in both cases. The absolute number expected in each bin is important, as well as the difference between expected and measured. The larger the expected number, the sterner the chi-squared test is to data which does not match the expected distribution. The chi-squared test is also sterner for less degrees of freedom. The less degrees of freedom one allows then the better one would hope to match the test distribution: for a limit of only 1 bin then all the measurements would be in that one bin for both distribution; for the limit of many bins then it is harder to get a correct match for all, so the chi-squared test is less demanding.

7 Code and checks

The codes to evaluate the expressions derived in the earlier chapters have been written using MATLAB version 5.3, a high level programming language. In this chapter the following code is presented:

- the matrix propagator reflection code, "matrix_prop_04_plus.m";
- the main code, "main_many_10_2.m", and subroutines used to calculate the scattering coefficient from a liquid / liquid interface for any number of surface realisations;
- the codes used for the Gaussian and Rayleigh data fitting;
- the subroutines used to calculate the liquid / solid scattered pressures, "p_calc_sol_09.m";
- the codes used to test the pulse and beam parameters.

All words after a % are comments.

7.1 Matrix propagator reflection coefficient calculations

This code consists of a "main" program which calls a series of sub-modules in turn. Some of the sub-modules are called within a loop which is iterated over the number of intermediate seabed layers between the sea and the seabed basement. The complete code and sub-modules are listed:

Main code	matrix_prop_04_file.m
Sub-modules	
To get the scenario parameters	m_scenario_05.m
To get the layer geoacoustic parameters	m_geo_02.m
To calculate the layer propagation angles	m_angles_01.m
To calculate the layer "A" matrix coefficients	matrix_coeffs_03.m
To calculate the system "A" matrix	matrix_A_01.m
To calculate V,W and P	m_VWP_02.m

7.1.1 The main code

This is the main code, "matrix_prop_04_plus.m".

```
%To implement the matrix propagator method for calculating the reflection coefficient for
%a series of solid layers below a top liquid layer. The sound is incident from the liquid.
%The expressions for the reflection and transmission coefficients V, W and P, were derived
%in the transfer report following the method outlined in Brekhovskikh and Godin's "Waves
%in Layered Media" but with the last part corrected.
%20/12/99 MATRIX_PROP_01: start writing the code.
%21/12/99 continued with code.
%In the transfer report...
%"it is assumed that the layers are numbered from the lower half-space (layer 1) to the fluid
%half-space (layer n+1) with z_n being at the top of layer j."
%Here the layers are numbered from the top, so will need to be careful...
%27/12/99: NOTE THAT THE a COEFFICIENTS RETURNED FROM MATRIX_COEFFS_02 ARE FOR LAYERS NUMBERED
%          WITH N=1 AS THE UPPERMOST LAYER, AND N=LAYERS AS THE LAYER DIRECTLY ABOVE THE
          BASEMENT.
%28/12/99: PUT IN LOOP OVER ALL INCIDENT ANGLES.
%06/05/00: GOT RID OF "CLOSE ALL", SO THAT I CAN OVERPLOT DIFFERENT RESULTS.
```

```
%23/08/00: CHANGED THE PLOTTING.
%23/08/00: CALCULATED THE PHASE CHANGE (uses "angle" = ATAN(V_imag/V_real)).
%24/08/00: CHANGED M_SCENARIO TO REMOVE LAYER LIMIT. NOW MATRIX_PROP_04.
%PhD VIVA PASSED 30/11/00. CORRECTIONS REQUIRED. COMPARISON WITH INCORRECT BREK AND GODIN
%SOLUTION IS WANTED.
%13/01/01: ADDITIONAL CODE TO GIVE BREK AND GODIN'S WRONG SOLUTION.


clear
conv_to_deg=180/pi;
deg_min=0.25; deg_max=89.75; delta_deg=0.25;       %set parameters for loop over incident angles
degs=deg_min:delta_deg:deg_max;                    %all the values of deg
k_0=0;k_c_base=0;k_b_base=0;            %initialise so they can be passed to m_scenario code
k_1=0;k_b=0;                            %initialise so they can be passed to m_geo code
dummy=1;                                %to use in the calls to various subroutines

for loop=1:length(degs)
   deg=degs(loop)    ;                  %set deg to the current value of degs

   if deg==deg_min

      [freq,c_0,rho_0,k_0,c_base,b_base,rho_base,layers,omega,...
            lambda_0,mu_base,lambda_base,depth,k_c_base,k_b_base]=m_scenario_05(dummy);

      if layers>0
         [rho_1,c_1,b_1,k_1,k_b,alpha_1,beta_1,mu_1,lambda_1]=m_geo_02(omega,layers);
      end

   end

   [epsilon,sin_theta_c_base,sin_theta_b_base,cos_theta_c_base,cos_theta_b_base,...

gamma_0,gamma_c_base,gamma_b_base,alpha_1,beta_1,theta_0]=m_angles_01(deg,k_0,k_c_base,...
      k_b_base,k_1,k_b,layers);

   A=diag(ones(1,4));                   %initialise the A matrix

   if layers>0


[a11,a12,a13,a14,a21,a22,a23,a24,a31,a32,a33,a34,a41,a42,a43,a44]=matrix_coeffs_03(omega,layers,e
psilon,rho_1,c_1,b_1,k_1,k_b,alpha_1,beta_1,mu_1,lambda_1,depth,c_base,b_base,rho_base,...
gamma_c_base,gamma_b_base,mu_base,lambda_base);

      [A]=matrix_A_01(a11,a12,a13,a14,a21,a22,a23,a24,a31,a32,a33,a34,a41,a42,a43,a44,layers);

   end

   [V,W,P,V_Brek,W_Brek,P_Brek]=m_VWP_02(A,omega,theta_0,rho_0,c_0,rho_base,sin_theta_c_base,...
      sin_theta_b_base,cos_theta_c_base,cos_theta_b_base,epsilon,gamma_c_base,...
      gamma_b_base,mu_base,k_b_base);

   V_arr(loop)=V;
   V_arr_Brek(loop)=V_Brek;

end

V_phase=conv_to_deg*angle(V_arr);
V_phase_Brek=conv_to_deg*angle(V_arr_Brek);


figure(4)
plot(degs,abs(V_arr.^2),'k-')
hold on
plot(degs,abs(V_arr_Brek.^2),'b-')
axis([0 deg_max 0 1])
title('Power reflection coefficient versus incident angle')
xlabel('Incident angle (degrees)')
ylabel('Power reflection coefficient')

figure(5)
plot(degs,abs(V_arr),'k-')
hold on
plot(degs,abs(V_arr_Brek),'b-')
axis([0 deg_max 0 1])
title('Absolute amplitude reflection coefficient versus incident angle')
xlabel('Incident angle (degrees)')
ylabel('Amplitude reflection coefficient')

figure(6)
plot(degs,V_phase,'k-')
hold on
plot(degs,V_phase_Brek,'b-')
axis([0 deg_max -180 180])
title('Phase change on reflection, versus incident angle')
xlabel('Incident angle (degrees)')
ylabel('Phase change (degrees)')
```

```
figure(7)
plot(degs,abs(V_arr.^2),'k-')
hold on
plot(degs,abs(V_arr_Brek.^2),'b-')
axis([0 deg_max 0 20])
title('Power reflection coefficient versus incident angle')
xlabel('Incident angle (degrees)')
ylabel('Power reflection coefficient')

figure(8)
plot(degs,abs(V_arr),'k-')
hold on
plot(degs,abs(V_arr_Brek),'b-')
axis([0 deg_max 0 20])
title('Absolute amplitude reflection coefficient versus incident angle')
xlabel('Incident angle (degrees)')
ylabel('Amplitude reflection coefficient')
```

7.1.2 Sub-modules

Below is the code to get the scenario parameters, "m_scenario_05.m".

```
%STEPHEN AINSWORTH 24/08/00
%Function to get the scenario variables required for the matrix propagator
%reflection code. Puts in defaults if the user hits the "return" key rather
%than typing in a value.
%27/12/99: NOTE THE DEPTH IS MEASURED DOWNWARDS HERE, WITH THE DEPTH AT THE SEA / SEABED
%INTERFACE BEING DEFINED AS ZERO.
%28/12/99: HAVE SEPARATED OUT THOSE PARAMETERS WHICH DEPEND UPON THE INCIDENT ANGLE.
%24/08/00: CHANGED TO REMOVE THE LAYER LIMIT, NOW M_SCENARIO_05.

function [freq,c_0,rho_0,k_0,c_base,b_base,rho_base,layers,omega,...
      lambda_0,mu_base,lambda_base,depth,k_c_base,k_b_base]=m_scenario_05(dummy);

freq_default=800;                       %Hz
rho_0_default=1000;                     %kg/m^3
c_0_default=1500;                       %m/s
rho_base_default=5000;                  %kg/m^3
c_base_default=3000;                    %m/s
b_base_default=2000;                    %m/s
alpha_c_base_default=0.000000001;       %dB per wavelength travelled
alpha_b_base_default=0.000000001;       %dB per wavelength travelled
layers_default=1;             %default number of layers between the sea and the basement
delta_depth_default=10;       %default layer thickness is 10m

freq=input('Frequency please (default 800Hz)');
if length(freq)==0
   freq=freq_default;
end
rho_0=input('Density 0 please (default 1000kg/m^3)');
if length(rho_0)==0
   rho_0=rho_0_default;
end
c_0=input('Sound speed 0 please (default 1500m/s)');
if length(c_0)==0
   c_0=c_0_default;
end
rho_base=input('Density of the basement please (default 5000kg/m^3)');
if length(rho_base)==0
   rho_base=rho_base_default;
end
c_base=input('Sound speed in the basement please (default 3000m/s)');
if length(c_base)==0
   c_base=c_base_default;
end
b_base=input('Transverse speed in the basement please (default 2000m/s)');
if length(b_base)==0
   b_base=b_base_default;
end
alpha_c_base=input('Attenuation for compressional wave (default 0 dB per wavelength travelled)');
if length(alpha_c_base)==0
   alpha_c_base=alpha_c_base_default;
end
alpha_b_base=input('Attenuation for transverse wave (default 0 dB per wavelength travelled)');
if length(alpha_b_base)==0
   alpha_b_base=alpha_b_base_default;
end
layers=input('Number of layers between sea and basement. Default 1.  ');
if length(layers)==0
   layers=layers_default;
elseif layers<0
   layers=1;
   disp('Number of layers has been set to one.')
```

```
end

depth(1)=0;                                %top of first layer is at 0m
if layers>1
   for n=2:layers
      temp=input('Depth please (default: depth (n-1) + 10m) ');%sensible input required. This is
      %the depth, not delta depth. So must make it deeper than the previous layer !!!
      if length(temp)==0
         temp=depth(n-1)+delta_depth_default;
      end
      depth(n)=temp;
   end
end

if layers>0
   temp=input('Basement depth please (default: last layer depth + 10m) ');
   if length(temp)==0
      temp=depth(layers)+delta_depth_default;
   end
   depth(layers+1)=temp;
end

omega=2*pi*freq;                           %angular frequency (radians per second)
c_base=c_base+(-c_base*alpha_c_base/54.575*i);     %complex sound speed in the basement
b_base=b_base+(-b_base*alpha_b_base/54.575*i);     %complex transverse wave speed in the basement
k_0=omega/c_0;                             %sound wave wavenumber in sea
k_c_base=omega/c_base;                     %sound wave wavenumber in basement
k_b_base=omega/b_base;                     %transverse wave wavenumber in basement
mu_base=rho_base*b_base.^2;                %Lame coefficient for the seabed basement
lambda_base=rho_base*c_base.^2-2*mu_base;%Lame coefficient for the seabed basement
lambda_0=rho_0*c_0.^2;                     %Lame coefficient for the sea
disp('have got all the scenario variables')
```

Below is the code to get the layer geoacoustic parameters, "m_geo_02.m".

```
%STEPHEN AINSWORTH 24/08/00
%Function to get the geoacoustic variables required for the matrix propagator
%reflection code. Puts in defaults if the user hits the "return" key rather
%than typing in a value.
%21/12/99: started.
%26/12/99: separated out parameters which depend on the incident angle.
%24/08/00: changed to run with matrix_prop_04_file

function
[rho_1,c_1,b_1,k_1,k_b,alpha_1,beta_1,mu_1,lambda_1]=m_geo_02_file(omega,layers,density,...
          sound_speed,shear_speed,atten_comp,atten_shear);

conv=pi/180;                                       %essential !!
rho_1_default=2000;                                %kg/m^3
c_1_default=2000;                                  %m/s
b_1_default=1200;                                  %m/s
alpha_c_1_default=0.000000001;                     %dB per wavelength travelled
alpha_b_1_default=0.000000001;                     %dB per wavelength travelled

for n=1:layers
   rho_1(n)=density(n);
   c_1(n)=sound_speed(n);
   b_1(n)=shear_speed(n);
   alpha_c_1(n)=atten_comp(n);
   alpha_b_1(n)=atten_comp(n);
end

c_1=c_1+(-c_1.*alpha_c_1/54.575*i);                %complex sound speed in the seabed
b_1=b_1+(-b_1.*alpha_b_1/54.575*i);                %complex transverse wave speed in the seabed
k_1=omega./c_1;                                    %sound wave wavenumber in seabed
k_b=omega./b_1;                                    %transverse wave wavenumber in seabed
mu_1=rho_1.*b_1.^2;                                %Lame coefficient for the seabed
lambda_1=rho_1.*c_1.^2-2.*mu_1;                    %Lame coefficient for the seabed
disp('have got all the geoacoustic variables')
```

Below is the code to calculate the layer propagation angles, "m_angles_01.m".

```
%STEPHEN AINSWORTH 28/12/99
%This is to update the angles and other parameters which depend upon the incident
%angle and hence will change with each value of deg.

function[epsilon,sin_theta_c_base,sin_theta_b_base,cos_theta_c_base,cos_theta_b_base,...
      gamma_0,gamma_c_base,gamma_b_base,alpha_1,beta_1,theta_0]=m_angles_01(deg,k_0,k_c_base,...
   k_b_base,k_1,k_b,layers)

conv=pi/180;                                       %to convert degrees to radians
theta_0=deg*conv;                                  %the incident angle in radians
```

```
epsilon=k_0*sin(theta_0);                          %epsilon_0 conserved - (smooth) horizontal
wavenumber
sin_theta_c_base=epsilon/k_c_base;                 %hence sound wave incident angle in seabed
sin_theta_b_base=epsilon/k_b_base;                 %hence transverse wave incident angle in seabed
cos_theta_c_base=sqrt(1-sin_theta_c_base^2);
cos_theta_b_base=sqrt(1-sin_theta_b_base^2);
gamma_0=k_0*cos(theta_0);                          %vertical wavenumber in the sea
gamma_c_base=k_c_base*cos_theta_c_base;  %vertical wavenumber in the seabed
gamma_b_base=k_b_base*cos_theta_b_base;  %transverse wave vertical wavenumber in the seabed

if layers>0
   sin_theta_l=epsilon./k_l;            %sound wave incident angle in seabed
   sin_theta_b=epsilon./k_b;            %transverse wave incident angle in seabed
   cos_theta_l=sqrt(1-sin_theta_l.^2);
   cos_theta_b=sqrt(1-sin_theta_b.^2);
   alpha_l=k_l.*cos_theta_l;            %compressional wave vertical wavenumber in the seabed
   beta_l=k_b.*cos_theta_b;             %transverse wave vertical wavenumber in the seabed
else
   alpha_l=1;                                      %default value to pass back, will not be used
   beta_l=1;                                       %default value to pass back, will not be used
end
```

Below is the code to calculate the layer "A" matrix coefficients, "matrix_coeffs_03.m".

```
%This defines the matrix coefficients for each of the number ("layers") of layers.
%In the transfer report...
%"it is assumed that the layers are numbered from the lower half-space (layer 1) to the fluid
%half-space (layer n+1) with z_n being at the top of layer j."
%Here the layers are numbered from the top, so will need to be careful...
%22/12/99 MATRIX_COEFFS_01: started writing.
%27/12/99 MATRIX_COEFFS_02: continued writing. NOTE THAT THESE a COEFFICIENTS ARE FOR LAYERS
%         NUMBERED WITH N=1 AS THE UPPERMOST LAYER, AND N=LAYERS AS THE LAYER DIRECTLY ABOVE
%         THE BASEMENT.
%28/12/99 MADE CORRECTIONS TO a21 AND a33.

function
[a11,a12,a13,a14,a21,a22,a23,a24,a31,a32,a33,a34,a41,a42,a43,a44]=matrix_coeffs_03(omega,layers,e
psilon...
   ,rho_1,c_1,b_1,k_1,k_b,alpha_1,beta_1,mu_1,lambda_1,depth,c_base,b_base,rho_base,...
   gamma_c_base,gamma_b_base,mu_base,lambda_base)

%*****************************************************************************************************
%DERIVE SIN_THETA TERMS
%*****************************************************************************************************

sin_theta_t=epsilon./k_b;
sin_theta_l=epsilon./k_l;

%*****************************************************************************************************
%DEFINE THE REST OF THE GEOMETRICAL TERMS
%*****************************************************************************************************

sin_sq_theta_t=sin_theta_t.^2;
cos_theta_t=sqrt(1-sin_sq_theta_t);
cos_sq_theta_t=cos_theta_t.^2;
cos_2_theta_t=cos_sq_theta_t-sin_sq_theta_t;
cos_sq_2_theta_t=cos_2_theta_t.^2;
sin_2_theta_t=2*sin_theta_t.*cos_theta_t;
sin_sq_2_theta_t=sin_2_theta_t.^2;
tan_theta_t=sin_theta_t./cos_theta_t;
cos_theta_l=sqrt(1-sin_theta_l.^2);
tan_theta_l=sin_theta_l./cos_theta_l;
cot_theta_l=1./tan_theta_l;

%*****************************************************************************************************
%DEFINE DELTA_Z: NOTE I HAVE Z MEASURED DOWNWARDS WITH DEPTH(N) AT THE TOP OF THE NTH LAYER, WITH
%DEPTH(1)=0. THE LAYERS ARE MEASURED WITH N INCREASING DOWNWARDS. THIS IS NOT A PROBLEM HERE BUT
%I WILL HAVE TO BE CAREFUL WHEN MULTIPLYING THE LAYER MATRICES LATER IN THE MAIN CODE.
%*****************************************************************************************************

for n=1:layers
   delta_z(n)=depth(n+1)-depth(n);      %NOTE THIS IS FOR LAYERS NUMBERED 1 TO N GOING DOWNWARDS
end

%*****************************************************************************************************
%DEFINE SOME MATRIX PARAMETERS
%*****************************************************************************************************

P=alpha_1.*delta_z;
Q=beta_1.*delta_z;
cos_P=cos(P);
sin_P=sin(P);
cos_Q=cos(Q);
sin_Q=sin(Q);

%*****************************************************************************************************
```

```
%DEFINE THE MATRIX COEFFICIENTS
%*************************************************************************************************

a11=2*sin_sq_theta_t.*cos_P+cos_2_theta_t.*cos_Q;
a12=i*(tan_theta_1.*cos_2_theta_t.*sin_P-sin_2_theta_t.*sin_Q);
a13=i*sin_theta_t.*(cos_Q-cos_P)./(omega*rho_1.*b_1);
a14=(tan_theta_1.*sin_theta_t.*sin_P+cos_theta_t.*sin_Q)./(omega*rho_1.*b_1);
a21=i*(2*cot_theta_1.*sin_sq_theta_t.*sin_P-tan_theta_t.*cos_2_theta_t.*sin_Q);
a22=cos_2_theta_t.*cos_P+2*sin_sq_theta_t.*cos_Q;
a23=(cot_theta_1.*sin_theta_t.*sin_P+sin_theta_t.*tan_theta_t.*sin_Q)./(omega*rho_1.*b_1);
a24=a13;
a31=-2*i*omega*rho_1.*b_1.*sin_theta_t.*cos_2_theta_t.*(cos_Q-cos_P);
a32=-
omega*rho_1.*b_1.*(tan_theta_1.*cos_sq_2_theta_t.*sin_P+sin_sq_2_theta_t.*tan_theta_t.*sin_Q)./si
n_theta_t;
a33=a22;
a34=a12;
a41=-
omega*rho_1.*b_1.*(4*cot_theta_1.*(sin_theta_t.^3).*sin_P+(cos_sq_2_theta_t./cos_theta_t).*sin_Q)
;
a42=a31;
a43=a21;
a44=a11;
```

Below is the code to calculate the system "A" matrix, "matrix_A_01.m".

```
%This calculates the matrix for the matrix propagator method for calculating the reflection
%and transmission coefficients from a system of smooth horizontal layers. It is assumed here
%that the layers are numbered with layer 1 at the top and the last layer just above the basement.
%This is different to the numbering scheme used in Brekhovskikh (and my transfer report) and so
%the order in which I have multiplied the matrices appears different in terms of indices but is
%actually the same.
%27/12/99  MATRIX_A_01: started writing.

function [A]=matrix_A_01(a11,a12,a13,a14,a21,a22,a23,a24,a31,a32,a33,a34,a41,a42,a43,a44,layers);

%*************************************************************************************************
%DEFINE THE PROPAGATED MATRIX
%*************************************************************************************************

A=diag(ones(1,4));                                  %initialise the matrix

for n=1:layers
   layer_A(1,:)=[a11(n) a12(n) a13(n) a14(n)];      %set the matrix rows for the nth layer
   layer_A(2,:)=[a21(n) a22(n) a23(n) a24(n)];      %set the matrix rows for the nth layer
   layer_A(3,:)=[a31(n) a32(n) a33(n) a34(n)];      %set the matrix rows for the nth layer
   layer_A(4,:)=[a41(n) a42(n) a43(n) a44(n)];      %set the matrix rows for the nth layer
   A=A*layer_A;                                     %right multiply the current matrix by the layer
matrix
end
```

Below is the code to calculate the reflection coefficient V , "m_VWP_02.m".

```
%This calculates the smooth surface reflection and transmission coefficients, V, W and P
%respectively, for a system of smooth horizontal layers.
%27/12/99  m_VWP_01: started writing.
%PhD VIVA PASSED 30/11/00. CORRECTIONS REQUIRED.
%13/01/01: m_VWP_02: to add Brek and Godin's incorrect solution.

function
[V,W,P,V_Brek,W_Brek,P_Brek]=m_VWP_02(A,omega,theta_0,rho_0,c_0,rho_base,sin_theta_c_base,...
   sin_theta_b_base,cos_theta_c_base,cos_theta_b_base,epsilon,gamma_c_base,...
   gamma_b_base,mu_base,k_b_base);


%*************************************************************************************************
%DEFINE A FEW GEOMETRICAL CONSTANTS
%*************************************************************************************************

sin_sq_theta_b_base=sin_theta_b_base^2;
cos_sq_theta_b_base=cos_theta_b_base^2;
sin_2_theta_b_base=2*sin_theta_b_base*cos_theta_b_base;
cos_2_theta_b_base=cos_sq_theta_b_base-sin_sq_theta_b_base;
cot_theta_c_base=cos_theta_c_base/sin_theta_c_base;
cot_theta_b_base=cos_theta_b_base/sin_theta_b_base;

%*************************************************************************************************
%DEFINE A FEW MORE CONSTANTS
%*************************************************************************************************

numerator=A(4,1)-A(4,2)*cot_theta_c_base+i*A(4,3)*mu_base*k_b_base*cos_2_theta_b_base...
   /sin_theta_b_base-2*A(4,4)*i*mu_base*k_b_base*sin_theta_b_base*cot_theta_c_base;
```

```
denominator=-A(4,1)*cot_theta_b_base-A(4,2)+2*i*A(4,3)*mu_base*k_b_base*cos_theta_b_base...
   +i*A(4,4)*mu_base*k_b_base*cos_2_theta_b_base/sin_theta_b_base;

q=numerator/denominator;

E_2=-A(2,1)*epsilon+A(2,2)*gamma_c_base-i*omega^2*rho_base*(A(2,3)*cos_2_theta_b_base...
   -A(2,4)*2*sin_sq_theta_b_base*cot_theta_c_base)-q*(A(2,1)*gamma_b_base+A(2,2)*epsilon...
   -i*omega^2*rho_base*(A(2,3)*sin_2_theta_b_base+A(2,4)*cos_2_theta_b_base));

E_3=-A(3,1)*epsilon+A(3,2)*gamma_c_base-i*omega^2*rho_base*(A(3,3)*cos_2_theta_b_base...
   -A(3,4)*2*sin_sq_theta_b_base*cot_theta_c_base)-q*(A(3,1)*gamma_b_base+A(3,2)*epsilon...
   -i*omega^2*rho_base*(A(3,3)*sin_2_theta_b_base+A(3,4)*cos_2_theta_b_base));

%*************************************************************************************
%DEFINE THE EQUIVALENT BREKHOVSKIKH AND GODIN CONSTANTS
%*************************************************************************************

M_21=A(2,1)-A(2,1)/A(4,1);
M_22=A(2,2)-A(2,1)/A(4,1);
M_23=A(2,3)-A(2,1)/A(4,1);
M_24=A(2,4)-A(2,1)/A(4,1);

M_31=A(3,1)-A(3,1)/A(4,1);
M_32=A(3,2)-A(3,1)/A(4,1);
M_33=A(3,3)-A(3,1)/A(4,1);
M_34=A(3,4)-A(3,1)/A(4,1);

E_2_Brek=M_22*gamma_c_base-i*omega^2*rho_base*(M_23*cos_2_theta_b_base+...
   M_24*2*sin_sq_theta_b_base*cot_theta_c_base)-q*(M_22*epsilon+i*omega^2*rho_base*...
   (M_23*sin_2_theta_b_base-M_24*cos_2_theta_b_base));

E_3_Brek=M_32*gamma_c_base-i*omega^2*rho_base*(M_33*cos_2_theta_b_base+...
   M_34*2*sin_sq_theta_b_base*cot_theta_c_base)-q*(M_32*epsilon+i*omega^2*rho_base*...
   (M_33*sin_2_theta_b_base-M_34*cos_2_theta_b_base));

%*************************************************************************************
%THE REFLECTION COEFFICIENT IS NOW WRITTEN IN ITS USUAL FORM
%*************************************************************************************

Z=rho_0*c_0/cos(theta_0);              %impedance of the upper liquid half-space

Z_inp=-E_3/(i*omega*E_2);              %input impedance of the layers and basement

V=(Z_inp-Z)/(Z_inp+Z);                 %reflection coefficient

Z_inp_Brek=-E_3_Brek/(i*omega*E_2_Brek); %Brek and Godin's incorrect input impedance

V_Brek=(Z_inp_Brek-Z)/(Z_inp_Brek+Z);   %Brek and Godin's incorrect reflection coefficient


%*************************************************************************************
%THE TRANSMISSION COEFFICIENTS
%*************************************************************************************

%NEED TO CHECK THESE - NOT CLEAR WHICH RHO AND OMEGA AND THETAS TO USE

W=1;
P=1;
W_Brek=1;
P_Brek=1;
```

7.2 Scattering strength from a liquid / liquid interface

The code has been written in a modular form, with a main program, "main_many_10_2.m", which calls 11 subroutines. These are listed below. One of these subroutines, "LS_plots_20.m", calls 2 subroutines itself, also listed below. The heart of the algorithm is the subroutine to calculate the scattered pressure for each surface, "p_calc_liq_09.m", and is called many times as two nested loops over harmonic and plane wave components are evaluated. The scattered pressure sum of these plane harmonic waves gives the solution for a pulsed beam, as described in chapter 6.

Name main_many_10_2.m

Sub-modules

To get the geoacoustic parameters		LL_geo8.m
To calculate the sound pulse parameters		pulse_params_04
To calculate the surface power spectrum	either	surf_power12.m
	or	thorsos_surf_power12.m
To include phases in surface realisations		add_phases_03.m
To calculate the sound beam parameters		beam_params_08.m
To calculate the pressure reflection coefficient		refls3.m
To calculate the scattered pressure for each surface		p_calc_liq_09.m
To sort the scattered pressures by outgoing angle		angle_sort_05.m
To interpolate over zero bins		smooth_03.m
To smooth data using box car mean		box_03.m
To smooth data, calculate statistics and plots		LS_plots_20.m
To plot best fit Gaussian distribution		gaussian_03.m
To plot best fit Rayleigh distribution		rayleigh_06.m
To calculate the chi squared values for each fit		chi_sq_03.m

7.2.1 The main code

```
clear                          %to get rid of old data from the workspace
conv=pi/180;                    %to convert degrees to radians
dummy=1;                        %to call the functions which need no variables passed
delta_f=0.5;                    %difference in frequency components in the pulse
nyq_factor=2;                   %factor that hydrophone spacing is less than Nyquist
angle_factor=5;                 %take outputs at 1/angle_factor degree spacing
all_angles=-90:(1/angle_factor):90;      %angles for scattered pressure output
hist_width=4;                            %no. of std each side of the mean for the histograms
hist_bin=0.0001;                         %bin width, linear, for histograms
num_angles=length(all_angles);           %the length of the all_angles array
cos_sq_all_angles=(cos(all_angles*conv)).^2;       %cos squared for all of the output angles
kappa_factor=1.0;                                  %such that all relevant angles are considered
delta_kappa=0.05;                                  %units of m^-1
imag_real_frac=0.01;                               %maximum allowed imaginary_gamma / real_gamma

[kappa,theta_centre,freq_centre,rho_0,c_0,rho_1,c_1,b_1,alpha_c_1,alpha_b_1,...
      m,k_0,k_1,k_b,no_hyd,h,l,chebgain,pulse_width,epsilon_centre,beamwidth]=LL_geo8...
   (kappa_factor,delta_kappa,nyq_factor);          %GEOACOUSTIC AND SURFACE DATA

box=beamwidth*angle_factor;                        %for the box-car smoothing

[freqs,n_freqs,w_freqs]=pulse_params_04(freq_centre,pulse_width,delta_f);%PULSE PARAMETERS
n_freqs

%*************************************************************************************************
%MUST manually switch between the surface being defined by: ka and ksigma (Thorsos) or sigma and
%corr (gaussian)
%[thorsos_amp,surface_amp,many_surfaces]=surf_power12(kappa,k_0,epsilon_centre);%SURFACE
%AMPLITUDE SPECTRUM
%[thorsos_amp,surface_amp,many_surfaces]=thorsos_surf_power12(kappa,k_0,epsilon_centre);%SURFACE
%AMPLITUDE SPECTRUM
%MUST manually switch between the surface being defined by: ka and ksigma (Thorsos) or sigma and
%corr (gaussian)
%*************************************************************************************************

%*************************************************************************************************
%MUST manually switch between enabling this assignment, to look at thorsos results, or not, to
%keep with gaussian
%surface_amp=thorsos_amp;
%MUST manually switch between enabling this assignment, to look at thorsos results, or not, to
%keep with gaussian
%*************************************************************************************************

tic                                    %to start timing the code

p_array=zeros(many_surfaces,num_angles); %array of scattered p_alpha for all surface realisations
p_rigid=zeros(many_surfaces,num_angles); %array of scattered p_solid for all surface realisations

[surface_amp_array]=add_phases_03(kappa,surface_amp,many_surfaces);    %ARRAY OF many_surfaces
PHASED surface_amp ROWS

%*************************************************************************************************
%LOOP OVER ALL REQUIRED HARMONIC WAVES AND ALL REQUIRED PLANE WAVE DIRECTIONS AND SUM WITH
%RESPECT TO WEIGHTS
%*************************************************************************************************
```

```
for f_index=1:n_freqs
   f_index
   freq=freqs(f_index);

[epsilons,gams_0,gams_1,gams_b,omega,thetas_0,n_theta_0,w_theta_0]=beam_params_08(theta_centre,..
freq,no_hyd,c_0,c_1,b_1,h,1,chebgain,nyq_factor);            %BEAM PARAMETERS
   for theta_0_index=1:n_theta_0
      theta_0=thetas_0(theta_0_index);   %incident angle for particular plane wave
      epsilon_0=epsilons(theta_0_index); %horizontal wavevector for particular plane wave
      gam_0=gams_0(theta_0_index);       %vertical wavevector for plane wave in the sea
      gam_1=gams_1(theta_0_index);       %vertical wavevector for plane sound wave in the seabed
      gam_b=gams_b(theta_0_index);%vertical wavevector for plane transverse wave in the seabed
      [V,W,P]=refls3(omega,theta_0,rho_0,c_0,rho_1,c_1,b_1); %CALCULATES SMOOTH SURFACE PRESSURE
COEFFICIENTS
      G=-m*(1+V);              %constant just to group some terms together
      E=gam_0-gam_0*V-gam_1*W; %constant just to group some terms together

[p_alpha,p_beta,p_solid,c_angle_out,c_angle_in,denom,gamma_alpha,gamma_beta,p_sol_unweighted]=
  p_calc_liq_09(k_0,k_1,epsilon_0,kappa,gam_0,gam_1,G,W,E,m,surface_amp_array,imag_real_frac);
%SCATTERED PRESSURES

[p_sorted,p_solid_sorted]=angle_sort_05(p_alpha,p_solid,c_angle_out,all_angles,angle_factor);
%BIN BY OUTGOING ANGLE

      [p_sorted]=smooth_03(p_sorted);    %interpolates over zeros for each row in p_sorted
      [p_solid_sorted]=smooth_03(p_solid_sorted);  %interpolates over zeros for each row in
p_solid_sorted

      [p_sorted]=box_03(p_sorted,box);   %to smooth p_sorted
      [p_solid_sorted]=box_03(p_solid_sorted,box); %to smooth p_solid_sorted

      p_sorted=p_sorted*w_freqs(f_index)*w_theta_0(theta_0_index);     %weight the harmonic plane
wave output array
      p_solid_sorted=p_solid_sorted*w_freqs(f_index)*w_theta_0(theta_0_index);   %weight the
harmonic plane wave output array

      p_array=p_array+p_sorted;%add pressure array for this freq and beam, for elastic scatter
      p_rigid=p_rigid+p_solid_sorted;    %add pressure array for this freq and beam, for rigid
scatter

   end
end

%*****************************************************************************************
%ALL SCATTERED PRESSURES HAVE NOW BEEN SUMMED WITH RESPECT TO THE WEIGHTS OF THE INCIDENT
%HARMONIC AND PLANE WAVES
%*****************************************************************************************
save latest_run;

toc                  %to stop the timing of the code running

tic                  %to time how long the smoothing and plotting takes

[scatter_strength_last,rigid_scatter_last,mean_scatter_strength,mean_rigid_scatter_strength,...
prob_back_gaussian,prob_forw_gaussian]=LS_plots_20(p_array,p_rigid,p_beta,conv,all_angles,k_0,k_1
,many_surfaces,cos_sq_all_angles,theta_centre,angle_factor,hist_width,hist_bin,beamwidth,no_hyd);
                     %PLOTS AND CHECKS

toc                  %to stop the clock on the smoothing and plotting
```

7.2.2 Sub-modules

The code below "LL_geo8.m", and is the subroutine to get the geometric and geoacoustic parameters. The user is asked to input the parameters, and defaults are provided. From these, other geoacoustic parameters are derived, as well as the beamwidth of the incident wave and range of surface wavenumbers to be used in the surface power spectral density.

```
function [kappa,theta_centre,freq_centre,rho_0,c_0,rho_1,c_1,b_1,alpha_c_1,alpha_b_1,...
      m,k_0,k_1,k_b,no_hyd,h,1,chebgain,pulse_width,epsilon_centre,beamwidth]=LL_geo8...
   (kappa_factor,delta_kappa,nyq_factor); %GEOACOUSTIC AND SURFACE DATA

%*****************************************************************************
%DEFAULT PARAMETERS
%*****************************************************************************

no_hyd_default=1;              %number of hydrophones in transmitter
```

```
h_default=100;                  %height of array from the seabed (metres)
chebgain_default=20;            %dB gain from Chebyshev weights on the hydrophone amplitudes
bw_max=10;                      %maximum beamwidth, degrees
beamscale=72.53;                %Width (degrees) = 72.53 / (L(metres)xf(kHz)).

pulse_width_default=1000;       %width of pulse from -3 sigma to +3 sigma from mean, in seconds

conv=pi/180;                    %essential !!
freq_centre_default=800;        %Hz
theta_centre_default=45*conv;   %radians (incident angle, measured from the normal)
rho_0_default=1000;             %kg/m^3
c_0_default=1500;               %m/s
rho_1_default=2000;             %kg/m^3
c_1_default=2000;               %m/s
b_1_default=0.01;               %m/s
alpha_c_1_default=0.00000001;   %dB per wavelength travelled
alpha_b_1_default=0.00000001;   %dB per wavelength travelled

%*******************************************************************************
%GEOMETRY AND PULSE PARAMETERS
%*******************************************************************************

theta_centre=input('Incident angle please (default 45 degrees) ?');
if length(theta_centre)==0
   theta_centre=theta_centre_default;
else
   theta_centre=theta_centre*conv;
end
no_hyd=input('Number of hydrophones in TX please (default 1) ?');
if length(no_hyd)==0
   no_hyd=no_hyd_default;
end
h=input('Height of TX array above the seabed please (default 100m) ?');
if length(h)==0
   h=h_default;
end
chebgain=input('Gain of main beam wrt sidelobes please (default 20dB) ?');
if length(chebgain)==0
   chebgain=chebgain_default;
end
freq_centre=input('Frequency please (default 800Hz)');
if length(freq_centre)==0
   freq_centre=freq_centre_default;
end
pulse_width=input('Pulse width please (default 1000 seconds)');
if length(pulse_width)==0
   pulse_width=pulse_width_default;
end

%*******************************************************************************
%GEOACOUSTIC PARAMETERS
%*******************************************************************************

rho_0=input('Density_0 please (default 1000kg/m^3)');
if length(rho_0)==0
   rho_0=rho_0_default;
end
c_0=input('Sound speed 0 please (default 1500m/s)');
if length(c_0)==0
   c_0=c_0_default;
end
rho_1=input('Density_1 please (default 2000kg/m^3)');
if length(rho_1)==0
   rho_1=rho_1_default;
end
c_1=input('Sound speed 1 please (default 2000m/s)');
if length(c_1)==0
   c_1=c_1_default;
end
b_1=input('Transverse speed 1 please (default 0.01m/s)');
if length(b_1)==0
   b_1=b_1_default;
end
alpha_c_1=input('Attenuation for compressional wave (default 0 dB per wavelength travelled)');
if length(alpha_c_1)==0
   alpha_c_1=alpha_c_1_default;
end
alpha_b_1=input('Attenuation for transverse wave (default 0 dB per wavelength travelled)');
if length(alpha_b_1)==0
   alpha_b_1=alpha_b_1_default;
end

%*******************************************************************************
%CALCULATE THE BEAMWIDTH
%*******************************************************************************

f_kHz=freq_centre/1000;                 %frequency in kHz
lambda=c_0/freq_centre;                 %incident wavelength
```

```
nyquist=lambda/2;                          %nyquist spacing
spacing=nyquist/nyq_factor;                %spacing of the array elements in metres
array_length=(no_hyd-1)*spacing;           %length of array in metres
beamwidth=beamscale/(array_length*f_kHz);%full width half maximum intensity, in degrees
if beamwidth>bw_max
   beamwidth=bw_max;
end
%*****************************************************************************
%DERIVED GEOACOUSTIC PARAMETERS
%*****************************************************************************

omega_centre=2*pi*freq_centre;             %centre angular frequency (radians per second)
l=-h*tan(theta_centre);%horizontal displacement of array centre from point of impact of beam
m=rho_1/rho_0;                             %dimensionless ratio
c_1=c_1+(-c_1*alpha_c_1/54.575*i);         %complex sound speed in the seabed
b_1=b_1+(-b_1*alpha_b_1/54.575*i);         %complex transverse wave speed in the seabed
k_0=omega_centre/c_0;                      %sound wave wavenumber in sea
epsilon_centre=k_0*sin(theta_centre);      %horizontal wavenumber
k_1=omega_centre/c_1;                      %sound wave wavenumber in seabed
k_b=omega_centre/b_1;                      %transverse wave wavenumber in seabed
disp('have got all the geoacoustic variables')

%*****************************************************************************
%DERIVED SURFACE WAVENUMBERS (KAPPA)
%*****************************************************************************

%max_k=max([abs(k_0) abs(k_1)]);           %maximum wavevector. Use if considering transmitted.
max_k=k_0;                                 %only considering reflected wave now.
kappa_min=-kappa_factor*(max_k+epsilon_centre); %minimum kappa value to be considered in the
power spec.
kappa_max=kappa_factor*(max_k-epsilon_centre); %maximum kappa value to be considered in the power
spec.


%want to make as many kappa values as possible symmetric about zero.

kappa_left=0:-delta_kappa:kappa_min;                          %from 0 to min
kappa_right=delta_kappa:delta_kappa:kappa_max;                %from delta_kappa to max
full_length=length(kappa_left)+length(kappa_right);
kappa(1:length(kappa_left))=kappa_left;
kappa(length(kappa_left)+1:full_length)=kappa_right;
kappa=sort(kappa);                                            %rough surface wavenumber
```

The code below is "pulse_params_04.m", and is the subroutine used to calculate the weights of the harmonic components of the incident sound pulse. The weights are calculated for a Gaussian pulse. The length of the pulse, input by the user (see LL_geo8) is taken to be ±3 standard deviations.

```
function [freqs,n_freqs,w_freqs]=pulse_params_04(freq_centre,pulse_width,delta_f);

%*****************************************************************************
%SET UP PARAMETERS
%*****************************************************************************

mu=freq_centre;                            %centre frequency of the pulse (Hz)
sigma=(1/2*pi)*(6/pulse_width);            %width of the pulse (Hz) for half width half maximum

%*****************************************************************************
%DERIVED PULSE COMPONENTS
%*****************************************************************************

fmin=mu-4*sigma;                           %minimum frequency component in the pulse
fmax=mu+4*sigma;                           %maximum frequency component in the pulse
freqs=fmin:delta_f:fmax;                   %array of frequency components in the pulse
n_freqs=length(freqs);                     %number of frequency components in the pulse

%*****************************************************************************
%FREQUENCY COMPONENT WEIGHTS
%*****************************************************************************

w_freqs=(1/sqrt(2*pi*sigma^2)).*exp((-(freqs-mu).^2)/(2*sigma^2));  %Gaussian weighting
w_freqs=w_freqs/sum(w_freqs); %normalise so that the weights sum to one
```

The code below is "surf_power12.m", one of the two power spectral density subroutines which the user must select by commenting the appropriate code in the main_many_10_2 code. This one is used to give a Gaussian power spectral density, defined in terms of the surface correlation length, with the root mean square surface height, σ, defined as a fixed (small) fraction of the mean incident wavelength. The subroutine also produces a "Thorsos" power spectral density with the same total power as the Gaussian, and with equal value at κ = 0. [Note: The fractal option should not be selected – this part of the code has not been maintained.]

```
function [thorsos_amp,surface_amp,many_surfaces]=surf_power12(kappa,k_0,epsilon_centre);

many_surfaces_default=1;       %default number of surface realisations to be summed over
epsilon_0=epsilon_centre;      %to keep code changes minimal
factor_default=0.1;            %correlation length factor default for Gaussian spectrum
wavelength_0=2*pi/k_0;         %incident wavelength
default_sigma_factor=0.2/(4*pi);         %default_sigma_factor << 1/4_pi for small Rayleigh
kappa_power_default=0.5;       %default power spectrum is 1/kappa^(0.5)
kappa_max=k_0-epsilon_0-0.01; %see page 144 of notebook, sub 0.01 otherwise get gamma_0 -> 0

sigma_factor = input('Sigma in terms of wavelength_0 (default 0.2/(4*pi)) ?');
if length(sigma_factor)==0
   sigma_factor=default_sigma_factor;
end
factor=input('Correlation length in terms of wavelength_0 (default 0.1) ?');
if length(factor)==0
   factor=factor_default;
end

sigma=sigma_factor*wavelength_0;
beta=k_0*sigma;                          %used in the Thorsos spectrum
corr=factor*wavelength_0;                %correlation length of the surface
exponential=exp(-(kappa.^2)*(corr.^2)/4);
surface_power=(sigma^2)*((corr*pi^0.5)/(2*pi))*exponential;  %Gaussian power spectrum for 1d
surface.

%*************************************************************************************************
%Looking at the type of power spectrum used in the Thorsos paper. This is normalised in two ways.
%Firstly the constants a and b are such that no-matter what ka is used, the total power (i.e.
%integral of %thorsos over kappa) equals that of the gaussian spectrum. Secondly, if the
%ka_default is used, the value of %thorsos at zero kappa equals that of the gaussian at zero
%kappa (as well as the total powers being equal).
%*************************************************************************************************

ka_default=k_0*(2*sigma^2)/(corr*pi^1.5);                %default value for ka, gives
thorsos(0)=gaussian(0)
ka=input('Value for ka please (Thorsos uses 0.0175)');
if length(ka)==0
   ka=ka_default;
end
a=ka/k_0;                                                 %for thorsos power spectrum
b=k_0*ka*pi/beta^2;                                       %for thorsos power spectrum
thorsos=a./(kappa.^2+b^2);

%*************************************************************************************************
*************

surface_amp=sqrt(surface_power);         %NOW RETURN SURFACE AMPLITUDE (NO PHASE YET)
thorsos_amp=sqrt(thorsos);               %RETURN SURFACE AMPLITUDE (NO PHASE YET)
figure(15)
plot(kappa,surface_amp,'r-')
hold on
plot(kappa,thorsos_amp,'b-')
title('Surface amplitude versus kappa for gaussian (red) and Thorsos (blue) spectra')
ylabel('Surface amplitude')
xlabel('Rough surface wavenumber, kappa')

%*************************************************************************************************

many_surfaces=input('Number of surface realisations (default 1) ?');   %surface realisations to
find scattering stats
if length(many_surfaces)==0
   many_surfaces=many_surfaces_default;
end
```

The code below is "thorsos_surf_power12.m", the second of the two power spectral density subroutines which the user must select by commenting the appropriate code in the main_many_10_2 code. This one is used to give a "Thorsos" power spectral density (see chapter 3), defined in terms of the products $k\sigma$, where σ is the root mean square surface height, and ka, where "a" is a parameter in the power spectral density. The subroutine also produces a Gaussian power spectral density with the same total power as the "Thorsos" one, and with equal value at $\kappa = 0$. [Note: The fractal option should not be selected – this part of the code has not been maintained.]

```
function [thorsos_amp,surface_amp,many_surfaces]=thorsos_surf_power12(kappa,k_0,epsilon_centre);

many_surfaces_default=1;                %default number of surface realisations to be summed over
epsilon_0=epsilon_centre;               %to keep code changes minimal
factor_default=0.1;                     %correlation length factor default for Gaussian spectrum
wavelength_0=2*pi/k_0;                  %incident wavelength
kappa_power_default=0.5;                %default power spectrum is 1/kappa^(0.5)
kappa_max=k_0-epsilon_0-0.01; %see page 144 of notebook, sub 0.01 otherwise get gamma_0 -> 0
ka_default=0.0175;            %used in the Thorsos spectrum
ksigma_default=0.2;           %used in the Thorsos spectrum

ksigma=input('Value for ksigma please (default 0.2)');
if length(ksigma)==0
   ksigma=ksigma_default;
end

ka=input('Value for ka please (default 0.0175)');
if length(ka)==0
   ka=ka_default;
end

sigma=ksigma/k_0;                       %for both spectra
a=ka/k_0;                               %for Thorsos power spectrum
b=k_0*ka*pi/ksigma^2;                   %for Thorsos power spectrum
corr_default=(2*sigma^2)/(a*pi^1.5);     %corr, gives thorsos(0)=Gaussian(0)

factor=input('Correlation length in terms of wavelength_0 (default gives thorsos(0)=gaussian(0))
?');
if length(factor)==0
   corr=corr_default;
else
   corr=factor*wavelength_0;
                                        %correlation length of the surface
end

%*************************************************************************************************
%Gaussian spectrum
%*************************************************************************************************

exponential=exp(-(kappa.^2)*(corr.^2)/4);
surface_power=(sigma^2)*((corr*pi^0.5)/(2*pi))*exponential;  %surface Gaussian power spectrum for
1d surface.

%*************************************************************************************************
%Looking at the type of power spectrum used in the Thorsos paper. This is normalised in two ways.
%Firstly the constants a and b are such that no-matter what ka and k_sigma are used, the total
%power (i.e. integral over kappa) equals that of the Gaussian spectrum. Secondly, if the
%corr_default is used, the value of thorsos at zero kappa equals that of the Gaussian at zero
%kappa (as well as the total powers being equal).
%*************************************************************************************************

thorsos=a./(kappa.^2+b^2);

%*************************************************************************************************

surface_amp=sqrt(surface_power);        %NOW RETURN SURFACE AMPLITUDE (NO PHASE YET)
thorsos_amp=sqrt(thorsos);              %RETURN SURFACE AMPLITUDE (NO PHASE YET)
figure(15)
plot(kappa,surface_amp,'r-')
hold on
plot(kappa,thorsos_amp,'b-')
title('Surface amplitude versus kappa for Gaussian (red) and Thorsos (blue) spectra')
ylabel('Surface amplitude')
xlabel('Rough surface wavenumber, kappa')

%*************************************************************************************************
```

```
many_surfaces=input('Number of surface realisations (default 1) ?');   %surface realisations to
find scattering stats
if length(many_surfaces)==0
   many_surfaces=many_surfaces_default;
end
```

The code below is "add_phases_03.m" and is the subroutine used to produce an array of surface amplitude spectra, each one having random phases on each of the spectral components. Each surface amplitude spectrum is therefore unique, and allows the scattering from a surface realisation to be calculated.

```
function [surface_amp_array]=add_phases_03(kappa,surface_amp,many_surfaces);%rows of phased
surface_amp

surf_amp_length=length(surface_amp);     %gives the number of cpts in the surface_amp array
a=ones(surf_amp_length,many_surfaces);   %set up a rectangular array of ones
b=diag(surface_amp);                     %array with non-zero diagonal only
a=(b*a)';                                %each row is now surface_amp
phases=rand(many_surfaces,surf_amp_length)*2*pi;%random phases from 0 to 2pi

last=length(kappa);                      %should be the same as length(surface_amp).
mid=find(kappa==0);
last=last-mid;
for n=1:last
   phases(:,mid+n)=-phases(:,mid-n);     %such that imag parts of exp(i*phase) sum to zero
end

surface_amp_array=a.*exp(i*phases);      %multiply by exp(i*phases) per array element
```

In the "main_many_10_2.m" code, a loop starts over all the harmonic waves which produce the required Gaussian pulse.

The code below is "beam_params_08.m", and is the subroutine used to calculate the plane wave components which produce a beam at the frequency which is being looped over. A beam is produced using Chebyshev weights which has sidelobes at a user defined number of dB below the main beam (default 20dB).

```
function
[epsilons,gams_0,gams_1,gams_b,omega,thetas_0,n_theta_0,w_theta_0]=beam_params_08(theta_centre,..
freq,no_hyd,c_0,c_1,b_1,h,l,chebgain,nyq_factor);

%*****************************************************************************************
%DERIVED PARAMETERS AND SCALES
%*****************************************************************************************

n_theta_0=no_hyd;              %there will be one (approximately) plane wave from each hydrophone
omega=2*pi*freq;               %angular frequency in radians per second
k=omega/c_0;                   %wavenumber in 1/metres
lambda=c_0/freq;               %wavelength of sound (metres)
nyq_space=lambda/2;            %Nyquist maximum hydrophone spacing (metres)
spacing=nyq_space/nyq_factor;  %hydrophone spacing (metres)
min_n=-round((no_hyd-1)/2);    %minimum value of n (counter for hydrophones)
max_n=-min_n;                  %maximum value of n (counter for hydrophones)
nvals=min_n:max_n;             %n, the counter for the hydrophones
cheb_weights=chebwin(no_hyd,chebgain);   %gets weighting coefficients for gain of "chebgain"
cheb_weights=cheb_weights';    %transpose to give a 1xN (row) matrix

%*****************************************************************************************
%GEOMETRICAL CONSTRUCTS
%*****************************************************************************************

r_0=sqrt(h^2+l^2);  %distance from array centre hydrophone to the point on the seabed (metres)
%phase=-l*nvals*spacing*2*pi/(r_0*lambda);%phase delay for the nth hydrophone (radians) so ADD
this phase
phase=-(sqrt(l^2+h^2+(nvals*spacing).^2+2*l*nvals*spacing)-r_0)*2*pi/lambda; %exact phase delay
(no sqrt approximation)
phase_factor=exp(i.*phase);    %so the phase can be added by multiplying by the phase_factor
hyd_x=l+nvals*spacing; %x positions for the array hydrophones wrt point of impact at (0,0).
hyd_y=h;               %y position for all the array hydrophones wrt point of impact at (0,0).
thetas_0=-atan(hyd_x./hyd_y); %the incident angles from each of the hydrophones to the point of
impact
epsilons=k.*sin(thetas_0);     %the horizontal wavenumbers
k_0=omega/c_0;                 %sound wave wavenumber in the sea
```

```
k_1=omega/c_1;                  %sound wave wavenumber in seabed
k_b=omega/b_1;                  %transverse wave wavenumber in seabed
thetas_1=asin(epsilons./k_1);   %sound wave incident angles in seabed
thetas_b=asin(epsilons./k_b);   %transverse wave incident angles in seabed
gams_0=k_0.*cos(thetas_0);      %vertical wavenumbers in the sea
gams_1=k_1.*cos(thetas_1);      %vertical wavenumbers in the seabed
gams_b=k_b.*cos(thetas_b);      %transverse wave vertical wavenumbers in the seabed

%*****************************************************************************************
%CALCULATE THE WEIGHTS FOR THE PLANE WAVES FROM THE HYDROPHONES, INCLUDING THE PHASE ADJUSTMENTS
%*****************************************************************************************

w_theta_0=cheb_weights.*phase_factor;    %weighting coefficients for the various plane waves,
including phase
w_theta_0=w_theta_0/(sum(w_theta_0));    %normalise such that sum(w_theta_0) = 1.
%w_theta_0=w_theta_0/(sqrt(sum(abs(w_theta_0.^2))));%normalise such that sum(abs(w_theta_0.^2)) =
1.
%*****************************************************************************************
```

In the "main_many_10_2.m" code, a nested loop starts over all plane waves.

The code below is "refls3.m" and is the subroutine used to calculate the pressure reflection and transmission coefficients for the particular harmonic and plane wave in the double nested loop.

```
function [V,W,P]=refls3(omega,theta,rho_0,c_0,rho_1,c_1,b_1);

theta_0=theta;                          %theta_0 is the input angle of incident
m=rho_1/rho_0;                          %rho_0,1 are in kg/m^3; m is dimensionless
k_0=omega/c_0;                          %set up the seabed angles and functions
epsilon=k_0*sin(theta_0);
k_1=omega/c_1;                          %set up the variables for within the seabed
kap_1=omega/b_1;
theta_1=asin(epsilon/k_1);
gamma_1=asin(epsilon/kap_1);
cos2gamma1=cos(2*gamma_1);    %a few angular variables
sin2gamma1=sin(2*gamma_1);
cossq2gamma1=cos2gamma1.^2;
sinsq2gamma1=sin2gamma1.^2;

Z_0=rho_0*c_0./cos(theta_0);  %set up impedances, "units" of rho_c
Z_1=rho_1*c_1./cos(theta_1);
Z_t=rho_1*b_1./cos(gamma_1);
Z_input=Z_1.*cossq2gamma1 + Z_t.*sinsq2gamma1;

V=(Z_input-Z_0)./(Z_input+Z_0);         %reflection and transmission coefficients
W=2*Z_1.*cos2gamma1./((Z_input+Z_0));   %note that these are "pressure" coefficients
P=2*Z_t.*sin2gamma1./((Z_input+Z_0));   %note that these are all dimensionless
```

The code below is "p_calc_liq_09.m", and is the guts of the scattering code. This calculates (for the particular harmonic plane wave under consideration in the double nested loop) the scattered pressure using the liquid / liquid equations derived in chapter 4. The scattered pressure from a rigid surface (standard case) is also calculated. Through multiplying by the surface amplitude spectrum array (generated in "add_phases_03", see above) the scattered pressures for each surface realisation are generated. The equivalent code for the liquid / solid case is shown later.

```
function
[p_v,p_w,p_p,p_solid,c_angle_out]=p_calc_sol_09(c_1,liq_flag,rho_0,rho_1,omega,k_0,k_1,k_b,epsilo
n_0,kappa,...
   gam_0,gam_1,gam_b,mu_1,lambda_1,lambda_0,m,I,V,W,P,surface_amp_array,imag_real_frac);

weights=surface_amp_array;    %now multiply pressures by weights rather than sqrt(weights)
epsilon=epsilon_0;            %to keep consistent with earlier code
alpha=gam_0;                          %to keep consistent with earlier code
alpha_1=gam_1;                        %to keep consistent with earlier code
beta_1=gam_b;                         %to keep consistent with earlier code

%*****************************************************************************************
%CALCULATE THE VERTICAL WAVENUMBERS AND THE PROPAGATION ANGLES (MEASURED WRT THE NORMAL)
%*****************************************************************************************
```

```
gamma_v=sqrt(k_0^2-(epsilon+kappa).^2);  %vertical wavenumber of reflected scattered cpts
gamma_w=sqrt(k_1^2-(epsilon+kappa).^2);  %vertical wavenumber of transmitted scattered W cpts
gamma_p=sqrt(k_b^2-(epsilon+kappa).^2);  %vertical wavenumber of transmitted scattered P cpts

c_angle_out=atan((epsilon+kappa)./(gamma_v));      %outgoing incident angles for reflected
angle_in_w=atan((epsilon+kappa)./(gamma_w));       %ingoing incident angles for transmitted W
angle_in_p=atan((epsilon+kappa)./(gamma_p));       %ingoing incident angles for transmitted P

%*****************************************************************************************
%CALCULATE A BUNCH OF COEFFICIENTS TO SIMPLIFY NOTATION
%*****************************************************************************************

C_1=(I+V)*(kappa*epsilon-alpha^2)-W*(kappa*epsilon-alpha_1^2)+P*beta_1*(kappa+epsilon);

C_2=-i*lambda_0*alpha*k_0^2*(I-V)+i*lambda_1*alpha_1*k_1^2*W+2*i*mu_1*alpha_1*epsilon*W*(epsilon-
2.*kappa);
C_2=C_2+2*i*mu_1*P*(beta_1^2*epsilon+(beta_1^2-epsilon^2).*kappa);

C_3=2*(i*kappa*(epsilon^2-alpha_1^2)-i*alpha_1^2*epsilon)*W-i*beta_1*(epsilon^2-
beta_1^2+4*kappa*epsilon)*P;

C_4=2*gamma_w.*(kappa+epsilon);

C_5=(kappa+epsilon).^2-gamma_p.^2;

C_6=lambda_1*k_1^2+2*mu_1*(kappa+epsilon).^2;

C_7=2*mu_1*gamma_p.*(kappa+epsilon);

C_8=i*gamma_w-i*(C_4./C_5).*(kappa+epsilon);

C_9=C_1-i*(C_3./C_5).*(kappa+epsilon);

C_10=lambda_0*k_0^2./(C_6-C_7.*C_4./C_5);

C_11=(C_2+C_7.*C_3./C_5)./(C_6-C_7.*C_4./C_5);

%*****************************************************************************************
%CALCULATE A_v WITH AS MANY DENOMINATOR-FREE COEFFICIENTS AS POSSIBLE
%*****************************************************************************************

N_1=C_5.*C_6-C_7.*C_4;                          %numerator coefficient
N_2=C_5.*C_1-i*C_3.*(kappa+epsilon);     %numerator coefficient
N_3=i*gamma_w.*C_5-i*C_4.*(kappa+epsilon);      %numerator coefficient
N_4=C_2.*C_5+C_7.*C_3;                          %numerator coefficient
D_1=N_1;                                        %denominator coefficient
D_2=i*gamma_v.*C_5;                      %denominator coefficient
D_3=N_3;                                        %denominator coefficient
D_4=lambda_0*(k_0^2).*C_5;               %denominator coefficient

A_v=(N_1.*N_2+N_3.*N_4)./(D_1.*D_2+D_3.*D_4);      %without weights

%*****************************************************************************************
%CALCULATE THE SCATTERED VELOCITY POTENTIALS' SPECTRAL AMPLITUDES
%*****************************************************************************************

A_w=C_10.*A_v-C_11;                        %without weights
A_p=(C_3-C_4.*A_w)./C_5;                   %without weights

%*****************************************************************************************
%CALCULATE THE SCATTERED PRESSURES' SPECTRAL AMPLITUDES
%*****************************************************************************************

p_v=A_v;                                        %reflected scattering pressure integrand at
(0,0)
b=diag(p_v);                                    %use to multiply the rows of the
surface_amp_array
p_v=(weights*b);                         %weighted reflected scattered pressure integrand at (0,0)
non_ind_v=find(gamma_v~=real(gamma_v));  %imaginary gamma_v will be attenuated, so set p=0
p_v(:,non_ind_v)=0;                      %these p will be rapidly attenuated so set to zero

p_w=A_w*m;                               %transmitted scattered pressure integrand at (0,0)
b=diag(p_w);                                    %use to multiply the rows of the
surface_amp_array
p_w=(weights*b);                         %weighted reflected scattered pressure integrand at (0,0)
non_ind_w=find(imag(gamma_w)>imag_real_frac*real(gamma_w));  %large imaginary gamma_w will be
rapidly attenuated
p_w(:,non_ind_w)=0; %these p will be rapidly attenuated so set to zero

p_p=A_p*m;          %transmitted scattered transverse wave pressure integrand at (0,0)
b=diag(p_p);                %use to multiply the rows of the surface_amp_array
p_p=(weights*b);            %weighted reflected scattered pressure integrand at (0,0)
non_ind_p=find(imag(gamma_p)>imag_real_frac*real(gamma_p));  %large imaginary gamma_p will be
rapidly attenuated
p_p(:,non_ind_p)=0; %these p will be rapidly attenuated so set to zero

p_solid=-2*i*(gam_0^2-kappa*epsilon_0)./gamma_v;%rigid surface scattering integrand at (0,0)
```

```
b=diag(p_solid);              %use to multiply the rows of the surface_amp_array
p_solid=(weights*b);%weighted rigid surface (reflected) scattered pressure
```

The code below is "angle_sort_05.m", and is the subroutine used to sort the scattered pressure output into "angle" bins, since they are calculated in "kappa" bins, which equate to different angles depending upon the particular plane wave under consideration (still in the double nested loop over harmonic and plane waves).

```
function
[p_sorted,p_solid_sorted]=angle_sort_05(p_alpha,p_solid,c_angle_out,all_angles,angle_factor);
 %BIN BY OUTGOING ANGLE

size_p_alpha=size(p_alpha);              %gets the (no._rows,no._columns) for p_alpha
p_sorted=zeros(size_p_alpha(1),length(all_angles));%initialise p_sorted over all angles to zero
p_solid_sorted=zeros(size_p_alpha(1),length(all_angles));    %initialise p_solid_sorted over all
angles to zero
conv=pi/180;                             %factor converts degrees to radians
angle_out=real(c_angle_out)./conv;       %convert angle_out to degrees
angle_array=angle_factor*angle_out; %make array with "angle_factor" times the range of degrees
array_elements=round(angle_array);  %make an array of array elements for the p_alpha
array_elements=array_elements+(90*angle_factor)+1; %shift elements so that they start at 1

for loop=1:size_p_alpha(2)     %do for each column in p_alpha and p_solid
   if (0<array_elements(loop))&(array_elements(loop)<=2*angle_factor*90+1)
      p_sorted(:,array_elements(loop))=p_sorted(:,array_elements(loop))+p_alpha(:,loop);

p_solid_sorted(:,array_elements(loop))=p_solid_sorted(:,array_elements(loop))+p_solid(:,loop);
   end
end
```

The code below is "smooth_03.m" and is the subroutine used to perform a linear interpolation over any angle bins with zeros in.

```
function [smoothed]=smooth_03(input_array);              %this smooths out each row

[rows,columns]=size(input_array);                        %get the size of the array
smoothed=zeros(rows,columns);                            %initialise the smoothed output

last_non_zero=1;                                         %last non-zero element
next_non_zero=1;                                         %next non-zero element
check_row=input_array(1,:);                              %use first row to check for zeros
non_zeros=find(check_row~=0);                            %non-zero columns

%*************************************************************************************************
%make sure that the start and end columns are non-zero
%*************************************************************************************************
if check_row(1)==0
   smoothed(:,1)=input_array(:,non_zeros(1));            %set to equal first non-zero element
   input_array(:,1)=input_array(:,non_zeros(1));         %so it will be picked up in the non-zeros
else
   smoothed(:,1)=input_array(:,1);
end
if check_row(columns)==0
   smoothed(:,columns)=input_array(:,non_zeros(length(non_zeros))); %set to last non-zero element
   input_array(:,columns)=input_array(:,non_zeros(length(non_zeros))); %to get into the non-zeros
else
   smoothed(:,columns)=input_array(:,columns);
end
%*************************************************************************************************

check_row=input_array(1,:);                              %use revised first row to check for zeros
non_zeros=find(check_row~=0);                            %re-do the non-zero columns

for j=2:columns-1
   if check_row(j)~=0
      smoothed(:,j)=input_array(:,j);
      last_non_zero=j;
   else
      next_non_zero=non_zeros(min(find(non_zeros>j)));  %find the next non-zero element
      diff=next_non_zero-last_non_zero;
      frac=(j-last_non_zero)/diff;

      r_two=abs(input_array(:,next_non_zero));
      r_one=abs(input_array(:,last_non_zero));
      r_int=frac*r_two+(1-frac)*r_one;
```

```
      theta_two=atan2(imag(input_array(:,next_non_zero)),real(input_array(:,next_non_zero)));
      theta_one=atan2(imag(input_array(:,last_non_zero)),real(input_array(:,last_non_zero)));
      theta_int=frac*theta_two+(1-frac)*theta_one;

      smoothed(:,j)=r_int.*exp(i*theta_int);
   end
end
```

The code below is "box_03.m" and is the subroutine used to smooth the scattering strength so that the accuracy of the presented results is consistent with the beamwidth of the receiver (assumed for convenience to be the same beamwidth as the incident beam, though in principle any beamwidth could be used).

```
function [box_mean]=box_03(input_array,box_size)

half_box_size=ceil(box_size/2);
[rows,columns]=size(input_array);

for j=1:half_box_size
   amplitudes=abs(input_array(:,1:(2*j-1)));
   phases=atan2(imag(input_array(:,1:(2*j-1))),real(input_array(:,1:(2*j-1))));
   mean_amplitudes=mean(amplitudes,2);
   mean_phases=mean(phases,2);
   box_mean(:,j)=mean_amplitudes.*exp(i*mean_phases);
end
for j=(columns-half_box_size+1):columns
   amplitudes=abs(input_array(:,(columns-2*(columns-j)):columns));
   phases=atan2(imag(input_array(:,(columns-2*(columns-j)):columns)),real(input_array(:,(columns-
2*(columns-j)):columns)));
   mean_amplitudes=mean(amplitudes,2);
   mean_phases=mean(phases,2);
   box_mean(:,j)=mean_amplitudes.*exp(i*mean_phases);
end
for j=(half_box_size+1):(columns-half_box_size)
   amplitudes=abs(input_array(:,(j-half_box_size+1):(j+half_box_size-1)));
   phases=atan2(imag(input_array(:,(j-half_box_size+1):(j+half_box_size-
1))),real(input_array(:,(j-half_box_size+1):(j+half_box_size-1))));
   mean_amplitudes=mean(amplitudes,2);
   mean_phases=mean(phases,2);
   box_mean(:,j)=mean_amplitudes.*exp(i*mean_phases);
end
```

In the "main_many_10_2.m" code the nested loop over plane waves ends now.
In the "main_many_10_2.m" code the loop over harmonic waves ends now.

The code below is "LS_plots_20.m" and is the subroutine used to smooth the scattered data, to calculate the scattering strength, to calculate the statistics of the backscatter and forward scatter, and to plot the results. In performing these functions a number of subroutines are called, these are also listed below.

```
function
[scatter_strength_last,rigid_scatter_last,mean_scatter_strength,mean_rigid_scatter_strength,...
prob_back_gaussian,prob_forw_gaussian]=LS_plots_20(p_array,p_rigid,p_beta,conv,all_angles,k_0,k_1
,many_surfaces,cos_sq_all_angles,theta_centre,angle_factor,hist_width,hist_bin,beamwidth,no_hyd);
%PLOTS AND CHECKS

%*************************************************************************************************
%CALCULATE SCATTERING STRENGTHS FOR ALL SURFACE REALISATIONS AND ANGLES
%*************************************************************************************************
bin_factor=50;                          %bin width = dist mean / bin_factor
all_angles=all_angles*conv;             %convert outgoing angles to radians
box=round(beamwidth*angle_factor);      %for the box meaning over angle
beamwidth=beamwidth*conv;               %to convert to radians
angle_factor=angle_factor/conv;         %convert 1/angle_factor to radians
plot_angle=all_angles/conv+90;          %so 0° is backscatter and 180° is forwardscatter

norm_factor=no_hyd^2;                   %since beamwidth ~ 1 / number of hydrophones
norm_factor=1;

ms_alpha=(k_0).*(abs(p_array.^2))*diag(cos_sq_all_angles);   %ms for all surface realisations,
elastic scatter
```

```
ms_solid=(k_0).*(abs(p_rigid.^2))*diag(cos_sq_all_angles);   %ms for all surface realisations,
rigid scatter

ms_alpha=ms_alpha*norm_factor;
ms_solid=ms_solid*norm_factor;

%*****************************************************************************************************
%NOW FOR THE STATISTICS OF THE LINEAR DATA
%*****************************************************************************************************

%*****************************************************************************************************
%CALCULATE FORWARD-SCATTERING STRENGTHS FOR ALL SURFACE REALISATIONS
%*****************************************************************************************************

fo_scat_ind=find((all_angles<=((theta_centre+beamwidth/2)))&(all_angles>=((theta_centre-
beamwidth/2))));
ms_alpha_forw=ms_alpha(:,fo_scat_ind);   %forward scatter
ms_alpha_forw=mean(ms_alpha_forw,2);     %take mean over columns (since fo_scat_ind is potentially
> one column)
mean_forw=mean(ms_alpha_forw)            %find mean to centre histogram
hist_bin=mean_forw/bin_factor;           %histogram bin width
std_forw=std(ms_alpha_forw)              %find st. deviation to use in width of histogram
h_range_forw=(0:hist_bin:(mean_forw+hist_width*std_forw));% 0 to + hist_width sigma
m=hist(ms_alpha_forw,h_range_forw);      %CALCULATE HISTOGRAM VALUES
[gaussian_forw]=gaussian_03(mean_forw,std_forw,many_surfaces,h_range_forw); %CALC. GAUSSIAN FIT
[rayleigh_forw]=rayleigh_06(m,h_range_forw,mean_forw,many_surfaces); %CALC. RAYLEIGH FIT

%*****************************************************************************************************
%CALCULATE BACK-SCATTERING STRENGTHS FOR ALL SURFACE REALISATIONS
%*****************************************************************************************************

bk_scat_ind=find((all_angles>=(-(theta_centre+beamwidth/2)))&(all_angles<=(-(theta_centre-
beamwidth/2))));
ms_alpha_back=ms_alpha(:,bk_scat_ind);   %backscatter
ms_alpha_back=mean(ms_alpha_back,2);     %take mean over columns (since bk_scat_ind is potentially
> one column)
mean_back=mean(ms_alpha_back);           %find mean to centre histogram
hist_bin=mean_back/bin_factor;           %histogram bin width
std_back=std(ms_alpha_back);             %find st. deviation to use in width of histogram
h_range_back=(0:hist_bin:(mean_back+hist_width*std_back));% 0 to + hist_width sigma
n=hist(ms_alpha_back,h_range_back);
[gaussian_back]=gaussian_03(mean_back,std_back,many_surfaces,h_range_back); %CALC. GAUSSIAN FIT
[rayleigh_back]=rayleigh_06(n,h_range_back,mean_back,many_surfaces); %CALC. RAYLEIGH FIT

%*****************************************************************************************************
%Now log the data to put into dB.
%*****************************************************************************************************

alpha_scatter_strength=10*log10(ms_alpha);         %scattering strength for elastic boundary
rigid_scatter_strength=10*log10(ms_solid);         %scattering strength for rigid boundary

alpha_scatter_strength_mean=mean(alpha_scatter_strength,1);  %mean scattering strength from
elastic boundary
rigid_scatter_strength_mean=mean(rigid_scatter_strength,1);  %mean scattering strength from rigid
boundary
smooth_alpha_scatter_strength_mean=box_02(alpha_scatter_strength_mean,box);
smooth_rigid_scatter_strength_mean=box_02(rigid_scatter_strength_mean,box);

smooth_alpha_scatter_strength=box_03(alpha_scatter_strength,box);%scattering strength for elastic
boundary
smooth_rigid_scatter_strength=box_03(rigid_scatter_strength,box);%scattering strength for rigid
boundary

smooth_alpha_scatter_strength_last=smooth_alpha_scatter_strength(many_surfaces,:);
smooth_rigid_scatter_strength_last=smooth_rigid_scatter_strength(many_surfaces,:);

%*****************************************************************************************************
save latest_scatters smooth_alpha_scatter_strength smooth_rigid_scatter_strength
%*****************************************************************************************************
%PLOTS
%*****************************************************************************************************

figure(3)
plot(h_range_forw,m,'r-')
hold on
title('Histogram of the forward scattering coefficient')
xlabel('forward scattering coefficient')
plot(h_range_forw,gaussian_forw,'k-')
plot(h_range_forw,rayleigh_forw,'k:')

figure(4)
plot(h_range_back,n,'b-')
hold on
title('Histogram of the backward scattering coefficient')
xlabel('backward scattering coefficient')
plot(h_range_back,gaussian_back,'k-')
plot(h_range_back,rayleigh_back,'k:')
```

```
figure(7)
hold on
plot(plot_angle,smooth_alpha_scatter_strength_mean,'b-')
axis([0 180 -100 0]);
hold on
plot(plot_angle,smooth_rigid_scatter_strength_mean,'r-')
plot(plot_angle,smooth_alpha_scatter_strength_last,'c:')
plot(plot_angle,smooth_rigid_scatter_strength_last,'k:')
axis([0 180 -40 20])
title('Scattering strength versus scattering angle')
xlabel('Scattering angle in degrees')
ylabel('Scattering strength (dB)')
```

The code below is "gaussian_03.m" and is the subroutine used to produce a Gaussian distribution function with required mean and standard deviation. This is called from the "LS_plots_20.m" subroutine.

```
function [gaussian]=gaussian_03(req_mean,req_sigma,realisations,h_range)

mu=req_mean;          %the mean of the real data distribution
sigma=req_sigma;      %the sigma of the real data distribution
z=h_range;            %same range as for the original histogram
hist_bin=abs(h_range(2)-h_range(1)); %for normalisation later
f=(1/sqrt(2*pi*sigma^2))*exp(-((z-mu).^2)/(2*sigma^2));%a gaussian distribution
gaussian=f*realisations*hist_bin;       %normalise to the number of surface realisations
```

The code below is "rayleigh_06.m" and is the subroutine used to produce a Rayleigh distribution function with required mean. The zero for the Rayleigh function is assumed to be the lowest unpopulated dB bin above the mean. This is called from the "LS_plots_20.m" subroutine.

```
function [rayleigh]=rayleigh_06(N_z,array_z,mean_z,many_surfaces);

size_factor=0.9;                        %generally gives a better fit

max_z_ind=find(N_z==max(N_z));
max_z_ind=round(mean(max_z_ind));       %for if there is more than one max peak
z_max=array_z(max_z_ind);
max_N=N_z(max_z_ind);
sigma=z_max;
factor=max_N/((1/sigma)*exp(-0.5));     %to scale the rayleigh to the data
factor=factor*size_factor;              %size_factor ensures a better fit to the data
rayleigh=factor*(array_z/(sigma^2)).*exp(-(array_z.^2)/(2*(sigma^2))); %Rayleigh PDF

figure(10)
plot(array_z,rayleigh,'r-')
hold on
plot(array_z,N_z)
```

The code below is "analysis_01.m" and is the routine used to analyse just the forward and backscattered pressures.

```
function
[m,gaussian_forw,rayleigh_forw,n,gaussian_back,rayleigh_back]=analysis_01(p_back,p_forw,conv,k_0,
k_1,many_surfaces,theta_scat,angle_factor,hist_width,hist_bin,beamwidth,no_hyd); %PLOTS AND
CHECKS

%*************************************************************************************************
%CALCULATE SCATTERING STRENGTHS FOR FORWARD AND BACKWARD SCATTER
%*************************************************************************************************
bin_factor=50;      %bin width = dist mean / bin_factor

bin_factor=25;

ms_forw=(k_0).*(abs(p_forw.^2))*(cos(theta_scat)^2);        %ms for all surface realisations,
elastic scatter
ms_back=(k_0).*(abs(p_back.^2))*(cos(theta_scat)^2);        %ms for all surface realisations,
elastic scatter

%*************************************************************************************************
%CALCULATE FORWARD-SCATTERING STRENGTHS FOR ALL SURFACE REALISATIONS
%*************************************************************************************************

ms_forw=mean(ms_forw,2);                %take mean over columns
```

```
mean_forw=mean(ms_forw);                %find mean to centre histogram
hist_bin=mean_forw/bin_factor;          %histogram bin width
std_forw=std(ms_forw);                  %find st. deviation to use in width of histogram
h_range_forw=(0:hist_bin:(mean_forw+hist_width*std_forw));   % 0 to + hist_width sigma
m=hist(ms_forw,h_range_forw);                                %CALCULATE HISTOGRAM VALUES
[gaussian_forw]=gaussian_03(mean_forw,std_forw,many_surfaces,h_range_forw); %CALC. GAUSSIAN FIT
[m_kept,rayleigh_forw,z_forw]=rayleigh_06_set1_forw(m,h_range_forw,many_surfaces); %CALC.
RAYLEIGH FIT

[elements,num,chi_sq_forw_R]=chi_sq_03(m_kept,rayleigh_forw)
prob_forw_rayleigh=1-gammainc(chi_sq_forw_R,num)

m_kept=m_kept(elements);
rayleigh_forw=rayleigh_forw(elements);
z_forw=z_forw(elements);
gaussian_forw=gaussian_forw(elements);

[elements,num,chi_sq_forw_G]=chi_sq_03(m_kept,gaussian_forw)
prob_forw_gaussian=1-gammainc(chi_sq_forw_G,num)

figure(1)
plot(z_forw,m_kept,'m.')
hold on
plot(z_forw,rayleigh_forw,'k-')
plot(z_forw,gaussian_forw,'k-')
title('Histogram of the forward scattering coefficient')
xlabel('forward scattering coefficient')

%*****************************************************************************************
%CALCULATE BACK-SCATTERING STRENGTHS FOR ALL SURFACE REALISATIONS
%*****************************************************************************************

ms_back=mean(ms_back,2);                %take mean over columns
mean_back=mean(ms_back);                %find mean to centre histogram
hist_bin=mean_back/bin_factor;          %histogram bin width
std_back=std(ms_back);                  %find st. deviation to use in width of histogram
h_range_back=(0:hist_bin:(mean_back+hist_width*std_back));   % 0 to + hist_width sigma
n=hist(ms_back,h_range_back);
[n_kept,rayleigh_back,z_back]=rayleigh_06_set1_back(n,h_range_back,many_surfaces); %CALC.
RAYLEIGH FIT
[gaussian_back]=gaussian_03(mean_back,std_back,many_surfaces,z_back); %CALC. GAUSSIAN FIT

[elements,num,chi_sq_back_R]=chi_sq_03(n_kept,rayleigh_back);
prob_back_rayleigh=1-gammainc(chi_sq_back_R,num);

n_kept=n_kept(elements);
rayleigh_back=rayleigh_back(elements);
z_back=z_back(elements);
gaussian_back=gaussian_back(elements);

[elements,num,chi_sq_back_G]=chi_sq_03(n_kept,gaussian_back);
prob_back_gaussian=1-gammainc(chi_sq_back_G,num);

figure(2)
plot(z_back,n_kept,'m.')
hold on
plot(z_back,rayleigh_back,'k-')
plot(z_back,gaussian_back,'k-')
title('Histogram of the backward scattering coefficient')
xlabel('backward scattering coefficient')


figure(3)
plot(z_back,n_kept,'m.')
hold on
plot(z_back,rayleigh_back,'r-')
plot(z_back,gaussian_back,'r:')
plot(z_forw,m_kept,'b.')
plot(z_forw,rayleigh_forw,'g-')
plot(z_forw,gaussian_forw,'g:')
```

The code below is "chi_sq_03.m" and is the subroutine used to calculate the chi square value for the fit between a "measured" distribution – the scattering data - and a known distribution – the Rayleigh or Gaussian distribution.

```
function[elements,num_elements,chi_sq]=chi_sq_03(event_dist,known_dist);

lowest=1;
elements=(find(known_dist>=lowest));
num_elements=length(elements);
known_dist=known_dist(elements);
event_dist=event_dist(elements);
```

```
to_be_summed=((event_dist-known_dist).^2)./known_dist;
chi_sq=sum(to_be_summed);
```

7.3 Scattered pressures for a liquid / solid interface

For the liquid / solid case the main code is of precisely the same structure as that shown above for the liquid / liquid case. The only differences are:

- the default values for the geoacoustic parameters;
- the reflection code is "refls6.m" and calculates reflection velocity potentials;
- the subroutine equivalent to "p_calc_liq_09.m" is, obviously, different. This is the subroutine "p_calc_sol_09.m" and is based on the scattering equations derived in chapter 5. The scattered velocity potentials calculated using these equations are converted into pressures, so that the output of the subroutine is scattered pressure. This subroutine is listed below.

```
function[p_v,p_w,p_p,p_solid,c_angle_out]=p_calc_sol_09(c_1,liq_flag,rho_0,rho_1,omega,k_0,k_1,k_
b,epsilon_0,kappa,gam_0,gam_1,gam_b,mu_1,lambda_1,lambda_0,m,I,V,W,P,surface_amp_array,imag_real_
frac);%GETS SCATTERING COEFFS

weights=surface_amp_array;     %now multiply pressures by weights rather than sqrt(weights)
epsilon=epsilon_0;             %to keep consistent with earlier code
alpha=gam_0;                            %to keep consistent with earlier code
alpha_1=gam_1;                          %to keep consistent with earlier code
beta_1=gam_b;                           %to keep consistent with earlier code

%*****************************************************************************************
CALCULATE THE VERTICAL WAVENUMBERS AND THE PROPAGATION ANGLES (MEASURED WITH RESPECT TO THE
NORMAL)
%*****************************************************************************************

gamma_v=sqrt(k_0^2-(epsilon+kappa).^2);  %vertical wavenumber of reflected scattered cpts
gamma_w=sqrt(k_1^2-(epsilon+kappa).^2);  %vertical wavenumber of transmitted scattered W cpts
gamma_p=sqrt(k_b^2-(epsilon+kappa).^2);  %vertical wavenumber of transmitted scattered P cpts

c_angle_out=atan((epsilon+kappa)./(gamma_v));      %outgoing incident angles
angle_in_w=atan((epsilon+kappa)./(gamma_w));       %ingoing incident angles
angle_in_p=atan((epsilon+kappa)./(gamma_p));       %ingoing incident angles

%*****************************************************************************************
%CALCULATE A BUNCH OF COEFFICIENTS TO SIMPLIFY NOTATION
%*****************************************************************************************

C_1=(I+V)*(kappa*epsilon-alpha^2)-W*(kappa*epsilon-alpha_1^2)+P*beta_1*(kappa+epsilon);

C_2=-i*lambda_0*alpha*k_0^2*(I-V)+i*lambda_1*alpha_1*k_1^2*W+2*i*mu_1*alpha_1*epsilon*W*(epsilon-
2.*kappa);
C_2=C_2+2*i*mu_1*P*(beta_1^2*epsilon+(beta_1^2-epsilon^2).*kappa);

C_3=2*(i*kappa*(epsilon^2-alpha_1^2)-i*alpha_1^2*epsilon)*W-i*beta_1*(epsilon^2-
beta_1^2+4*kappa*epsilon)*P;

C_4=2*gamma_w.*(kappa+epsilon);

C_5=(kappa+epsilon).^2-gamma_p.^2;

C_6=lambda_1*k_1^2+2*mu_1*(kappa+epsilon).^2;

C_7=2*mu_1*gamma_p.*(kappa+epsilon);

C_8=i*gamma_w-i*(C_4./C_5).*(kappa+epsilon);

C_9=C_1-i*(C_3./C_5).*(kappa+epsilon);

C_10=lambda_0*k_0^2./(C_6-C_7.*C_4./C_5);

C_11=(C_2+C_7.*C_3./C_5)./(C_6-C_7.*C_4./C_5);

%*****************************************************************************************
%CALCULATE A_v WITH AS MANY DENOMINATOR-FREE COEFFICIENTS AS POSSIBLE
%*****************************************************************************************

N_1=C_5.*C_6-C_7.*C_4;                          %numerator coefficient
N_2=C_5.*C_1-i*C_3.*(kappa+epsilon);     %numerator coefficient
```

```
N_3=i*gamma_w.*C_5-i*C_4.*(kappa+epsilon);          %numerator coefficient
N_4=C_2.*C_5+C_7.*C_3;                              %numerator coefficient
D_1=N_1;                                            %denominator coefficient
D_2=i*gamma_v.*C_5;                          %denominator coefficient
D_3=N_3;                                            %denominator coefficient
D_4=lambda_0*(k_0^2).*C_5;                   %denominator coefficient

A_v=(N_1.*N_2+N_3.*N_4)./(D_1.*D_2+D_3.*D_4);       %without weights

%*****************************************************************************************************
%CALCULATE THE SCATTERED VELOCITY POTENTIALS' SPECTRAL AMPLITUDES
%*****************************************************************************************************

A_w=C_10.*A_v-C_11;                           %without weights
A_p=(C_3-C_4.*A_w)./C_5;                      %without weights

%*****************************************************************************************************
%CALCULATE THE SCATTERED PRESSURES' SPECTRAL AMPLITUDES
%*****************************************************************************************************

p_v=A_v;                                      %reflected scattering pressure integrand at (0,0)
b=diag(p_v);                                  %use to multiply the rows of the surface_amp_array
p_v=(weights*b);                              %weighted reflected scattered pressure integrand at (0,0)
non_ind_v=find(gamma_v~=real(gamma_v));  %imaginary gamma_v will be attenuated, so set p=0
p_v(:,non_ind_v)=0;                           %these p will be rapidly attenuated so set to zero

p_w=A_w*m;                           %transmitted scattered sound wave pressure integrand at (0,0)
b=diag(p_w);                                  %use to multiply the rows of the surface_amp_array
p_w=(weights*b);                              %weighted reflected scattered pressure integrand at (0,0)
non_ind_w=find(imag(gamma_w)>imag_real_frac*real(gamma_w));  %large imaginary gamma_w will be
rapidly attenuated
p_w(:,non_ind_w)=0;                  %these p will be rapidly attenuated so set to zero

p_p=A_p*m;                %transmitted scattered transverse wave pressure integrand at (0,0)
b=diag(p_p);                         %use to multiply the rows of the surface_amp_array
p_p=(weights*b);                     %weighted reflected scattered pressure integrand at (0,0)
non_ind_p=find(imag(gamma_p)>imag_real_frac*real(gamma_p));  %large imaginary gamma_p will be
rapidly attenuated
p_p(:,non_ind_p)=0; %these p will be rapidly attenuated so set to zero

p_solid=-2*i*(gam_0^2-kappa*epsilon_0)./gamma_v;%rigid surface scattering integrand at (0,0)
b=diag(p_solid);                     %use to multiply the rows of the surface_amp_array
p_solid=(weights*b);%weighted rigid surface (reflected) scattered pressure
```

7.4 Beamforming

Below is the listing for the code used to check the validity of the beam calculation.

```
%*****************************************************************************************************
%SET UP PARAMETERS
%*****************************************************************************************************

conv=pi/180;          %essential in any code!!
no_hyd=107;           %number of hydrophones
freq=1000;%frequency in Hz
c=1500;               %sound speed in m/s
h=100;                %height of array from the seabed (metres)
l=-50;                %horizontal displacement of array (metres)
points=1001;          %number of points in the line perpendicular to the centre hydrophone
direction
length=150;           %full length of the line perp to centre hydrophone direction
chebgain=20;          %dB gain through using a Chebyshev weighting function on hydrophone
amplitudes

%*****************************************************************************************************
%DERIVED PARAMETERS AND SCALES
%*****************************************************************************************************

omega=2*pi*freq;                              %angular frequency in radians per second
k=omega/c;                           %wavenumber in 1/metres
theta_0=atan(abs(l)/h);                       %the incident angle (radians)
lambda=c/freq;                                %wavelength of sound (metres)
nyq_space=lambda/2;                  %Nyquist maximum hydrophone spacing (metres)
spacing=nyq_space/2;                 %hydrophone spacing (metres)
min_n=-round((no_hyd-1)/2);          %minimum value of n (counter for hydrophones)
max_n=-min_n;                                 %maximum value of n (counter for hydrophones)
nvals=min_n:max_n;                   %n, the counter for the hydrophones
middle_hyd=(no_hyd+1)/2;                      %middle hydrophone number
middle_length=(points+1)/2;          %number of the middle position on the line
```

```
cheb_weights=chebwin(no_hyd,chebgain);  %gets weighting coefficients for gain of "chebgain"
cheb_weights=cheb_weights/(sum(cheb_weights));%normalises the amplitudes to sum to one.

%*************************************************************************************************
%GEOMETRICAL CONSTRUCTS
%*************************************************************************************************

r_0=sqrt(h^2+l^2);%distance from array centre hydrophone to the point on the seabed (metres)
%phase=-l*nvals*spacing*2*pi/(r_0*lambda);        %phase delay for the nth hydrophone (radians)
so ADD
phase=-(sqrt(l^2+h^2+(nvals*spacing).^2+2*l*nvals*spacing)-r_0)*2*pi/lambda; %exact phase delay
hyd_x=l+nvals*spacing;                  %x positions for the array hydrophones (metres)
hyd_y=h;                                %y position for all the array hydrophones (metres)
length_steps=length/(points-1);         %length between the points on the line (metres)
lengths=-(points-1)/2:(points-1)/2;%points now either side of zero
lengths=lengths*length_steps;  %now have all the lengths to the points on the line (metres)
xlengths=lengths*cos(theta_0); %x values of the positions on the line (metres)
ylengths=lengths*sin(theta_0); %y values of the positions on the line (metres)
beam=zeros(1,points);                   %initial amplitude of the beam
wbeam=zeros(1,points);                  %initial amplitude of the weighted beam
db3=ones(1,points);           %will use this to draw horizontal line at 3dB below max
wdb3=ones(1,points);          %will use this to draw horizontal line at 3dB below max

%*************************************************************************************************
%CALCULATE THE AMPLITUDES FOR ALL HYDROPHONES FOR ALL POINTS ON THE LINE
%*************************************************************************************************

for n=1:no_hyd      %loop over each position on the line perp to centre hydrophone direction
   ranges=sqrt((hyd_x(n)-xlengths).^2+(hyd_y-ylengths).^2);  %ranges of n'th hydrophone (metres)
   beamvals=exp(i*(k*ranges+phase(n)));  %for the unweighted case
   beam=beam+beamvals;
end
beam=beam/no_hyd;   %normalise the sum by the number of hydrophones

for n=1:no_hyd      %loop over each position on the line perp to centre hydrophone direction
   ranges=sqrt((hyd_x(n)-xlengths).^2+(hyd_y-ylengths).^2);  %ranges of n'th hydrophone (metres)
   wbeamvals=cheb_weights(n)*exp(i*(k*ranges+phase(n)));     %for the weighted case
   wbeam=wbeam+wbeamvals;
end

%*************************************************************************************************
%DISPLAYS
%*************************************************************************************************

log_beam_intensity=10*log10(beam.*conj(beam));
db3=(max(log_beam_intensity)-3)*db3;

wlog_beam_intensity=10*log10(wbeam.*conj(wbeam));
wdb3=(max(wlog_beam_intensity)-3)*wdb3;

figure(1)
plot(lengths,log_beam_intensity,'r-')
hold on
plot(lengths,wlog_beam_intensity,'b-')
plot(lengths,db3,'g-')
plot(lengths,wdb3,'c-')
title('Beam log intensities versus width')
xlabel('Width from beam centre (metres)')
ylabel('Log intensity (dimensionless)')

figure(2)
plot(xlengths,ylengths,'b*')
hold on
plot(hyd_x,hyd_y,'r*')
plot([hyd_x(middle_hyd) xlengths(middle_length)],[hyd_y ylengths(middle_length)],'g-')
title('Geometry of array and beam')
xlabel('x distance (metres)')
ylabel('y distance (metres)')

figure(3)
plot(lengths,(beam.*conj(beam)),'r-')
hold on
plot(lengths,(wbeam.*conj(wbeam)),'b-')
title('Beam intensities versus width')
xlabel('Width from beam centre (metres)')
ylabel('Intensity (dimensionless)')
```

7.5 Generating a pulse

Below is the listing for the code used to check the validity of the pulse calculation.

```
%*************************************************************************************
```

```
%SET UP PARAMETERS
%*****************************************************************************

mu=30;                                  %centre frequency of the pulse (Hz)
sigma=1;                                %width of the pulse (Hz)
t=-1:0.001:1;                           %array of times

%*****************************************************************************
%DERIVED PARAMETERS AND SCALES
%*****************************************************************************

fmin=mu-4*sigma;                        %minimum frequency in the sum over frequencies
fmax=mu+4*sigma;                        %maximum frequency in the sum over frequencies
delta_f=0.01;                           %difference in frequencies summed over
freqs=fmin:delta_f:fmax;                %array of frequencies to be summed over
omegas=2*pi*freqs;            %array of angular frequencies
phase=omegas'*t;                        %array of phases for all frequencies and all times

%*****************************************************************************
%WEIGHTS AND SIGNALS
%*****************************************************************************

gauss=(1/sqrt(2*pi*sigma^2)).*exp((-(freqs-mu).^2)/(2*sigma^2));       %frequency weights
sum_gauss=sum(gauss);                   %to normalise with later
gauss=gauss'*ones(1,length(t));         %Gaussian weights for the frequency amplitudes
unweighted=cos(phase);                  %unweighted amplitudes for each frequency
sig=gauss.*cos(phase);                  %weighted amplitudes for each frequency
clear gauss phase                       %to clear the memory
sig=sum(sig,1);                         %sum over frequencies to get the full pulse
sig=sig/(sum_gauss);          %normalise by sum of weights
unweighted=sum(unweighted,1); %sum over frequencies to get the unweighted pulse
unweighted=unweighted/(length(freqs));  %normalise by number of components

%*****************************************************************************
%DISPLAYS
%*****************************************************************************

figure(1)
plot(t,sig,'r-')
hold on
plot(t,unweighted,'b-')
title('Pulse amplitude versus time')
xlabel('Time (seconds)')
ylabel('Pulse amplitude (dimensionless)')
```

8 Further work

Notwithstanding the developments made in recent years it is clear that there is much still to be done to gain a complete understanding of the role of the seabed in the reflection and scattering of sound. These developmental areas may be looked at from the separate viewpoints of reflection and scattering theories, and then looked at from a joint perspective.

In terms of single interfaces the theory of sound reflection is fairly mature. In practice, this is not enough. Two main areas for development remain. The first is to understand and address the numerical limits of the matrix propagator method with regard to including attenuation within the sediment layers. It was explained in chapter 2 that the problem arises due to taking the cosines and sines of complex terms. These arise due to the use of a complex wavenumber which is used to model an attenuating medium. A solution to this problem may be to dispense with the use of this complex wavenumber. Then, it would be necessary to treat the wave propagation and the wave attenuation separately. The first of these (wave propagation) keeps track of the phase of the waves; the second (wave attenuation) keeps track of the wave amplitude. This approach would firstly require that the wavenumber be made a purely real number (corresponding to zero attenuation). Secondly, the attenuation for each layer would have to be included separately as a (real) multiplying factor on the equation linking the interface to interface displacement-stress vectors (equation 2-37). This factor may be calculated for each layer and for each wave (compressional or shear wave) as the product of: the cosine of the incident angle for the wave (which will be real); the (real) attenuation coefficient (assumed in dB per wavelength, i.e. linear with frequency); the thickness of the layer; and the reciprocal of the wavelength.

The second area for development concerns the model used to represent the seabed. In terms of its ability to represent any vertically inhomogeneous set of layers, the matrix propagator method is perfectly capable, as demonstrated in chapter 2. The problem is more in understanding and finding the correct approach to dealing with sediments which are not rigid solids. It is shown in chapter 2 that rigidity, or the ability to support shear waves, has a profound effect on the relative proportion of energy reflected from the interface. Not only is the pertinent question "Does the sediment support shear waves ?" but "*How much* does it support shear waves ?" since the degree of shear elasticity represented by the shear modulus, μ, has a non-linear relationship with the reflected energy. The problem may be even more complicated than this. It is showed by BUCKINGHAM (1998) that certain sediments may not be treated as either fluids or solids in the usual sense: for porous fluid-filled sediments which exhibit a dissipative characteristic with memory (or hysteresis), he shows that a shear wave solution may be derived even though the shear (or elastic) modulus is zero. Thus the description of a solid as having a non-zero shear modulus, and hence supporting shear waves, and a liquid having zero shear modulus, and not supporting shear waves, is not always valid, and the whole approach may need reviewing for these cases. This would involve going back to fundamentals, and re-evaluating the applicability of Hooke's

law (equation 2-14, right at the start of the development shown at Appendix 2A) and its use in deriving the wave propagation equations. BUCKINGHAM (1998) has looked at this problem, and the challenge initially is to look at how this type of approach could be used within a multilayer reflection model, and to ascertain precisely when such an approach is justified in preference to the standard methods. The next step would then be to determine whether this approach could be used within a perturbation theory roughness model.

In the model developed here there are some clear assumptions and limitations which could be relaxed in order to develop a more complete scattering solution. The equations developed in chapters 4 and 5 gave solutions for the transmitted scattered waves as well as reflected scattered waves. These have not been looked at in detail here, though would be a necessary inclusion in a model which considered a scattering sediment overlying a smooth basement. An involved, but straightforward extension would be to consider the transmitted scattered energy reflecting from a smooth seabed and then interacting again with the sediment / sea interface, and calculating how much extra energy is returned to the sea by this mechanism. Using scattered pressures for a liquid sediment, the "input impedance method" (see chapter 2) would be the model to extend for this case. If a solid sediment was used then the matrix propagator method (see chapter 2) would be the one to extend.

It was mentioned in chapter 6 that the liquid / solid code, developed to implement the solution developed in chapter 5, is unstable. This is a loose end which should be tidied up, so that the liquid / solid model can be used as the general interface scattering model.

Although the model which was coded up was for a corrugated rough surface, i.e. a surface which is rough in one dimension only, the theoretical developments necessary for a 2 dimensional rough surface have been detailed where relevant in each chapter. It is shown that in terms of the power spectra, the zero order reflection coefficient, and the beam and pulse considerations, the modifications required for a 2 dimensional rough surface are fairly simple. In terms of the boundary conditions for the rough surface perturbation theory the modifications are not trivial, and the modifications to the treatment of the surface and normal derivatives are simple but significantly increase the algebraic manipulations required. Also, for more practical use, a non-gaussian rough surface power spectrum would be used. The development shown in chapters 3, 4 and 5 allows for any surface power spectrum to be used, a gaussian spectrum was used to produce the plots for since this is the standard spectrum used for comparison with other work in the literature.

One of the aims of this thesis is to show the effect on the scattered energy of using real geoacoustic parameters rather than assuming the scattering medium to be either solid or vacuum (for the pressure release case). It is clear, however, that an equally significant effect on the scattered energy comes from the assumed rough surface power spectral density (PSD). Depending on the form of the PSD (Gaussian, power law, etc.) and the way in which it is parameterised, in terms of root mean square (rms) height or in terms of surface correlation length, certain statistical properties of the rough surface become very significant. For the gaussain PSD used in various places throughout this thesis, an accurate estimate of

the rms height is essential. It is of interest, then, to find out which power spectra are valid for which scattering approaches (small perturbations method, tangent plane method) and what the factors are which limit their key parameters.

In chapter 6 it was shown how the scattering strengths from a number of surface realisations can be found and how the statistics of these can be investigated. This was done for a few arbitrary cases to show the utility of the method. It is clear that the methodology presented here can be used to conduct a more purposeful statistical study in its own right. It was explained in chapter 6 that the spread of the scattering strength at a particular outgoing angle is due to the surface power spectral density function used to describe the surface; the mean value at any angle is due to both this and the geoacoustic parameters at the interface. The precise dependence on the type of PSD, and on key parameters such as rms height and the surface correlation length, with respect to the incident sound wavelength, should be investigated.

Looking outside the model developed here, it is clear that surface roughness theories and models based on the tangent plane approximation and the small perturbations approach are fairly mature now. These apply only for large scale and small scale roughness respectively, where large and small are functions of the incident sound frequency and geometry. The challenge still remains to design a model which covers all scales of surface roughness. It is not immediately clear how such a model may be derived, since the large and small scale theories are fundamentally different in approach.

A first step would be to try to extend the work done (in the literature) on multiscale modelling. This is really combining the small and large scale approaches by putting small scale roughness on top of large scale roughness. The scales in the middle are omitted. For an incident pulsed beam this approach has potential, since a pulsed beam will be incident at a particular location on the rough surface, and so the tangent plane approximation only needs to be considered at that particular location. The extension required to the model developed here would be therefore to allow a local mean surface angle (in degrees) to be specified. The new first step in the model would then be to calculate the beam's incident angle with respect to the surface normal, and then the model would continue as it does now, with the calculations all being with respect to this mean surface reference frame. On calculating the scattering with respect to this co-ordinate system, the absolute scattered angles would be calculated by rotating back to the absolute reference frame. It can be seen that this approach, using an incident beam, rather than a single incident plane wave, means that although there is added complexity in deriving the incident beam (as the weighted sum of plane waves) there is a clear benefit in that the "integral over the whole surface" usually required for the tangent plane approach is reduced to considering only one part of the surface. The shadowing effects associated with this method, so often a problem when considering the whole of the surface, can also be treated more directly on an individual basis.

A recent theory which addresses both small and large scale roughness is one based on the small slope approximation: this is an approximation which is common to both the small perturbation theory (used for small scale roughness) and the tangent plane theory (used for large scale roughness). This model is being developed by TATARSKI and looks promising.

Sediment volume scattering, mentioned in chapter 1, is a major field of study in its own right, with some of the developments in this area having been mentioned earlier (see chapter 1). To extend the model developed here towards one that aimed to completely describe the interaction of sound with the seabed it would be necessary to include both surface roughness scattering and sediment volume scattering as separate modules, before attempting to describe the interaction between the two. An attempt to model volume scattering as an effective surface roughness has been made by CHU et al (1997). This is done for a regime where there is a low impedance mismatch at the sea / seabed interface, and so where the scattering is mainly due to the sediment volume. A surface bubble scattering model is developed, which has parameters set such that it represents the scattering from the whole of the inhomogeneous sediment volume. For an interface with significant impedance mismatch, such an approach could be combined with a standard surface roughness model in order to investigate the relative effects of each scattering mechanism on an "equal footing".

A longer term aim to include sediment volume scattering in a more formal manner would involve modelling the surface roughness and sediment volume scattering mechanisms separately, but consistently. For this, a model would have to keep track of and coherently sum the sound scattered by a number of mechanisms. *Firstly*, sound reflected and scattered from the rough sea / seabed interface. This is the first source of scattering from the seabed. *Secondly*, sound would be scattered from an inhomogeneous sediment volume. Such scattering has been modelled by PACE (1995), HINES (1990) and others, following the development by CHERNOV (1967). In a self-consistent scattering model, the incident field upon the scattering volume would be made up of the field transmitted (and scattered) through the rough sea / seabed interface. The transmitted scattered field is developed naturally in chapters 3, 4 and 5 as a result of the self-consistent manner in which the rough surface interaction is modelled, and is expressed in terms of plane wave components. The interaction of each of these plane waves with the sediment volume would be dealt with using a CHERNOV (1967) type model, and the results coherently summed to give a resultant volume scattered field. *Thirdly*, the resultant volume scattered field would be then incident upon the rough sea / seabed interface (from the seabed side). Whatever was transmitted (and scattered) through this interface would then be a second source of scattering from the seabed. The first and second sources of scattering from the seabed would then be added coherently.

This sort of approach has been tried by HOLLAND and NEUMANN (1998) in an attempt to understand the discrepancies seen in bottom scattering strength between

intermediate and low grazing angles. As well as backscatter, such a self consistent model will, naturally, also predict forward scatter. Their model also includes a basement layer beneath the sediment, though how useful this additional factor is will depend largely on the thickness and attenuating properties of the sediment layer. A similar model was compared to data for both backscatter and forward scatter by WILLIAMS and JACKSON (1998): they concluded that multiple scattering effects may be needed to fully model the particular site where the data was taken.

It was mentioned in chapter 6 that the pulse and beam types used here were relatively straightforward. Using a normal modes approach, GINGRAS (1998) shows that by a judicious use of multiple sources with appropriate weightings and phases one can minimise the backscatter generated from a seabed by exciting the first mode within a particular frequency band. He also shows that the sediment type (as part of the geoacoustic profile) is also an important factor in determining the reduction in backscatter and attenuation. These ideas are not used here, though would provide a suitable direction in which to progress further work. Care must be taken when using a normal modes approach to include the interactions between the incident and the scattered modes; and also to be aware of similar interference effects generated by the periodicity of the surface, for surfaces with non-zero correlation length (see LeMOND and KOCH (1997)).

As for all theoretical models, the justification for the model developed here must ultimately be gauged from how well it compares to experimental data. The comparisons given in chapters 4 and 5 show how this model compares to the standard limits of textbook perturbation theory approaches (BREKHOVSKIKH and LYSANOV (1990)) and the PSD used have been compared to those used by THORSOS (1999). While these comparisons provide evidence that the approach used here is consistent with practice elsewhere in the field, the best evidence for *correctness* must be derived from analysis of sea trials data.

9 References

Ainslie, M. A. (1995) J. Acoust. Soc. Am., 954, 97.

Ainslie, M. A. and Burns, P. W. (1995) J. Acoust. Soc. Am., 2836, 98.

Ainslie, M. A. (1996) J. Acoust. Soc. Am., 893, 99.

Ainslie, M. A., Robins, A. J. and Prior, M. K., "Benchmark solutions of plane wave bottom reflection loss", JASA December 1998 Volume 104, Issue 6, pp. 3305-3312.

Alenitsyn, A., "Double wave of Stoneley type on the interface of a stratified fluid layer and an elastic solid half-space", JASA February 1998 Volume 103, Issue 2, pp. 795-800.

Allen, J. R. L. (1968) *Current Ripples* (North Holland Publishing Company).

Badiey, M. H., Cheng, A. H-D. and Jaya, I., (1996) J. Acoust. Soc. Am., 903, 99.

Bergem, O., Pouliquen, E., Canepa, G., and Pace, N. G., "Time-evolution modeling of seafloor scatter. II. Numerical and experimental evaluation", JASA June 1999 Volume 105, Issue 6, pp. 3142-3150.

Berman, D. H., "Reverberation in waveguides with rough surfaces", JASA February 1999 Volume 105, Issue 2, pp. 672-686.

de Billy, M. and Quentin, G., "Backscattering of acoustic waves by randomly rough surfaces of elastic solids immersed in water", J. Acoust. Soc. Am., August 1982, 72, 591-601.

Biot, M. A., "Theory of Propagation of Elastic waves in a Fluid-Saturated Porous Solid. I. Low-Frequency Range", J. Acoust. Soc. Am., March 1956, 28, pp168-78.

Blakemore, M., "Scattering of acoustic waves by the rough surface of an elastic solid", Ultrasonics, 1993, 31, pp161-174.

Boehme, H., Chotiros, N.P., Rolleigh, L. D., Pitt, S. P., Garcia, A. L., Goldsberry, T. G. and Lamb, R. A., "Acoustic backscattering at low grazing angles from the ocean bottom. Part I. Bottom backscattering strength", J. Acoust. Soc. Am, March 1985, 77, pp962-974.

Bowles, F. A., "Observations on attenuation and shear-wave velocity in fine-grained, marine sediments", JASA June 1997 Volume 101, Issue 6, pp. 3385-3397.

Bradley, C. R. and Stephen, R. A., "Modeling of seafloor wave propagation and acoustic scattering in 3-D heterogeneous media", J. Acoust. Soc. Am., July 1996, 100, pp225-236.

Brekhovskikh, L. M. and Godin, O. A. (1990) *Acoustics of layered media I* (Springer Verlag).

Brekhovskikh, L. M. and Lysanov, Yu. P. (1990) *Fundamentals of ocean acoustics* (Springer Verlag).

Buckingham, M. J., "Theory of acoustic attenuation, dispersion, and pulse propagation in unconsolidated granular materials including marine sediments", JASA November 1, 1997 Volume 102, Issue 5, pp. 2579-2596.

Buckingham, M. J., "Theory of compressional and shear waves in fluidlike marine sediments", JASA January 1998 Volume 103, Issue 1, pp. 288-299.

Carbo, R. (1997) J. Acoust. Soc. Am, 227, 101.

Caruthers, J. W. and Novarini, J. C., "Modeling Bistatic Bottom Scattering Strength Including a Forward Scatter Lobe", IEEE Journal of Oc. Eng., April 1993, 18, pp100-107.

Caruthers, J. W. and Novarini, J. C., "The Partition Wavenumber in Acoustic backscattering from a Two-Scale Rough Surface Described by a Power-Law Spectrum", IEEE Journal of Oc. Eng., April 1994, 19, pp200-207.

Chambers, J. P. and Berthelot, Y. H., "An experimental investigation of the propagation of sound over a curved, rough, rigid surface", JASA August 1997 Volume 102, Issue 2, pp. 707-714.

Chernov, L. A. (1967) *Wave propagation in a random medium* (McGraw-Hill 1967).

Chu, D., Williams, K. L., Tang, D. and Jackson, D. R., "High-frequency bistatic scattering by sub-bottom gas bubbles", JASA August 1997 Volume 102, Issue 2, pp. 806-814.

Collins, M. D. and Kuperman, W. A., "Overcoming ray chaos", J. Acoust. Soc. Am, June 1994, 95, pp3167-3170.

Cook, R. K., "Lord Rayleigh and reciprocity in physics", J. Acoust. Soc. Am., January 1996, 99, pp24-29.

Cooper Jr., H. F. (1967) J. Acoust. Soc. Am., 42, 1064.

DeSanto, J. A. and Martin, P. A., "On the derivation of boundary integral equations for scattering by an infinite one-dimensional rough surface", JASA July 1997 Volume 102, Issue 1, pp. 67-77.

Ellis, D. D. and Crowe, D. V., "Bistatic reverberation calculations using a three-dimensional scattering function", J. Acoust. Soc. Am, May 1991, 89, pp2207-2214.

Essen, H-H., "Scattering from a rough sedimental seafloor containing shear and layering", J. Acoust. Soc. Am., March 1994, 95, pp1299-1310.

Fawcett, J. A., Fox, W. L. J. and Maguer, A., "Modeling of scattering by objects on the seabed", JASA December 1998 Volume 104, Issue 6, pp. 3296-3304.

Feuillade, C. and Nero, R. W., "A viscous-elastic swimbladder model for describing enhanced-frequency resonance scattering from fish", JASA June 1998 Volume 103, Issue 6, pp. 3245-3255.

Gardner, T. N., "An acoustic study of soils that model seabed sediments containing gas bubbles", JASA January 2000 Volume 107, Issue 1, pp. 163-176.

Gingras, D. F., "Single mode excitation, attenuation, and backscatter in shallow water", JASA January 1998 Volume 103, Issue 1, pp. 195-204.

Goff, J. A., "The relationship between local- and global-scale scattering functions for fractal surfaces under a separation of scales hypothesis", J. Acoust. Soc. Am., March 1995, 97, pp1586-1595.

Hamilton, E. L., "Geoacoustic modeling of the sea floor", J. Acoust. Soc. Am., November 1980, 68, pp1313-1340.

Heezen, B. C. and Hollister, C. D. (1971) *The Face of the Deep* (Oxford University Press).

Hines, P. C., "Theoretical model of acoustical backscatter from a smooth seabed", J. Acoust. Soc. Am, July 1990, 88, pp324-334.

Hines, P. C., "Theoretical model of in-plane scatter from a smooth sediment seabed", J. Acoust. Soc. Am., February 1996, 99, pp836-844.

Holland, C. W. and Neumann, P., "Sub-bottom scattering: A modeling approach", JASA September 1998 Volume 104, Issue 3, pp. 1363-1373.

Hwang, W. S., "A boundary integral method for acoustic radiation and scattering", JASA June 1997 Volume 101, Issue 6, pp. 3330-3335.

Ivakin, A. N., "A unified approach to volume and roughness scattering", JASA February 1998 Volume 103, Issue 2, pp. 827-837.

Ivakin, A. N. and Jackson, D. R., "Effects of shear elasticity on sea bed scattering: Numerical examples", JASA January 1998 Volume 103, Issue 1, pp. 346-354.

Jackson, D. R.and Briggs, K. B., "High-frequency bottom backscattering: Roughness versus sediment volume scattering", J. Acoust. Soc. Am, August 1992, 92, pp962-977.

Jackson, D. R., Winnebrenner, D. P. and Ishimaru, A., "Comparison of perturbation theories for rough surface scattering", J. Acoust. Soc. Am., March 1988, 83, pp961-969.

Jackson, D. R. and Ivakin, A. N., "Scattering from elastic sea beds: First-order theory", JASA January 1998 Volume 103, Issue 1, pp. 336-345.

Kinney, W. A. and Clay, C. S., "Insufficiency of surface spatial power spectrum for estimating scattering strength and coherence: Numerical studies", J. Acoust. Soc. Am., November 1985, 78, pp1777-1784.

Kinney, W. A. and Clay, C. S. (1988) J. Acoust. Soc. Am., 2126, 83.

Kuo, E. Y. T., "Wave Scattering and Transmission at Irregular Surfaces", J. Acoust. Soc. Am, November 1964, 36, pp2135-2142.

Kuperman, W. A., "Coherent component of specular reflection and transmission at a randomly rough two-fluid interface", J. Acoust. Soc. Am., August 1975, 58, pp365-370.

Kuperman, W. A. and Schmidt, H., "Rough surface elastic wave scattering in a horizontally stratified ocean", J. Acoust. Soc. Am., June 1986, 79, pp1767-1777.

Kuperman, W. A. and Schmidt, H., "Self-consistent perturbation approach to rough surface scattering in stratified elastic media", J. Acoust. Soc. Am., October 1989, 86, pp1511-1522.

Leeder, M. R. (1985) *Sedimentology* (George Allen and Unwin Ltd).

LeMond, J. E. and Koch, R. A., "Finite correlation and coherent propagation effects in the normal-mode description of bottom reverberation", JASA July 1997 Volume 102, Issue 1, pp. 266-277.

LePage, K., "Bottom reverberation in shallow water: Coherent properties as a function of bandwidth, waveguide characteristics, and scatterer distributions", JASA December 1999 Volume 106, Issue 6, pp. 3240-3254.

Lupien, V., "The role of scale structure in scattering from random rough surfaces", JASA April 1999 Volume 105, Issue 4, pp. 2187-2202.

Lyons, A. P. and Abraham, D. A., "Statistical characterization of high-frequency shallow-water seafloor backscatter", JASA September 1999 Volume 106, Issue 3, pp. 1307-1315.

Lyons, A. P. and Anderson, A. L., "Acoustic scattering from the seafloor: Modeling and data comparison", J. Acoust. Soc. Am, May 1994, 95, pp2441-2451.

Mackenzie, K. V., "Bottom Reverberation for 530- and 1030-cps Sound in Deep Water", (1961) J. Acoust. Soc. Am, November 1961, 33, pp1498-1504.

Maguer, A., Fox, W. L. J., Schmidt, H., Pouliquen, E. and Bovio, E., "Mechanisms for subcritical penetration into a sandy bottom: Experimental and modeling results", JASA March 2000 Volume 107, Issue 3, pp. 1215-1225.

Marsh, H. W., "Exact Solution of wave Scattering by Irregular Surfaces", J. Acoust. Soc. Am, March 1961, 33, pp330-333.

Marsh, H. W., Schulkin, M. and Kneale, S. G., "Scattering of Underwater Sound by the Sea Surface", J. Acoust. Soc. Am, March 1961, 33, pp334-340.

Marsh, H. W., "Sound Reflection and Scattering from the Sea Surface", J. Acoust. Soc. Am, February 1963, 35, pp240-244.

Mast, D. T., Nachman, A. I. and Waag, R. C., "Focusing and imaging using eigenfunctions of the scattering operator", JASA August 1997 Volume 102, Issue 2, pp. 715-725.

Mathews, J. and Walker, R. L. (1970) "Mathematical methods of physics", Addison Wesley.

MATLAB, high level programming language for data manipulation and analysis, produced by "The MathWorks" ©, Cambridge Control Ltd., Matrix House, Cowley Park, Cambridge, England, CB4 0HH (www.camcontrol.co.uk).

McDaniel, S. T. and Gorman, A. D., "Spectral spread of sea-surface reverberation", J. Acoust. Soc. Am, July 1983, 74, pp241-248.

McKinney, C. M. and Anderson, C. D., "Measurements of Backscattering of Sound from the Ocean Bottom", J. Acoust. Soc. Am, January 1964, 36, pp158-163.

Moe, J. E. and Jackson, D. R., "Near-field scattering through and from a two-dimensional fluid–fluid rough interface", JASA January 1998 Volume 103, Issue 1, pp. 275-287.

Mourad, P. D. and Jackson, D. R., "A model / data comparison for low-frequency bottom backscatter", J. Acoust. Soc. Am, July 1993, 94, pp344-358.

Nagy, P. B. and Adler, L., "Surface roughness induced attenuation of reflected and transmitted ultrasonic waves", J. Acoust. Soc. Am., July 1987, 82, pp193-197.

Nolle, A. W., "Acoustical Properties of Water-Filled Sands", J. Acoust. Soc. Am, September 1963, 35, pp1394-1408.

Ogilvy, J. A. (1992) Theory of wave scattering from random rough surfaces (Institute of Physics)

Pace, N. G. (1992) *Low Frequency Acoustic Backscatter from the Seabed* University of Bath (report for the Defence Research Agency).

Pace, N. G. (1993) *Low frequency acoustic backscatter from the seabed : final report* University of Bath (report for the Defence Research Agency).

Pace, N. G. (1995) *Bistatic scatter from the seabed: final report* University of Bath (report for the Defence Research Agency).

Pace, N. G., Cowley, A. and Campbell, A. M., "Short pulse acoustic excitation of microbubbles", JASA September 1997 Volume 102, Issue 3, pp. 1474-1479.

Parkins, B. E., "Omnidirectional Scattering of Acoustic Waves by Rough, Imperfectly reflecting Surfaces", J. Acoust. Soc. Am, 1967, 41, pp126-134.

Patterson, R. B., "Relationships between Acoustic Backscatter and Geological Characteristics of the Deep Ocean Floor", J. Acoust. Soc. Am, October 1969, 46, pp756-761.

Porter, M. B., "Acoustic Models and Sonar Systems", IEEE Journal of Oceanic Engineering, October 1993, 18, pp425-437.

Press, W. H., Teukolsky, S. A., Vetterling, W. T. and Flannery, B. P., "Numerical Recipes in C", Second Edition, Cambridge University Press, 1992.

Pouliquen, E., Bergem, O. and Pace, N. G., "Time-evolution modeling of seafloor scatter. I. Concept", JASA June 1999 Volume 105, Issue 6, pp. 3136-3141.

Purcell, A., "The Rayleigh equations for a multi-sinusoidal periodic surface", JASA February 1998 Volume 103, Issue 2, pp. 683-694.

Qian, Z. W., "Wave scattering on a fractal surface", JASA January 2000 Volume 107, Issue 1, pp. 260-262.

Rasmussen, R. A., "Remote detection of turbulence from observations of reverberation spectra", J. Acoust. Soc. Am, January 1978, 63, pp101-110.

Riley, K. F., "Mathematical Methods for the Physical Sciences", Cambridge University Press, 1987.

Robins, A. J (1991) J. Acoust. Soc. Am., 1686, 89.

Robins, A. J., "Plane-wave reflection from a solid layer with nonuniform density, sound speed, and shear speed", JASA March 1998 Volume 103, Issue 3, pp. 1337-1345.

Rose, J. H. and Bilgen, M., "Acoustic double-reflection and transmission at a rough water-solid interface", J. Acoust. Soc. Am, June 1994, 95, pp3242-3251.

Schmidt, H. and Jensen, F. B. (1985) J. Acoust. Soc. Am., 813, 77.

Schmidt, H. and Lee, J., "Physics of 3-D scattering from rippled seabeds and buried targets in shallow water", JASA March 1999 Volume 105, Issue 3, pp. 1605-1617.

Schultz, C. A. and Toksoz, M. N., "Experimental study of enhanced backscattering from a highly irregular acoustic-elastic interface", J. Acoust. Soc. Am., February 1996, 99, pp880-891.

Smith, E., "Benchmarking virtual backscatter in parabolic evolution", JASA November 1, 1997 Volume 102, Issue 5, pp. 2626-2636.

Stephen, R. A., "Optimum and standard beam widths for numerical modeling of interface scattering problems", JASA March 2000 Volume 107, Issue 3, pp. 1095-1102.

Stride, A. H. (1982) *Offshore Tidal Sands* (Chapman and Hall Ltd).

Tang, D., "A note on scattering by a stack of rough interfaces", J. Acoust. Soc. Am., March 1996, 99, pp1414-1418.

Thomson, W. T., "Transmission of Elastic waves through a Stratified Solid Medium", J. Applied Physics, February 1950, 21, pp 89 – 93.

Thorsos, E. I., "The validity of the Kirchhoff approximation for rough surface scattering using a Gaussian roughness spectrum", J. Acoust. Soc. Am., January 1988, 83, pp78-92.

Thorsos, E, I. "A practical model for rough surface scattering: the small slope approximation", paper presented to the IOA International Conference, Cambridge, 15-17 Dec. 1999.

Thorsos, E. I. and Jackson, D. R., "The validity of the perturbation approximation for rough surface scattering using a Gaussian roughness spectrum J. Acoust. Soc. Am., July 1989, 86, pp261-277.

Thorsos, E. I., Jackson, D. R. and Williams, K. L., "Modeling of subcritical penetration into sediments due to interface roughness", JASA January 2000 Volume 107, Issue 1, pp. 263-277.

Tollefsen, D., "Thin-sediment shear-induced effects on low-frequency broadband acoustic propagation in a shallow continental sea", JASA November 1998 Volume 104, Issue 5, pp. 2718-2726.

Tolstoy, I., "Acoustic scatter from a slightly rough boundary between a fluid and an elastic solid", J. Acoust. Soc. Am., November 1985, 78, pp1727-1734.

Tracey, B. H. and Schmidt, H., "A self-consistent theory for seabed volume scattering", JASA November 1999 Volume 106, Issue 5, pp. 2524-2534.

Trucco, A., "A least-squares approximation for the delays used in focused beamforming", JASA July 1998 Volume 104, Issue 1, pp. 171-175.

Turgut, A., "Inversion of bottom/subbottom statistical parameters from acoustic backscatter data", JASA August 1997 Volume 102, Issue 2, pp. 833-852.

Vidmar, P. J. (1980) J. Acoust. Soc. Am., 68, 634.

Vidmar, P. J. (1980) J. Acoust. Soc. Am., 86, 1442.

Vidmar, P. J. and Foreman, T. L. (1979) J. Acoust. Soc. Am., 66, 1830.

Voronovich, A. G. (1994) *Wave scattering from rough surfaces* (Springer Verlag).

Waite, A. D. "Sonar For Practising Engineers", Thomson Marconi Sonar Ltd, printed by Epic Printing Services, Dorchester (1998).

Westwood, E. K. (1989) J. Acoust. Soc. Am., 85, 1872.

Westwood, E. K. and Vidmar, P. J. (1987) J. Acoust. Soc. Am., 81, 912.

Williams, K. W. and Jackson, D. R., "Bistatic bottom scattering: Model, experiments, and model / data comparison", JASA January 1998 Volume 103, Issue 1, pp. 169-181.

Yamamoto, T., "Acoustic scattering in the ocean from velocity and density fluctuations in the sediments", J. Acoust. Soc. Am., February 1996, 99, pp866-879.